Flavin-binding fluorescent proteins as genetically encoded singlet oxygen photosensitizers

Joaquim Torra Nonell

DOCTORAL THESIS

Title	Flavin-binding fluorescent proteins as genetically encoded singlet oxygen photosensitizers
Presented by	Joaquim Torra Nonell
Centre	IQS School of Engineering
Department	Analytical and Applied Chemistry
Directed by	Prof. Dr. Santi Nonell Marrugat Dr. Rubén Ruiz González

La llibertat és un estat permanent
sense fronteres,
és oferir amor clandestí
com una droga
a plena llum del dia,
és no claudicar en l'intent,
és sincerar-te.

La llibertat és conviure
amb el desordre del desig
i no justificar-te,
és blasfemar
i fugir dels visionaris,
és condemnar-te a l'oblit
dels capatassos,
és dignificar mots tals com
Revolució, Insurgència,
Autoorganització.

La llibertat és desmitificar
i fer caure totes les estàtues,
és suprimir, definitivament, la falsa amistat
amb traïdoria,
és profanar la voluntat de control del
misticisme,
és oblidar el pecat, la mala consciència,
els remordiments de la moral
perversa, que t'han incultat en escoles
tenebroses
com palaus,
com presons,
amb patis enormes
on només podies donar voltes.

La llibertat és un hemicicle buit,
un mentider coix, un dictador mut,
una rumba dansant al voltant d'una foguera,
les calces de la cambrera fent de bandera
negra
a l'estenedor de les il·lusions
complertes, de les utopies acabades,
de les conviccions que han deixat de presumir,
de les cançons que han deixat de ser himnes,
mentre l'últim ideari ens escalfa els peus,
i ens ajuda a fer el sopar...

La llibertat és treballar poc i llegir molt,
és abandonar el llibre sempre que puguis,
és suprimir el prefix de la paraula sexual,
és estimar i punt.
És descobrir el plaer i potenciar-lo,
és emancipar-te del tedi,
és la vida juganera,
creativa, la pervivència del dubte,
l'abolició de la condemna,

I tu, de quin color dius que és
la llibertat?

La llibertat
David Caño

Als pares, germà i àvia,
i a la Meme.

ACKNOWLEDGMENTS

Molts col·legues doctors m'han comentat que l'escriptura de la tesi doctoral és un procés lent i esgotador, i que quan finalment un arriba als agraïments ja no té esma ni ganes d'allargar-se ni una paraula més. Certament ha estat un període llarg, estressant en moltes ocasions i les forces han anat minvant pel camí. Però precisament si estic ara i aquí és gràcies a totes les persones que en un moment o altre m'han acompanyat en aquesta etapa i a les que vull dedicar unes paraules per mostrar el meu sincer agraïment.

En primer lloc, i fugint dels estrictes formalismes que omplen les línies dedicades als "jefes", vull agrair al Dr. Santi Nonell la oportunitat de fer la tesi doctoral al seu grup, en el que el rigor, l'exigència i les grans dosis de *multitasking* prometen emocions fortes, però finalment esdevenen les verdaderes claus de l'èxit. També vull fer menció especial al Dr. Rubén Ruiz, co-director d'aquesta tesi, per agrair-li afectuosament la seva dedicació, el suport i especialment l'acompanyament científic i personal durant aquests anys.

Imprescindibles són també totes les persones que m'han acompanyat el dia a dia d'aquesta història i que saben de primera mà les penes i alegries que hem viscut. Vull tenir un record pels flamants Dr. Oriol Planas i Dra. Beatriz Rodríguez, al qui és un orgull (i encara m'impressiona) anomenar-los doctors, i al Roger Bresolí, amb una ment científica brillant i que ben aviat també es doctorarà. Oriol, Bea i Roger, hem fet la tesi junts i això implica tantes coses que recordar-les ompliria una segona tesi. Ha estat un autèntic plaer. A la Dra. Ester Boix vull agrair-li l'acollida al grup i el suport que em va oferir als inicis de la tesi. Vull mostrar el meu agraïment i admiració a la Dra. Íngrid Nieves, pels ànims i consells, per la seva alegria i sentit de l'humor i per la seva vàlua personal. Aprovecho para mandar un fuerte abrazo al Dr. Renzo Zanocco y agradecerle sus sabios consejos y su apoyo. També vull incloure unes paraules pels nous membres del grup de FOTOQ; en Jaume Nos, en Cormac Hally i l'Elena de las Heras, a qui desitjo tota la sort i força en la seva etapa fotoquímica. No vull oblidar-me de l'Elisabeth Bou i d'en Raul Ondoño, als que vull agrair molt especialment el recolzament constant i les dosis de bon humor que han fet que tot fos una mica més fàcil i divertit. Finalment, també voldria tenir un record per totes les persones que en un moment o altre ha passat pel laboratori de fotoquímica..

Vull expressar el meu agraïment a la Dra. Montserrat Agut per oferir-me la oportunitat de desenvolupar la part microbiana de la tesi al seu laboratori i pel seu suport. Així mateix, agraeixo al Dr. Òscar Gulías els nombrosos consells i ajudes que m'ha ofert en els estudis amb bacteris.

A la incombustible, vital y siempre sonriente Dra. Pepa Blanco mi más sincera gratitud y admiración. Ha sido un placer entrar al mundo de la calidad y aprender tanto a su lado.

Vull agrair als Dr. Jordi Martorell i Dr. Marc Carnicer per facilitar-me l'ús d'equips i espais per dur a terme assajos cel·lulars, així com per les discussions científiques i consells.

Quiero saludar a Isabel y a Pilar de IQS con la misma sonrisa y alegría que me brindan siempre. Ha sido un placer compartir tantos pequeños momentos, ya sea temprano por las mañanas como en tantas horas intempestivas por la noche cuando los pasillos están tranquilos.

Vull agrair especialment a la Dra. Àngels Fabra i al seu equip el temps i l'esforç que han dedicat amb les cèl·lules de melanoma. Els agraeixo molt l'interès i la voluntat que han mostrat constantment en buscar i provar mètodes i processos de transfecció i anàlisi alternatius.

A la Dra. Cristina Flors quiero agradecerle junto a los miembros de su equipo la amable y calurosa bienvenida que me ofrecieron y la oportunidad de trabajar en su laboratorio.

I want to thank Dr. Thomas Gensch and his team in Jülich for giving me the opportunity to learn and work with advanced imaging techniques. I would also like to thank Dr. Thomas Drepper and his team for their work on FbFPs engineering and for helpful discussions.

I thank especially Dr. Xiaokun Shu from the UCSF for the fantastic opportunity to work in a cutting-edge laboratory. I am sincerely grateful for the warm welcome and for letting me participate in such impressive projects. I also want to thank the great guys working in Shu's lab for their help and support.

Vull tenir un record especial i agrair a tots els amics i amigues més propers la seva comprensió en els moments més complicats i el seu suport incondicional i constant. Els seus ànims i força m'han permès sens dubte tirar endavant i aconseguir els objectius. Així mateix, vull agrair a tantes altres persones que en un moment o altre han posat el seu granet de sorra per ajudar-me a arribar fins aquí.

Als meus pares, els autèntics herois d'aquesta historia, tot el meu agraïment i reconeixement. Per arribar-hi cal certament anar-hi, anar-hi i anar-hi, i de ben segur que jo no seria aquí sense la vostra estimada ajuda. Vull incloure una dedicació i especial a la meva estimada àvia per tantes i tantes coses que m'ha donat i ensenyat, i un sentit record per la meva estimada i enyorada Meme, a qui dedico aquesta tesi.

Financial support for this research has been provided by La Fundació la Marató de Tv3 (grant No. 20133133) and by the Spanish Ministerio de Economía y Competitividad (grants No. CTQ2013-48767-C3-1-R and CTQ2016-78454-C2-1-R).

ABSTRACT

This thesis reports the study of flavin-binding fluorescent proteins as genetically encodable singlet oxygen photosensitizers in photodynamic therapy.

Biological photosensitizers are a powerful alternative to conventional light-sensitive drugs owing to their superior targeting potential and localized accumulation in critical organelles, conferred by the genetic control of cell expression. A novel family of fluorescent proteins encasing flavin mononucleotide as the chromophore is gaining much attention since flavoproteins produce higher amounts of singlet oxygen than the proteins derived from the green fluorescent protein family. In this work, the photophysical, photosensitizing and antimicrobial properties of eleven flavoproteins derived from different organisms have been evaluated. All the proteins studied are capable of producing singlet oxygen and most of them are highly phototoxic when expressed in *E. coli* cells. Although they encase the same chromophore, their photophysical properties differ remarkably from one protein to another. For example, some of them are efficient photosensitizers and kill bacterial cells but show rapid photobleaching. Others produce little amounts of singlet oxygen but exhibit high photostability. The results presented herein expand the toolbox of photoactive flavoproteins and provide valuable guides for choosing the best candidate for a given application.

MiniSOG was the first flavoprotein rationally developed for singlet oxygen applications. Since then, it has been a matter of intense research; however, its photochemistry is complex and a number of controversial observations and fundamental questions remain unexplained. The combination of structural and spectroscopic studies has allowed to rationalize its modest singlet oxygen production, elucidate the transformations that it undergoes upon photolysis and establish a sound scientific basis for the rational design and development of new genetically encoded singlet oxygen photosensitizers. Novel miniSOG mutants with improved photosensitizing properties have been characterized as well as flavoprotein heterodimers that combine complementary photophysical properties. It has also been demonstrated that miniSOG and selected mutants induce mammalian cell killing selectively upon light exposure and that it is possible to combine photoactive proteins with fluorescent cell reporters.

The application of photodynamic therapy for the treatment of melanoma remains one of the main challenges in the biomedical sciences. In this study, miniSOG has been selected to test the suitability of the genetically encoded approach in melanoma cell lines. Unfortunately, it has not been possible to ascertain the correct expression of the photoactive protein, which has prevented further studies and the possibility of drawing conclusions.

RESUMEN

Esta tesis profundiza en el estudio de proteínas fluorescentes que unen flavina como compuestos fotosensibilizadores de oxígeno singlete codificables genéticamente para su uso en terapia fotodinámica.

Los fotosensibilizadores biológicos son una poderosa alternativa a los fármacos convencionales sensibles a la luz debido a su mayor especificidad frente a células sanas y a su capacidad para acumularse en orgánulos críticos, gracias al control genético de la expresión celular. Una nueva familia de proteínas fluorescentes que encapsulan el mononucleótido de flavina ha despertado un gran interés por su mayor capacidad de generar oxígeno singlete en comparación con la proteína verde fluorescente y sus derivados. En este trabajo se han evaluado las propiedades fotofísicas, fotosensibilizantes y antimicrobianas de once flavoproteínas provenientes de diferentes organismos. Todas ellas producen oxígeno singlete y la mayoría son altamente fototóxicas una vez expresadas en células *E. coli*. Aunque comparten el mismo cromóforo, las propiedades fotofísicas difieren notablemente de una a otra proteína. Por ejemplo, algunas son fotosensibilizadores eficientes y destruyen las células bacterianas, pero fotoblanquean rápidamente. Otras producen pequeñas cantidades de oxígeno singlete, pero son más fotoestables. Los resultados obtenidos amplían el abanico de flavoproteínas fotoactivas disponibles y proporcionan una guía útil para elegir la mejor opción para cada aplicación.

MiniSOG fue la primera flavoproteína racionalmente desarrollada para generar oxígeno singlete. A pesar de haber sido analizada en numerosos estudios, su fotoquímica es compleja y hay observaciones controvertidas e incógnitas que restan por resolver. Su caracterización estructural y espectroscópica ha permitido comprender los factores que limitan su modesta producción de oxígeno singlete, dilucidar las transformaciones que sufre bajo irradiación y establecer una base científica sólida para el desarrollo de nuevos fotosensibilizadores codificados genéticamente. Además, se han caracterizado nuevos mutantes de miniSOG más eficientes así como heterodímeros de flavoproteínas que combinan propiedades fotofísicas complementarias. También se ha demostrado que miniSOG y ciertos mutantes inducen selectivamente la muerte de células de mamífero cuando se iluminan con luz azul y que es posible combinar proteínas fotoactivas con reporteros fluorescentes de procesos celulares.

La aplicación de la terapia fotodinámica para el tratamiento del melanoma sigue siendo uno de los principales desafíos en la biomedicina. En este estudio se ha propuesto la expresión de miniSOG para tratar celulas de melanoma. Sin embargo, no ha sido posible comprobar la expresión correcta de la proteína fotoactiva, por lo que no se ha podido evaluar la idoneidad del enfoque ni sacar conclusiones adicionales.

RESUM

Aquesta tesi profunditza en l'estudi de les proteïnes fluorescents que uneixen flavina com a fotosensibilitzadors d'oxigen singlet codificables genèticament per a la teràpia fotodinàmica.

Els fotosensibilitzadors biològics són una alternativa poderosa als fàrmacs convencionals sensibles a la llum degut a la major especificitat front a cèl·lules sanes i a la capacitat d'acumular-se preferentment en orgànuls crítics, gràcies al control genètic de l'expressió cel·lular. Una nova família de proteïnes fluorescents que contenen mononucleòtid de flavina com a cromòfor ha despertat molt d'interès ja que produeixen majors quantitats d'oxigen singlet que la proteïna verda fluorescent i els seus derivats. En aquest treball s'han avaluat les propietats fotofísiques, fotosensibilitzants i antimicrobianes d'onze flavoproteïnes provinents de diferents organismes. Totes les proteïnes estudiades són capaces de produir oxigen singlet i la majoria són altament fototòxiques quan s'expressen en cèl·lules *E. coli*. Malgrat que comparteixen el mateix cromòfor, les propietats fotofísiques de les proteïnes difereixen notablement d'una a l'altra. Per exemple, algunes són fotosensibilitzadors eficients i són capaces de provocar la mort de cèl·lules bacterianes però fotoblanquegen ràpidament. D'altres produeixen petites quantitats d'oxigen singlet però exhibeixen una elevada fotostabilitat. Els resultats presentats en aquest treball amplien el ventall de flavoproteïnes fotoactives i proporcionen una guia útil per triar la millor opció per a cada aplicació.

MiniSOG va ser la primera flavoproteïna desenvolupada racionalment amb l'objectiu de produir d'oxigen singlet. Des de llavors ha estat emprada en nombrosos estudis, però les seves propietats fotoquímiques són complexes i encara resten qüestions pendents de resoldre. Mitjançant estudis estructurals i espectroscòpics s'ha aconseguit racionalitzar la seva modesta producció d'oxigen singlet, dilucidar les transformacions que experimenta quan s'irradia amb llum i establir una base científica sòlida pel desenvolupament racional de nous fotosensibilitzadors d'oxigen singlet codificats genèticament. Així mateix, s'han caracteritzat nous mutants de miniSOG més eficients, així com heterodímers de flavoproteïnes que combinen propietats fotofísiques complementàries. També s'ha demostrat que miniSOG i certs mutants indueixen selectivament la mort de cèl·lules de mamífer quan s'il·luminen amb llum blava, i que és possible combinar proteïnes fotoactives amb reporters fluorescents de processos cel·lulars.

L'aplicació de la teràpia fotodinàmica pel tractament del melanoma continua sent un dels principals reptes biomèdics. En aquest estudi, s'ha proposat utilitzar miniSOG per tractar cèl·lules de melanoma. Lamentablement, no ha estat possible comprovar l'expressió correcta de la proteïna fotoactiva, pel que no s'ha pogut avaluar la idoneïtat de la proposta ni extreure'n conclusions.

TABLE OF CONTENTS

CHAPTER 1

Introduction

A general introduction to the subject of the thesis is given in this chapter, and the main objectives are described. The molecular basis, as well as the components that constitute the photodynamic approach for the treatment of cancer and microbial infections, are discussed. Its current limitations and the novel strategies that are being developed to overcome them are also revised. Special attention is given to biological photosensitizers and the promising advantages that genetic control offers. Relevant contributions and the state of art of genetically encoded systems are reviewed and future directions for more efficient outcomes are presented.

Sometimes it's the very people no one imagines anything of
who do the things that no one can imagine.
Alan Turing

1.1. Photodynamic Therapy: an overview

The therapeutic use of light has a long history. Thousands of years ago, ancient cultures used the combined action of plant extracts with sunlight in attempts to treat various diseases. However, phototherapy disappeared for many centuries and it was not until the end of the 1800s that the beneficial effects of light were rediscovered.[1,2] For more than a hundred years, photodynamic therapy (PDT) has been a matter of extensive research and over the last four decades it has become a powerful therapeutic tool in modern medicine and surgery, and new technology and promising applications continue to be discovered.

PDT is a currently clinically approved, minimally invasive medical treatment against solid tumors and localized microbial infections.[3] It relies on the combination of three individually non-toxic components: (1) a phototoxic agent referred to as photosensitizer (PS), (2) light of a specific wavelength, which is specifically absorbed by the PS and (3) molecular oxygen (O_2). Light excitation of the PS leads to the local formation of cytotoxic reactive oxygen species (ROS) that are responsible for tumor-associated vascular damage, activation of antitumor immune responses and the killing of the tumor cells or microbial cells.[3–5]

In PDT, the PS concentrates predominantly within the malignant tissue and then light is applied focused on the lesion during a controlled time. Moreover, ROS are short-lived species that rapidly react with nearby biomolecules. Therefore, the therapeutic action is limited and confined in time and space to the illuminated region, providing high specificity and selectivity and reducing the adverse side-effects. In addition, PDT can also be applied in conjunction with other clinical modalities (e.g., post-surgery). Noteworthy, the multi-target approach of PDT, derived from the high reactivity and non-specificity of ROS is believed to hamper the development of cellular defense mechanisms or resistances.[6] In this regard, PDT is particularly attractive for diseases that are resistant to conventional treatments, such as for aggressive types of cancer.[6] All these advantages have stimulated and triggered the use of PDT in the modern medicine as an attractive alternative to conventional treatments for cancer and also microbial infections. Clinical success of PDT has been reported, however, it is not widespread due to some limitations. The current drawbacks of PDT as well as the novel smart strategies developed to render it a more effective and more widely available option are reviewed and discussed in the following sections.

1.2. Molecular basis of photodynamic therapy

The photophysical processes in PDT are illustrated in the Jablonski diagram (Figure 1.1). In the ground state, the PS molecule ($^1PS_0$) is a singlet because it has two electrons with opposite spins. Upon absorption of light with the appropriate quantum energy or wavelength (λ) one electron is shifted to a higher-energy orbital, yielding an excited singlet state ($^1PS^*$). The electron rapidly falls to the first excited singlet state ($^1PS_1^*$), via vibrational relaxation (VR) or internal conversion (IC). These processes are called non-radiative because there is no light emission and the energy is dissipated as heat. Singlet states are usually very short-lived (~10^{-9} s) since the spin number is preserved in both states. From $^1PS_1^*$, the molecule may return to $^1PS_0$ either as emission of light, a process called fluorescence or as production of heat, via IC. According to Kasha's rule, fluorescence emission starts from the lowest vibrational level of $^1PS_1^*$ and therefore the spectrum does not depend on the light wavelength used for excitation. Moreover, the emitted light has lower energies (and λ) than those used for excitation. This energy difference is known as the Stokes shift. From $^1PS_1^*$ the electron may also undergo a process called intersystem crossing (ISC) to the excited triplet state ($^3PS^*$) with parallel spins. Triplet states are relatively long-lived (10^{-6} to 1 s) because the transition to the singlet ground state is a "spin forbidden process" due to the change in spin number. As a consequence, competing to non-radiative (back ISC to the singlet state) and radiative (phosphorescence) processes, the long lifetime of $^3PS_1^*$ allows it sufficient time to react with molecules nearby. Photochemical reactions are therefore more likely to occur from triplet states than from the short-lived singlet states. These reactions are generally classified in Type-I and Type-II for electron transfer and energy transfer processes, respectively (Figure 1.1).

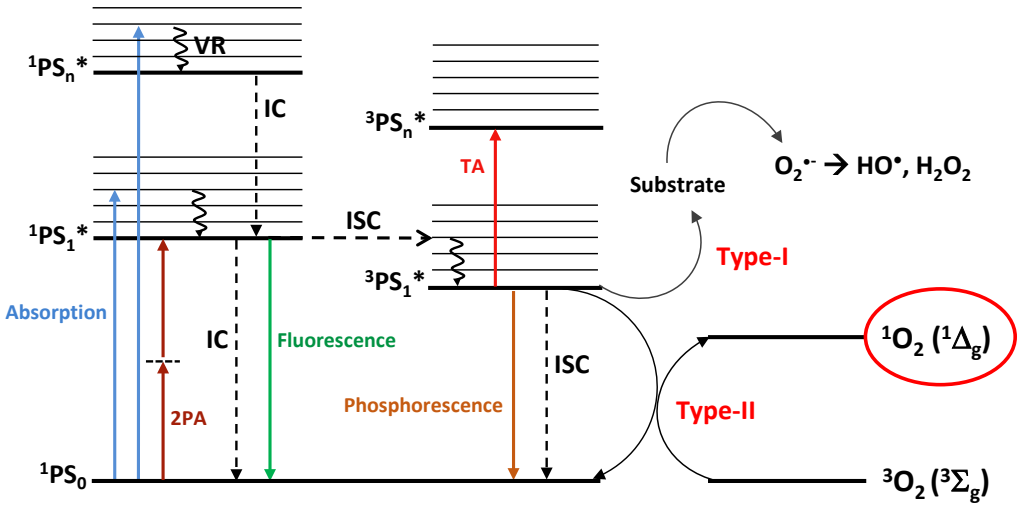

Figure 1.1. Jablonski diagram illustrating the photophysical processes in PDT. ^1PS and ^3PS denote singlet and triplet excited states, respectively. VR: vibrational relaxation; IC: internal conversion; ISC: intersystem crossing; 2PA: two-photon absorption; TA: triplet absorption.

Most PSs are capable of undergoing both processes whereby the outcome of the competition being strongly conditioned by the PS micro-environment. Type-I processes involve an electron transfer to the triplet state PS from another substrate, initiating a cascade of radical reactions which in the presence of O_2 may culminate in the formation of various types of ROS, including the hydroxyl radical ($HO^{\bullet}$) or the superoxide radical anion ($O_2^{\bullet -}$). This latter is not particularly reactive in biological systems and only reacts at a few specific protein sites,[7,8] but it can react to produce hydrogen peroxide (H_2O_2), which can easily pass through biological membranes and induce damage in different cellular compartments, reacting particularly with cysteine residues.[9] Type-II reactions comprise the transfer of energy from the $^3PS^*$ to triplet ground state molecular oxygen, which is unique in being a triplet in its ground state and is typically denotes ad $^3O_2$. This step leads to the formation of the highly reactive singlet oxygen ($^1O_2$). During this process, the sensitizer returns to the ground state and it is then ready to absorb another photon, catalytically restarting the photosensitization cycle.[10] Indeed, it has been estimated that the turnover rate can be as high as 10^6 or 10^7 cycles per second per molecule of PS,[11] although photobleaching and photodegradation processes are frequently unavoidable and lead to the loss of the photosensitizing ability. Most PSs used in PDT are thought to act through Type-II reactions, which are mechanistically more simple than Type-I. Therefore, $^1O_2$ is regarded as the central molecule causing oxidative cellular damage[3,12] and significant efforts are actively being made to develop methods for improving its generation and detection.

Other authors have also claimed the participation of Type-III and Type-IV mechanisms in PDT in which direct tissue damage is achieved in the absence of oxygen.[13] In Type-III reaction, a process called triplet-doublet interaction is produced between the activated PS and native free radicals present in the system as a result of biochemical processes.[14] This process, also known as the modified Type I (MTO) mechanism, is suggested to compete, although to a lesser extent, with Type-I and Type-II photosensitization.[15] The Type-IV mechanism involves a PS that cannot initially bind to its molecular target, however, upon light excitation it undergoes intramolecular remodeling (by photoisomerization) that then allows the binding to its cellular target site.[13]

Novel approaches for PDT are based on the so-called two-photon absorption (2PA) or two-photon excitation (2PE) process. It involves the excitation of a molecule in the ground state to an excited state upon the simultaneous absorption of two photons of lower energy than the energy gap between the two states[16] (Figure 1.1, dark red arrows). If the excited molecule is fluorescent, it can emit a single photon of fluorescence as if it were excited by a single higher energy photon. Alternatively, the excited singlet state can undergo ISC to the excited triplet

state and further react with surrounding molecules as described previously for single-photon excitation.

2PA is a nonlinear process.[17] This is because it depends on the two photons both interacting with the molecule nearly simultaneously (10^{-16} s),[17] resulting in a quadratic dependence on the light intensity rather than the linear dependence of conventional single-photon excitation. In other words, the probability of 2PA is extremely small and it is only achieved with high-intensity laser pulses focused at a very small volume (focal point).[16] Away from the focal plane, the probability drops off rapidly so that no appreciable excitation of the molecules occurs. Therefore, 2PA provides an alternative to improve the spatial precision of the treatment as well as to achieve deeper tissue penetration as a result of the long wavelength light used for excitation, as described below. These advantages have been extensively exploited for microscopy, however, the use of 2PA in PDT has been typically limited due to the low two-photon cross-sections of the PSs available,[18,19] which characterizes the probability of the simultaneous absorption of two photons whose energies add up to match the molecular transition energy.[20] The development of new PSs with improved 2PA properties has reactivated the interest for the 2PA-PDT application and it has already shown encouraging results,[3,21] including the precise targeting of individual blood vessels,[22] and to enhance the efficiency of the treatment deep in tumor xenografts.[23] Furthermore, 2PA-PDT has been suggested as a promising approach to overcome light attenuation limitations, such as in pigmented melanoma tumors,[3] although there has been no report on 2PA-PDT for melanoma so far.[24]

1.3. Light, singlet oxygen and photosensitizers in photodynamic therapy

a) Light

The use of light for healing offers several advantages as compared to conventional treatments based on chemical systems that induce biological responses. Light is readily modulated in space, time, frequency (or wavelength) and intensity, allowing for precise stimulation of a system with exceptional spatiotemporal resolution. In addition, light is an inexpensive, highly specific and immediate substrate that can be delivered or removed completely by the flick of a switch.

The increasing attention towards PDT has stimulated the development of advanced optic systems that can deliver light within the sub-millisecond scales and with the spot size down to the theoretical diffraction limit.[25,26] Numerous light sources are currently available, ranging from broadband sources (lamps) to lasers of specific wavelengths. Laser light can be delivered

to areas inside the body through fiber optic cables (thin fibers that transmit light). Both lamps and lasers have been employed in PDT and the superiority of one over the other has not been demonstrated.[27] Therefore, the choice of the light source depends on the specific application (i.e., the location of the tumor, the light dose required or the PS employed).

However, the use of light in therapy has also some limitations. Because PDT depends on localized light delivery, it is essential that light reaches the targeted tissue. This may seem quite obvious, but in practice, it turns out to be the primary drawback that hampers a broader and more efficient application of PDT. Tumors localized in internal organs such as lungs or esophagus must be illuminated using a fiber optic cable that can be inserted through an endoscope. However, illuminating the surface of the tumor tissue is usually not enough for an effective treatment. This is because light interacts with tissues by processes such as refraction, reflection, absorption and scattering that result in attenuation of the incident light energy.[28] Moreover, there are several endogenous chromophores in tissues, including hemoglobin derivatives and melanin, that have strong absorption of visible light (i.e., light comprised within the range of 400 – 700 nm of the electromagnetic spectrum and responsible for the sense of sight to the human eye). In addition, light of longer wavelengths (infrared, IR) is absorbed by water molecules present in tissues. As a consequence, effective penetration depth is limited and wavelength-dependent. Endogenous chromophores have a minimal absorbance in the region between approximately 600 and 1400 nm, which is often called the optical or therapeutic window. (Figure 1.2). However, light of wavelength longer than 850 nm has not sufficient energy to produce $^1O_2$,[29] so the active optical window is narrowed to 850 nm as the upper limit. For this reason, red and near-infrared (NIR) lights are preferentially selected to perform PDT, however, the treatment is not limited to these wavelengths, particularly for superficial lesions.

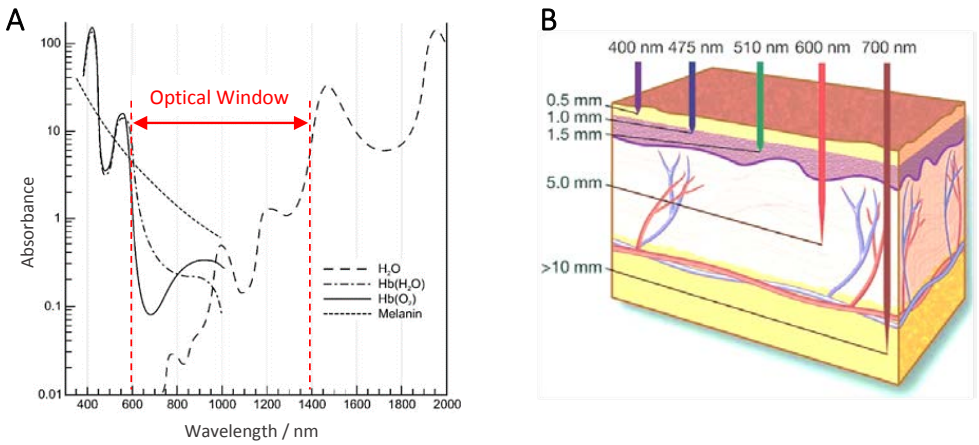

Figure 1.2. A) Absorbance of endogenous tissue chromophores and the optical window range. Adapted from Ref. 28. B) Wavelength dependency of light penetration in tissues. Adapted from Ref. 30.

b) Singlet Oxygen. Formation, detection and biological implications

Molecular oxygen (O_2) is a diatomic homonuclear molecule which constitutes 21% of Earth's atmosphere and is indispensable for aerobic life. Despite being the second most electronegative element in the periodic table, it is rather inert. This is because O_2 has a triplet electronic configuration in its ground state ($^3O_2$),[31,32] and thus its reaction with spin singlet reactants (^{1}R-H) is forbidden in terms of the spin angular momentum since the spins of the reactants are not conserved in the products[33,34] (Scheme 1.1).

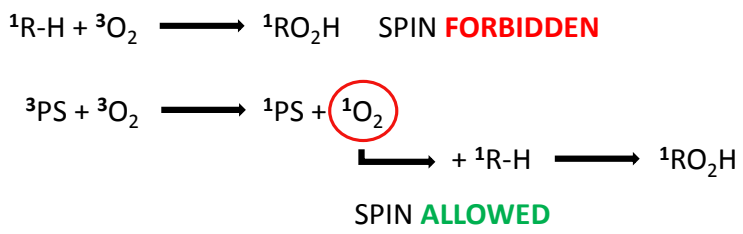

Scheme 1.1. Reactivity of triplet and singlet state molecular oxygen.

The first two electronically excited states of O_2 are known as the first and the second excited states, designed as $^1\Delta_g$ and $^1\Sigma_g^+$, respectively, and are both singlet.[35] The excited states lie approximately 94 kJ mol^{-1} and 157 kJ·mol^{-1}, respectively, above the ground state[36,37] (Figure 1.3). Because of the large amount of energy needed to reach $^1\Sigma_g^+$ and its very fast conversion (~picoseconds) to the first singlet excited state,[38] the $^1\Delta_g$ state is the primary species involved in most chemical and biological applications. For this reason, $^1O_2$ ($^1\Delta_g$) is therefore commonly referred to as singlet oxygen and expressed as $^1O_2$ to simplify the nomenclature.

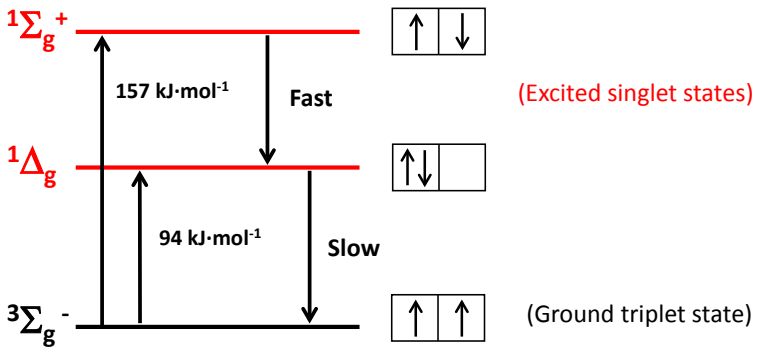

Figure 1.3. Schematic representation of the electronic states of molecular oxygen.

$^1O_2$ can be generated in a variety of ways,[32,39] however, photosensitization is the most common, convenient and controllable method, requiring only O_2, light of a specific wavelength

and a PS, as described previously. The photosensitized production of $^1O_2$ via the Type-II mechanism is essentially a two-step process in which light is first absorbed by a PS resulting in the formation of the sensitizer's triplet state, $^3PS^*$, and then the energy is transferred to ground state triplet oxygen, (Scheme 1.2).

$$^1PS + h\nu \longrightarrow {}^1PS^* \longrightarrow {}^3PS^*$$

$$^3PS + {}^3O_2 \longrightarrow {}^1PS + {}^1O_2$$

Scheme 1.2. Two-step process for $^1O_2$ photosensitization.

The $^1O_2$ generating ability of a PS is measured by its quantum yield (Φ_Δ) and is determined by three factors,[40,41] according to Equation 1.1. (i) the ability of PS molecules to undergo ISC to produce $^3PS^*$, named quantum yield of triplet formation (Φ_T), (ii) the ability of O_2 to trap $^3PS^*$ molecules, expressed by $P_T^{O_2}$, and (iii) the efficiency of energy transfer from $^3PS^*$ to O_2, $f_{T,\Delta}^{O_2}$.

$$\Phi_\Delta = \Phi_T \, x \, P_T^{O_2} \, x \, f_{T,\Delta}^{O_2} \qquad \textbf{Equation 1.1.}$$

$^1O_2$ is an elusive molecule and its detection and quantification have long been a major challenge in the field of ROS chemistry. Once produced, $^1O_2$ can undergo non-radiative decay, react oxidizing surrounding molecules or emit NIR phosphorescence, around 1275 nm. This latter is the only one direct method to detect $^1O_2$ and has become a highly valuable spectroscopic tool.[41,42] The NIR phosphorescence of $^1O_2$ is extremely weak and requires very sensitive NIR detectors, however, modern time-resolved detection systems endowed with higher sensitivity have allowed not only the confirmation of its presence but also detailed information on its formation and decay kinetics (Figure 1.4).

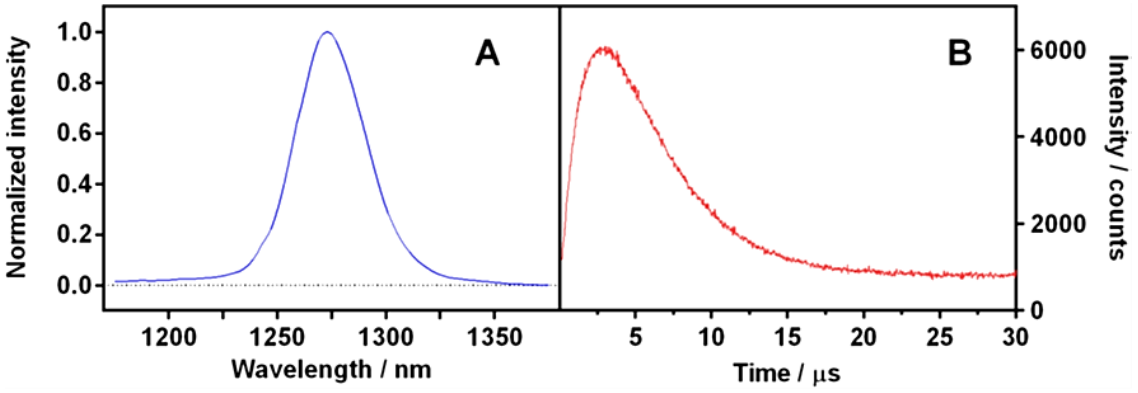

Figure 1.4. A) Near-infrared phosphorescence spectrum of $^1O_2$. B) Rise-and-decay time-resolved NIR phosphorescence signal in water. Image from Ref. 41.

Indirect detection methods are based on the high reactivity of $^1O_2$ towards organic compounds, inducing chemical transformations that can be analyzed by different techniques, such as photothermal and photoacoustic methods, electron-paramagnetic resonance (EPR), microwave spectroscopy or absorption and emission spectroscopy, among others.[32,43] In particular, spectroscopic methods have gained much attention because of their high sensitivity, simplicity in data collection, and high spatial resolution in microscopic imaging techniques.[44,45] They are typically based on chemical probes that react with $^1O_2$ yielding an oxidized product that can be detected by means of absorption or fluorescence techniques. A great variety of $^1O_2$ traps have been developed and extensively used,[46] however, there are some drawbacks regarding their specificity and cross-reactivity with other ROS that limit their broader expansion.

In biological systems, $^1O_2$ is produced by chemical, enzymatic and photosensitized reactions and it functions as a double-edged sword, ranging from cell proliferation to cell death.[47–49] For instance, low levels of $^1O_2$ and other ROS play important roles in maintaining cell homeostasis, acting as signaling messengers and also protecting our body from invading organisms.[50–53] Cells have a variety of redox regulatory mechanisms to regulate the balance between the formation and elimination of $^1O_2$ and other ROS. However, these mechanisms may not be capable of neutralizing all the ROS generated, particularly when acute levels of ROS are produced unexpectedly. $^1O_2$ is highly reactive towards different cellular components, including proteins, membrane lipids, as well as DNA and RNA and rapidly oxidizes the biomolecules in close proximity to its production site,[6,54,55] (Figure 1.5). The imbalance between the amount of ROS generation and the defensive scavenging processes produces the so-called oxidative stress processes that may cause damage to some cellular constituents leading to cell death as the ultimate consequence.

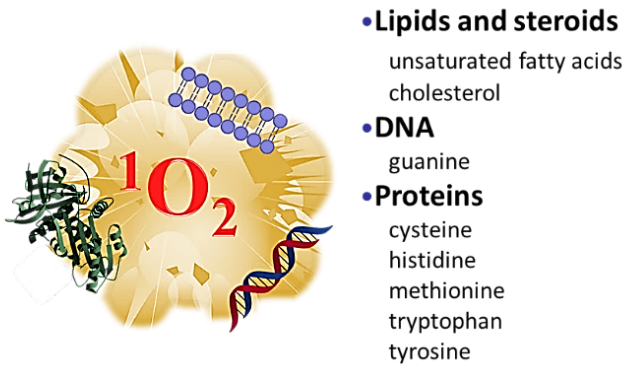

Figure 1.5. Main biological targets of $^1O_2$-induced photooxidation.

c) Molecular photosensitizers

Most of PSs used in PDT are commonly organic molecules with highly delocalized π-orbitals capable of transferring electrons or energy to O_2. A PS should ideally be a pure compound endowed with the following properties (i) efficient triplet formation (Φ_T); (ii) long triplet excited state lifetime (τ_T) to increase the probability to react with O_2 and (iii) to have a triplet excited state of appropriate energy (E_T>95 kJ·mol^{-1}) to allow for efficient energy transfer to ground state O_2.[56] Additionally, other desired properties include: (iv) high extinction coefficients (Ɛ) in the spectral region of the light excitation, ideally in the therapeutic window, (v) high photostability, (vi) water solubility, (vii) no dark toxicity and (viii) relatively rapid clearance from healthy tissues.

Typical PSs in PDT are cyclic tetrapyrroles, comprising substituted derivatives of porphyrin, chlorin, and bacteriochlorin (Figure 1.6A). Indeed, the first PS clinically approved for PDT was a porphyrin named 'hematoporphyrin derivative' or Photofrin®. However, Photofrin® is far from being an ideal PS because it is a mixture of compounds whose precise composition is not known, it has a relatively low absorbance in the red region of the spectrum and it induces long-lasting skin photosensitivity.[57] This has stimulated intense research during the last years and a palette of photosensitizing compounds have been developed, covering a broad part of the electromagnetic spectrum, from the ultraviolet (UV) with aromatic ketones to the NIR with porphyrin-like compounds and its derivatives (Figure 1.6B).

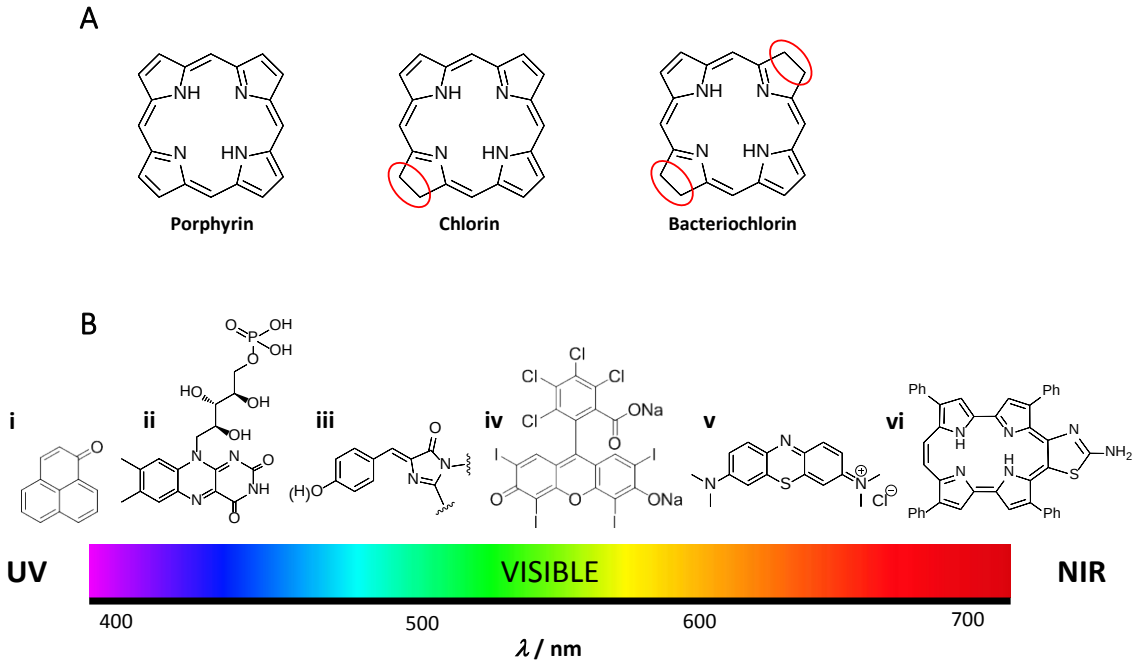

Figure 1.6. A) Chemical structures of porphyrin, chlorin and bacteriochlorin. B) Spectral diversity of selected PSs: i) Phenalenone; ii) Flavin mononucleotide; iii) Green Fluorescent Protein's chromophore; iv) Rose Bengal; v) Methylene Blue and vi) expanded Porphycene.

However, despite the considerable research effort and promising advances in the design and synthesis of novel PSs, only a relatively small number of photosensitizing drugs have received approval for clinical use so far.[58] This is due to some typical drawbacks that have long precluded their broader application in PDT. First, poor water solubility and high toxicity-inducing side effects of most organic PSs hampers its direct administration to the patient. In this regard, smart strategies in nanomedicine have been developed to deliver the PS to the target tissue by means of a carrier vehicle that also protects it from external factors.[59] Several nano-sized drug delivery systems have been engineered and including metal and ceramic nanoparticles, liposomes, micelles, proteins and dendrimers and have been successfully applied in various biological fields.[59–62]

The second major limitation lies on the difficulties to precisely control the localization of the PS in the tumor tissue. It is critical to selectively induce damage only to the malignant tissue and not to the surrounding healthy cells. However, because ROS are intrinsically non-specific, both healthy and unhealthy cells will be damaged equally if the PS is randomly distributed. Moreover, since light can diffuse through tissues, it is highly unlikely to specifically irradiate tumor cells (i.e. healthy cells in or proximal to the lesion are also irradiated). Modifications on the PS itself and/or on the nanovehicle are the most common approaches for targeting the drug to a specific location. Targeted-PDT and photoimmunotherapy (PIT) are new modalities for light therapy that have attracted much attention in the recent years because provide higher selectivity towards malignant cells.[61,63,64] They are commonly based on the functionalization of the surface of the delivery system with specific ligands that bind with high affinity to specific biomolecules that are unique or overexpressed in target cells. Frequently used ligands include antibodies and antibody fragments, proteins and peptides and small molecules such as folic acid and sugars.[65–67] However, limited reproducibility of the conjugate synthesis and the loss of activity of the antibody or the PS are still unsolved disadvantages of this approach.

Once the PS is selectively delivered to the target cells, it is fundamental, of course, that the ROS produced upon illumination induce sufficient damage to cause cell death. For this reason, PSs that generate $^1O_2$ in high yield have been typically sought as potential candidates for PDT. While producing high amounts of $^1O_2$ will undoubtedly induce some degree of cell damage, it may not be enough to kill the cells. This is due to the presence of antioxidant compounds and the activation of other defense mechanisms upon induction of oxidative stress. Interestingly, the cellular response to photodamage is strongly dependent on multiple factors of which PS localization is the key for the outcome of the treatment.[54,56,68] It is known that certain cellular organelles are more critical for the cell survival and, indeed, organelle-targeted PSs that

specifically accumulate in these hypersensitive subcellular locations have provided higher levels of photodamage.[69] Examples of targeted organelles include the cell nucleus,[70] the plasma membrane,[71] mitochondria[72,73] and lysosomes.[74] In addition, the intracellular site of photodynamic action plays a significant part in the fate of the cell. And even though photodynamic action affects many targets, three major mechanisms of cell death have been described: apoptosis, necrosis and autophagy. For instance, photodamage at mitochondria and lysosomes has been reported to induce apoptosis; photodynamic action at the ER elicits autophagy; whereas targeting to the plasma membrane induces necrosis.[3,54,75]

Of course, targeting an intracellular organelle implies that the PS have to diffuse throw the cell membrane either by passive diffusion or active uptake. However, some organic dyes are not cell permeable, which typically results in a weaker phototoxic effect (Figure 1.7). This is because the oxidative damage of proteins and fatty acids appears only at the localization site,[76,77] due to the high reactivity, short lifetime and limited diffusion of the generated ROS, as described previously. In addition, although significant improvements have been made to provide controllable photosensitization in specific organelles, these strategies still show some off-target effects from nonspecific localization. In this regard, it is recognized that the precise localization of chemical PSs are only relative and distribution in multiple subcellular sites are quite common.[78,79] More severely, mitochondria-targeted PSs have been reported to induce severe dark toxicity, probably due to the highly cationic nature of the molecules required to cross the negative potential mitochondrial membrane.[80,81] Moreover, nuclear-targeted PSs are also not favorable because of the high risk of causing genetic variation.[54,82] Therefore, selectively targeting PSs with high specificity and low potential for side effects remains an essential goal in PDT-associated cancer therapy.[79]

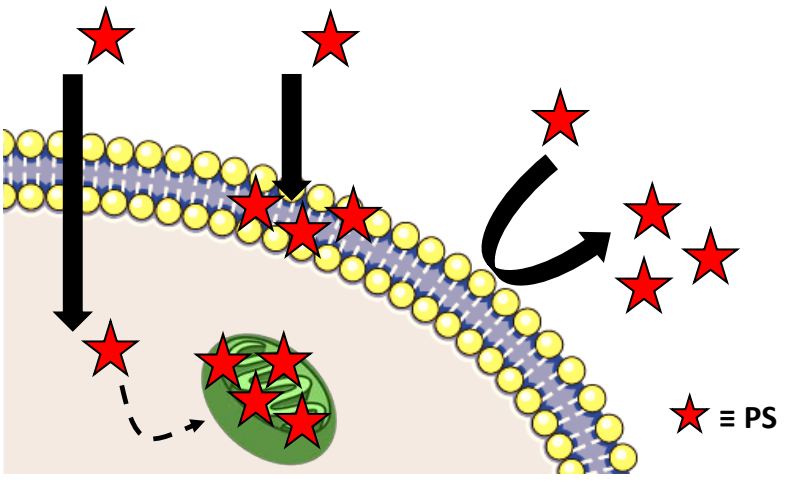

Figure 1.7. Schematic representation of the interactions between PS molecules and cell membrane. PSs capable of crossing the lipid bilayer can be targeted to specific organelles such as mitochondria to induce higher photodamage.

1.4. Antimicrobial photodynamic therapy

Over the last decades, infectious diseases have become a global threat, causing about 17 million annual deaths.[83] The rise in the malignancy of pathogenic infections is commonly attributed to the appearance of new diseases as well as to the re-emergence of infections previously controlled. Moreover, the excessive or inappropriate prescription of antibiotics and the failure of some patients to complete their treatment regimens have contributed significantly to a worldwide inexorable growth of multi-drug resistant bacteria. The situation has reached a global emergency limit and it is finally acknowledged by all the leading health organizations and governments that the currently available antibiotics will no longer be effective against certain pathogens. In this line, a report from 2014[84] garnered much attention when it delivered the alarming forecast that by 2050, 10 million more people would be expected to die every year if resistance was kept to today's level, that is, more than 300 million premature deaths, and an estimated cost of 100 trillion USD to the world economy. It is absolutely and urgently needed to develop new methodologies for the treatment of infectious diseases.[85,86]

The antimicrobial properties of the light therapy were first reported at the beginning of the twentieth century, however, their potential has been largely unappreciated. Now, at the end of the antibiotic era, antimicrobial photodynamic therapy (aPDT) (also named photodynamic inactivation, PDI) emerges as a safe, easy to implement and up-and-coming alternative to treat localized infections[87] (Figure 1.8).

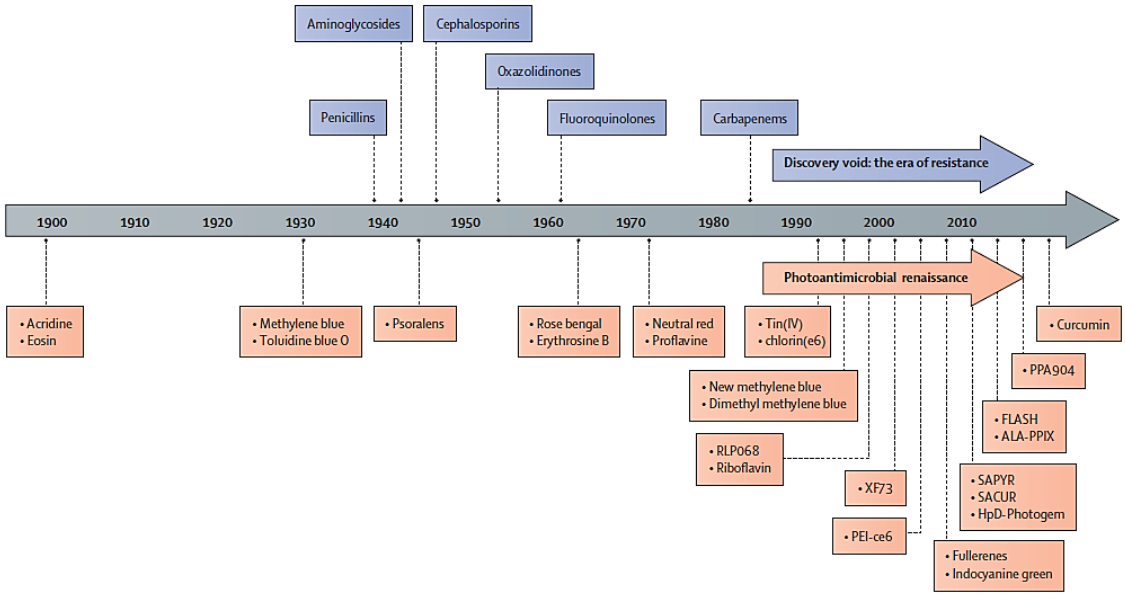

Figure 1.8. Timeline for conventional and photoantimicrobial discovery. Image from Ref. 88.

Likewise for PDT of cancer, aPDT relies on the combination of light, O_2 and a PS. Again, the non-specificity of the ROS simultaneously attack various biomolecular targets offering both multiple and variable sites of action. The locally and rapid oxidation of cellular compounds provides two tremendous advantages as compared to conventional chemical antibiotics. First, aPDT is a broad-spectrum therapy which has been proven effective against different families of microbial pathogens,[89] including bacteria, virus, fungi and other parasites, while antibiotics are only effective towards bacterial infections (Figure 1.9). Moreover, the photodynamic action exerts its killing effects much more rapidly than conventional agents that might take hours or days to become active, even against susceptible strains. Secondly, the multi-target approach also circumvents conventional mechanisms of resistance and inhibits the development of resistance to the agents.[88] The high and non-specific reactivity of ROS prevents bacteria to react adequately by overexpression of a protective protein shield. For this reason, aPDT has long been believed to completely avoid any resistance, however, recent works have already reported initial signs of defending mechanism after the treatment.[90,91]

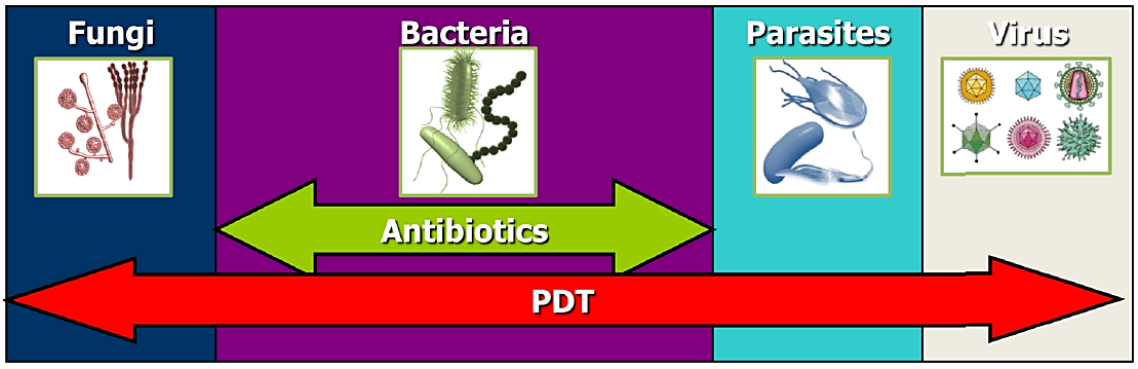

Figure 1.9. Broad-spectrum treatment of localized infections with aPDT, contrarily to the limited use of antibiotics. Image from Ref. 89.

Most of the PSs described for PDT have also been employed for performing aPDT. Novel PSs are smartly designed so they selectively bind to microbial cells, while not binding to host mammalian cells.[92] This is generally achieved by using cationic PSs, taking advantage of the negative charges that are present in the cell envelope of many microorganisms (i.e Gram-negative bacteria). In addition, the binding of the PS to the microbial cells is relatively rapid, while uptake of the cationic PS by mammalian cells is slow.[89,93] Although less specific, neutral or anionic PSs are also employed for aPDT as they bind efficiently to the cytoplasmic membrane of Gram-positive bacteria, which is surrounded by a relatively porous peptidoglycan layer that allows PS to cross. There are no particular target structures (e.g. enzymes, chromosomes, ribosomes) in aPDT, however, as described previously, the efficiency of the treatment strongly

depends on the localization of the PS, being much more phototoxic when found within the cell membrane or inside the cell that when it remains dissolved in the external media. Therefore, the biochemical composition of cell walls plays an essential role in the inactivation of bacteria and it frequently limits the use of certain PSs. For instance, there are several examples of anionic PSs that killed Gram-positive bacteria but did not inactivate Gram-negative cells.[94–96]

Although new and improved PSs are being synthesized and reported, exogenously applied dyes have several intrinsic limitations as PS, including their poor water solubility, selectivity and restricted membrane permeability. Furthermore, identification of the sites of binding of the photosensitizing molecules in bacteria is a complicated issue to address with conventional microscopy due to the limit of resolution.[97,98] This type of information is generally retrieved from indirect experimental evidence, based on the efficiency of cell inactivation, photophysical measurements, and laborious analysis of cell damage products. Methods for direct observation of the drug localization to verify its internalization are highly desired but not widely available yet for routine spectroscopic techniques. Therefore, alternative PSs with exclusively selectivity towards bacteria, improved cell permeability and novel approaches to ensure their internal localization and higher cell-killing efficiency still need to be developed.

1.5. Genetically-encoded photosensitizers as biological drugs

Despite significant efforts have been made and smart approaches have been designed to address the main limitations of conventional and currently available PSs both for cancer and antimicrobial PDT, these drawbacks are still a real and unresolved problem that precludes their widespread use. Unfortunately, some of these limitations seem to be intrinsic and irretrievably linked to all externally-administered PSs. For this reason, research attention has focused on light-active endogenous compounds that are already present in biological systems in order to find potential PSs. There is a variety of natural-occurring chromophores, including amino acids, flavins, bilirubin or porphyrins in the human body.[99,100] Although these compounds are reported to induce photodamage in the long term (e.g., photoaging),[100] they are not particularly efficient PSs due to deactivation processes that occur when they are bound to other biomolecules. Therefore, direct excitation of purely endogenous chromophores does not provide a feasible alternative for PDT applications and other roads have been explored.

A major approach relies on the ability to alter the cell function and behavior by means of genetic manipulation, which has led to considerable advances in cell biology.[101] However, classical genetic approaches (including overexpression, RNA interference (RANi) and

knockdown/knockouts) typically offer little control over spatial or temporal variation in a target pathway, and cannot be applied during development or house-keeping genes in general.[102,103] On the other hand, the use of light to induce biological transformations offers unprecedented precision for the study of cell events in time and in space and has opened up a new window for a different range of applications in the biomedical field. The use of light to control cells in living tissue, which has been genetically modified to express light-sensitive biomolecules, has yielded a brand new field named optogenetics.[104] Early strategies to optically control processes involved signaling molecule analogs that could be specifically caged or uncaged in response to light. Later on, the discovery of light-responsive proteins in the eye, plants, fungi, jellyfish, coral, bacteria, and algae provided an excellent platform for developing novel systems that could be genetically encoded. The modern optogenetic toolbox includes fluorescent sensors to visualize signaling events in living cells and optogenetic entities enabling manipulation of numerous cellular activities with single-cell resolution in a light-dependent manner.[105]

The use of genetically encoded actuators for photosensitizing purposes was initially explored as selective targeting entities, and three main tagging approaches have been developed: (1) Small genetic tags encoding tetracysteine motifs (Cys-Cys-Xaa-Xaa-Cys-Cys) were demonstrated to non-covalently bind with high affinity and specificity biarsenical PSs.[106–108] These dyes are membrane-permeant and non-fluorescent in solution; however, they become fluorescent and generate modest amounts of $^1O_2$ upon binding to the motif. Nevertheless, this approach did not completely solve the issue of nonspecific localization, required antidotes to prevent cell toxicity, needed careful precautions to reduce nonspecific background signal and have been difficult to apply to multicellular tissues and organisms.[109,110] (2) A similar strategy was the SNAP-tag system.[111] Covalent labeling with a small molecule is achieved through the mammalian O^6-alkylguanine-DNA-alkyltransferase (hAGT), which is irreversibly labeled using O^6-benzylguanine derivatives that can be conjugated with organic dyes.[112] Compared to the tetracysteine tag, SNAP-tag allows highly specific labeling without restrictions on the cellular compartment and without the need for additional reagents to suppress background.[113] Further developments yielded CLIP-tag,[114] which reacts specifically with O^2-benzylcytosine derivatives. Because SNAP-tag and CLIP-tag possess orthogonal substrate specificities, SNAP and CLIP fusion proteins can be labeled simultaneously and specifically with different molecular probes in living cells. (3) A third approach, named HALO-tag[115] was developed from a modified prokaryotic dehalogenase (DhaA). It reacts irreversibly and specifically with primary alkyl halides, that can also be conjugated with chemical probes or PSs. However, all these cell-based fluorescence imaging or photosensitizing methods that rely on organic dyes typically suffer from cytotoxicity, poor cell

permeability, and high levels of background fluorescence arising from the need to remove the excess of unlabeled dye.[110]

Another example whereby an exogenous ligand binds to a genetically engineered protein has been recently reported.[116] In this approach, the authors designed a genetically encoded fluorogen-activating protein that binds an iodinated version of malachite green which absorbs NIR light. The dye is non-fluorescent and non-photosensitizing when dissolved in solution, however, the binding to the protein suppresses the non-radiative relaxation and *activates* the PS.

However, all these strategies that have introduced genetic approaches are still based on molecular PSs that need to be externally-administered. The real revolution in cell biology and optogenetics came with the discovery, expression and development of the Green Fluorescent Protein (GFP), which was awarded the Chemistry Nobel Prize in 2008.[117,118] Since then, GFP-like proteins have been of general use to visualize and keep track of relevant processes in living cells and whole organisms.[119,120] Over the last years, new fluorescent proteins (FPs) with novel characteristics and enhanced optical properties have been developed.[121] The diversity of currently available FPs covers nearly the entire visible spectrum and part of the NIR, providing numerous alternative possibilities for multicolor labeling of cellular structures and studies of protein interaction.[118]

It was soon realized that FPs could be used for purposes other than visualizing cellular events. The ability to report bioprocesses in real time has attracted much attention and over 100 different genetically encoded reporters have been engineered insofar and successfully used in a broad range of applications and targets, as diverse as ions, molecules and enzymes, providing unprecedented insight into the inner workings of a cell.[122–125] In parallel, engineering a genetically encoded PSs has been long pursued as a valuable tool for mechanistic intracellular studies (e.g., chromophore-assisted light inactivation of proteins, CALI),[126–128] for advanced microscopy techniques (e.g., correlative light and electron microscopy (CLEM)[129] and as a promising alternative to exogenous PSs for therapeutic applications (e.g., PDT).[130] In this approach, is no longer a molecular PS but a biological PS, which is delivered to the cell by means of a DNA fragment and, therefore, the very target cell becomes the generator of the photoactive agent. Of note, biological PSs are produced without the addition of any exogenous cofactor, which circumvents typical problems for externally administered PSs. Moreover, they can be fused to specific targeting sequences (e.g. leader peptides or antibodies) to selectively direct the recombinant protein to particular cellular structures, compartments or cell types of interest with

much higher precision than counterpart drugs that are exogenous-administered. Therefore, the use of proteins as fully genetically encoded PSs is currently the best possible approach for controlling the intracellular localization of the PSs and the $^1O_2$ generation site with exquisite and unprecedented spatiotemporal resolution. On the other hand, biological PSs are intrinsically much more complex systems and therefore new difficulties may arise when it comes to their production, handling and their characterization.

In the last decade, two major families of proteins as biological PSs have been developed. The first family encompasses fluorescent proteins of GFP family,[130–133] whereas the second uses flavin-binding fluorescent proteins (FbFPs) that are derived from natural blue light photoreceptor domains[134–136] (Figure 1.10).

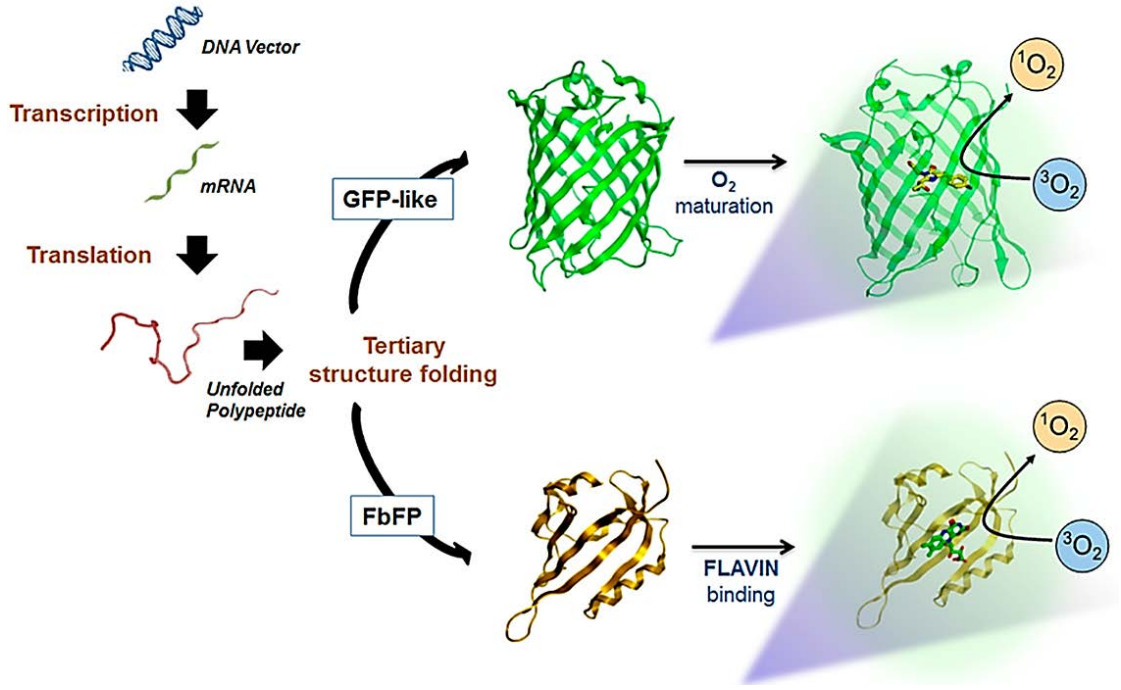

Figure 1.10. Genetic production of FPs derived from the GFP family and FbFPs. Image from Ref. 137.

1.5.1. Green Fluorescent Proteins

GFP is a fluorescent protein naturally present in *Aequorea 19ictoria* jellyfish.[117,118] It is formed by 238 amino acids arranged in an eleven-stranded β-barrel (one large β-sheet) and an α-helix penetrating through the cylinder that hosts a chromophore approximately in the middle of the cavity. The GFP chromophore, 4-hydroxybenzylidene-1,2-dimethylimidazoline (HBDI), is produced by autocatalytic cyclization of a tripeptide, typically serine, tyrosine and glycine (Ser65–Tyr66–Gly67) in a multistage maturation process that requires the presence of O_2[138,139] (Figure 1.11).

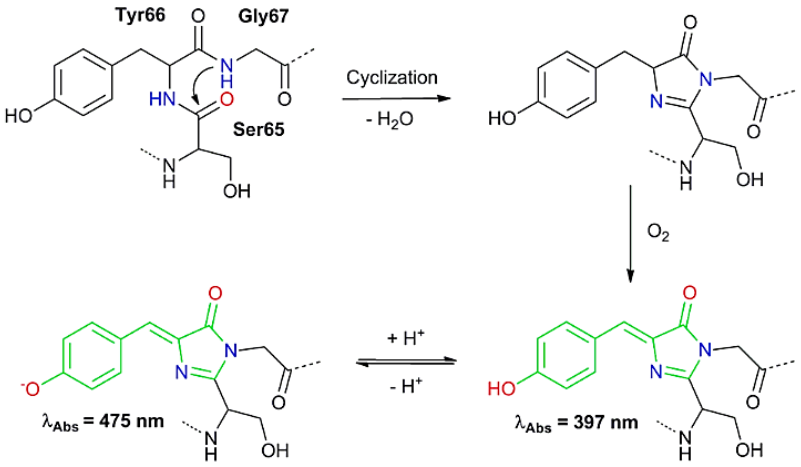

Figure 1.11. Proposed mechanism of autocatalytic formation of the GFP chromophore.

First attempts to use proteins as $^1O_2$ generators focused their attention on GFP. Early studies reported that GFP could inactivate proteins specifically upon illumination, yet the efficiency was very small.[126] Later experiments revealed that GFP photobleaching was partially linked to oxygenation processes derived from self-generated $^1O_2$ production upon illumination.[131,140] The potential application of this effect was recognized for mechanistic studies and the Enhanced Green Fluorescent Protein[141,142] (EGFP; Figure 1.12A) was shown to be a valuable agent for CALI.[143,144] In 2008, the production of $^1O_2$ by EGFP was unequivocally demonstrated through the direct detection of $^1O_2$ NIR phosphorescence at 1275 nm.[132] The Φ_Δ could not be quantified but its HDBI chromophore produced $^1O_2$ with yield Φ_Δ= 0.004.[132] The low efficiency in ROS production was reasoned by the hindered chromophore's accessibility to O_2,[133] even though the oxidative maturation of the chromophore inside the GFP demonstrates that O_2 can indeed diffuse through the protein. In addition, those results suggested $^1O_2$ quenching by the protein, which would also detract from its ability to release $^1O_2$ to the external medium. Two additional mutants, namely GFPmut2 and GFPmut2 H148G, were prepared in an attempt to alleviate such problems, although with modest results.[133]

A real breakthrough was the development of the red FP KillerRed derived from the *Hydrozoan* chromoprotein anm2CP,[130] as the first FP designed *de novo* specifically to act as an endogenous PS. Its photosensitizing ability has been extensively studied in cell cultures and other biological systems[130,145–149] However, the main ROS produced by KillerRed is not $^1O_2$ but $O_2^{\bullet-}$ and H_2O_2, formed via Type-I processes.[146,150–152] Both theoretical and experimental structural studies have been conducted in attempts to rationalize the photosensitization ability of KillerRed, concluding that it has a unique water-filled channel reaching the chromophore

through which O_2 can readily diffuse and may therefore be responsible for its prominent phototoxic nature over the original GFP.[150,153,154] KillerRed has been fused to several organelle-targeted sequences and used as an optogenetic tool in different cell lines and organisms.[78] However, the fact that KillerRed is a dimeric protein (Figure 1.12B) causes mistargeting and aggregation of fused constructs, hindering or even precluding its use as a fusion tag.[155]

Many efforts have been devoted to overcoming this problem, not only found in KillerRed but also in all naturally FPs with emission maxima above 550 nm discovered so far.[156] In 2007, Merzlyak *et* al. developed TagRFP,[156] a bright red monomeric protein derived from the *Entacmaea quadricolor* FP TurboRFP (Figure 1.12C). Interestingly, its photobleaching and photoconversion rates showed a sharp oxygen dependence,[157] which suggested higher oxygen accessibility to the chromophore and the alleged participation of self-sensitized ROS. This hypothesis was confirmed experimentally by direct detection of its $^1O_2$ production, obtaining a Φ_Δ = 0.004.[158] In addition, it was later demonstrated that TagRFP was capable of killing *E. coli* bacteria by endogenously-generated $^1O_2$ upon green light irradiation.[159] Surprisingly, TagRFP lacks the water channel connecting the chromophore with the bulk solvent observer for KillerRed. It was proposed that diffusion of $^1O_2$ could be facilitated by the presence of temporal permeable gates in the protein due to dynamical breathing,[158] as reported for other GFP-like proteins. The development of other monomeric mutants yielded the so-called mFruits (e.g. mOrange, mCherry, mPlum, etc.), however, most of them suffered from low brightness[119] and were less able to photoinactivate bacteria than TagRFP.[160] The latest developments in the GFP arena are proteins engineered from KillerRed, called KillerOrange[161] (Figure 1.12D) and SuperNova[162] (Figure 1.12E). The former is a dimeric and blue-shifted protein as compared to the parental KillerRed that has been expressed in bacterial and mammalian cells and has exhibited cell damage upon blue and green light irradiation. However, the mechanism and the ROS involved in KillerOrange phototoxicity remains unknown. Supernova is spectrally similar to its precursor and retains the ability to generate ROS. Most importantly, unlike KillerRed, Supernova is monomeric and it allows the proper protein expression and localization without perturbing the normal function of the target protein.[162]

(Note: As this thesis was going through revision and printing, a new photosensitizing protein was reported, named SuperNova Green,[163] which emits green light and produces ROS other than $^1O_2$, and induces photo-inducible protein inactivation and cell ablation).

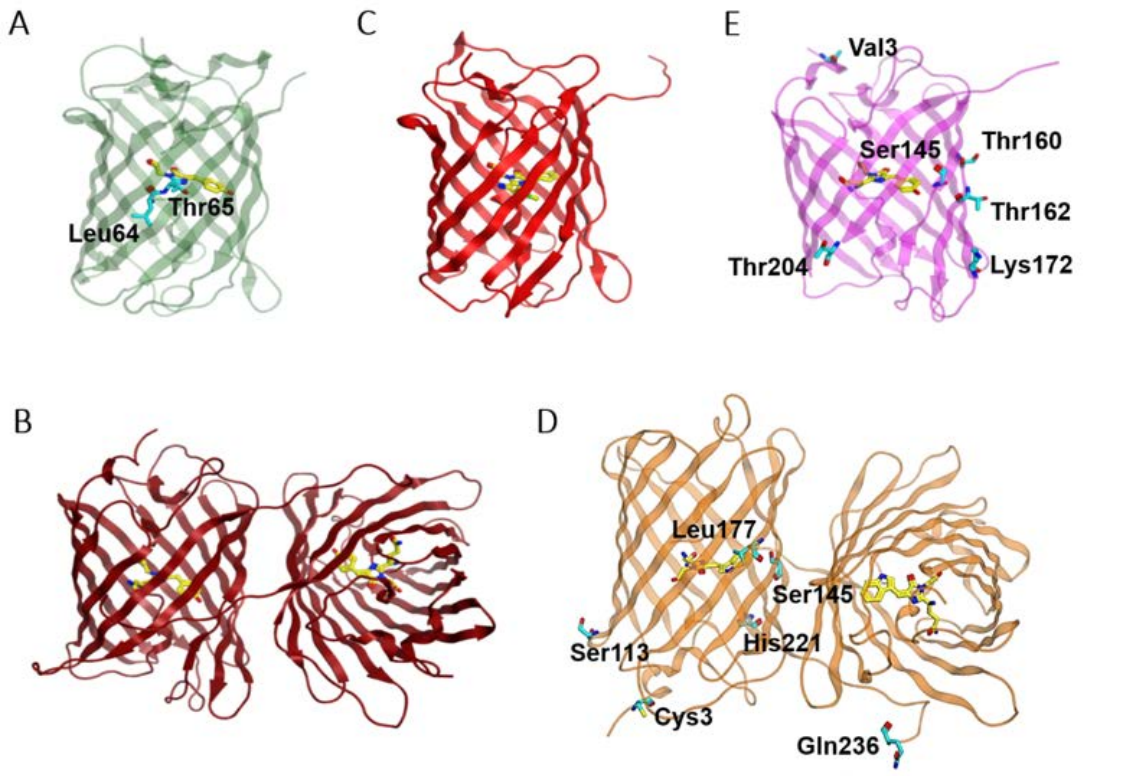

Figure 1.12. Protein structure of GFP-like photosensitizing proteins. A: EGFP structure. Mutations made from GFP are highlighted. (PDB ID: 2Y0G); (B) KillerRed structure (PDB ID: 3GB3); (C) TagRFP structure (PDB ID: 3M22); (D) KillerOrange structure. Mutations from KillerRed are highlighted on the left monomer PDB ID: 4ZFS) and e) SuperNova structure. Mutations made from KillerRed are highlighted. (PDB ID: 3WCK).

1.5.2. Flavin-binding Fluorescent Proteins

Flavoprotein is the term referring to proteins harboring riboflavin (RF, vitamin B2) or its derivatives as prosthetic group. This family of compounds is involved in a wide array of biological processes, including photosynthesis, DNA repair and bioluminescence among others.[164–166] Due to their importance for versatile and essential biochemical reactions in most organisms, the potential of flavoproteins as targets of pharmacological treatment is immense.[167] On the other hand, their photophysical properties have also been exploited as a source of FPs, biosensors, and optogenetic tools.[135,168]

Flavins are ubiquitous molecules based upon the nitrogen heterocycle 7,8-dimethyl isoalloxazine, present in living systems and performing essential biological functions such as mitochondrial electron transport, fatty acid oxidation, and vitamin metabolism.[169] Flavins are broadly distributed in tissues, but little is present as free molecules in solution. The majority is found in flavoproteins, mainly as flavin adenine dinucleotide (FAD), and in lesser amounts as flavin mononucleotide (FMN), which are generated from RF. The chemical structures of flavins

are shown in Figure 1.13. RF can be synthesized *de novo* by plants, many bacteria and fungi, but not by animals, which must therefore obtain it from dietary sources.[170]

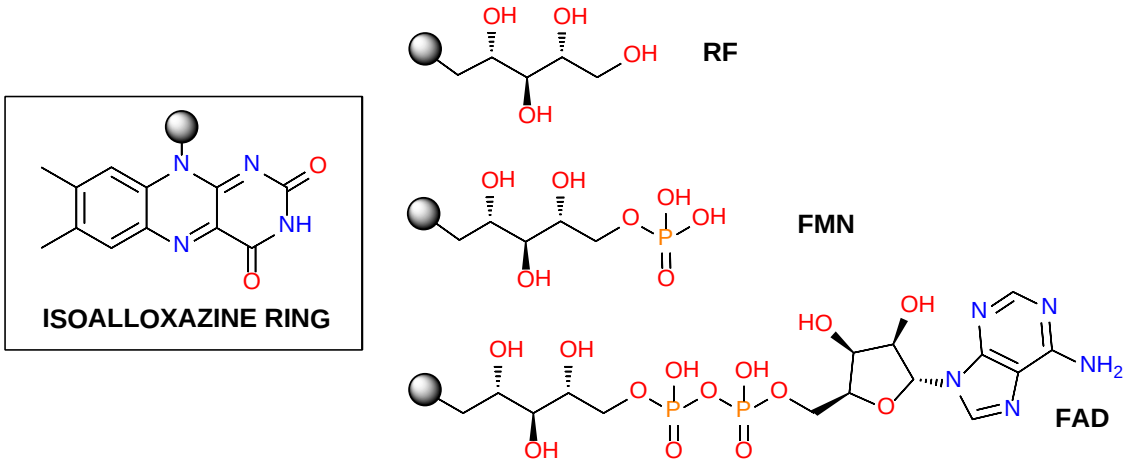

Figure 1.13. Chemical structures of flavin chromophores in flavoproteins.

The general properties of flavins in free solution and when bound to flavoproteins have been the subject of intense research over the past 50 years.[171–173] The high chemical versatility of flavins and particularly, their rich photochemistry has extensively been exploited in catalysis, synthesis and as redox partners in one-electron and two-electron transfer processes.[169] In solution, flavins in their neutral and oxidized form exhibit strong absorption in the UV and visible region, with four peaks around 445, 375, 265 and 220 nm.[174] All the absorption maxima possess high-molar absorptivities ($\varepsilon > 10^4$ M^{-1} cm^{-1}), indicative of π-π* transitions. Most flavins fluoresce in the long-blue to the green part of the spectrum with moderate fluorescence quantum yield ($\Phi_F = 0.2 - 0.3$).[172] In addition, ISC populates efficiently the triplet excited state ($\Phi_T = 0.5 - 0.7$),[172] which in turn is reflected in relatively high yields of $^1O_2$ production ($\Phi_\Delta = 0.51$).[175]

In nature, three major classes of flavoprotein light sensors, namely Light, Oxygen and Voltage (LOV) domains, blue light sensor using FAD (BLUF) proteins and cryptochromes (CRYs), regulate diverse biological activities in response to blue light.[176] In each of those families, photoreceptor proteins undergo distinct photochemical reactions upon blue light exposure, which are mainly linked to conformational changes in the protein, and allowing for blue light-dependent physiological responses of the respective host.[177] The biological role of flavoproteins has been extensively studied and it has been found to participate regulating in a myriad of different processes, including light phototropism, cell and organelle motility, regulation of photosynthesis, stress responses, organismal development and entrainment of circadian rhythms.[166,178–181]

In flavoproteins from the LOV domain, the flavin chromophore is tightly and noncovalently bound in the active pocket. Absorption of blue light by the FMN chromophore results in the formation of a thiol adduct between the C(4a) position of the isoalloxazine ring of FMN and a conserved cysteine (Cys) residue within the protein.[182] In the darkness, this reaction thermally goes in the reversible direction within a few seconds to hours or even days, depending on the specific environment[177] (Figure 1.14).

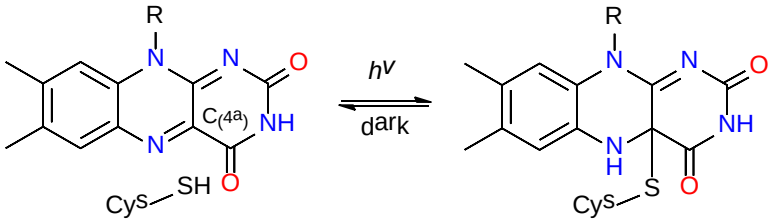

Figure 1.14. Upon blue light absorption, a covalent flavin-cysteine adduct is formed which recovers back thermally in the dark.

The flavin chromophore bestows the LOV domain a weak intrinsic green fluorescence, however, because the formation of the cystenyl photoadduct is very fast, quenching of the triplet excited state by O_2 cannot efficiently compete.[136] Therefore, in order to engineer fluorescent variants of the LOV proteins, the photoadduct was abolished through mutation of the active cysteine residue to alanine (Ala).[183] The Cys to Ala mutation indeed prevented the formation of the covalent adduct, thereby opening a molecular framework to engineer flavin-binding fluorescent proteins (FbFPs). Since then, several fluorescent flavoproteins have been developed and used as fluorescent reporters for the study of bioprocesses in bacterial and mammalian cells. FbFPs have gained much attention in the recent years because they address some of the limitations associated with the counterparts derived from the GFP.[184] Firstly, their smaller size (12 kDa, less than half the size of GFP) and rapid maturation time is a key advantage to study intact tissues and the function of specific proteins without significant perturbations. Secondly, they do not need O_2 to develop the chromophore, which is particularly convenient for the study of biological processes that operate under conditions of hypoxia.[183] Finally, FbFPs are stable over a wider range of pH and temperature as compared to GFPs. On the other hand, LOV-based FPs engineered thus far exhibit lower brightness and photostability than GFPs, which has stimulated a continuous development of improved variants.[185–187]

It was not until 2011 that the photosensitizing properties of FbFPs were explored. The first LOV-based PS was miniSOG[129] (for mini Singlet Oxygen Generator), a 106 residue monomeric protein engineered from the LOV2 domain of *Arabidopsis thaliana* (Figure 1.15). MiniSOG was

developed rationally aiming at preserving the innate FMN capacity of $^1O_2$ generation. This could be achieved by replacing, among other mutations, the conserved cysteine residue into glycine (instead of alanine) to abolish the formation of the photoadduct and giving more space for O_2 to arrive closely to FMN.[129] MiniSOG absorbs blue light and fluoresces with a maximum around 495 nm, which is slightly blue-shifted as compared to the free flavin chromophore. MiniSOG was initially reported to exhibit a Φ_Δ value of 0.47,[129] which was obtained by ROS-oxidation of a chemical trap. This value was later reassessed as Φ_Δ = 0.03 by both direct $^1O_2$ phosphorescence detection and indirect methods.[188,189] Although relatively low compared to organic PSs, this value was at the time a record for a fully genetically encoded PS.

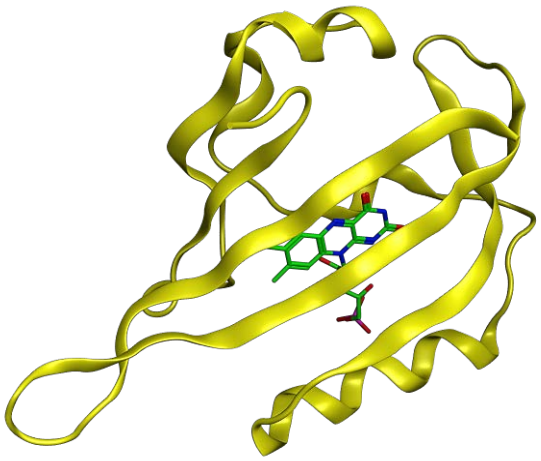

Figure 1.15. Modeled miniSOG encasing the FMN chromophore. Based on the structure of a LOV2 flavoprotein (PDB ID: 4EET).

MiniSOG was originally developed for photooxidation-based CLEM.[129] This method relies on the local polymerization of 3,3'-diaminobenzidine (DAB) by a PS to form an insoluble osmiophilic polymer, which provides contrast in EM after staining with osmium tetroxide.[190–192] This reaction can also be initiated by a genetically encoded peroxidase and hydrogen peroxide, but the short lifetime and diffusion length of $^1O_2$ result in a much improved spatial resolution. Indeed, exquisite protein localization and 3D reconstruction of complex protein structures within persevered subcellular organelles have been obtained with high resolution (8–10 nm) using miniSOG as a genetically encoded tag.[193–195] For instance, CLEM using miniSOG has made progress in understanding the role of α-synuclein accumulation in neurons affected by Parkinson's disease.

MiniSOG has also been used in another fluorescence imaging modality called "singlet oxygen triplet energy transfer-based" (STET) imaging.[196] STET relies on the ability of $^1O_2$ to diffuse tens of nanometers away from its generation site and react at relatively remote sites. Therefore, STET

extends the range of conventional "molecular rulers" such as FRET (Förster resonance energy transfer), which typically allow a detection range below 10 nm, and is thus particularly useful to study processes and structures of large protein complexes. In STET, two different proteins, which are expected to form a protein complex in a particular cellular process, are separately fused to a PS and a $^1O_2$ fluorescent sensor, both genetically encoded. Irradiation of the PS generates $^1O_2$ that diffuses until it encounters and reacts with the sensor. The enhancement of the sensor fluorescence directly depends on the distance at which $^1O_2$ is generated (i.e., the closer the two proteins are, the higher the amount of $^1O_2$ that reaches the sensor).

Aside from CLEM, miniSOG has been widely used as a powerful optogenetic tool, with major contributions in the field of neuroscience.[105,197] Despite its modest production of $^1O_2$, successful examples in photo-induced cell ablation in *Caenorhabditis elegans* and *Drosophila melanogaster*[198–200] as well as photokilling of cancer cells[201,202] have been reported. MiniSOG, as a fully genetically encoded PS, has been fused to specific proteins and expressed at different subcellular localizations, confirming the superior phototoxicity when critical organelles are selectively damaged. For example, It has been demonstrated that cytosolic expression is not particularly toxic whereas targeting to mitochondria and cell membrane yields more cell death.[134] Furthermore, miniSOG has also been fused to antibodies for the precise targeting of tumor cells. The applicability of the immunophotosensitizer strategy has already been demonstrated for the selective photokilling of cancer cells,[202,203] however, it requires the external administration of the conjugate and it therefore deviates from the fully genetically encoded approach.

A novel alternative has been recently proposed by Shramova and co-workers.[204] In this study, the authors fused miniSOG to a luciferase named NanoLuc, which emits blue bioluminescence upon oxidation of its substrate fumarimazine. Interestingly, miniSOG is excited by NanoLuc by means of a bioluminescence energy transfer process (BRET) and is capable of inducing cell death in a stably transfected cell line. This approach may circumvent the main limitation of light delivery to certain organs or thick tissues. However, it still suffers from the need to add the substrate exogenously.

Extensive progress has been made since the first report of miniSOG and better mutants and novel applications are continuously emerging. Nevertheless, a full understanding of miniSOG is still lacking and there are fundamental questions that remain unresolved, strongly limiting further improvements for miniSOG, and by extension, for other flavoproteins considered for photosensitizing applications. For example, the crystal structure of miniSOG has not been solved

and all the mechanistic and rational design studies performed so far have been based on artificially modeled structures of a parental protein. Moreover, the factors that dramatically reduce the Φ_Δ of FMN encased in miniSOG as compared to the value for free flavin in solution have not been rationalized. Finally, other photoprocesses such as the 10-fold enhancement in the Φ_Δ value upon photolysis of miniSOG observed by Ruiz-González and co-workers[188] also remains unexplained. Therefore, there are still new lessons to be learned and there is much room for improvement in the miniSOG's and other FbFP's photochemistry.

The growing interest in photosensitizing fluorescent proteins is quickly expanding its potential and uses for the other applications. In addition to cell damaging purposes and advanced imaging techniques, the fluorescent properties of miniSOG and other genetically encoded PSs have found a niche in the cutting-edge field of theranostics.[205,206] This concept is coined from the combination of therapy and diagnosis from a single agent. Theranostics allow the simultaneous specific diagnosis of the tumor location and its selective destruction which is of particular interests in surgery. In a typical surgical procedure, the surgeon, aided with computed tomography and magnetic resonance images recorded before the surgery, removes all the malignant tissue and sends it to the pathologist for analysis.[207] The standard pathology report takes typically several days to be obtained, while the patient is recovering from the operation. If the pathologic report indicates the presence of positive tumor margins, then the patient is often asked to go through another surgical procedure, which is neither convenient nor practical.[207] Fluorescence image-guided surgery in combination with PDT provides intra-operative tools for both finely differentiate the tumor margins in real time and selectively kill any remaining malignant cell that has not been extirpated (Figure 1.16).

The use of miniSOG and other FPs as genetically encoded PSs has therefore great potential also for theranostic applications. The combination of their fluorescence and photosensitizing properties with their superior targeting capacity to different types of cells or specific organelles is currently emerging as a powerful, safe and feasible tool for modern medicine and surgery.

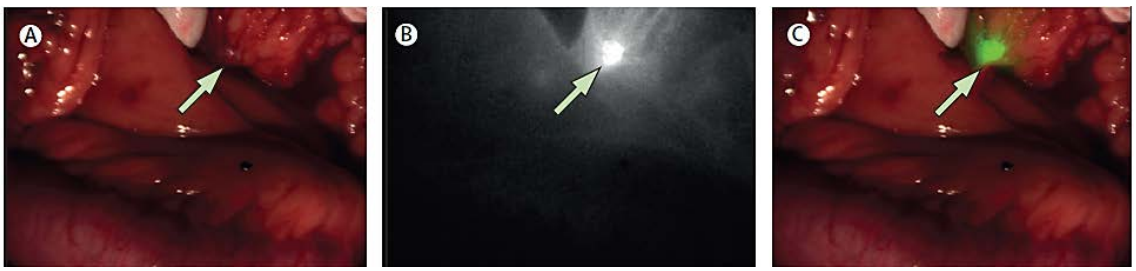

Figure 1.16. A real case of intraoperative imaging by A) white light imaging and B) molecular fluorescence-guided surgery. C) overlay images. Adapted from Ref. 208.

1.6. Photodynamic therapy of melanoma skin cancer

Malignant melanoma is a type of cancer that arises from melanocytes, the primary cells responsible for the production of melanin which is the pigment that protects the skin from sun damage by absorbing UV light.[209,210] Although melanoma is less common than some other types of skin cancer (it accounts for only 4% of skin cancer cases), it causes 79% of all skin cancer-related deaths.[211] Melanoma can be classified into three categories: cutaneous melanoma (91.2%), ocular melanoma, also known as uveal melanoma or choroidal melanoma (5.3%), and mucosal melanoma (1.3%).[212,213] Melanomas are also classified in relation to melanin content. Most types of melanomas are melanotic, containing various degrees and types of pigmentation; however, any clinical subtype of primary cutaneous melanoma or metastatic melanoma may be amelanotic, presenting the absence of pigmentation in the tumor. Amelanotic melanoma represents 1.8-8.1% of all such tumors.[214]

The incidence of melanoma has been continuously increasing over the past decades, to the point that it has been claimed that there has been an epidemic of melanoma in white populations worldwide. Melanoma is currently being diagnosed at more than double the rate it was in 1986, increasing faster than any other major cancer. If diagnosed early, surgery and adjuvant therapy enable improved outcomes in thin lesions, however, melanoma is barely responsive towards current therapies in the majority of cases and the prognosis is generally poor once metastases occur.[210,215] Furthermore, the rapid increase in malignant melanoma incidence has not been paralleled by the development new and improved chemotherapeutic drugs suitable for the conventional treatments.[216]

Novel strategies for treatment of melanoma such as immunotherapy, gene therapy, and molecularly-targeted therapy have been developed.[213,217,218] In this regard, PDT could be applied as an alternative treatment alone or in combination with current therapeutics to combat melanoma,[219] however, its successful application remains one of the main challenges in the area. More severely, melanoma has generally been considered to be resistant to PDT.[24] Resistance is due to several, highly active mechanisms, including defects in the apoptotic pathways, pigmentation, PS sequestration inside melanosomes, efflux of PS by multi-drug transporters and increased oxidative stress defense.[211,220] Various approaches to overcome this PDT resistance are being evaluated such as the use of agents that overcome the apoptotic defects, hinder the efflux of PS, or the use of methods to reduce the quantity or the pigmentation of the melanin.[24,220] These strategies in combination with the development of more efficient PSs are

showing encouraging results of the efficacy of PDT in melanoma,[221–223] however there are still some limitations unsolved regarding selectivity and cellular uptake.[224]

Genetically encoded PSs may therefore offer a working alternative to conventional PSs owing to the superior targeting potential conferred by the genetic control of cell expression and precise targeting and damaging of crucial organelles for cell viability.

1.7. Objectives

The main goal of this thesis is to explore the potential of flavoproteins as genetically encoded photosensitizers $^1O_2$ for PDT and aPDT. MiniSOG, the most renowned photosensitizing flavoprotein is studied in detail to understand its photosensitization mechanisms, which may help in the design and development of improved mutants. This primary goal is further set to the following specific objectives:

- Characterization of the photophysical, photosensitizing and antimicrobial properties of novel flavin-binding fluorescent proteins.
- Study of the singlet oxygen photosensitization processes in miniSOG. Analysis of the factors the limit its ability to produce singlet oxygen and the phototransformations that it undergoes upon photolysis.
- Study of the potential of flavin-binding fluorescent proteins for imaging and optogenetic applications. Expression of miniSOG in mammalian cells and evaluation of its ability for the photodynamic therapy of melanoma.

1.8. References

(1) Dolmans, D. E. J. G. J.; Fukumura, D.; Jain, R. K. Photodynamic Therapy for Cancer. *Nat Rev Cancer* **2003**, *3* (5), 380–387.

(2) Daniell, M. D.; Hill, J. S. A History of Photodynamic Therapy. *Aust. N. Z. J. Surg.* **1991**, *61* (5), 340–348.

(3) Agostinis, P.; Berg, K.; Cengel, K. A.; Foster, T. H.; Girotti, A. W.; Gollnick, S. O.; Hahn, S. M.; Hamblin, M. R.; Juzeniene, A.; Kessel, D.; et al. Photodynamic Therapy of Cancer: An Update. *CA. Cancer J. Clin.* **2011**, *61* (4), 250–281.

(4) Krammer, B. Vascular Effects of Photodynamic Therapy. *Anticancer Res.* **2001**, *21* (6B), 4271–4277.

(5) Fan, W.; Huang, P.; Chen, X. Overcoming the Achilles' Heel of Photodynamic Therapy. *Chem. Soc. Rev.* **2016**, *45* (23), 6488–6519.

(6) van Straten, D.; Mashayekhi, V.; de Bruijn, H. S.; Oliveira, S.; Robinson, D. J. Oncologic Photodynamic Therapy: Basic Principles, Current Clinical Status and Future Directions. *Cancers (Basel).* **2017**, *9* (2), 1–54.

(7) Fee, J. A. Is Superoxide Important in Oxygen Poisoning? *Trends Biochem. Sci.* **1982**, *7* (3), 84–86.

(8) Winterbourn, C. C. Reconciling the Chemistry and Biology of Reactive Oxygen Species. *Nat. Chem. Biol.* **2008**, *4* (5), 278–286.

(9) Sharman, W. M.; Allen, C. M.; van Lier, J. E. Role of Activated Oxygen Species in Photodynamic Therapy. *Methods Enzymol.* **2000**, *319*, 376–400.

(10) Brown, S. B.; Brown, E. A.; Walker, I. The Present and Future Role of Photodynamic Therapy in Cancer Treatment. *Lancet Oncol.* **2004**, *5* (8), 497–508.

(11) Brown, J. E.; Brown, S. B.; Vernon, D. I. Photosensitising Drugs- Their Potential in Oncology. *Expert Opin Investig Drugs* **1999**, *8* (12), 1967–1979.

(12) Martinez De Pinillos Bayona, A.; Mroz, P.; Thunshelle, C.; Hamblin, M. R. Design Features for Optimization of Tetrapyrrole Macrocycles as Antimicrobial and Anticancer Photosensitizers. *Chem. Biol. Drug Des.* **2017**, *89* (2), 192–206.

(13) M. Scherer, K.; H. Bisby, R.; W. Botchway, S.; W. Parker, A. New Approaches to Photodynamic Therapy from Types I, II and III to Type IV Using One or More Photons. *Anticancer. Agents Med. Chem.* **2017**, *17* (2), 171–189.

(14) Gál, D. Effect of Photosensitizers in Chemical and Biological Processes: The MTO Mechanism in Photodynamic Therapy. *Biochem. Biophys. Res. Commun.* **1992**, *186* (2), 1032–1036.

(15) Kriska, T.; Malt'seva, E.; Gál, D. In Vivo Experimental Studies on the Role of Free Radicals in Photodynamic Therapy. III. Photodynamic Effect on Free Radicals Generated in Cell Cultures. *Biochem. Biophys. Res. Commun.* **1997**, *233* (1), 173–176.

(16) Pawlicki, M.; Collins, H. A.; Denning, R. G.; Anderson, H. L. Two-Photon Absorption and the Design of Two-Photon Dyes. *Angew. Chemie - Int. Ed.* **2009**, *48* (18), 3244–3266.

(17) Zipfel, W. R.; Williams, R. M.; Webb, W. W. Nonlinear Magic: Multiphoton Microscopy in the Biosciences. *Nat. Biotechnol.* **2003**, *21* (11), 1369–1377.

(18) Bhawalkar, J. D.; Kumar, N. D.; Zhao, C. F.; Prasad, P. N. Two-Photon Photodynamic Therapy. *J Clin Laser Med Surg* **1997**, *15* (5), 201–204.

(19) Karotki, A.; Khurana, M.; Lepock, J. R.; Wilson, B. C. Simultaneous Two-Photon Excitation of Photofrin in Relation to Photodynamic Therapy. *Photochem. Photobiol.* **2006**, *82* (9), 443–452.

(20) Drobizhev, M.; Makarov, N. S.; Tillo, S. E.; Hughes, T. E.; Rebane, A. Two-Photon Absorption Properties of Fluorescent Proteins. *Nat. Methods* **2011**, *8* (5), 393–399.

(21) Brown, S. Photodynamic Therapy: Two Photons Are Better than One. *Nat. Photonics* **2008**, *2* (7), 394–395.

(22) Collins, H. A.; Khurana, M.; Moriyama, E. H.; Mariampillai, A.; Balaz, M.; Kuimova, M. K.; Drobizhev, M.; Yang, V. X. D.; Rebane, A.; Wilson, B. C.; et al. Blood Vessel Closure Using Photosensitisers Engineered for Two-Photon Excitation. *Nat. Photonics* **2008**, *2*, 420–424.

(23) Starkey, J. R.; Rebane, A. K.; Drobizhev, M. A.; Meng, F.; Gong, A.; Elliott, A.; McInnerney, K.; Spangler, C. W. New Two-Photon Activated Photodynamic Therapy Sensitizers Induce Xenograft Tumor Regressions after near-IR Laser Treatment through the Body of the Host Mouse. *Clin. Cancer Res.* **2008**, *14* (20), 6564–6573.

(24) Sharma, S. K.; Huang, Y.-Y.; Hamblin, M. R. Resistance to Photodynamic Therapy in Cancer. In *Resistance to Photodynamic Therapy in Cancer*; Rapozzi, V., Jori, G., Eds.; Springer, 2015; Vol. 5, pp 229–246.

(25) Shkryl, V. M.; Maxwell, J. T.; Blatter, L. A. A Novel Method for Spatially Complex Diffraction-Limited Photoactivation and Photobleaching in Living Cells. *J. Physiol.* **2012**, *590* (5), 1093–1100.

(26) Kowalik, L.; Chen, J. K. Illuminating Developmental Biology through Photochemistry. *Nat. Chem. Biol.* **2017**, *13* (6), 587–598.

(27) Brancaleon, L.; Moseley, H. Laser and Non-Laser Light Sources for Photodynamic Therapy. *Lasers Med. Sci.* **2002**, *17* (3), 173–186.

(28) Plaetzer, K.; Krammer, B.; Berlanda, J.; Berr, F.; Kiesslich, T. Photophysics and Photochemistry of Photodynamic Therapy: Fundamental Aspects. *Lasers Med. Sci.* **2009**, *24* (2), 259–268.

(29) Juzeniene, A.; Peng, Q.; Moan, J. Milestones in the Development of Photodynamic Therapy and Fluorescence Diagnosis. *Photochem. Photobiol. Sci.* **2007**, *6* (12), 1234–1245.

(30) Keereweer, S.; Van Driel, P. B. A. A.; Snoeks, T. J. A.; Kerrebijn, J. D. F.; De Jong, R. J. B.; Vahrmeijer, A. L.; Sterenborg, H. J. C. M.; Löwik, C. W. G. M. Optical Image-Guided Cancer Surgery: Challenges and Limitations. *Clin. Cancer Res.* **2013**, *19* (14), 3745–3754.

(31) Kasha, M.; Khan, A. U. Physics, Chemistry, and Biology of Singlet Molecular Oxygen. *Ann. N. Y. Acad. Sci.* **1970**, *171* (1), 5-.

(32) Kearns, D. R. Physical and Chemical Properties of Singlet Molecular Oxygen. *Chem.Rev.* **1971**, *71* (4), 395–427.

(33) Long, C.; Kearns, D. R. Selection Rules for the Intermolecular Enhancement of Spin Forbidden Transitions in Molecular Oxygen. *J. Chem. Phys.* **1973**, *59* (10), 5729.

(34) Ho, R. Y. N.; Liebman, J. F.; Valentine, J. S. Active Oxygen in Chemistry. *Act. Oxyg. Chem.* **1996**, 1–23.

(35) Ogilby, P. R. Singlet Oxygen: There Is Indeed Something New under the Sun. *Chem. Soc. Rev.* **2010**, *39* (8), 3181–3209.

(36) DeRosa, M. C.; Crutchley, R. J. Photosensitized Singlet Oxygen and Its Applications. *Coord. Chem. Rev.* **2002**, *233–234*, 351–371.

(37) Boix-Garriga, E.; Rodríguez-Amigo, B.; Planas, O.; Nonell, S. Properties of Singlet Oxygen. In *Singlet Oxygen: Applications in Biosciences and Nanosciences*; Nonell, S., Flors, C., Eds.; Royal Society of Chemistry, 2016; pp 23–46.

(38) Schweitzer, C.; Schmidt, R. Physical Mechanisms of Generation and Deactivation of Singlet Oxygen. *Chem. Rev.* **2003**, *103* (5), 1685–1758.

(39) Krinsky, N. I. Singlet Oxygen in Biological Systems. *Trends Biochem. Sci.* **1977**, *30* (9), 35–38.

(40) Nonell, S.; Braslavsky, S. E. Time-Resolved Singlet Oxygen Detection. *Methods Enzymol.* **2000**, *319*, 37–49.

(41) Nonell, S.; Flors, C. Chapter 25. Steady-State and Time-Resolved Singlet Oxygen Phosphorescence Detection in the Near-IR. In *Singlet Oxygen: Applications in Biosciences and Nanosciences*; Nonell, S., Flors, C., Eds.; Royal Society of Chemistry, 2016; pp 7–26.

(42) Jiménez-Banzo, A.; Ragàs, X.; Kapusta, P.; Nonell, S. Time-Resolved Methods in Biophysics. 7. Photon Counting vs. Analog Time-Resolved Singlet Oxygen Phosphorescence Detection. *Photochem. Photobiol. Sci.* **2008**, *7* (9), 1003–1010.

(43) Wilkinson, F.; Helman, W. P.; Ross, A. B. Quantum Yields for the Photosensitized Formation of the Lowest Electronically Excited State of Molecular Oxygen in Solution. *J. Phys. Chem. Ref. Data* **1993**, *22* (1), 113–262.

(44) Gomes, A.; Fernandes, E.; Lima, J. L. F. C. Fluorescence Probes Used for Detection of Reactive Oxygen Species. *J. Biochem. Biophys. Methods* **2005**, *65* (2–3), 45–80.

(45) Chen, X.; Tian, X.; Shin, I.; Yoon, J. Fluorescent and Luminescent Probes for Detection of Reactive Oxygen and Nitrogen Species. *Chem. Soc. Rev.* **2011**, *40* (9), 4783–4804.

(46) Ruiz-González, R.; Zanocco, A. L. Singlet Oxygen Fluorescent Probes. In *Singlet Oxygen : Applications in Biosciences and Nanosciences, Volume 2*; Nonell, S., Flors, C., Eds.; The Royal Society of Chemistry, 2016; pp 103–120.

(47) Boonstra, J.; Post, J. A. Molecular Events Associated with Reactive Oxygen Species and Cell Cycle Progression in Mammalian Cells. *Gene* **2004**, *337* (SUPPL.), 1–13.

(48) Valko, M.; Leibfritz, D.; Moncol, J.; Cronin, M. T. D.; Mazur, M.; Telser, J. Free Radicals and Antioxidants in Normal Physiological Functions and Human Disease. *Int. J. Biochem. Cell Biol.* **2007**, *39* (1), 44–84.

(49) Blázquez-Castro, A.; Breitenbach, T.; Ogilby, P. R. Singlet Oxygen and ROS in a New Light: Low-Dose Subcellular Photodynamic Treatment Enhances Proliferation at the Single Cell Level. *Photochem. Photobiol. Sci.* **2014**.

(50) Ray, P. D.; Huang, B.-W.; Tsuji, Y. Reactive Oxygen Species (ROS) Homeostasis and Redox Regulation in Cellular Signaling. *Cell. Signal.* **2012**, *24* (5), 981–990.

(51) D'Autréaux, B.; Toledano, M. B. ROS as Signalling Molecules: Mechanisms That Generate Specificity in ROS Homeostasis. *Nat. Rev. Mol. Cell Biol.* **2007**, *8* (10), 813–824.

(52) Flannagan, R. S.; Cosío, G.; Grinstein, S. Antimicrobial Mechanisms of Phagocytes and Bacterial Evasion Strategies. *Nat. Rev. Microbiol.* **2009**, *7* (5), 355–366.

(53) Schumacker, P. Reactive Oxygen Species in Cancer: A Dance with the Devil. *Cancer Cell* **2015**, *27* (2), 156–157.

(54) Bacellar, I. O. L.; Tsubone, T. M.; Pavani, C.; Baptista, M. S. Photodynamic Efficiency : From Molecular Photochemistry to Cell Death. *Int. J. Mol. Sci.* **2015**, *16*, 20523–20559.

(55) Benov, L. Photodynamic Therapy: Current Status and Future Directions. *Med. Princ. Pract.* **2015**, *24* (suppl 1), 14–28.

(56) Castano, A. P.; Demidova, T. N.; Hamblin, M. R. Mechanisms in Photodynamic Therapy: Part One - Photosensitizers, Photochemistry and Cellular Localization. *Photodiagnosis Photodyn. Ther.* **2004**, *1* (4), 279–293.

(57) Nyman, E. S.; Hynninen, P. H. Research Advances in the Use of Tetrapyrrolic Photosensitizers for Photodynamic Therapy. *J. Photochem. Photobiol. Biol.* **2004**, *73* (1–2), 1–28.

(58) Rodríguez-Amigo, B.; Planas, O.; Bresolí-Obach, R.; Torra, J.; Ruiz-González, R.; Nonell, S. Photosensitisers for Photodynamic Therapy: State of the Art and Perspectives. In *Photodynamic Medicine: From Bench to Clinic*; Kostron, H., Hasan, T., Eds.; The Royal Society of Chemistry, 2016; pp 23–62.

(59) Lucky, S. S.; Soo, K. C.; Zhang, Y. Nanoparticles in Photodynamic Therapy. *Chem. Rev.* **2015**, *115* (4), 1990–2042.

(60) Ferrari, M. Cancer Nanotechnology: Opportunities and Challenges. *Nat. Rev. Cancer* **2005**, *5* (3), 161–171.

(61) Chatterjee, D. K.; Fong, L. S.; Zhang, Y. Nanoparticles in Photodynamic Therapy: An Emerging Paradigm. *Adv. Drug Deliv. Rev.* **2008**, *60* (15), 1627–1637.

(62) Abrahamse, H.; Kruger, C. A.; Kadanyo, S.; Mishra, A. Nanoparticles for Advanced Photodynamic Therapy of Cancer. *Photomed. Laser Surg.* **2017**, *XX* (Xx), pho.2017.4308.

(63) Shirasu, N.; Nam, S. O.; Kuroki, M. Tumor-Targeted Photodynamic Therapy. *Anticancer Res.* **2013**, No. 33, 2823–2831.

(64) Cho, K.; Wang, X.; Nie, S.; Chen, Z. G.; Shin, D. M. Therapeutic Nanoparticles for Drug Delivery in Cancer. *Clin. Cancer Res.* **2008**, *14* (5), 1310–1316.

(65) Solban, N.; Rizvi, I.; Hasan, T. Targeted Photodynamic Therapy. *Lasers Surg. Med.* **2006**, *38* (5), 522–531.

(66) Bugaj, A. M. Targeted Photodynamic Therapy--a Promising Strategy of Tumor Treatment. *Photochem. Photobiol. Sci.* **2011**, *10* (7), 1097–1109.

(67) Lim, C.-K.; Heo, J.; Shin, S.; Jeong, K.; Seo, Y. H.; Jang, W.-D.; Park, C. R.; Park, S. Y.; Kim, S.; Kwon, I. C. Nanophotosensitizers toward Advanced Photodynamic Therapy of Cancer. *Cancer Lett.* **2013**, *334* (2), 176–187.

(68) Oliveira, C. S.; Turchiello, R.; Kowaltowski, A. J.; Indig, G. L.; Baptista, M. S. Major Determinants of Photoinduced Cell Death: Subcellular Localization versus Photosensitization Efficiency. *Free Radic. Biol. Med.* **2011**, *51* (4), 824–833.

(69) Rosenkranz, A. A.; Jans, D. A.; Sobolev, A. S. Targeted Intracellular Delivery of Photosensitizers to Enhance Photodynamic Efficiency. *Immunol. Cell Biol.* **2000**, *78* (4), 452–464.

(70) Zheng, X.; Morgan, J.; Pandey, S. K.; Chen, Y.; Tracy, E.; Baumann, H.; Missert, J. R.; Batt, C.; Jackson, J.; Bellnier, D. A.; et al. Conjugation of 2-(1'-Hexyloxyethyl)-2-Devinylpyropheophorbide-a (HPPH) to Carbohydrates Changes Its Subcellular Distribution and Enhances Photodynamic Activity in Vivo. *J. Med. Chem.* **2009**, *52* (14), 4306–4318.

(71) Mitsunaga, M.; Ogawa, M.; Kosaka, N.; Rosenblum, L. T.; Choyke, P. L.; Kobayashi, H. Cancer Cell–selective in Vivo near Infrared Photoimmunotherapy Targeting Specific Membrane Molecules. *Nat. Med.* **2011**, *17* (12), 1685–1691.

(72) Kessel, D.; Luo, Y. Mitochondrial Photodamage and PDT-Induced Apoptosis. *J. Photochem. Photobiol. B Biol.* **1998**, *42* (2), 89–95.

(73) Hilf, R. Mitochondria Are Targets of Photodynamic Therapy. *J. Bioenerg. Biomembr.* **2007**, *39* (1), 85–89.

(74) Berg, K.; Moan, J. Lysosomes as Photochemical Targets. *Int. J. cancer.Journal Int. du cancer* **1994**, *59* (6), 814–822.

(75) Abrahamse, H.; Hamblin, M. R. New Photosensitizers for Photodynamic Therapy. *Biochem. J* **2016**, *473*, 347–364.

(76) Dougherty, T. J.; Gomer, C. J.; Henderson, B. W.; Jori, G.; Kessel, D.; Korbelik, M.; Moan, J.; Peng, Q. Photodynamic Therapy. *J. Natl. Cancer Inst.* **1998**, *90* (12), 889–905.

(77) Rajendran, L.; Knölker, H. J.; Simons, K. Subcellular Targeting Strategies for Drug Design and Delivery. *Nat. Rev. Drug Discov.* **2010**, *9* (1), 29–42.

(78) Jiang, H. N.; Li, Y.; Cui, Z. J. Photodynamic Physiology—Photonanomanipulations in Cellular Physiology with Protein Photosensitizers. *Front. Physiol.* **2017**, *8* (April), 1–13.

(79) Zhou, Z.; Song, J.; Nie, L.; Chen, X. Reactive Oxygen Species Generating Systems Meeting Challenges of Photodynamic Cancer Therapy. *Chem. Soc. Rev.* **2016**, *45* (23), 6597–6626.

(80) Modica-napolitano, J. S.; John, L.; Ara, G.; Oseroff, A. R.; Aprille, J. R. Mitochondrial Toxicity of Cationic Photosensitizers for Photochemotherapy1. *Cancer Res.* **1990**, *50*, 7876–7881.

(81) Morgan, J.; Oseroff, A. R. Mitochondria-Based Photodynamic Anti-Cancer Therapy. *Adv. Drug Deliv. Rev.* **2001**, *49* (1–2), 71–86.

(82) Castano, A. P.; Demidova, T. N.; Hamblin, M. R. Mechanisms in Photodynamic Therapy: Part Two: Cellular Signaling, Cell Metabolism and Modes of Cell Death. *Photodiagnosis and photodynamic therapy*. Elsevier January 2005, pp 1–23.

(83) Denis, T. G. S.; Dai, T.; Izikson, A.; Astrakas, C.; Anderson, R. R.; Hamblin, M. R.; Tegos, G. P. All You Need Is Light. *Virulence* **2011**, *2* (6), 1–12.

(84) O'Neill, J. Antimicrobial Resistance: Tackling a Crisis for the Health and Wealth of Nations. *Rev. Antimicrob. Resist. Chaired by Jim O'Neill* **2014**, No. December, 4–16.

(85) Boucher, H. W.; Talbot, G. H.; Bradley, J. S.; Edwards, J. E.; Gilbert, D.; Rice, L. B.; Scheld, M.; Spellberg, B.; Bartlett, J. Bad Bugs, No Drugs: No ESKAPE! An Update from the Infectious Diseases Society of America. *Clin. Infect. Dis.* **2009**, *48* (1), 1–12.

(86) Piddock, L. J. V. The Crisis of No New Antibiotics-What Is the Way Forward? *Lancet Infect. Dis.* **2012**, *12* (3), 249–253.

(87) Hamblin, M. R. Antimicrobial Photodynamic Inactivation: A Bright New Technique to Kill Resistant Microbes. *Curr. Opin. Microbiol.* **2016**, *33*, 67–73.

(88) Wainwright, M.; Maisch, T.; Nonell, S.; Plaetzer, K.; Almeida, A.; Tegos, G. P.; Hamblin, M. R. Photoantimicrobials-Are We Afraid of the Light? *Lancet Infect. Dis.* **2017**, *17* (2), 49–55.

(89) Dai, T.; Huang, Y. Y.; Hamblin, M. R. Photodynamic Therapy for Localized Infections- State of the Art. *Photodiagnosis Photodyn. Ther.* **2009**, *6* (3–4), 170–188.

(90) Maisch, T. Resistance in Antimicrobial Photodynamic Inactivation of Bacteria. *Photochem. Photobiol. Sci.* **2015**, *14* (8), 1518–1526.

(91) Kashef, N.; Hamblin, M. R. Can Microbial Cells Develop Resistance to Oxidative Stress in Antimicrobial Photodynamic Inactivation? *Drug Resist. Updat.* **2017**, *31* (April), 31–42.

(92) Hamblin, M. R.; Hasan, T. Photodynamic Therapy: A New Antimicrobial Approach to Infectious Disease? *Photochem. Photobiol. Sci.* **2004**, *3* (5), 436–450.

(93) Sharma, S. K.; Mroz, P.; Dai, T.; Huang, Y.-Y.; Denis, T. G. St.; Hamblin, M. R. Photodynamic Therapy for Cancer and for Infections: What Is the Difference? *Isr. J. Chem.* **2012**, *52* (8–9), 691–705.

(94) Malik, Z.; Ladan, H.; Nitzan, Y. Photodynamic Inactivation of Gram-Negative Bacteria: Problems and Possible Solutions. *J. Photochem. Photobiol. B Biol.* **1992**, *14* (3), 262–266.

(95) Valduga, G.; Bertoloni, G.; Reddi, E.; Jori, G. Effect of Extracellularly Generated Singlet Oxygen on Gram-Positive and Gram-Negative Bacteria. *J. Photochem. Photobiol. Biol.* **1993**, *21* (1), 81–86.

(96) Sperandio, F. F.; Huang, Y.-Y.; Hamblin, M. R. Antimicrobial Photodynamic Therapy to Kill Gram-Negative Bacteria. *Recent Pat. Antiinfect. Drug Discov.* **2013**, *8* (2), 108–120.

(97) Hell, S. W. Toward Fluorescence Nanoscopy. *Nat. Biotechnol.* **2003**, *21* (11), 1347–1355.

(98) Delcanale, P.; Pennacchietti, F.; Maestrini, G.; Rodríguez-Amigo, B.; Bianchini, P.; Diaspro, A.; Iagatti, A.; Patrizi, B.; Foggi, P.; Agut, M.; et al. Subdiffraction Localization of a Nanostructured Photosensitizer in Bacterial Cells. *Sci. Rep.* **2015**, *5*, 15564.

(99) Dalle Carbonare, M.; Pathak, M. a. Skin Photosensitizing Agents and the Role of Reactive Oxygen Species in Photoaging. *J. Photochem. Photobiol. Biol.* **1992**, *14* (1–2), 105–124.

(100) Young, A. R. Chromophores in Human Skin. *Phys. Med. Biol.* **1997**, *42* (5), 789–802.

(101) Repina, N. A.; Rosenbloom, A.; Mukherjee, A.; Schaffer, D. V.; Kane, R. S. At Light Speed: Advances in Optogenetic Systems for Regulating Cell Signaling and Behavior. *Annu. Rev. Chem. Biomol. Eng.* **2017**, *8* (1), 13–39.

(102) Fenno, L.; Yizhar, O.; Deisseroth, K. The Development and Application of Optogenetics. *Annu. Rev. Neurosci.* **2011**, *34* (1), 389–412.

(103) Mühlhäuser, W. W. D.; Fischer, A.; Weber, W.; Radziwill, G. Optogenetics - Bringing Light into the Darkness of Mammalian Signal Transduction. *Biochim. Biophys. Acta - Mol. Cell Res.* **2017**, *1864* (2), 280–292.

(104) Deisseroth, K. Optogenetics. *Nat. Methods* **2011**, *8* (1), 26–29.

(105) Rost, B. R.; Schneider-Warme, F.; Schmitz, D.; Hegemann, P. Optogenetic Tools for Subcellular Applications in Neuroscience. *Neuron* **2017**, *96* (3), 572–603.

(106) Griffin, B. a. Specific Covalent Labeling of Recombinant Protein Molecules Inside Live Cells. *Science (80-.).* **1998**, *281* (5374), 269–272.

(107) Gaietta, G.; Deerinck, T. J.; Adams, S. R.; Bouwer, J.; Tour, O.; Laird, D. W.; Sosinsky, G. E.; Tsien, R. Y.; Ellisman, M. H. Multicolor and Electron Microscopic Imaging of Connexin Trafficking. *Science* **2002**, *296* (5567), 503–507.

(108) Tour, O.; Meijer, R. M.; Zacharias, D. A.; Adams, S. R.; Tsien, R. Y. Genetically Targeted Chromophore-Assisted Light Inactivation. *Nat. Biotechnol.* **2003**, *21* (12), 1505–1508.

(109) Hoffmann, C.; Gaietta, G.; Zürn, A.; Adams, S. R.; Terrillon, S.; Ellisman, M. H.; Tsien, R. Y.; Lohse, M. J. Fluorescent Labeling of Tetracysteine-Tagged Proteins in Intact Cells. *Nat. Protoc.* **2010**, *5* (10), 1666–1677.

(110) Ellisman, Mark H, Deerinck T., Shu, X. Sosinsky, G. Picking Faces out If a Crowd: Genetic Labels for Identification of Proteins in Correlated Light and Electron Microscopy Imaging. *Methods Cell Biol.* **2012**, No. Lm, 1–16.

(111) Keppler, A.; Gendreizig, S.; Gronemeyer, T.; Pick, H.; Vogel, H.; Johnsson, K. A General Method for the Covalent Labeling of Fusion Proteins with Small Molecules in Vivo. *Nat. Biotechnol.* **2003**, *21* (1), 86–89.

(112) Juillerat, A.; Gronemeyer, T.; Keppler, A.; Gendreizig, S.; Pick, H.; Vogel, H.; Johnsson, K. Directed Evolution of O6-Alkylguanine-DNA Alkyltransferase for Efficient Labeling of Fusion Proteins with Small Molecules In Vivo. *Cell Chem. Biol.* **2003**, *10* (F), 313–317.

(113) Keppler, A.; Pick, H.; Arrivoli, C.; Vogel, H.; Johnsson, K. Labeling of Fusion Proteins with Synthetic Fluorophores in Live Cells. *Proc. Natl. Acad. Sci.* **2004**, *101* (27), 9955–9959.

(114) Gautier, A.; Juillerat, A.; Heinis, C.; Corrêa, I. R.; Kindermann, M.; Beaufils, F.; Johnsson, K. An Engineered Protein Tag for Multiprotein Labeling in Living Cells. *Chem. Biol.* **2008**, *15* (2), 128–136.

(115) Los, G. V; Darzins, A.; Zimprich, C.; Karassina, N.; Learish, R.; McDougall, M. G.; Encell, L. P.; Friedman-Ohana, R.; Wood, M.; Vidugiris, G.; et al. One Fusion Protein: Multiple Functions. *Promega Notes* **2005**, No. 89, 2–6.

(116) Jianjun He; Yi Wang; Maria A Missinato; Ezenwa Onuoha; Lydia A Perkins; Simon C Watkins; Claudette M St Croix; Michael Tsang; Marcel P Bruchez. A Genetically Targetable Near-Infrared Photosensitizer. *Nat. Methods* **2016**, No. August 2015.

(117) Shimomura, O. Discovery of Green Fluorescent Protein, GFP. *Methods Biochem. Anal.* **2008**, *47*, 1–13.

(118) Tsien, R. Y. Constructing and Exploiting the Fluorescent Protein Paintbox (Nobel Lecture). *Angew. Chemie Int. Ed.* **2009**, *48* (31), 5612–5626.

(119) Day, R. N.; Davidson, M. W. The Fluorescent Protein Palette: Tools for Cellular Imaging. *Chem. Soc. Rev.* **2009**, *38* (10), 2887–2921.

(120) Chudakov, D. M.; Matz, M. V; Lukyanov, S.; Lukyanov, K. A. Fluorescent Proteins and Their Applications in Imaging Living Cells and Tissues. *Physiol Rev* **2010**, *90*, 1103–1163.

(121) Rodriguez, E. A.; Campbell, R. E.; Lin, J. Y.; Lin, M. Z.; Miyawaki, A.; Palmer, A. E.; Shu, X.; Zhang, J.; Tsien, R. Y. The Growing and Glowing Toolbox of Fluorescent and Photoactive Proteins. *Trends Biochem. Sci.* **2017**, *42* (2), 111–129.

(122) Frommer, W. B.; Davidson, M. W.; Campbell, R. E. Genetically Encoded Biosensors Based on Engineered Fluorescent Proteins. *Chem. Soc. Rev.* **2009**, *38* (10), 2833–2841.

(123) Palmer, A. E.; Qin, Y.; Park, J. G.; McCombs, J. E. Design and Application of Genetically Encoded Biosensors. *Trends Biotechnol.* **2011**, *29* (3), 144–152.

(124) Enterina, J. R.; Wu, L.; Campbell, R. E. Emerging Fluorescent Protein Technologies. *Curr. Opin. Chem. Biol.* **2015**, *27*, 10–17.

(125) Thorn, K. Genetically Encoded Fluorescent Tags. **2016**, No. Figure 1.

(126) Surrey, T.; Elowitz, M. B.; Wolf, P.-E. E.; Yang, F.; Nedelec, F.; Shokat, K.; Leibler, S.; Nédélec, F.; Shokat, K.; Leibler, S.; et al. Chromophore-Assisted Light Inactivation and Self-Organization of Microtubules and Motors. *Proc. Natl. Acad. Sci. U. S. A.* **1998**, *95* (8), 4293–4298.

(127) Jacobson, K.; Rajfur, Z.; Vitriol, E.; Hahn, K. Chromophore-Assisted Laser Inactivation in Cell Biology. *Trends Cell Biol.* **2008**, *18* (9), 443–450.

(128) Sano, Y.; Watanabe, W.; Matsunaga, S. Chromophore-Assisted Laser Inactivation - towards a Spatiotemporal-Functional Analysis of Proteins, and the Ablation of Chromatin, Organelle and Cell Function. *J. Cell Sci.* **2014**, *127* (Pt 8), 1621–1629.

(129) Shu, X.; Lev-Ram, V.; Deerinck, T. J.; Qi, Y.; Ramko, E. B.; Davidson, M. W.; Jin, Y.; Ellisman, M. H.; Tsien, R. Y. A Genetically Encoded Tag for Correlated Light and Electron Microscopy of Intact Cells, Tissues, and Organisms. *PLoS Biol.* **2011**, *9* (4), e1001041.

(130) Bulina, M. E.; Chudakov, D. M.; Britanova, O. V; Yanushevich, Y. G.; Staroverov, D. B.; Chepurnykh, T. V; Merzlyak, E. M.; Shkrob, M. A.; Lukyanov, S.; Lukyanov, K. A. A Genetically Encoded Photosensitizer. *Nat. Biotechnol.* **2006**, *24* (1), 95–99.

(131) Greenbaum, L.; Rothmann, C.; Lavie, R.; Malik, Z. Green Fluorescent Protein Photobleaching: A Model for Protein Damage by Endogenous and Exogenous Singlet Oxygen. *Biol. Chem.* **2000**, *381* (12), 1251–1258.

(132) Jiménez-Banzo, A.; Nonell, S.; Hofkens, J.; Flors, C. Singlet Oxygen Photosensitization by EGFP and Its Chromophore HBDI. *Biophys. J.* **2008**, *94* (1), 168–172.

(133) Jiménez-Banzo, A.; Ragàs, X.; Abbruzzetti, S.; Viappiani, C.; Campanini, B.; Flors, C.; Nonell, S. Singlet Oxygen Photosensitisation by GFP Mutants: Oxygen Accessibility to the Chromophore. *Photochem. Photobiol. Sci.* **2010**, *9* (10), 1336–1341.

(134) Wojtovich, A. P.; Foster, T. H. Optogenetic Control of ROS Production. *Redox Biol.* **2014**, *2*, 368–376.

(135) Shcherbakova, D. M.; Shemetov, A. A.; Kaberniuk, A. A.; Verkhusha, V. V.; Ahmad, I. *Natural Photoreceptors as a Source of Fluorescent Proteins, Biosensors, and Optogenetic Tools*; 2015; Vol. 84.

(136) Losi, A.; Gärtner, W. Solving Blue-Light Riddles: New Lessons from Flavin-Binding LOV Photoreceptors. *Photochem. Photobiol.* **2016**, n/a-n/a.

(137) Planas, O.; Boix-Garriga, E.; Rodríguez-Amigo, B.; Torra, J.; Bresolí-Obach, R.; Flors, C.; Viappiani, C.; Agut, M.; Ruiz-González, R.; Nonell, S. Chapter 9: Newest Approaches to Singlet Oxygen Photosensitisation in Biological Media. In *Photochemistry*; Fasani, E., Albini, A., Eds.; Special Periodical Reports; Royal Society of Chemistry, 2015; Vol. 42, pp 233–278.

(138) Cody, C. W.; Prasher, D. C.; Westler, W. M.; Prendergast, F. G.; Ward, W. W. Chemical Structure of the Hexapeptide Chromophore of the Aequorea Green-Fluorescent Protein. *Biochemistry* **1993**, *32* (1979), 1212–1218.

(139) Heim, R.; Prasher, D. C.; Tsien, R. Y. Wavelength Mutations and Posttranslational Autoxidation of Green Fluorescent Protein. *Proc. Natl. Acad. Sci. U. S. A.* **1994**, *91* (26), 12501–12504.

(140) Bell, A. F.; Stoner-Ma, D.; Wachter, R. M.; Tonge, P. J. Light-Driven Decarboxylation of Wild-Type Green Fluorescent Protein. *J. Am. Chem. Soc.* **2003**, *125* (23), 6919–6926.

(141) Cubitt, A. B.; Heim, R.; Adams, S. R.; Boyd, A. E.; Gross, L. A.; Tsien, R. Y. Understanding, Improving and Using Green Fluorescent Proteins. *Trends Biochem. Sci.* **1995**, *20* (11), 448–455.

(142) Cormack, B. P.; Valdivia, R. H.; Falkow, S. FACS-Optimized Mutants of the Green Fluorescent Protein (GFP). *Gene* **1996**, *173* (1 Spec No), 33–38.

(143) Rajfur, Z.; Roy, P.; Otey, C.; Romer, L.; Jacobson, K. Dissecting the Link between Stress Fibres and Focal Adhesions by CALI with EGFP Fusion Proteins. *Nat. Cell Biol.* **2002**, *4* (4), 286–293.

(144) Vitriol, E. A.; Uetrecht, A. C.; Shen, F.; Jacobson, K.; Bear, J. E. Enhanced EGFP-Chromophore-Assisted Laser Inactivation Using Deficient Cells Rescued with Functional EGFP-Fusion Proteins. *Proc. Natl. Acad. Sci. U. S. A.* **2007**, *104* (16), 6702–6707.

(145) Waldeck, W.; Mueller, G.; Wiessler, M.; Brom, M.; Toth, K.; Braun, K.; Tóth, K.; Braun, K.; Toth, K.; Braun, K. Autofluorescent Proteins as Photosensitizer in Eukaryontes. *Int. J. Med. Sci.* **2009**, *6* (6), 365–373.

(146) Serebrovskaya, E. O.; Edelweiss, E. F.; Stremovskiy, O. A.; Lukyanov, K. A.; Chudakov, D. M.; Deyev, S. M. Targeting Cancer Cells by Using an Antireceptor Antibody-Photosensitizer Fusion Protein. *Proc. Natl. Acad. Sci. U. S. A.* **2009**, *106* (23), 9221–9225.

(147) Del Bene, F.; Wyart, C.; Robles, E.; Tran, A.; Looger, L.; Scott, E. K.; Isacoff, E. Y.; Baier, H. Filtering of Visual Information in the Tectum by an Identified Neural Circuit. *Science (80-.).* **2010**, *330*, 669–674.

(148) Williams, D. C.; Bejjani, R. El; Ramirez, P. M.; Coakley, S.; Kim, S. A.; Lee, H.; Wen, Q.; Samuel, A.; Lu, H.; Hilliard, M. a; et al. Rapid and Permanent Neuronal Inactivation in Vivo via Subcellular Generation of Reactive Oxygen with the Use of KillerRed. *Cell Rep.* **2013**, *5* (2), 553–563.

(149) Zhuo, L.-G.; Liao, W.; Yu, Z.-X. A Frontier Molecular Orbital Theory Approach to Understanding the Mayr Equation and to Quantifying Nucleophilicity and Electrophilicity by Using HOMO and LUMO Energies. *Asian J. Org. Chem.* **2012**, *1* (4), 336–345.

(150) Pletnev, S.; Gurskaya, N. G.; Pletneva, N. V; Lukyanov, K. A.; Chudakov, D. M.; Martynov, V. I.; Popov, V. O.; Kovalchuk, M. V; Wlodawer, A.; Dauter, Z.; et al. Structural Basis for Phototoxicity of the Genetically Encoded Photosensitizer KillerRed. *J. Biol. Chem.* **2009**, *284* (46), 32028–32039.

(151) Vegh, R. B.; Solntsev, K. M.; Kuimova, M. K.; Cho, S.; Liang, Y.; Loo, B. L. W.; Tolbert, L. M.; Bommarius, A. S. Reactive Oxygen Species in Photochemistry of the Red Fluorescent Protein "Killer Red." *Chem. Commun.* **2011**, *47* (17), 4887–4889.

(152) Kim, S.; Tachikawa, T.; Fujitsuka, M.; Majima, T. Far-Red Fluorescence Probe for Monitoring Singlet Oxygen during Photodynamic Therapy. *J. Am. Chem. Soc.* **2014**, *136* (33), 11707–11715.

(153) Carpentier, P.; Violot, S.; Blanchoin, L.; Bourgeois, D. Structural Basis for the Phototoxicity of the Fluorescent Protein KillerRed. *FEBS Lett.* **2009**, *583* (17), 2839–2842.

(154) Roy, A.; Carpentier, P.; Bourgeois, D.; Field, M. Diffusion Pathways of Oxygen Species in the Phototoxic Fluorescent Protein KillerRed. *Photochem. Photobiol. Sci.* **2010**, *9* (10), 1342–1350.

(155) Chudakov, D. M.; Lukyanov, S.; Lukyanov, K. A. Fluorescent Proteins as a Toolkit for in Vivo Imaging. *Trends Biotechnol.* **2005**, *23* (12).

(156) Merzlyak, E. M.; Goedhart, J.; Shcherbo, D.; Bulina, M. E.; Shcheglov, A. S.; Fradkov, A. F.; Gaintzeva, A.; Lukyanov, K. A.; Lukyanov, S.; Gadella, T. W. J.; et al. Bright Monomeric Red Fluorescent Protein with an Extended Fluorescence Lifetime. *Nat. Methods* **2007**, *4* (7), 555–557.

(157) Shaner, N. C.; Lin, M. Z.; McKeown, M. R.; Steinbach, P. A.; Hazelwood, K. L.; Davidson, M. W.; Tsien, R. Y. Improving the Photostability of Bright Monomeric Orange and Red Fluorescent Proteins ESI. *Nat. Methods* **2008**, *5* (6), 545–551.

(158) Ragàs, X.; Cooper, L. P.; White, J. H.; Nonell, S.; Flors, C. Quantification of Photosensitized Singlet Oxygen Production by a Fluorescent Protein. *Chemphyschem* **2011**, *12* (1), 161–165.

(159) Ruiz-González, R.; White, J. H.; Agut, M.; Nonell, S.; Flors, C. A Genetically-Encoded Photosensitiser Demonstrates Killing of Bacteria by Purely Endogenous Singlet Oxygen. *Photochem. Photobiol. Sci.* **2012**, *11* (9), 1411–1413.

(160) Waldeck, W.; Heidenreich, E.; Mueller, G.; Wiessler, M.; Tóth, K.; Braun, K. ROS-Mediated Killing Efficiency with Visible Light of Bacteria Carrying Different Red Fluorochrome Proteins. *J. Photochem. Photobiol. B.* **2012**, *109*, 28–33.

(161) Sarkisyan, K. S.; Zlobovskaya, O. A.; Gorbachev, D. A.; Bozhanova, N. G.; Sharonov, G. V.; Staroverov, D. B.; Egorov, E. S.; Ryabova, A. V.; Solntsev, K. M.; Mishin, A. S.; et al. KillerOrange, a Genetically Encoded Photosensitizer Activated by Blue and Green Light. *PLoS One* **2015**, *10* (12), e0145287.

(162) Takemoto, K.; Matsuda, T.; Sakai, N.; Fu, D.; Noda, M.; Uchiyama, S.; Kotera, I.; Arai, Y.; Horiuchi, M.; Fukui, K.; et al. SuperNova, a Monomeric Photosensitizing Fluorescent Protein for Chromophore-Assisted Light Inactivation. *Sci. Rep.* **2013**, *3* (2629), 1–7.

(163) Riani, Y. D.; Matsuda, T.; Takemoto, K.; Nagai, T. Green Monomeric Photosensitizing Fluorescent Protein for Photo-Inducible Protein Inactivation and Cell Ablation. *BMC Biol.* **2018**, *16* (50), 1–12.

(164) Briggs, W. R.; Christie, J. M. Phototropins 1 and 2: Versatile Plant Blue-Light Receptors. *Trends Plant Sci.* **2002**, *7* (5), 204–210.

(165) Christie, J. M. Phototropin Blue-Light Receptors. *Annu. Rev. Plant Biol.* **2007**, *58*, 21–45.

(166) Losi, A.; Gärtner, W. The Evolution of Flavin-Binding Photoreceptors: An Ancient Chromophore Serving Trendy Blue-Light Sensors. *Annu. Rev. Plant Biol.* **2012**, *63*, 49–72.

(167) Jortzik, E.; Lihui, W.; Jiapeng, M.; Becker, K. Flavins and Flavoproteins: Applications in Medicine. In *Flavins and Flavoproteins: Methods and Protocols*; Weber, S., Schleicher, E., Eds.; Springer Science+Business Media, New York, 2013; Vol. 1146, pp 113–157.

(168) Möglich, A.; Moffat, K. Engineered Photoreceptors as Novel Optogenetic Tools. *Photochem. Photobiol. Sci.* **2010**, *9*, 1286–1300.

(169) Massey, V. The Chemical and Biological Versatility of Riboflavin. *Biochem. Soc. Trans.* **2000**, *28* (4), 283–296.

(170) Colibus, L. De; Mattevi, A. New Frontiers in Structural Flavoenzymology. *Curr. Opin. Struct. Biol.* **2006**, *16*, 722–728.

(171) Grodowski, M. S.; Veyret, B.; Weiss, K. Photochemistry of Flavins II. Photophysical Properties of Alloxazines and Isoalloxazines. *Photochem. Photobiol.* **1977**, *26*, 341–352.

(172) Heelis, P. F. The Photophysical and Photochemical Properties of Flavins (Isoalloxazines). *Chem. Soc. Rev.* **1982**, *11*, 15–39.

(173) Edwards, A. M. General Properties of Flavins. *Flavin Photochem. Photobiol.* **2006**, 1–11.

(174) Ahmad, I.; Vaid, F. H. M. Photochemistry of Flavins in Aqueous and Organic Solvents. In *Flavins photochemistry and photobiology:*; Silva, E., Edwards, A. M., Eds.; Cambridge: Royal Society of Chemistry, 2006; pp 13–40.

(175) Baier, J.; Maisch, T.; Maier, M.; Engel, E.; Landthaler, M.; Bäumler, W. Singlet Oxygen Generation by UVA Light Exposure of Endogenous Photosensitizers. *Biophys. J.* **2006**, *91* (4), 1452–1459.

(176) Conrad, K. S.; Manahan, C. C.; Crane, B. R. Photochemistry of Flavoprotein Light Sensors. *Nat. Chem. Biol.* **2014**, *10* (10), 801–809.

(177) Möglich, A.; Yang, X.; Ayers, R. A.; Moffat, K. Structure and Function of Plant Photoreceptors. *Annu. Rev. Plant Biol.* **2010**, *61* (1), 21–47.

(178) Herrou, J.; Crosson, S. Function, Structure and Mechanism of Bacterial Photosensory LOV Proteins. *Nat. Rev. Microbiol.* **2011**, *9* (10), 713–723.

(179) Chaves, I.; Pokorny, R.; Byrdin, M.; Hoang, N.; Ritz, T.; Brettel, K.; Essen, L.-O.; van der Horst, G. T. J.; Batschauer, A.; Ahmad, M. The Cryptochromes: Blue Light Photoreceptors in Plants and Animals. *Annu. Rev. Plant Biol.* **2011**, *62*, 335–364.

(180) Zoltowski, B. D.; Gardner, K. H. Tripping the Light Fantastic: Blue-Light Photoreceptors as Examples of Environmentally Modulated Protein-Protein Interactions. *Biochemistry* **2011**, *50* (1), 4–16.

(181) Masuda, S. Light Detection and Signal Transduction in the BLUF Photoreceptors. *Plant Cell Physiol.* **2013**, *54* (2), 171–179.

(182) Swartz, T. E.; Corchnoy, S. B.; Christie, J. M.; Lewis, J. W.; Szundi, I.; Briggs, W. R.; Bogomolni, R. A. The Photocycle of a Flavin-Binding Domain of the Blue Light Photoreceptor Phototropin. *J. Biol. Chem.* **2001**, *276* (39), 36493–36500.

(183) Drepper, T.; Eggert, T.; Circolone, F.; Heck, A.; Krauss, U.; Guterl, J. K.; Wendorff, M.; Losi, A.; Gärtner, W.; Jaeger, K. E. Reporter Proteins for in Vivo Fluorescence without Oxygen. *Nat. Biotechnol.* **2007**, *25* (4), 443–445.

(184) Chapman, S.; Faulkner, C.; Kaiserli, E.; Garcia-Mata, C.; Savenkov, E. I.; Roberts, A. G.; Oparka, K. J.; Christie, J. M. The Photoreversible Fluorescent Protein ILOV Outperforms GFP as a Reporter of Plant Virus Infection. *Proc. Natl. Acad. Sci. U. S. A.* **2008**, *105* (50), 20038–20043.

(185) Christie, J. M.; Hitomi, K.; Arvai, A. S.; Hartfield, K. A.; Mettlen, M.; Pratt, A. J.; Tainer, J. A.; Getzoff, E. D. Structural Tuning of the Fluorescent Protein ILOV for Improved Photostability ESI. *J. Biol. Chem.* **2012**, *287* (26), 22295–22304.

(186) Wingen, M.; Potzkei, J.; Endres, S.; Casini, G.; Rupprecht, C.; Fahlke, C.; Krauss, U.; Jaeger, K.-E.; Drepper, T.; Gensch, T. The Photophysics of LOV-Based Fluorescent Proteins – New Tools for Cell Biology. *Photochem. Photobiol. Sci.* **2014**, *13* (6), 875–883.

(187) Mukherjee, A.; Weyant, K. B.; Agrawal, U.; Walker, J.; Cann, I. K. O.; Schroeder, C. M.; Mukherjee, A.; Weyant, K. B.; Agrawal, U.; Walker, J.; et al. Engineering and Characterization of New LOV-Based Fluorescent Proteins from Chlamydomonas Reinhardtii and Vaucheria Frigida. *ACS Synth. Biol.* **2014**, 140725083743009.

(188) Ruiz-González, R.; Cortajarena, A. L.; Mejias, S. H.; Agut, M.; Nonell, S.; Flors, C. Singlet Oxygen Generation by the Genetically Encoded Tag MiniSOG. *J. Am. Chem. Soc.* **2013**, *135* (26), 9564–9567.

(189) Pimenta, F. M.; Jensen, R. L.; Breitenbach, T.; Etzerodt, M.; Ogilby, P. R. Oxygen-Dependent Photochemistry and Photophysics of "MiniSOG," a Protein-Encased Flavin. *Photochem. Photobiol.* **2013**, *89* (5), 1116–1126.

(190) Deerinck, T. J.; Martone, M. E.; Lev-Ram, V.; Green, D. P.; Tsien, R. Y.; Spector, D. L.; Huang, S.; Ellisman, M. H. Fluorescence Photooxidation with Eosin: A Method for High Resolution Immunolocalization and in Situ Hybridization Detection for Light and Electron Microscopy. *J. Cell Biol.* **1994**, *126* (4), 901–910.

(191) Meisslitzer-Ruppitsch, C.; Röhrl, C.; Neumüller, J.; Pavelka, M.; Ellinger, A. Photooxidation Technology for Correlated Light and Electron Microscopy. *J. Microsc.* **2009**, *235* (3), 322–335.

(192) De Boer, P.; Hoogenboom, J. P.; Giepmans, B. N. G. Correlated Light and Electron Microscopy: Ultrastructure Lights Up! *Nat. Methods* **2015**, *12* (6), 503–513.

(193) Ludwig, A.; Howard, G.; Mendoza-Topaz, C.; Deerinck, T.; Mackey, M.; Sandin, S.; Ellisman, M. H.; Nichols, B. J. Molecular Composition and Ultrastructure of the Caveolar Coat Complex. *PLoS Biol.* **2013**, *11* (8).

(194) Boassa, D.; Berlanga, M. L.; Yang, M. A.; Terada, M.; Hu, J.; Bushong, E. A.; Hwang, M.; Masliah, E.; George, J. M.; Ellisman, M. H. Mapping the Subcellular Distribution of Alpha-Synuclein in Neurons Using Genetically Encoded Probes for Correlated Light and Electron Microscopy: Implications for Parkinson's Disease Pathogenesis. *J. Neurosci.* **2013**, *33* (6), 2605–2615.

(195) Ou, H. D.; Deerinck, T. J.; Bushong, E.; Ellisman, M. H.; O'Shea, C. C. Visualizing Viral Protein Structures in Cells Using Genetic Probes for Correlated Light and Electron Microscopy. *Methods* **2015**, 1–10.

(196) To, T.-L.; Fadul, M. J.; Shu, X. Singlet Oxygen Triplet Energy Transfer-Based Imaging Technology for Mapping Protein-Protein Proximity in Intact Cells. *Nat. Commun.* **2014**, *5* (May), 1–9.

(197) Souslova, E. A.; Mironova, K. E.; Deyev, S. M. Applications of Genetically Encoded Photosensitizer MiniSOG: From Correlative Light Electron Microscopy to Immunophotosensitizing. *J. Biophotonics* **2016**, *15*, 1–15.

(198) Qi, Y. B.; Garren, E. J.; Shu, X.; Tsien, R. Y.; Jin, Y. Photo-Inducible Cell Ablation in Caenorhabditis Elegans Using the Genetically Encoded Singlet Oxygen Generating Protein MiniSOG. *Proc. Natl. Acad. Sci. U. S. A.* **2012**, *109* (19), 7499–7504.

(199) Lin, J. Y.; Sann, S. B.; Zhou, K.; Nabavi, S.; Proulx, C. D.; Malinow, R.; Jin, Y.; Tsien, R. Y. Optogenetic Inhibition of Synaptic Release with Chromophore-Assisted Light Inactivation (CALI). *Neuron* **2013**, *79* (2), 241–253.

(200) Makhijani, K.; To, T.-L.; Ruiz-González, R.; Lafaye, C.; Royant, A.; Shu, X. Precision Optogenetic Tool for Selective Single- and Multiple-Cell Ablation in a Live Animal Model System. *Cell Chem. Biol.* **2017**, *24* (1), 110–119.

(201) Ryumina, A. P.; Serebrovskaya, E. O.; Shirmanova, M. V; Snopova, L. B.; Kuznetsova, M. M.; Turchin, I. V; Ignatova, N. I.; Klementieva, N. V; Fradkov, A. F.; Shakhov, B. E.; et al. Flavoprotein MiniSOG as a Genetically Encoded Photosensitizer for Cancer Cells. *Biochim. Biophys. Acta* **2013**, *1830* (11), 5059–5067.

(202) Mironova, K. E.; Proshkina, G. M.; Ryabova, A. V.; Stremovskiy, O. A.; Lukyanov, S. A.; Petrov, R. V.; Deyev, S. M. Genetically Encoded Immunophotosensitizer 4D5scFv-MiniSOG Is a Highly Selective Agent for Targeted Photokilling of Tumor Cells in Vitro. *Theranostics* **2013**, *3* (11), 831–840.

(203) Proshkina, G. M.; Shilova, O. N.; Ryabova, A. V; Stremovskiy, O. A.; Deyev, S. M. A New Anticancer Toxin Based on HER2 / Neu-Specific DARPin and Photoactive Flavoprotein MiniSOG. *Biochimie* **2015**, *118*, 116–122.

(204) Shramova, E. I.; Proshkina, G. M.; Chumakov, S. P.; Khodarovich, Y. M.; Deyev, S. M. Flavoprotein MiniSOG Cytotoxicity Can Be Induced By Bioluminescence Resonance Energy Transfer. *Acta Naturae* **2016**, *8* (31), 118–123.

(205) Lammers, T.; Aime, S.; Hennink, W. E.; Storm, G.; Kiessling, F. Theranostic Nanomedicine. *Acc. Chem. Res.* **2011**, *44* (10), 1029–1038.

(206) Kelkar, S. S.; Reineke, T. M. Theranostics: Combining Imaging and Therapy. *Bioconjugate Chem.* **2011**, *22* (10), 1879–1903.

(207) Hally, C.; Rodríguez-amigo, B. Photodynamic Therapy. In *Theranostics and Image Guided Drug Delivery*; 2014; pp 86–122.

(208) Harlaar, N. J.; Koller, M.; de Jongh, S. J.; van Leeuwen, B. L.; Hemmer, P. H.; Kruijff, S.; van Ginkel, R. J.; Been, L. B.; de Jong, J. S.; Kats-Ugurlu, G.; et al. Molecular Fluorescence-Guided Surgery of Peritoneal Carcinomatosis of Colorectal Origin: A Single-Centre Feasibility Study. *Lancet Gastroenterol. Hepatol.* **2016**, *1* (4), 283–290.

(209) Slominski, A.; Desmond, T. J.; Shibahara, S.; Wortsman, J. Melanin Pigmentation in Mammalian Skin and Its Hormonal Regulation. *Physiol. Rev.* **2004**, *84* (4), 1155–1228.

(210) Gray-Schopfer, V.; Wellbrock, C.; Marais, R. Melanoma Biology and New Targeted Therapy. *Nature* **2007**, *445* (7130), 851–857.

(211) Baldea, I.; Filip, A. G. Photodynamic Therapy in Melanoma - an Update. *J. Physiol. Pharmacol.* **2012**, *63* (7), 109–118.

(212) Chang, A. E.; Karnell, L. H.; Menck, H. R. The National Cancer Data Base Report on Cutaneous and Noncutaneous Melanoma. *Cancer* **1998**, *83* (8), 1664–1678.

(213) Kawczyk-Krupka, A.; Bugaj, A. M.; Latos, W.; Zaremba, K.; Sieroń, A. Photodynamic Therapy in Treatment of Cutaneous and Choroidal Melanoma. *Photodiagnosis Photodyn. Ther.* **2013**, *10* (4), 503–509.

(214) Koch, S. E.; Lange, J. R. Amelanotic Melanoma: The Great Masquerader. *J. Am. Acad. Dermatol.* **2000**, *42* (5 I), 731–734.

(215) Jilaveanu, L. B.; Aziz, S. A.; Kluger, H. M. Chemotherapy and Biologic Therapies for Melanoma: Do They Work? *Clin. Dermatol.* **2009**, *27* (6), 614–625.

(216) Monge-Fuentes, V.; Muehlmann, L. A.; de Azevedo, R. B. Perspectives on the Application of Nanotechnology in Photodynamic Therapy for the Treatment of Melanoma. *Nano Rev.* **2014**, *5* (1), 24381.

(217) Lo, J. A.; Fisher, D. E. The Melanoma Revolution: From UV Carcinogenesis to a New Era in Therapeutics. *Science (80-.).* **2014**, *346* (6212), 945–949.

(218) Vera, R. E.; Lamberti, M. J.; Rivarola, V. A.; Rumie Vittar, N. B. Developing Strategies to Predict Photodynamic Therapy Outcome: The Role of Melanoma Microenvironment. *Tumor Biol.* **2015**, *36* (12), 9127–9136.

(219) Davids, L. M.; Kleemann, B. Combating Melanoma: The Use of Photodynamic Therapy as a Novel, Adjuvant Therapeutic Tool. *Cancer Treat. Rev.* **2011**, *37* (6), 465–475.

(220) Huang, Y.; Vecchio, D.; Avci, P.; Yin, R.; Garcia-Diaz, M.; Hamblin, M. R. Melanoma Resistance to Photodynamic Therapy : New Insights. *Biol. Chem.* **2014**, *394* (2), 239–250.

(221) Mroz, P.; Huang, Y. Y.; Szokalska, A.; Zhiyentayev, T.; Janjua, S.; Nifli, A. P.; Sherwood, M. E.; Ruzie, C.; Borbas, K. E.; Fan, D.; et al. Stable Synthetic Bacteriochlorins Overcome the Resistance of Melanoma to Photodynamic Therapy. *FASEB J.* **2010**, *24* (9), 3160–3170.

(222) Pereira, N. A. M.; Laranjo, M.; Pineiro, M.; Serra, A. C.; Santos, K.; Teixo, R.; Abrantes, A. M.; Gonçalves, A. C.; Sarmento Ribeiro, A. B.; Casalta-Lopes, J.; et al. Novel 4,5,6,7-Tetrahydropyrazolo[1,5-a]Pyridine Fused Chlorins as Very Active Photodynamic Agents for Melanoma Cells. *Eur. J. Med. Chem.* **2015**, *103*, 374–380.

(223) Baldea, I.; Olteanu, D. E.; Bolfa, P.; Tabaran, F.; Ion, R. M.; Filip, G. A. Melanogenesis and DNA Damage Following Photodynamic Therapy in Melanoma with Two Meso-Substituted Porphyrins. *J. Photochem. Photobiol. B Biol.* **2016**, *161*, 402–410.

(224) Pereira, N. A. M.; Laranjo, M.; Sarmento-ribeiro, A. B.; Pi, M.; Gonçalves, A. C.; Melo, S. De; Botelho, M. F.; Pinho, T. M. V. D.; S, J. Advances on Photodynamic Therapy of Melanoma through Novel Ring-Fused 5 , 15-Diphenylchlorins. *Eur. J. Med. Chem.* **2018**, *146*, 395–408.

CHAPTER 2

General techniques and methods

This chapter describes the common photophysical techniques and methods that have been employed in this work and the general aspects of the fluorescence microscopy techniques used.

I've always been attracted to colors.
Color helps make the work more interesting and endurable.
It helps when things aren't going well.
Roger Y. Tsien

2.1. Steady-state optical techniques

In steady-state spectroscopies the samples are continuously irradiated with a beam of light at a very low intensity, creating and eliminating excited states in a continuous manner and reaching eventually a steady-state where their concentration remains constant.[1] This facilitates the measurement of weak signal levels at the expense of losing kinetic information. Steady-state spectroscopies are best applied to the measurement of absorption and emission spectra.

All spectroscopic measurements were performed using 1 cm path quartz cuvettes (Hellma), at room temperature and under magnetic stirring. Purified proteins were diluted in H_2O or D_2O-based solutions of Phosphate Buffered Saline at pH 7.4 (hereafter PBS and dPBS, respectively).

2.1.1. Absorbance

Absorption spectra were recorded on a double beam Cary 6000i UV-Vis-NIR spectrophotometer (Agilent Technologies, Santa Clara, CA, USA).

2.1.2. Fluorescence

Fluorescence excitation and emission spectra were registered in a Fluoromax-4 spectrofluorometer (Horiba Jobin-Yvon, Edison, NJ).

Fluorescence quantum yields ($\Phi_{F,}$) were determined by comparing the area under the emission curve (AUC) for optically matched solutions of the protein sample, and FMN, as the fluorescent reference, with $\Phi_{F,FMN} = 0.25$.[2] The absorbance of the sample and reference solutions was adjusted to be below 0.1 at the excitation wavelength to prevent inner filter effects.

$$\phi_{\mathrm{F}} = \phi_{\mathrm{F,Ref}} \left(\frac{\mathrm{AUC_{prot}}}{\mathrm{AUC_{Ref}}} \right) \qquad \textbf{Equation 2.1.}$$

2.2. Time-resolved optical techniques

Time-resolved optical techniques enable the detection of excited states or intermediate species upon pulsed irradiation of a sample with a light source whose intensity fluctuates as a function of time. Once these species are formed, they can be monitored through changes in the signal intensity of an analyzing beam (for absorption spectroscopy) or through photon emission (in the case of fluorescence or phosphorescence spectroscopy), in all cases the detection being

temporally resolved.[1,3] Therefore, time-resolved spectroscopies provide kinetic information at the expense of a lower sensitivity compared to steady-state techniques.

Nowadays these techniques are usually coupled to photon counting detectors due to their better time resolution, better sensitivity and lower interference from sensitizer luminescence or scattered laser light compared to analog detectors. Photomultiplier tubes (PMTs) are detectors the response of which is based on the initiation and amplification of a pulse of electrical current when a photon strikes their surface,[4] a principle that has inspired the photon counting mode. There are mainly three photon counting techniques, namely gated photon counting (GPC), multichannel scaling (MCS) and time-correlated single photon counting (TCSPC).[4] In the present work, only the last two have been employed to perform the experiments.

2.2.1. Time-correlated single photon counting

This method is common for time-resolved fluorescence measurements and it is based on the precisely timed registration of the first single photon arrival to the detector from the emitting sample.[5] Therefore, when a photon is detected, the time of the corresponding detector pulse in the signal period is measured. The cumulative signal obtained from repetitive cycles is a histogram of photon arrivals per time bin which represents the time decay one would have obtained from the observation of a single excitation-emission cycle[6] (Figure 2.1). This approach provides the most accurate timing of the photon among all photon-counting techniques, down to a few picoseconds per channel. For this reason, TCSPC is the technique of choice when time resolution is the prime need, at the expense of a much longer acquisition time to build up the count histogram.[4] In addition, this technique requires keeping the probability of registering more than one photon per cycle low, that is, to keep the count rate at the detector equal or below 1% of the excitation rate.[4]

The effective resolution of a TCSPC experiment is characterized by its instrument response function (IRF). The IRF contains the pulse shape of the light source used, the temporal dispersion in the optical system, the transit time spread in the detector, and the timing jitter in the recording electronics.[5] Measurement of the IRF is typically achieved by placing scattering medium at the sample compartment and collecting the scattered excitation light. Finally, deconvolution of the measured fluorescence decay and the IRF is performed by proper software for data analysis.

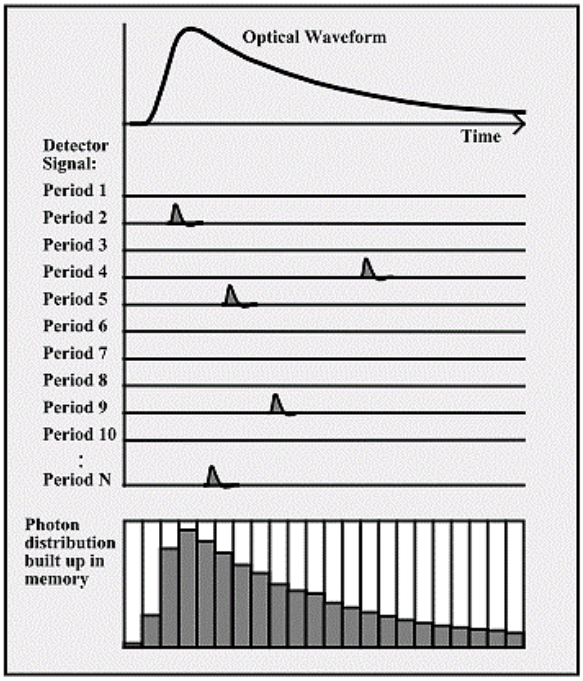

Figure 2.1. Principle of classic TCSPC. Image from Ref. 6.

Time-resolved fluorescence measurements were carried out using a customized PicoQuant Fluotime 200 fluorescence lifetime system (PicoQuant GmbH, Berlin, Germany) and the FluoFit 5.0 software for data analysis. Excitation was achieved by means of a pulsed LED source emitting at 405 nm or a picosecond diode laser at 375 nm (PicoQuant, 10 MHz repetition rate, 50 ps pulse width), depending on the study. Absorbance of the samples was kept below 0.1 at the excitation wavelength in all cases and the photon counting rate was kept below 1%. The IRF signal was measured by placing a cuvette with a suspension of Ludox® in water.

2.2.2. Time-resolved NIR phosphorescence detection

This technique is commonly used for direct and specific monitoring of the $^1O_2$ formation and decay, measure its lifetime (τ_Δ) and quantify its photogeneration quantum yield (Φ_Δ). It is based on the time-resolved detection of its weak NIR phosphorescence centered at 1275 nm. In this case, the photon-counting method is MCS, in which all detected photons are counted and sorted out in the different positions of a board memory, thus the time distribution of the detected photons is obtained at once.[4] Direct optical detection of $^1O_2$ is used broadly for three main purposes: (1) as an analytical tool to demonstrate that $^1O_2$ has indeed been created in a system, (2) to quantify the amount of $^1O_2$ created, and (3) to obtain kinetic information related to its production, diffusion, and decay.[7]

The $^1O_2$ detection system is mainly composed by a light source to photoexcite the sample, a NIR detector, a monochromator or bandpass filters to isolate the $^1O_2$ emission and a set of lenses to collect and focus the emitted photons onto the detector. A scheme of the typical $^1O_2$ detection setup is shown in Figure 2.2, which has been reproduced from the recent review in direct $^1O_2$ NIR phosphorescence detection methods from Nonell and Flors.[7]

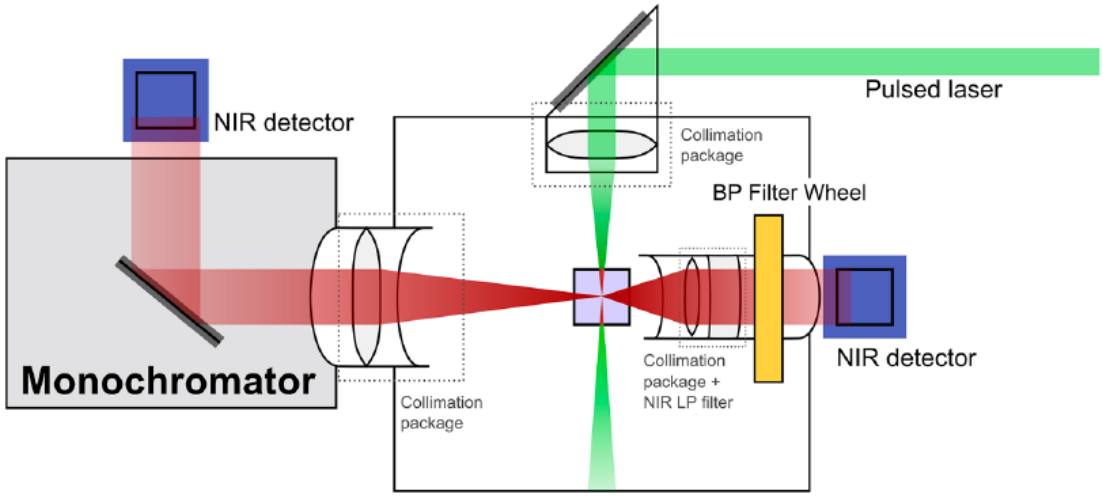

Figure 2.2. Generic scheme of the direct $^1O_2$ NIR phosphorescence detection system. Image from Ref. 7.

Time-resolved NIR phosphorescence signals at 1275 nm were measured using a customized PicoQuant Fluotime 200 lifetime system. Two different pulsed lasers were employed depending on the wavelength used for excitation. On one hand, irradiation at 355 nm or 532 nm was achieved with the frequency-tripled or doubled output of a diode-pumped pulsed Nd:YAG laser (FTSS355-Q, Crystal Laser, Berlin, Germany), respectively, working a 1 kHz repetition rate, which produces 1 ns pulse width laser pulses at either 355 nm (0.5 mW, or 0.5 μJ per pulse) or at 532 nm (1.2 mW, 1.2 mJ per pulse). On the other hand, an AO-Z-473 solid state acousto-optic modulator (AOM) Q-switched laser (Changchun New Industries Optoelectronics Technology Co., China) was used for excitation at 473 nm, working at 1.5 kHz repetition rate (<1.5 mW average power). For both lasers sources, an uncoated SKG-5 filter (CVI Laser Corporation, Albuquerque, U.S.A.) was placed at the exit port of the laser to remove any residual NIR component. The luminescence exiting from the sample was filtered by an 1100 nm long-pass filter (Edmund Optics, York, U.K.) and a narrow bandpass filter at 1275 nm (bk-1270-70-B, bk Interfernzoptik, Germany) to remove any scattered laser radiation and isolate the singlet oxygen emission. A thermoelectric-cooled near-IR sensitive photomultiplier tube assembly (H9170−45, Hamamatsu Photonics Hamamatsu City, Japan) in combination with an MCS (NanoHarp 250, PicoQuant

Gmbh, Germany) was used as photon-counting detector. The time-resolved $^1O_2$ emission decays were analyzed by fitting Equation 2.2[8] to the data using GraphPad Prism 5.

$$S(t) = S_0 \frac{\tau_\Delta}{\tau_\Delta - \tau_T} \left(e^{-\frac{t}{\tau_\Delta}} - e^{-\frac{t}{\tau_T}} \right) \quad \textbf{Equation 2.2.}$$

where τ_T and τ_Δ are the lifetimes of the PS triplet excited state and of $^1O_2$, respectively, and S_0 is a quantity proportional to Φ_Δ.[7] Thus, the transient signal obtained from direct optical detection of $^1O_2$ provides valuable information on both the efficiency and kinetics of $^1O_2$ production.

For some protein samples, two independent populations of triplet excited states were observed, each producing $^1O_2$ with its own set of kinetics and yields. In these cases, $^1O_2$ signals were analyzed with Equation 2.3.[9]

$$S(t) = S_{01} \frac{\tau_\Delta}{\tau_\Delta - \tau_{T_1}} \left(e^{-\frac{t}{\tau_\Delta}} - e^{-\frac{t}{\tau_{T_1}}} \right) + S_{02} \frac{\tau_\Delta}{\tau_\Delta - \tau_{T_2}} \left(e^{-\frac{t}{\tau_\Delta}} - e^{-\frac{t}{\tau_{T_2}}} \right) \quad \textbf{Equation 2.3.}$$

The quantum yield of singlet oxygen production, Φ_Δ, was calculated by comparing the fitted S_0 values for the protein of interest and for optically-matched solutions of the reference PS, according to Equation 2.4 or Equation 2.5,[8] depending on the existence of one or two ^{3}PS*. Selected reference PSs were FMN, Φ_Δ= 0.57[10], sodium 1H-phenalen-1-one-2-sulphonate (PNS), Φ_Δ= 0.97[11,12] and Rose Bengal, Φ_Δ= 0.75.[13]

$$\phi_\Delta = \phi_{\Delta_{\mathrm{Ref}}} \frac{S_{0\mathrm{Prot}}}{S_{0_{\mathrm{Ref}}}} \quad \textbf{Equation 2.4.}$$

$$\phi_\Delta = \phi_{\Delta_{\mathrm{Ref}}} \frac{S_{01\mathrm{Prot}} + S_{02\mathrm{Prot}}}{S_{0_{\mathrm{Ref}}}} \quad \textbf{Equation 2.5.}$$

The absorbance of the sample and reference solutions at the excitation wavelength was again kept below 0.1 to prevent inner-filter effects.

2.2.3. UV-Vis nanosecond laser flash photolysis

This technique is typically employed to study the properties of triplet excited states in a time-resolved manner. It allows studying the disappearance of the excited state, the formation of reactive intermediates, and the formation of photochemically generated products. Laser flash photolysis (LFP) is a pump-and-probe technique in which the sample is excited by a strong pulse of light (called pump beam) from a laser of nano-, pico-, or femtosecond pulse, at a wavelength where ground state absorption occurs, and a broadband light source in the UV-Vis-NIR spectral

range (called probe beam) to probe the changes in absorbance (ΔA). In a typical LFP experiment, a fast shutter exposes the sample to the probe beam shortly before the laser pulse hits the sample, and is closed after the end of data collection to prevent its photobleaching.[1] A schematic representation of the common setup is depicted in Figure 2.3.

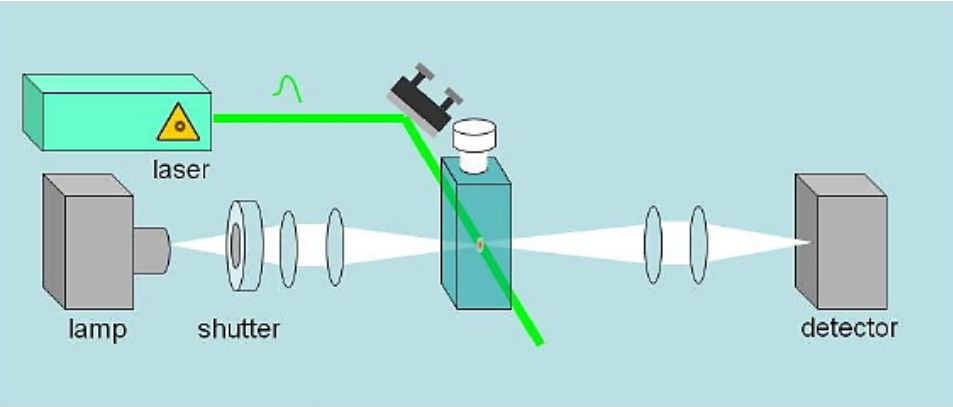

Figure 2.3. Illustration of the experimental setup for nanosecond UV-VIS laser flash photolysis, from Ref. 1.

Transient absorption experiments in the UV-Vis region were carried out using a home-built nanosecond LFP system. In this instrument, the 3rd harmonic (355 nm) of a Continuum Surelite I-10 Nd:YAG laser (5 ns pulse width, 7.5 mJ per pulse) was directed to the sample. The luminescence exiting from the sample was filtered by a 610 nm long-pass filter (CVI Laser Corporation, NM, USA). Changes in the sample absorbance were detected at 715 nm using a Hamamatsu R928 photomultiplier to monitor the intensity variations of an analysis beam produced by a 75 W short arc Xe lamp (USHIO) and spectral discrimination was obtained using a PTI 101 monochromator. The signal was fed to a Lecroy Wavesurfer 454 oscilloscope for digitizing and averaging (1 - 10 shots) and finally transferred to a PC for data storage and analysis. The TTL sync output of the laser was used to trigger the oscilloscope. The energy of the laser pulse was varied using neutral density filters and measured with a pyroelectric energy meter (RJP 735 and RJ 7610) from Laser Precision Corp. The system was controlled using the in-house-developed LKS software (LabView, National Instruments).

2.3. Bright field and fluorescence microscopy

Optical or light microscopy is a key tool in modern cell biology. This technique employs microscopes to closely view a sample through the magnification of a lens with visible light. The evolution of microscopes over the past centuries has been a matter of intense research aiming

at improving resolution and contrast. Modern instruments and techniques now allow unprecedented detail of visualization and study of subcellular structures and bioprocesses, even in a 4D (x-y-z-t) situation.[14,15] The field has been very active and only in the last years several improvements have pushed optical microscopy towards single molecule tracking and imaging systems, allowing to coin the term optical nanoscopy.[16] Not surprisingly, the development of super-resolution microscopy techniques was awarded the Nobel Prize in Chemistry in 2014.

There is a large variety of light microscopy modalities that allow different approaches for the study of cellular events. However, these techniques are commonly classified into two categories: bright field and fluorescence microscopy[17] (Figure 2.4).

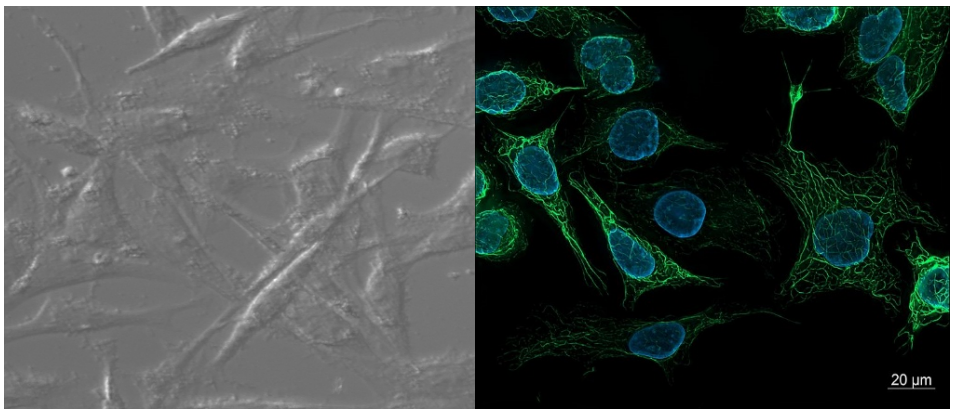

Figure 2.4. Examples of bright field image of melanoma cells (left) and fluorescence microscopy (right). The right picture is from ZEISS Microscopy and licensed in Wikimedia Commons.

2.3.1. Bright field microscopy

In bright field microscopy, the specimen is illuminated with transmitted light, this is, the light source and the detection objective are placed on opposite sides of the sample and the sample is imaged by its effect on the light passing through it. This yields dark objects on a bright background and because most cells are thin and transparent, they do not absorb much light and so are difficult to see without adding optical modifications. The two most commonly used techniques in bright field microscopy are phase contrast, which causes cells to appear dark on a light background and differential interference contrast (DIC), which gives a pseudo–three-dimensional (3D) shaded appearance to cells.[18] Bright field is usually sufficient to see the general outlines of cells, but phase contrast or DIC is necessary to achieve detailed, high-contrast bright field images.[17]

2.3.2. Fluorescence microscopy: wide field, confocal and fluorescence lifetime imaging

Fluorescence microscopy requires that the objects of interest fluoresce since they are themselves the light source. This constitutes one essential advantage over bright field microscopy since even when a structure is too small to be resolved by a light microscope, the emitted light remains visible. However, most molecules in the cell are not very fluorescent and therefore, fluorophores have to be incorporated into the specimen. It can be achieved either by the addition of organic dyes or by the genetic introduction of a fluorescent protein. The current available fluorescent dyes and FPs provide specific subcellular targeting as well as numerous color alternatives.[19–21]

Fluorescence microscopy is typically performed using epifluorescence, in which excitation of the fluorophore and detection of the fluorescence are done through the same light path (objective) by means of a fluorescence filter cube that contains a barrier filter and a dichroic mirror.[14] These microscopes are broadly used in biology for routine imaging, such as with the wide field microscope and are the basis for more advanced microscope designs, including the confocal microscope.

In a conventional wide field optical epifluorescence microscope, the entire specimen is bathed in light from a mercury or xenon source and the image can be viewed directly by eye or projected onto an image capture device or photographic film.[22] When using such microscopes, secondary fluorescence emitted by the specimen often occurs through the excited volume and obscures resolution of features that lie in the objective focal plane.[17] This situation is especially problematic for specimens having a thickness greater than about 2 micrometers, which usually exhibit such a high degree of fluorescence emission that most of the fine detail is lost.[19]

Confocal microscopy provides higher resolution. This is firstly achieved by the use of lasers for illumination, which narrows the excitation range to 2–3 nm. This is around 10 times narrower than the range of wavelengths one typically gets when using excitation filters.[23] Additionally, confocal microscopes obtain the image from just one focal plane, while removing the fluorescence from out-of-focus planes. Furthermore, it has the capability to collect serial optical sections from thick specimens such as rounded cells and tissue sections.[20,24] This is accomplished by illuminating the specimen with a focused scanning laser beam (point scanning) and by placing a pinhole aperture in the image plane in front of an electronic photon detector.[18,19] An improved approach is the spinning disk confocal microscopy which relies on the use of a disk of pinholes that sweep across the sample, improving the time resolution and generating a real confocal image that can be directly viewed by the eye or captured by high-sensitivity camera.[25]

Fluorescence lifetime imaging microscopy (FLIM) is a technique in which the mean fluorescence lifetime of a chromophore is measured at each spatially resolvable element of a microscope image.[26] The main advantage in FLIM is that the nanosecond excited-state lifetime is mostly independent of variations in fluorophore concentration, illumination intensity or processes such as photobleaching or leakage.[26] Furthermore, FLIM is dependent upon excited-state reactions such as (FRET). These properties of fluorescence lifetimes allow exploration of the molecular environment of fluorophores that are spectrally identical.[26–28] Among FLIM, additional improvement can be achieved by 2PE. Because of the nonlinear properties of 2PE, the generated fluorescence is restricted only to the small focal volume. The low-energy NIR light and the highly localized excitation strongly reduce global photobleaching of the fluorophore and tissue damage. Moreover, the NIR light used in 2P microscopy allows deeper tissue penetration and imaging.[29,30]

In the present work, two confocal and a 2P-FLIM microscope have been employed. At the Jülich Forschungszentrum (Germany) under the supervision of Dr. Thomas Gensch, confocal imaging was performed a confocal laser scanning microscope (cLSM 710, Carl Zeiss, Germany) equipped with laser lines at 405, 488, 561, and 633 nm and an EC plan-Neofluar 40×/1.30 Ph3 oil-immersion objective. Live cell imaging was performed under cell culture conditions (37 °C and 5% CO_2). Image acquisition and analysis were carried out with the manufacturer's software (ZEN, Carl Zeiss). 2P-FLIM imaging was performed upright fluorescence microscope (A1 MP; Nikon, Amsterdam, The Netherlands) equipped with a 25x water immersion objective (Numerical Aperture (NA) 1.1; WD 2 mm; XYZ, Nikon), fluorescence was stimulated by 100 fs light pulses (λ_{exc} = 880 nm) by 2PE. Laser pulses were generated at a frequency of 80 MHz by a mode-locked Titan-Sapphire laser (Mai Tai DeepSee, Newport Spectra Physics; Irvine, CA; output power 2.3 W at 880 nm). Mean fluorescence lifetimes were measured using multidimensional TCSPC. Lifetime images were analyzed using SPCImage 4.8 (Becker & Hickl).

At the University of California San Francisco UCSF (USA), under the supervision of Dr. Xiaokun Shu, confocal microscopy was performed on a Nikon Eclipse Ti Inverted Microscope equipped with a CSU-W1 confocal scanner unit (Yokogawa), a digital ORCA-Flash4.0 CMOS camera (Hamamatsu), an ASI MS-2000 XYZ Automated Stage (Applied Scientific Instrumentation) and a Nikon Plan Apo λ 20x air (NA 0.75) objective. Laser inputs were provided by an Integrated Laser Engine (Spectral Applied Research) equipped with laser lines of 405 nm, 488 nm, 561 nm, and 640 nm (Coherent). The confocal scanning unit was equipped with the following emission filters: 460/50 nm, 525/50 nm, 610/60 nm, 661/20 nm, 732/60 nm, and 731/137 nm. Images were analyzed and processed with ImageJ.

2.4. References

(1) Nonell, S.; Viappiani, C. Basic Spectroscopy. In *Photobiological Sciences Online*; Lee, J., Smith, K. C., Eds.; American Society for Photobiology, 2007.

(2) Wingen, M.; Potzkei, J.; Endres, S.; Casini, G.; Rupprecht, C.; Fahlke, C.; Krauss, U.; Jaeger, K.-E.; Drepper, T.; Gensch, T. The Photophysics of LOV-Based Fluorescent Proteins – New Tools for Cell Biology. *Photochem. Photobiol. Sci.* **2014**, *13* (6), 875–883.

(3) Abbruzzetti, S.; Bruno, S.; Faggiano, S.; Grandi, E.; Mozzarelli, A.; Viappiani, C. Time-Resolved Methods in Biophysics. 2. Monitoring Haem Proteins at Work with Nanosecond Laser Flash Photolysis. *Photochem. Photobiol. Sci.* **2006**, *5* (12), 1109–1120.

(4) Jiménez-Banzo, A.; Ragàs, X.; Kapusta, P.; Nonell, S. Time-Resolved Methods in Biophysics. 7. Photon Counting vs. Analog Time-Resolved Singlet Oxygen Phosphorescence Detection. *Photochem. Photobiol. Sci.* **2008**, *7* (9), 1003–1010.

(5) Becker, W. *Advanced Time-Correlated Single Photon Counting Techniques*; Castleman, A. W., Toennies, J. P., Zinth, W., Eds.; Springer Series in Chemical Physics; Springer Berlin Heidelberg: Berlin, Heidelberg, 2005; Vol. 81.

(6) Becker, W.; Bergmann, A.; Biscotti, G.; Rück, A. Advanced Time-Correlated Single Photon Counting Technique for Spectroscopy and Imaging in Biomedical Systems. *Springer* **2004**, *5340*, 1–9.

(7) Nonell, S.; Flors, C. Chapter 25. Steady-State and Time-Resolved Singlet Oxygen Phosphorescence Detection in the Near-IR. In *Singlet Oxygen: Applications in Biosciences and Nanosciences*; Nonell, S., Flors, C., Eds.; Royal Society of Chemistry, 2016; pp 7–26.

(8) Nonell, S.; Braslavsky, S. E. Time-Resolved Singlet Oxygen Detection. *Methods Enzymol.* **2000**, *319*, 37–49.

(9) Torra, J.; Burgos-Caminal, A.; Endres, S.; Wingen, M.; Drepper, T.; Gensch, T.; Ruiz-González, R.; Nonell, S. Singlet Oxygen Photosensitisation by the Fluorescent Protein Pp2FbFP L30M, a Novel Derivative of Pseudomonas Putida Flavin-Binding Pp2FbFP. *Photochem. Photobiol. Sci.* **2015**, *14* (2), 280–287.

(10) Rodríguez-Pulido, A.; Cortajarena, A. L.; Torra, J.; Ruiz-González, R.; Nonell, S.; Flors, C. Assessing the Potential of Photosensitizing Flavoproteins as Tags for Correlative Microscopy. *Chem. Commun.* **2016**, *52* (54), 8405–8408.

(11) Nonell, S.; González, M.; Trull, F. R. 1H-Phenalen-1-One-2-Sulfonic Acid: An Extremely Efficient Singlet Molecular Oxygen Sensitizer for Aqueous Media. *Afinidad* **1993**, *44*, 445–450.

(12) Martí, C.; Jürgens, O.; Cuenca, O.; Casals, M.; Nonell, S. Aromatic Ketones as Standards for Singlet Molecular Oxygen Photosensitization. Time-Resolved Photoacoustic and near-IR Emission Studies. *J. Photochem. Photobiol. A Chem.* **1996**, *97* (1–2), 11–18.

(13) Allen, M. T.; Lynch, M.; Lagos, A.; Redmond, R. W.; Kochevar, I. E. A Wavelength Dependent Mechanism for Rose Bengal-Sensitized Photoinhibition of Red Cell Acetylcholinesterase. *BBA - Gen. Subj.* **1991**, *1075* (1), 42–49.

(14) Lichtman, J. W.; Conchello, J.-A. Fluorescence Microscopy. *Nat. Methods* **2005**, *2* (12), 910–919.

(15) Lavagnino, Z.; Sancataldo, G.; D'Amora, M.; Follert, P.; De Pietri Tonelli, D.; Diaspro, A.; Cella Zanacchi, F. 4D (x-y-z-t) Imaging of Thick Biological Samples by Means of Two-Photon Inverted Selective Plane Illumination Microscopy (2PE-ISPIM). *Sci. Rep.* **2016**, *6* (March), 1–9.

(16) Hell, S. W. Toward Fluorescence Nanoscopy. *Nat. Biotechnol.* **2003**, *21* (11), 1347–1355.

(17) Thorn, K. A Quick Guide to Light Microscopy in Cell Biology. *Mol. Biol. Cell* **2016**, *27* (2), 219–222.

(18) Murphy, D. B. *Fundamentals of Light Microscopy and Electronic Imaging*; John Wiley & Sons, Inc., 2001; Vol. 83.

(19) Stephens, D. J.; Allan, V. J. Light Microscopy Techniques for Live Cell Imaging. *Science (80-.).* **2003**, *300* (5616), 82–86.

(20) Spring, K. R.; Davidson, M. W. Introduction to Fluorescence Microscopy https://www.microscopyu.com/techniques/fluorescence/introduction-to-fluorescence-microscopy (accessed Feb 14, 2018).

(21) Ettinger, A.; Wittmann, T. *Fluorescence Live Cell Imaging*, 1st ed.; Elsevier Inc., 2014; Vol. 123.

(22) Paddock, S. W.; Fellers, T. J.; Davidson, M. W. Introductory Confocal Concepts https://www.microscopyu.com/techniques/confocal/introductory-confocal-concepts (accessed Feb 14, 2018).

(23) Epifluorescence Microscope Basics https://www.thermofisher.com/es/es/home/life-science/cell-analysis/cell-analysis-learning-center/molecular-probes-school-of-fluorescence/fundamentals-of-fluorescence-microscopy/epifluorescence-microscope-basics.html (accessed Feb 14, 2018).

(24) Fellers, T. J.; Davidson, M. W. Concepts in Confocal Microscopy https://www.olympus-lifescience.com/en/microscope-resource/primer/techniques/confocal/confocalintro/ (accessed Feb 14, 2018).

(25) Nakano, A. Spinning-Disk Confocal Microscopy -- a Cutting-Edge Tool for Imaging of Membrane Traffic. *Cell Struct. Funct.* **2002**, *27*, 349–355.

(26) Bastiaens, P. I.; Squire, A. Fluorescence Lifetime Imaging Microscopy: Spatial Resolution of Biochemical Processes in the Cell. *Trends Cell Biol.* **1999**, *9* (98), 48–52.

(27) Suhling, K.; French, P. M. W.; Phillips, D. Time-Resolved Fluorescence Microscopy. *Photochem. Photobiol. Sci.* **2005**, *4* (1), 13–22.

(28) Becker, W. Fluorescence Lifetime Imaging - Techniques and Applications. *J. Microsc.* **2012**, *247* (2), 119–136.

(29) Zipfel, W. R.; Williams, R. M.; Webb, W. W. Nonlinear Magic: Multiphoton Microscopy in the Biosciences. *Nat. Biotechnol.* **2003**, *21* (11), 1369–1377.

(30) Hille, C.; Lahn, M.; Dosche, C. Two-Photon Fluorescence Lifetime Imaging (2P-FLIM) for Ion Sensing in Living Cells. *PicoQuant* **2008**, 1–5.

CHAPTER 3

Methods for the characterization of genetically encoded photosensitizers

Initial attempts to characterize the photophysical and photosensitizing properties of FbFPs have suffered from lack of reproducibility throughout the study. In particular, both the ability and the kinetics of singlet oxygen production have shown remarkable changes over time. This has motivated the development of a new methodology for the in-house protein production, which has allowed the robust and reproducible characterization of fresh protein samples.

…que la vida que ens hem perdut,
simplement no existeix.
Manel

3.1. Motivation

Since the pioneering work of Drepper *et al*.[1] that restored the fluorescent properties of FMN in flavoproteins by abolishing the cysteine photoadduct formation, flavin-binding fluorescent proteins (FbFPs) have become an attractive alternative to GFP as fluorescent reporters of cellular events.[2,3] The group of Dr. Drepper in collaboration with the group of Dr. Gensch, both at the Jülich Forschungszentrum in Germany, have been actively working on the development of novel FbFPs and they have engineered new variants from microbial and plant LOV photoreceptors. The early characterization of the fundamental photophysical properties revealed some interesting spectroscopic differences between them,[4] particularly regarding the Φ_F and photostability. Therefore, although all the flavoproteins encase the same FMN chromophore, its interactions with the surrounding amino acids notably modulates the optical properties. On the other hand, neither the ability to photosensitize $^1O_2$ nor the antimicrobial properties have been studied in detail so far. Because these fluorescent proteins are evolved from different organisms, the exploration of both the photosensitizing and photokilling abilities can provide new insights on the interactions between FMN and nearby residues and allow a better understanding of the factors that affect the $^1O_2$ production. This information will be of great value to rationalize the development of new variants with higher potential as fully genetically encoded PSs.

At the beginning of the project, fractions containing the purified proteins in PBS buffer were received from the group of Dr. Drepper (Figure 3.1).

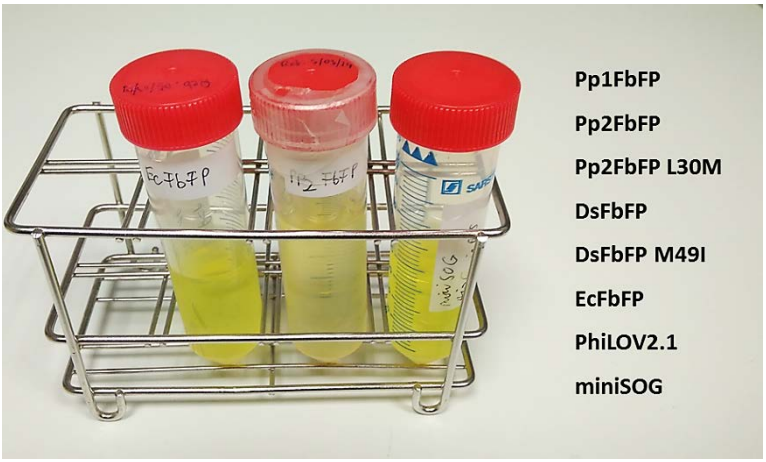

Figure 3.1. Examples and list of the purified proteins received from the group of Dr. Drepper.

All the protein samples were initially characterized in the original PBS buffer, as received. Both the absorption and fluorescence spectra were routinely recorded prior to the study of both the $^1O_2$ photosensitization and the properties of the triplet excited state of the flavin

chromophore, ^{3}FMN*. First attempts to quantify the $^1O_2$ production were performed in PBS using a pulsed laser illuminating at λ_{ex} = 355 nm for excitation. The frequency of the laser had to be ten-fold decreased in order to allow the study of long triplet lifetimes observed for these proteins. In these conditions, the $^1O_2$ signal was extremely weak and prolonged irradiation times of up to three hours were required to obtain reliable data suitable for analysis (Figure 3.2). Furthermore, common strategies to enhance the $^1O_2$ signal such as solvent deuteration, which increases the $^1O_2$ lifetime (τ_Δ) and facilitates its detection,[5] turned out to be impractical because of severe protein dilution, which decreased $^1O_2$ signal intensities even more. Despite all these limitations, early studies on the $^1O_2$ production were carried out, and particular attention was primarily focused on the Pp2FbFP L30M mutant, whose characterization led to the publication cited in Reference 6.

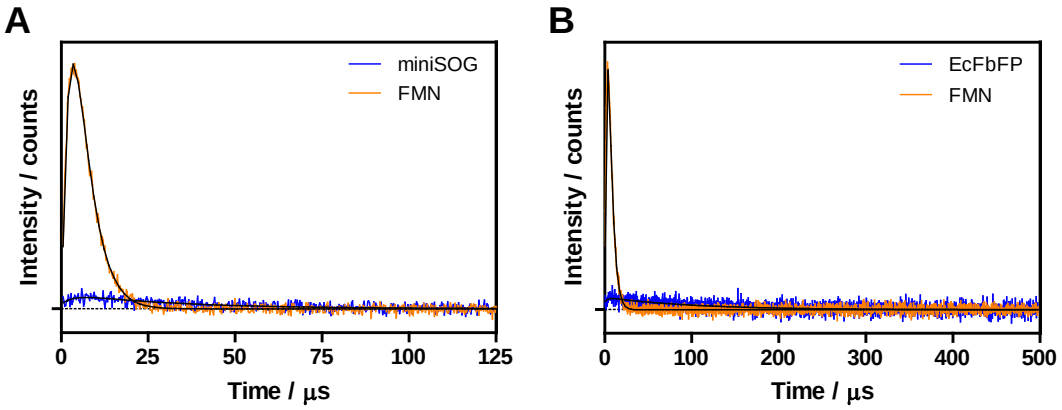

Figure 3.2. Representative $^1O_2$ transients from optically matched solutions of (A) miniSOG and FMN and (B) EcFbFP and FMN (right), in PBS. Notice the difference in the time scale between the two proteins. Fitting lines are in black. λ_{ex} = 355 nm and the irradiation time was 2 hours for each protein and for free FMN references.

3.1.1 Pp2FbFP L30M, first case of study.

The photophysical properties of Pp2FbFP L30M were characterized in PBS (Figure 3.3). The absorption and fluorescence spectra were slightly blue-shifted relative to those of FMN and showed more vibronic structure, indicating that the chromophore is tightly bound and confined to the protein active pocket (Figure 3.3A). Interestingly, the $^1O_2$ kinetics were more complex than previously reported studies on FbFPs and a tri-exponential decay was observed (Figure 3.3B). A comprehensive study of the triplet excited state properties was performed by means of laser flash photolysis and revealed the existence of two independent FMN triplet states; a short-lived (~2.6 µs) and a long-lived (~84 µs) in air-saturated PBS (Figure 3.3 C).

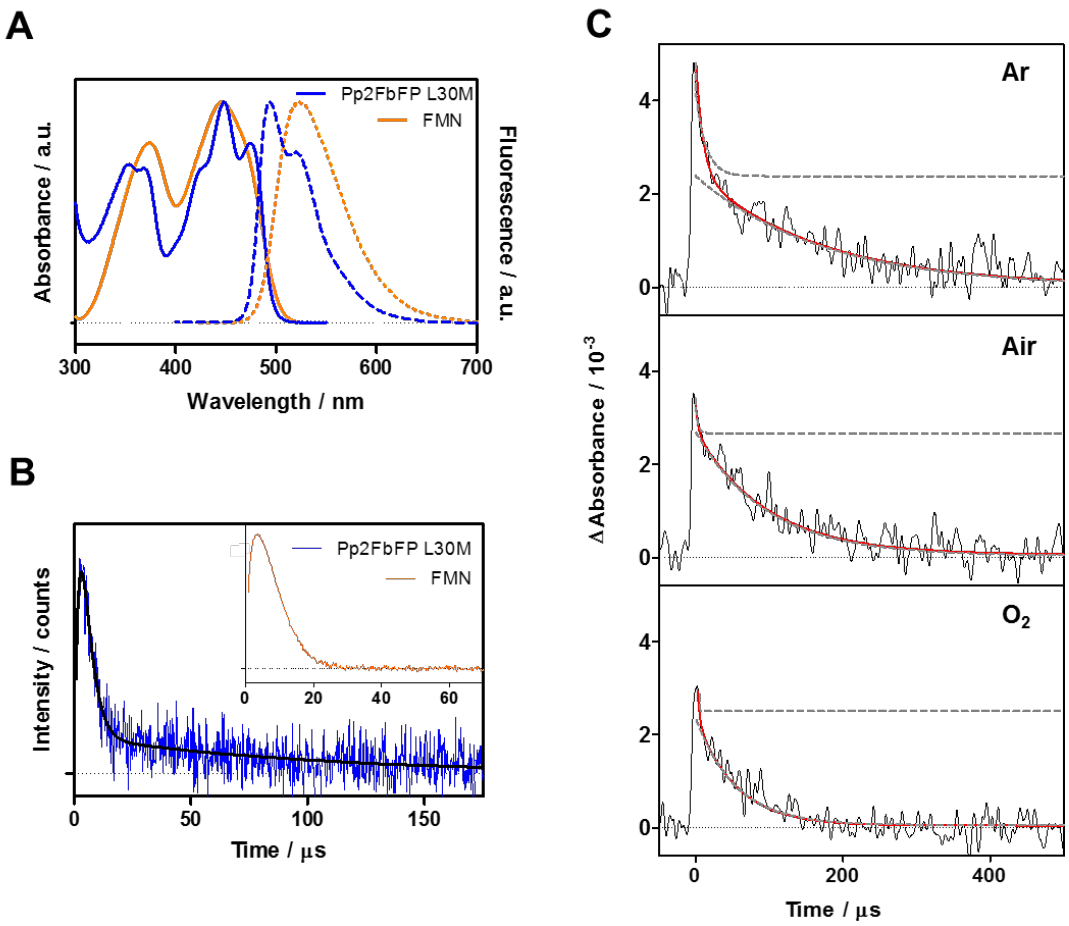

Figure 3.3. A) Normalized absorption (solid lines) and emission (dashed lines) spectra of Pp2FbFP L30M (blue) and FMN (orange) in PBS, pH 7.4, λ_{exc} = 355 nm. B) Time-resolved $^1O_2$ phosphorescence in air-saturated PBS solution. The corresponding trace for FMN is shown in the inset for comparison; notice the absence of the long-lived tail. Fitted function in black. The Y-axes are in log scale. λ_{exc} = 355 nm; λ_{obs} = 1275 nm. C) Transient absorption decays in argon (Ar), air and oxygen (O_2)-saturated PBS solutions. The overall fit (solid line) and individual decay components (dashed lines) are shown for comparison of their relative contributions to the overall signal. Transients are the average of 4 shots. λ_{exc} = 355 nm and λ_{obs} = 700 nm. Images adapted from Ref.6.

The oxygen concentration in the solution was modified by circulating solvent-saturated oxygen or argon over the solution surface for at least 30 minutes, while stirring the solution, to avoid protein denaturation at the air-water interference of bubbles that occur when passing the gas through the solution. This allowed the determination of the rate constants for oxygen quenching of ^{3}FMN* ($k_q^{O_2}$), which provides information on the accessibility of oxygen to the flavin within the protein, and the proportion of triplets quenched by oxygen ($P_T^{O_2}$), which reflects the ability of oxygen to trap ^{3}FMN* molecules before the decay. Equations 3.1 and 3.2 were used for the calculation of $k_q^{O_2}$ and $P_T^{O_2}$, respectively.

$$\frac{1}{\tau_T} = \frac{1}{\tau_T^0} + k_q^{O_2}[O_2] \quad \text{Equation 3.1.}$$

$$P_T^{O_2} = 1 - \frac{\tau_T}{\tau_T^0} \quad \text{Equation 3.2.}$$

where τ_T^0 and τ_T are the triplet lifetimes in the absence and presence of oxygen, respectively.

For the short-lived triplet, the $k_q^{O_2}$ was similar to that of free FMN, indicating a very exposed flavin, which allows for an efficient trapping by molecular oxygen. In contrast, the long-lived triplet was far less accessible and the trapping efficiency was much lower. The properties of the first singlet and triplet excited states of Pp2FbFP L30M and free FMN in solution are collected in Table 3.1 and Table 3.2, respectively.

Table 3.1. Spectroscopic data for the singlet state of Pp2FbFP L30M and FMN in PBS.

	λ_{abs} / nm	λ_{em} / nm	τ_F / ns	Φ_F
Pp2FbFP L30M	448	494	3.5 (70) 5.2 (30)	0.25±0.01
FMN	445	521	4.38[4]	0.25[4]

λ_{abs} and λ_{em} are the positions of the absorption and emission maxima, respectively, τ_F is the fluorescence lifetime of the two fluorophore populations and their corresponding relative amplitudes in parentheses, and Φ_F is the fluorescence quantum yield.

Table 3.2. Spectroscopic and photophysical data for the triplet state of Pp2FbFP L30M and FMN in PBS.

	τ_T / µs	Φ_T	Φ_Δ	$k_q^{O_2}$ / 10^9 M^{-1} s^{-1}	$P_T^{O_2}$
Pp2FbFP L30M	2.6	0.30±0.06	0.09±0.01	1.9±0.2	0.83
	84			0.0086±0.002	0.22
FMN	2.7	0.26 – 0.65[7,8]	0.51[9]	1.0±0.2[9]	0.91

τ_T is the triplet lifetime of the short and long triplets, Φ_T is the triplet quantum yield, Φ_Δ is the $^1O_2$ quantum yield, $k_q^{O_2}$ is the rate constant for oxygen quenching of each triplet state of Pp2FbFP L30M and $P_T^{O_2}$ is the proportion of each triplet quenched by oxygen.

Given the complexity of the $^1O_2$ kinetics, the common rise-and-decay mathematical model which is broadly used to analyze $^1O_2$ phosphorescence transients (Equation 3.3) did not allow proper fitting of the experimental data. Similar phenomena have been observed in heterogeneous systems such as biological media, and more complex kinetic models rate laws have been developed to fit the data.[10–12] In connection with chromophores embedded into a protein matrix, Lepeshkevich *et al.* have proposed a model that distinguishes between $^1O_2$ populations inside and outside the protein.[13] However, this model assumes a single population

of triplet states, a condition that does not hold in the protein samples of Pp2FbFP L30M. Therefore, a new model that considers two independent flavins, each producing $^1O_2$ with its own set of kinetics and yields was proposed and developed (Scheme 3.1).

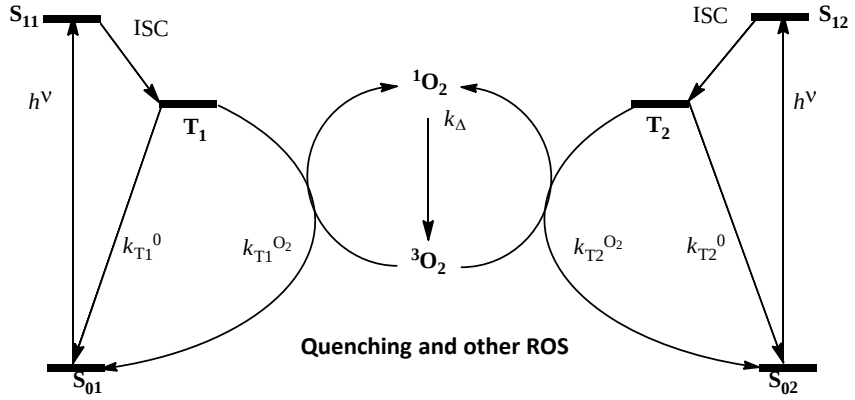

Scheme 3.1. Kinetic model of $^1O_2$ generation from two independent triplet excited states. From Ref. 6.

According to this model, a few ns after the laser pulse the initial triplet concentrations $[T_1]_0$ and $[T_2]_0$ are formed. In the absence of oxygen, the triplets decay back to the ground state with a rate constant k_T^0. If oxygen is allowed into the system, additional decay channels arise for the triplet, in which it is quenched by oxygen to produce $^1O_2$ (and perhaps other ROS). Finally, $^1O_2$ deactivates with a rate constant k_Δ. With this model in mind, the rise-and decay Equation 3.3 was rewritten as Equation 3.4.

$$S(t) = S_0 \frac{\tau_\Delta}{\tau_\Delta - \tau_T} \left(e^{-\frac{t}{\tau_\Delta}} - e^{-\frac{t}{\tau_T}} \right) \quad \text{Equation 3.3.}$$

$$S(t) = S_{01} \frac{\tau_\Delta}{\tau_\Delta - \tau_{T_1}} \left(e^{-\frac{t}{\tau_\Delta}} - e^{-\frac{t}{\tau_{T_1}}} \right) + S_{02} \frac{\tau_\Delta}{\tau_\Delta - \tau_{T_2}} \left(e^{-\frac{t}{\tau_\Delta}} - e^{-\frac{t}{\tau_{T_2}}} \right) \quad \text{Equation 3.4.}$$

Fitting the multiexponential $^1O_2$ signal with Equation 3.4 allowed the determination of the triplet lifetimes for the two populations, and the data thus obtained was in excellent agreement with the laser flash photolysis experiments. In addition, S_0 parameters for each triplet flavin obtained from Equation 3.4 were used in Equation 3.5 to calculate the overall Φ_Δ of Pp2FbFP L30M. A value $\Phi_\Delta = 0.09$ was determined (Table 3.2), which was at that time the highest reported Φ_Δ value for any FP.

$$\phi_\Delta = \phi_{\Delta_{\mathrm{Ref}}} \frac{S_{01\mathrm{Prot}} + S_{02\mathrm{Prot}}}{S_{0_{\mathrm{Ref}}}} \quad \text{Equation 3.5.}$$

Further analysis of the individual S_{01} and S_{02} values indicated that 30% of the protein $^1O_2$ signal arises from the short-lived, oxygen-accessible triplet, whereas 70% arises from the long-lived, less-accessible one, despite the oxygen trapping efficiencies being the opposite (Table 3.2). This could be explained by a higher Φ_T for the longest-lived triplet, in agreement with the transient absorption results shown in Figure 3.3C. A structural interpretation of the enhanced photosensitization ability was unfortunately not possible since the structures of Pp2FbFP L30M or its parental proteins had not been solved so far. Regarding the existence of two independent ^{3}FMN*, it was attributed to the unavoidable binding of different flavin derivatives (i.e., FMN, FAD, RB) into the active pocket, since these compounds are naturally present in cells. Indeed, HPLC analysis of the chromophores in Pp2FbFP L30M revealed the presence of FMN and FAD to a similar extent in addition to small amounts of RF. Furthermore, the contributions of different protein conformers and/or the formation of protein dimers could not be excluded.

All in all, despite its higher complexity, Pp2FbFP L30M outperformed miniSOG in terms of $^1O_2$ photosensitization by a factor of approximately 3. These results confirmed the potential of FbFPs for $^1O_2$ applications, such as genetically encoded PSs and provided solid arguments to explore other flavoproteins to expand the toolbox of biological PSs.

3.2. Problems in FbFPs characterization.

Following the experimental procedure described for Pp2FbFP L30M, the optical and photosensitizing properties of the other fluorescent flavoproteins were characterized. In addition to the flash photolysis studies as well as the direct detection of $^1O_2$ NIR phosphorescence, indirect $^1O_2$ measurements using uric acid (UA) as a $^1O_2$ chemical trap were carried out for all the proteins. This method relies on the irreversible reaction between UA and $^1O_2$ which can be monitored by the changes in absorbance of UA at 292 nm.[14] Upon reaction with $^1O_2$, UA forms a hydroperoxide intermediate that undergoes additional ($^1O_2$-independent) reaction steps to final degradation products such as triuret, urea and cyanuric acid.[15,16] For UA experiments, absorbance values at 292 nm were plotted versus irradiation time at λ = 450 nm of optically matched solutions of free FMN and each flavoprotein in PBS, both supplemented with 50 μM UA. The Φ_Δ value was obtained by comparing the UA degradation rates.

Unfortunately, once all the proteins had been spectroscopically characterized, the entire collected data had to be quarantined since lack of reproducibility was detected when comparing results obtained at different times along the study. It is worth noting that the complete

photophysical characterization of all proteins comprised about six months, analyzing one FbFP at a time. Throughout the study, some proteins progressively showed signs of degradation (i.e., formation of small precipitates and turbidity and gradually losing its innate yellow color), although all the protein samples had been carefully stored at 4°C and in the dark. Indeed, re-measuring the flavoproteins after their complete characterization revealed that the photosensitizing properties for most of them were changing over time, even for samples that did not show any visual signs of degradation. Of note, protein samples were still fluorescent and the absorption spectra showed the characteristic vibronic features indicating that the FMN remained bound into the active pocket (Figure 3.4). For this reason, it was highly unlikely to detect this phenomenon in advance by routine spectroscopy techniques. It was only when studying the $^1O_2$ production that marked changes could be observed when comparing measurements of the same FbFP at different storage times. Interestingly, these differences between fresh and evolved (or aged) protein samples modified both the ability and the kinetics of $^1O_2$ production severely (Figure 3.4).

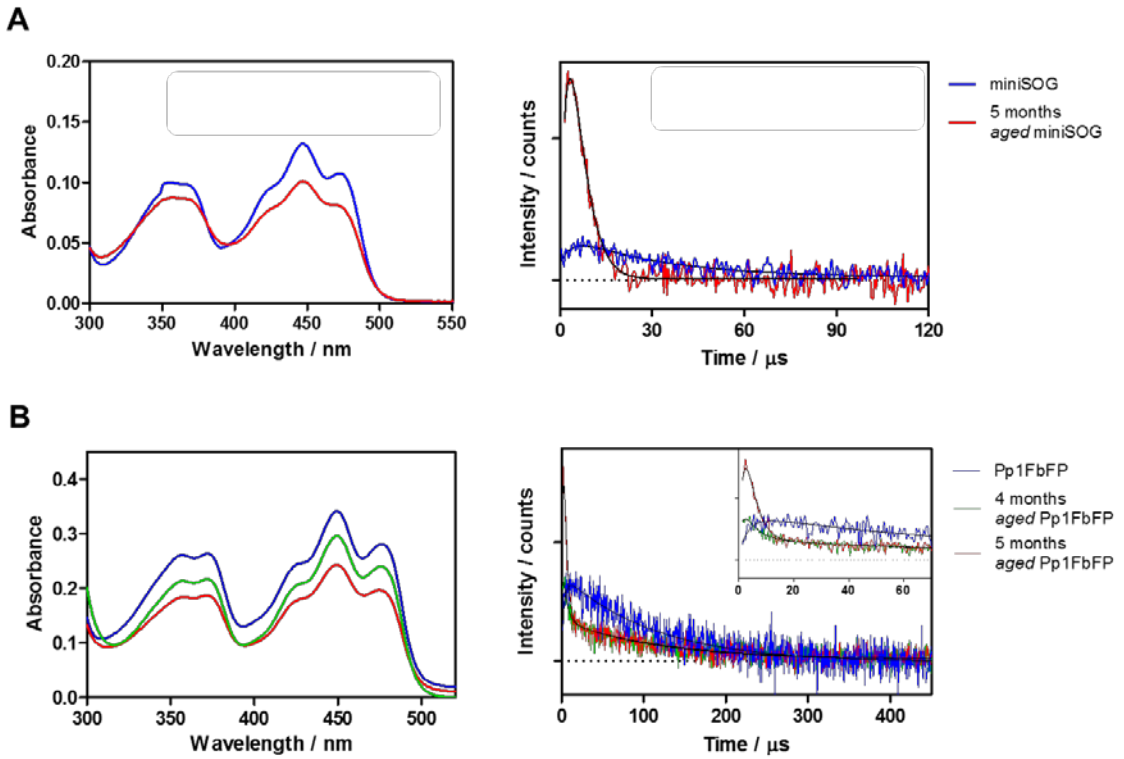

Figure 3.4. Selected examples to show the evolution of the protein absorbance and $^1O_2$ time-resolved NIR phosphorescence, throughout the course of protein characterization. A) miniSOG and B) Pp1FbFP. The inset shows a zoomed-in imaged of the $^1O_2$ signals.

The aging effect was totally unexpected. After the initial characterization of Pp2FbFP L30M, all the other proteins had been studied consecutively, without any major reason or preference

for the order of analysis. Therefore, it was not possible to know whether or not a given protein had already evolved at the time of the study, and/or to which extent. In other words, all the spectroscopic data collected so far may not describe the putative properties of the proteins of interest. For this reason, all this photophysical data was quarantined, and no further discussion is provided. For the interested reader, a summarized compilation of all these results is presented below in Figure 3.5 (experimental details are given in the figure caption) and the spectroscopic values are collected in Table 3.1. (Note: the absorption and fluorescence spectra of these FbFPs are not shown herein Chapter 3. All these data are presented and discussed in Chapter 4 for freshly purified proteins).

Since long-term storage of the proteins had been shown to induce unknown transformations that affected their photosensitizing ability, the only way to study the real properties was to analyze fresh protein samples. Therefore, the whole process to produce the FPs had to be developed from scratch. From learning the basic techniques to the designing, adapting and ultimately performing the experimental procedures, all process including bacterial transformation, bacterial growth, protein induction and expression and protein purification were one by one integrated into the microbiology and photochemistry laboratories.

a) Pp1FbFP

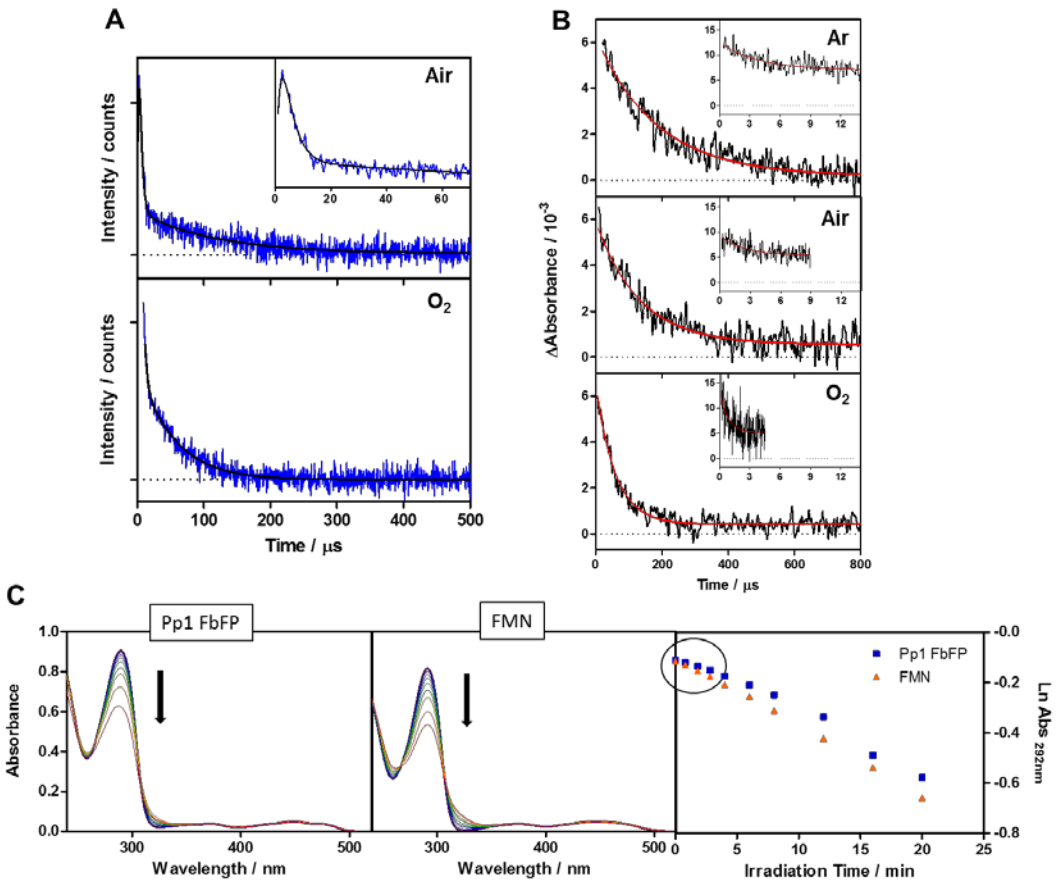

b) Pp2FbFP

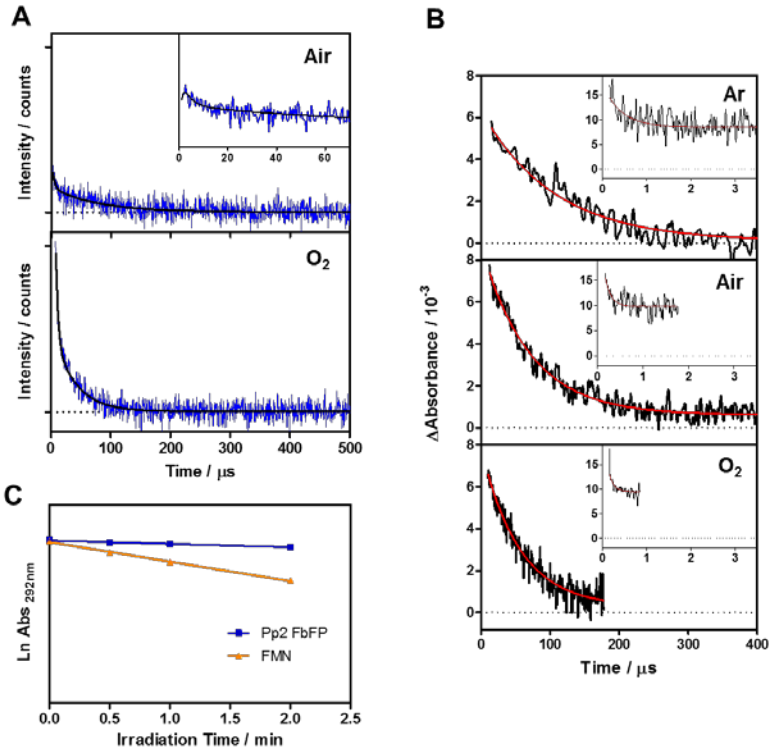

c) DsFbFP

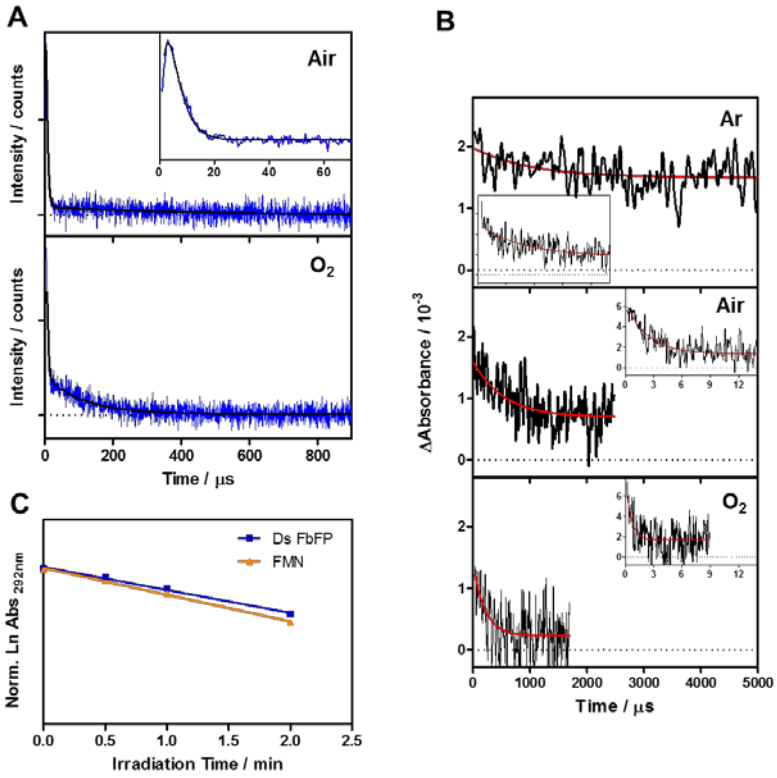

d) DsFbFP M49I

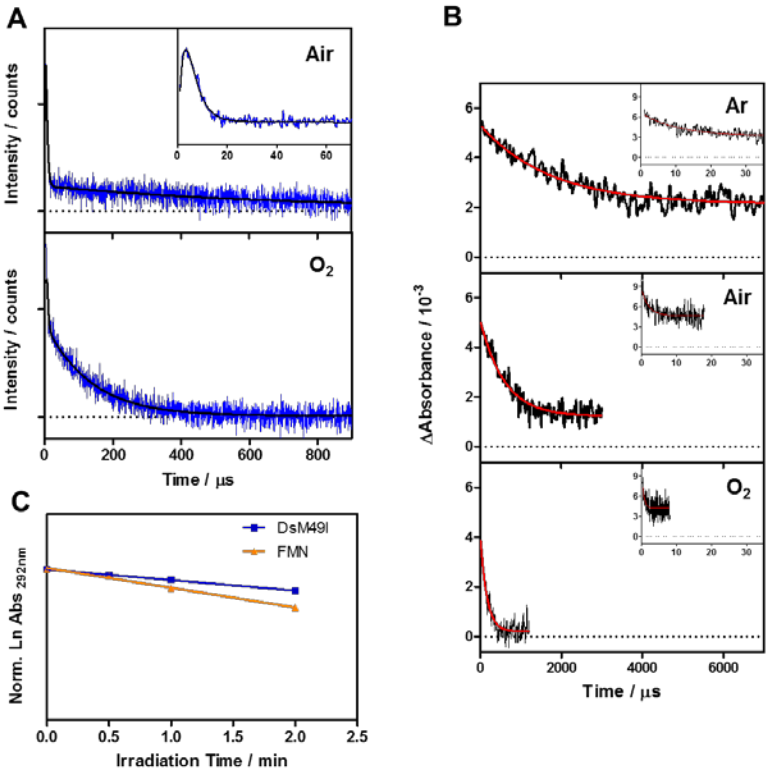

e) EcFbFP

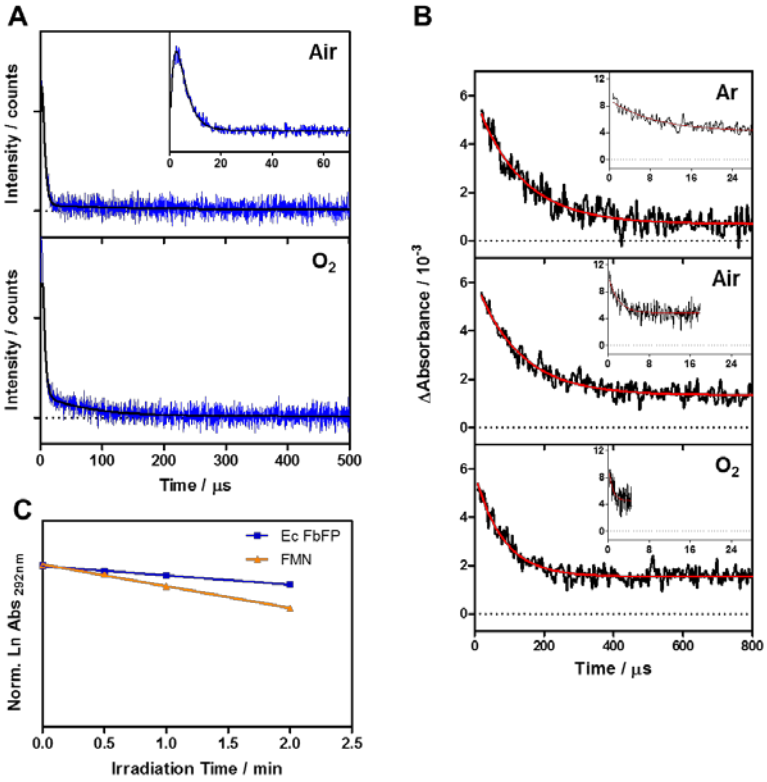

f) PhiLOV2.1

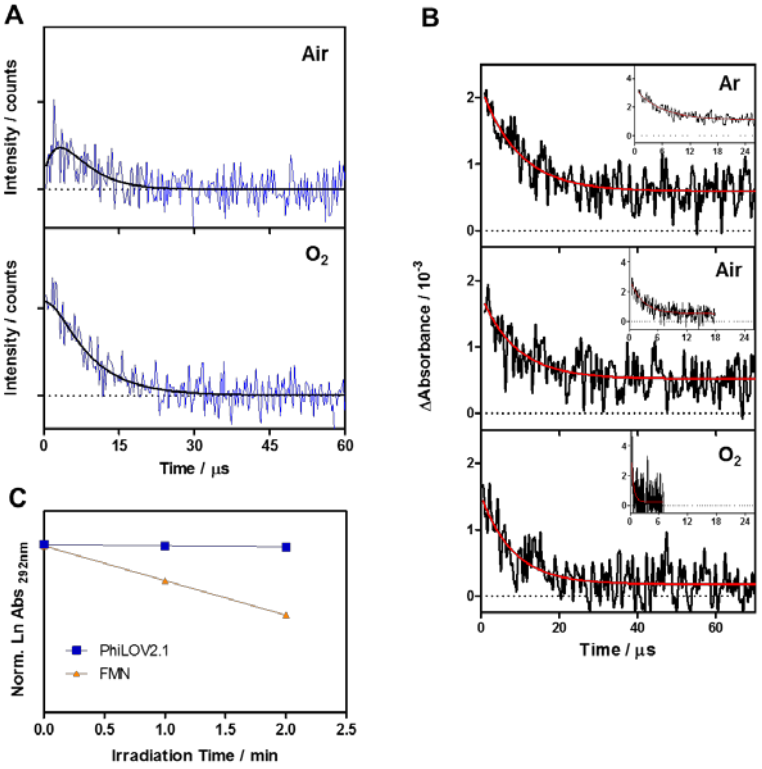

g) miniSOG

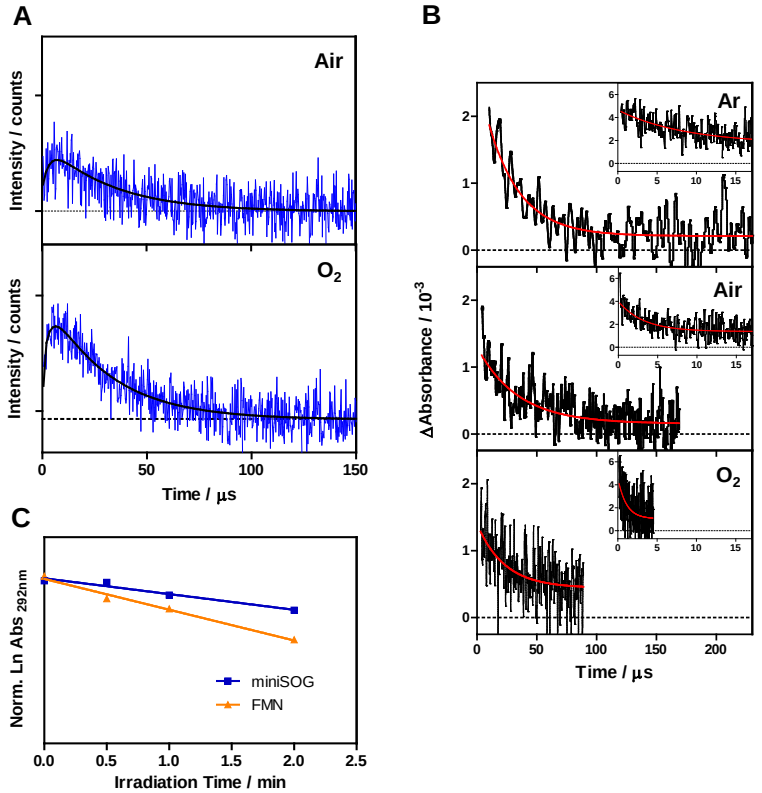

Figure 3.5. A) Time-resolved $^1O_2$ decays for the protein samples in air and O_2-saturated PBS solution. Insets show a zoomed-in transient at shorter times. Fitting lines are in black. The Y-axes are in log scale. B) Transient absorption decays in Ar, air and O_2-saturated PBS solutions. Insets show the decays for the short-lived triplet. Fitting lines are in red. C) Degradation of UA by illumination at λ = 450 nm of the FbFPs or free FMN. The black circle in the right panel in Pp1FbFP shows the linear part of the plot that has been used for calculations.

Table 3.3. Compilation of photophysical data for the FbFPs characterized.

	$^1O_2$ NIR Phosphorescence (λ_{ex} = 355 nm, λ_{obs} = 1275 nm)				Transient Absorption (λ_{ex} = 355 nm, λ_{obs} = 700 nm)											Uric Acid
	τ_{short} / µs	τ_{long} / µs	τ_Δ / µs	Φ_Δ	τ_{short} Ar / µs	τ_{long} Ar / µs	τ_{short} Air / µs	τ_{long} Air / µs	τ_{short} O_2 / µs	τ_{long} O_2 / µs	$k_q^{O2}{}_{short}$ / $M^{-1}\cdot s^{-1}$	$k_q^{O2}{}_{long}$ / $M^{-1}\cdot s^{-1}$	$P_T^{O2}{}_{short}$	$P_T^{O2}{}_{long}$	$\Phi_{T,AP}$	Φ_Δ UA
Pp2FbFP L30M *(dim)*	2.6 (0.9)	84 (65)	3.3	0.09	18	154	2,6	92	0.75	65	$1.9\cdot10^9$	$0.0086\cdot10^9$	83 (96)	22 (59)	0.30	0.20
Pp1FbFP *(dim)*	1.6 (0.54)	113 (50)	3.4	0.19	3.8	190	2.3	128	0.8	58	$1.0\cdot10^9$	$0.0118\cdot10^9$	39 (79)	33 (69)	0.38	0.30
Pp2FbFP *(dim)*	1.4 (0.39)	71 (33)	3.5	0.07	n.d	103	n.d	71	n.d	54	n.d	$0.0079\cdot10^9$	n.d	34 (48)	n.d	0.08
DsFbFP *(dim)*	2.6 - 6.2 (0.7)	> 400 (134)	3.4	0.18 - 0.44	6.4	932	2.3	577	0.62	216	$1.5\cdot10^9$	$0.0036\cdot10^9$	64 (90)	38 (77)	0.30	0.44
DsFbFP M49I *(dim)*	2.3 (0.67)	> 400 (126)	3.3	0.32 - 0.70	11	1807	2.2	589	0.65	168	$1.4\cdot10^9$	$0.0054\cdot10^9$	80 (94)	67 (91)	0.52	0.34
EcFbFP *(dim)*	2.0 (0.57)	127 (71)	3.4	0.08	8.8	138	2.0	125	0.78	82	$1.1\cdot10^9$	$0.0050\cdot10^9$	77 (91)	9 (41)	0.61	0.20
PhiLOV2.1 *(mon)*	2.4 (0.6)	7.2 (6.6)	3.5	0.02	5.7	9.6	2.7	9.0	0.54	8.2	$1.7\cdot10^9$	$0.0017\cdot10^9$	53 (91)	4 (15)	0.11	0.02
miniSOG *(mon)*	2.4 (0.8)	32 (28)	3.4	0.03 - 0.18	8.5	33	2.4	30	0.84	25	$1.0\cdot10^9$	$0.0093\cdot10^9$	72 (90)	9 (24)	0.30	0.26

Note: Pp2FbFP and PhiLOV2.1 degraded particularly quickly during the course of the experiments. For PhiLOV2.1 evidence was found suggesting the presence of free FMN in the solution (i.e., not bound to the protein). *Dim* and *mon* denote the dimeric or monomeric conformation of the protein, respectively.

3.3. Specific techniques and methods for the purification and characterization of flavin-binding fluorescent proteins

The processes and protocols for protein production and purification are well known and routinely performed in laboratories specialized in protein biotechnology. The main steps can be broadly summarized in the following stages (Figure 3.6):

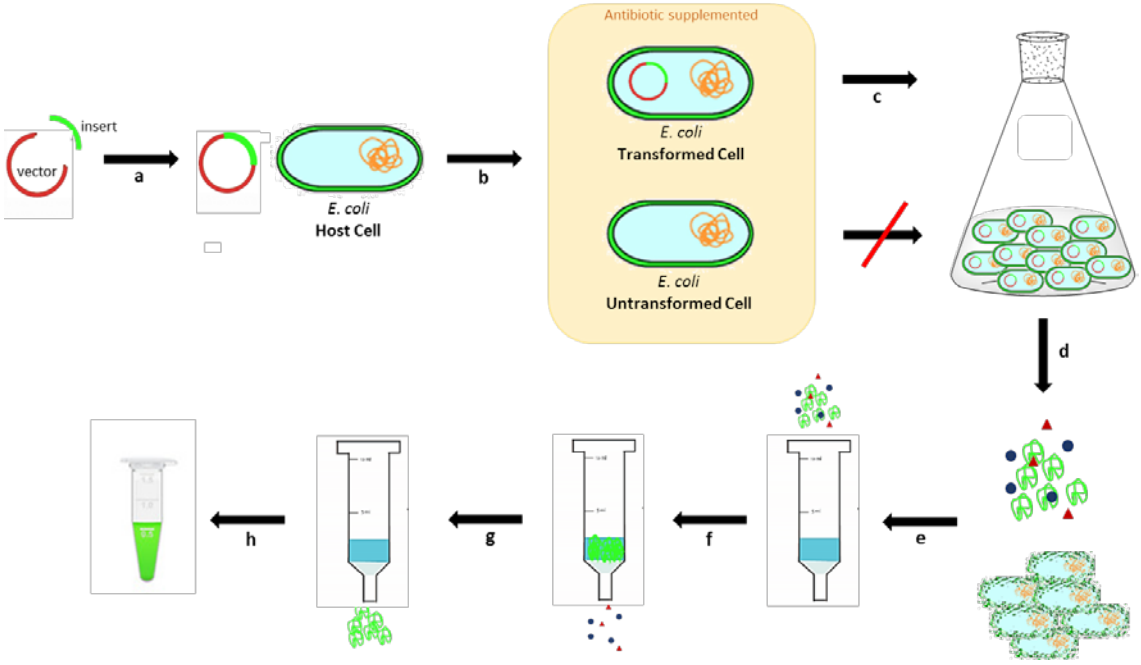

Figure 3.6. Schematic illustration of the protein production and purification processes using the affinity chromatography method.

a. Cloning a plasmid vector encoding the protein of interest. Typically, the plasmid also encodes resistance to a certain antibiotic which provides selectivity of the transformed cells over untransformed.
b. Introduction of the plasmid inside the bacterial cells, a process called transformation. Many methods have been developed for this purpose, but amongst them, thermal shock is one of the most used because of its simplicity and efficiency.
c. Bacterial growth in media supplemented with a suitable antibiotic. Induction of protein expression by addition of specific compounds called inducers (i.e., arabinose or derivatives of lactose metabolites), which depend on the type of plasmid selected.
d. Cell harvesting by centrifugation and lysis by physical or chemical methods.
e. Loading of the soluble fraction onto the purification column. There is a variety of chromatographic methods to separate the protein of interest from the rest of soluble cellular components, including reverse phase chromatography, ion-exchange chromatography, size-

exclusion chromatography and affinity chromatography. The latter is usually the method of choice because it gives the purest results and highest specific activity compared to other techniques.

f. The protein of interest remains bound in the column while the other biomolecules elute away.
g. Selective and controlled elution of the recombinant protein is achieved by the addition of specific chemical substrates that interact with the stationary phase.
h. Further steps can be performed in order to exchange the buffer solution or concentrate the protein.

Of course, this general procedure is opportunely modified and adapted for the specific properties of the protein of interest and every laboratory has optimized the process for their convenience. Therefore, a wide array of instruments, protein kits, laboratory materials and reagents have been developed and most of them are commercially available.

Plasmid vectors encoding the FbFPs were received from Dr. Drepper's group. Three additional proteins, namely SOPP, iLOV and CreiLOV were also included, expanding the initial palette of eight FbFPs up to eleven proteins. The following protocol was carried out for all the FbFP samples.

1) Preparation of competent cells

A single colony of *E. coli* BL21(DE3) cells (Novagen) was picked from an agar plate using a sterile, straight loopneedle. The loopneedle with the bacteria was then plunged deep into 3 mL LB medium (Fisher Scientific) and the solution was shaken overnight (ON) at 37 °C. In the following morning, 0.5 mL was used to inoculate 50 mL of LB and the suspension was incubated until the optical density measured at 600 nm (OD_{600}) reached 0.3. Then, the cells were put on ice for 20 minutes and then collected by centrifugation at 5000 revolutions per minute (rpm) for 5 minutes. The supernatant was decanted and the pellet was gently resuspended in 25 mL sterile, cold 0.1 M $CaCl_2$. After 10 minutes incubation on ice, cells were centrifuged as previously described, the supernatant was discarded and cells were gently resuspended in 5 mL sterile, cold 0.1 M $CaCl_2$. Aliquots of 47 µL of cells in $CaCl_2$ supplemented with 20% glycerol were immediately frozen at -80 °C for long-term storage.

2) Bacterial cell growth and induction of protein expression

For bacterial transformation, 1 µL of pET28a expression vector (Novagen/Merck) encoding each FbFP was added into aliquots of 47 µL of BL21(DE3) competent cells and incubated on ice for 30 minutes. pET28a plasmids also carried kanamycin resistance and a sequence of six histidine residues (6xHis) fused to the recombinant protein for purification. Afterward, heat shock was performed by incubating the cells for exactly 45 seconds at 42 °C in a water bath and cells were put back on ice for 5 minutes. Finally, 500 µL pre-warmed LB medium was added, the suspension was incubated for 1 hour at 37°C and 100 µL was plated on LB agar plates supplemented with 50 µg/mL kanamycin (Gibco). No cells were found in NO-DNA control experiments using 1 µL PBS instead of plasmid for cell transformation, thus confirming the antibiotic resistance of the transformed cells.

3) Bacterial cell growth and induction of protein expression

Bacterial cells encoding FbFPs were picked from single colonies and grown in 200 mL LB supplemented with 50 µg/mL Kanamycin. At OD_{600} ~ 0.6, protein expression was induced by addition of Isopropyl β-D-1-thiogalactopyranoside (IPTG) (Sigma-Aldrich). Several conditions for protein expression were tested, including IPTG concentration, temperature and induction time, and the production of the protein was conveniently monitored by measuring the flavin's fluorescence (Figure 3.7). A rational compromise between high expression levels and induction time was achieved with 0.4 mM IPTG, at 37°C and at 4 hours after the addition of IPTG. Therefore, these expression conditions were applied for the production of all FbFPs. Cell growth, as well as protein expression, were always performed under red light or in the dark.

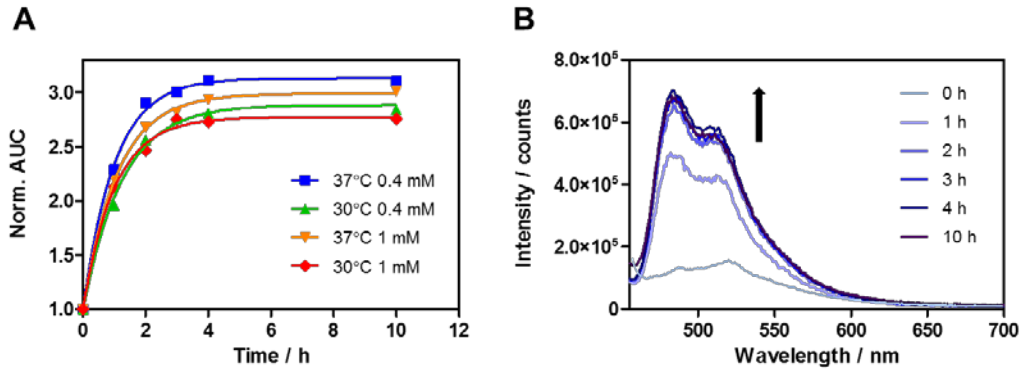

Figure 3.7. A) Normalized evolution of the AUC for SOPP as a selected example of FbFP during the expression of the protein in *E. coli* cells. B) Increase in fluorescence emission at 37°C upon addition of 0.4 mM IPTG. All spectra were normalized by OD_{600} at each expression time.

4) Protein purification

Bacterial cells expressing the FbFPs were harvested by centrifugation and the supernatant was discarded. The expression of proteins could be readily observed from the yellow color and bright fluorescence of the pellet under near UVA light (Figure 3.8A). Cells were lysed with B-PER lysis buffer (Thermo Scientific) complemented with a protease inhibitor cocktail (Sigma). Insoluble material was removed by centrifugation and the soluble extract was loaded onto Ni-NTA agarose column (Qiagen, Figure 3.8B) pre-equilibrated with buffer A (50 mM Tris(hydroxymethyl)aminomethane hydrochloride (Tris-HCl) (Sigma-Aldrich) pH 8.0, 300 mM NaCl (Panreac) and 10 mM imidazole (Sigma). In the Ni-NTA system, the 6xHis sequence fused to the recombinant protein binds to the immobilized metal ions in the resin of the column while unspecific proteins elute off. The column was washed with more than ten column volumes of buffer A and the fusion protein was then eluted with buffer B (50 mM Tris-HCl pH 8.0, 300 mM NaCl and 300 mM imidazole). The high concentration of imidazole competes with the His-tag for binding to the metal-charged resin. However, it must be completely removed afterwards from the protein solution, especially for characterizing the photosensitizing properties since imidazole is an efficient quencher of $^1O_2$.[17] The elution fraction containing the purified proteins was loaded on a PD-10 column (GE Healthcare) for buffer exchange and elimination of imidazole (Figure 3.8C). Fluorescent proteins were concentrated (Figure 3.8D) using Amicon® Ultra 0.5 mL or 2 mL centrifugal concentrators with a 10.000 Dalton molecular weight cut-off (Merck). All steps of protein purification were always performed under red light or in the dark.

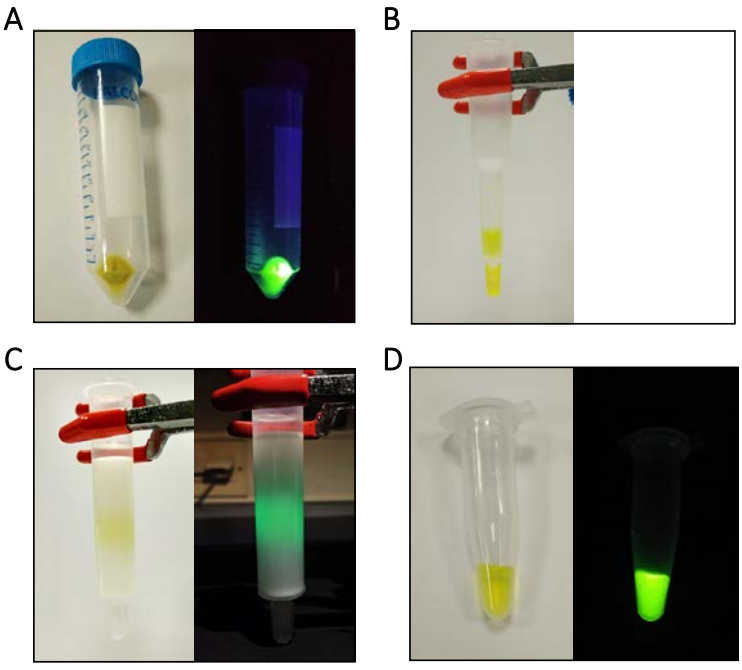

Figure 3.8. Protein purification steps, under white room light (left) and near UVA light (right).

5) $^1O_2$ NIR phosphorescence measurements

Early experiments on direct detection of $^1O_2$ NIR phosphorescence were carried out with a pulsed laser emitting at 355 nm. However, the low laser frequency (1 kHz) required for the study of long ^{3}FMN* lifetimes reduced the light intensity of the laser significantly and therefore prolonged irradiation times were needed to obtain decent $^1O_2$ signals. Therefore, it was pertinent to incorporate a new pulsed laser more suitable for the study of FbFPs. A powerful blue laser emitting at 473 nm was integrated into our $^1O_2$ detection system (Figure 3.9) and carefully optimized for FbFPs excitation. The higher light intensity as well as the possibility to finely tune the repetition rate remarkably improved the sensibility of the method while dramatically reducing the irradiation time required (Figure 3.10).

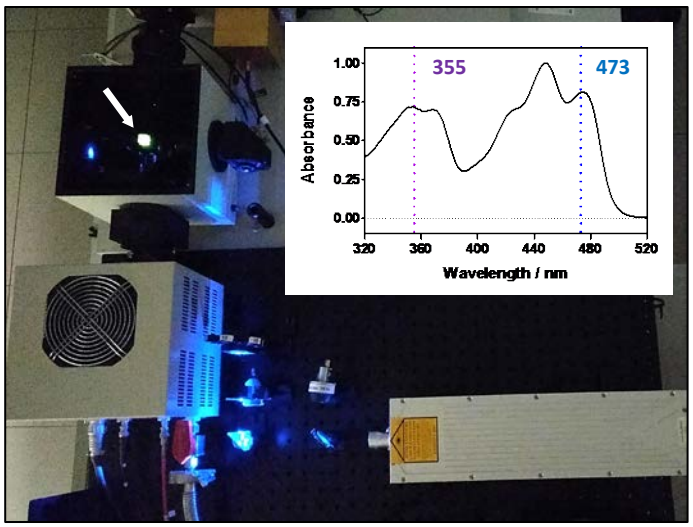

Figure 3.8. Optimized system for $^1O_2$ photosensitization and detection upon laser irradiation at 473 nm. The white arrow on the top left shows the position of the cuvette containing the fluorescent FbFP. The inset shows the two wavelengths used for FbFP excitation, superimposed on the absorption spectra of Pp2FbFP L30M.

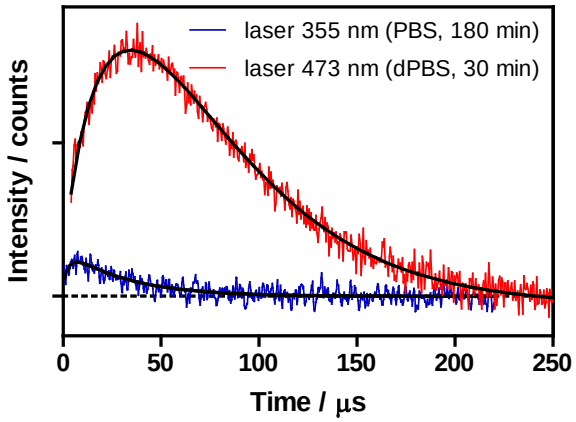

Figure 3.10. $^1O_2$ phosphorescence signal improvements for fresh miniSOG using optimized buffer and irradiation conditions at 473 nm (red) as compared to the early measurements at 355 nm (blue). Notice the differences in the irradiation time. Protein's concentration was comparable in the two experiments.

3.4. Conclusions

Initial attempts to characterize FbFPs have been hampered by the lack of reproducibility of the results observed during the study of the proteins, a process that has been called aging. The chemical transformations behind the aging process remain unclear; however, early results suggest the participation of light since aging was not observed for samples stored under strict dark conditions. The results presented in this study are intended to help those researchers interested in photoactive proteins to avoid undesired (photo)transformations. The observation of aging has motivated the development of a new methodology for the in-house production and characterization of the flavoproteins. Starting from the preparation of competent cells, followed by bacterial transformation with DNA vectors encoding FbFPs, cell growth and induction of protein expression, purification of the FbFP to the ultimate optimization of the $^1O_2$ photosensitization and detection system, all processes have been step by step successfully incorporated. It has allowed the study of fresh proteins on the same day of their extraction, which has provided reliable spectroscopic data that were consistent with the literature values and were reproducible over time. With the new methodology, it has been possible to use deuterated buffers without suffering from limitations derived from sample dilution, which has greatly improved the intensity the $^1O_2$ signal and made its analysis much more convenient and robust. All in all, the combination of freshly prepared proteins with the new blue laser has remarkably increased the quality of the signal while significantly reduced the irradiation time required for each experiment, from 2-3 hours to 30 minutes (Figure 3.10). The new procedure now enables the proper characterization of the photophysical and photosensitizing properties of FbFPs.

3.5. References

(1) Drepper, T.; Eggert, T.; Circolone, F.; Heck, A.; Krauss, U.; Guterl, J. K.; Wendorff, M.; Losi, A.; Gärtner, W.; Jaeger, K. E. Reporter Proteins for in Vivo Fluorescence without Oxygen. *Nat. Biotechnol.* **2007**, *25* (4), 443–445.

(2) Buckley, A. M.; Petersen, J.; Roe, A. J.; Douce, G. R.; Christie, J. M. LOV-Based Reporters for Fluorescence Imaging. *Curr. Opin. Chem. Biol.* **2015**, *27*, 39–45.

(3) Mishin, A. S.; Belousov, V. V; Solntsev, K. M.; Lukyanov, K. A. Novel Uses of Fluorescent Proteins. *Curr. Opin. Chem. Biol.* **2015**, *27*, 1–9.

(4) Wingen, M.; Potzkei, J.; Endres, S.; Casini, G.; Rupprecht, C.; Fahlke, C.; Krauss, U.; Jaeger, K.-E.; Drepper, T.; Gensch, T. The Photophysics of LOV-Based Fluorescent Proteins – New Tools for Cell Biology. *Photochem. Photobiol. Sci.* **2014**, *13* (6), 875–883.

(5) Schweitzer, C.; Schmidt, R. Physical Mechanisms of Generation and Deactivation of Singlet Oxygen. *Chem. Rev.* **2003**, *103* (5), 1685–1758.

(6) Torra, J.; Burgos-Caminal, A.; Endres, S.; Wingen, M.; Drepper, T.; Gensch, T.; Ruiz-González, R.; Nonell, S. Singlet Oxygen Photosensitisation by the Fluorescent Protein Pp2FbFP L30M, a Novel Derivative of Pseudomonas Putida Flavin-Binding Pp2FbFP. *Photochem. Photobiol. Sci.* **2015**, *14* (2), 280–287.

(7) Islam, S. D. M.; Penzkofer, A.; Hegemann, P. Quantum Yield of Triplet Formation of Riboflavin in Aqueous Solution and of Flavin Mononucleotide Bound to the LOV1 Domain of Phot1 from Chlamydomonas Reinhardtii. *Chem. Phys.* **2003**, *291* (1), 97–114.

(8) Losi, A. Flavin-Based Blue-Light Photosensors: A Photobiophysics Update. *Photochem. Photobiol.* **2007**, *83* (6), 1283–1300.

(9) Baier, J.; Maisch, T.; Maier, M.; Engel, E.; Landthaler, M.; Bäumler, W. Singlet Oxygen Generation by UVA Light Exposure of Endogenous Photosensitizers. *Biophys. J.* **2006**, *91* (4), 1452–1459.

(10) Nonell, S.; Braslavsky, S. E. Time-Resolved Singlet Oxygen Detection. *Methods Enzymol.* **2000**, *319*, 37–49.

(11) Fu, Y.; Kanofsky, J. R. Singlet Oxygen Generation from Liposomes: A Comparison of Time-Resolved 1270 Nm Emission with Singlet-Oxygen Kinetics Calculated from a One Dimensional Model of Singlet-Oxygen Diffusion and Quenching. *Photochem. Photobiol.* **1995**, *62* (4), 692–702.

(12) Fu, Y.; Sima, P. D.; Kanofsky, J. R. Singlet-Oxygen Generation from Liposomes : A Comparison of 6p-Cholesterol Hydroperoxide Formation with Predictions from a One-Dimensional Model of Singlet-Oxygen Diffusion and Quenching. *Photochem. Photobiol.* **1996**, *63* (4), 468–476.

(13) Lepeshkevich, S. V.; Parkhats, M. V.; Stasheuski, A. S.; Britikov, V. V.; Jarnikova, E. S.; Usanov, S. A.; Dzhagarov, B. M. Photosensitized Singlet Oxygen Luminescence from the Protein Matrix of Zn-Substituted Myoglobin. *J. Phys. Chem. A* **2014**, *118* (10), 1864–1878.

(14) Rabello, B. R.; Gerola, A. P.; Pellosi, D. S.; Tessaro, A. L.; Aparício, J. L.; Caetano, W.; Hioka, N. Singlet Oxygen Dosimetry Using Uric Acid as a Chemical Probe: Systematic Evaluation. *J. Photochem. Photobiol. A Chem.* **2012**, *238*, 53–62.

(15) Matsuura, T.; Saito, I. Photoinduced Reactions—XXI : Photosensitized Oxygenation of N-Unsubstituted Hydroxypurines. *Tetrahedron* **1968**, *24* (22), 6609–6614.

(16) Ruiz-González, R.; Cortajarena, A. L.; Mejias, S. H.; Agut, M.; Nonell, S.; Flors, C. Singlet Oxygen Generation by the Genetically Encoded Tag MiniSOG. *J. Am. Chem. Soc.* **2013**, *135* (26), 9564–9567.

(17) Tour, O.; Meijer, R. M.; Zacharias, D. A.; Adams, S. R.; Tsien, R. Y. Genetically Targeted Chromophore-Assisted Light Inactivation. *Nat. Biotechnol.* **2003**, *21* (12), 1505–1508.

CHAPTER 4

4. Photochemical, photophysical and antimicrobial characterization of flavin-binding fluorescent proteins

The photochemical, photophysical and antimicrobial properties of eleven FbFPs have been characterized. Protein samples were produced in *E. coli* cells, purified and analyzed on the same day, allowing the proper study of their genuine properties. The spectroscopic data thus obtained for miniSOG were fully consistent with the reported values, providing compelling validation of the whole process. All proteins produce $^1O_2$ and time-resolved signals showed the typical rise-and-decay profile, revealing the generation of a single population of triplet state proteins. In addition, most FbFPs are potent biological PSs for aPDT applications.

Per véncer cal anar-hi, anar-hi i anar-hi!
Antoni Massaguer

4.1. Introduction

The lack of reproducibility observed for long-term stored protein samples hampered their early characterization and all the spectroscopic data obtained thus far had to be quarantined. An alternative approach for the home production, purification and irradiation of FbFPs with a new blue-light laser has been developed, allowing a more robust study of freshly purified protein samples. All plasmids encoding FbFPs were engineered by the group of Dr. Drepper. The new experimental procedure was validated using miniSOG since this protein was the first FbFP explicitly developed for $^1O_2$ photosensitization purposes, and consequently, it has been studied in more detail than other FbFPs and the reported data can therefore be used as reference values. The spectroscopic properties of freshly home-purified miniSOG are shown in Figure 4.1 and listed in Table 4.1. Literature values are also included for comparison.

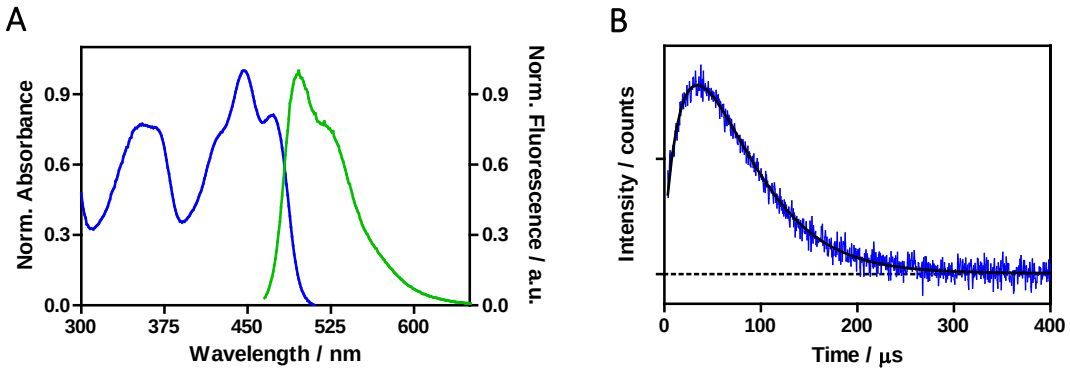

Figure 4.1. A) Normalized absorption (blue) and fluorescence (green) spectra and B) time-resolved $^1O_2$ NIR phosphorescence decay for miniSOG in air-saturated dPBS upon excitation at λ = 473 nm. Fitting line is in black.

Table 4.1. Photophysical data for miniSOG from this study and reported values.

	λ_{abs} / nm	λ_{em} / nm	τ_F / ns	Φ_F	τ_T / µs	Φ_Δ
This study	447	496	5.0	0.39	30	0.04
Published data	447[1]	497[1]	5.1[2]	0.41[1]	31[3]	0.03[2,3]

The spectroscopic data obtained for fresh miniSOG was consistent with previously reported values and provided compelling validation of the whole process for protein production, purification and characterization. Therefore, the procedure was systematically performed for the study of the initial nine FbFPs (see Chapter 3) and the three additional LOV proteins received afterward. In total, the photophysical and photosensitizing properties of eleven freshly purified flavoproteins were characterized.

4.2. Results

4.2.1. Spectroscopic characterization

All FbFPs were studied on the same day of their extraction from bacterial *E. coli* cells, following the procedure described in Chapter 3. In addition, at the last step of the purification process, recombinant proteins were concentrated and buffer-exchanged to dPBS in Amicon® centrifugal filters. Protein samples were prepared by diluting the concentrated stock solution to a final absorbance between 0.05 and 0.1 at 473 nm in dPBS. Protein handling and sample preparation were always performed under red light or in the dark. Absorption and fluorescence spectra, as well as $^1O_2$ time-resolved NIR phosphorescence at 1275 nm upon light excitation at 473 nm, are shown in Figure 4.2. FbFPs spectroscopic data are collected in Table 4.2. It is worth noting that, unlike the data obtained in Chapter 3, the $^1O_2$ signal from fresh proteins revealed a single population of ^{3}FMN* in all the flavoproteins, and therefore all $^1O_2$ transients were conveniently fitted and analyzed by a biexponential decay.

a) Pp1FbFP

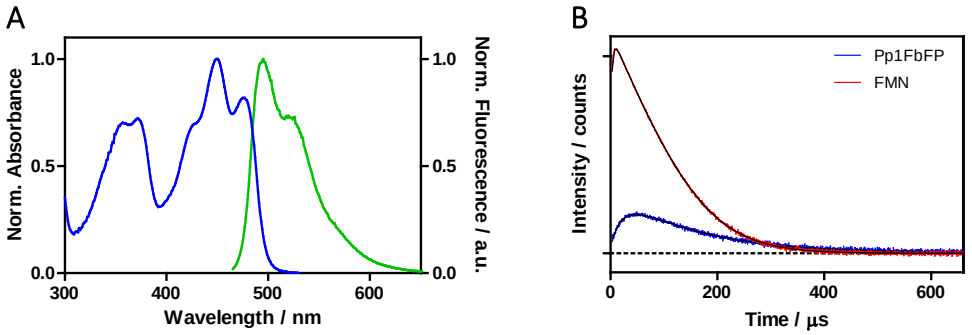

b) Pp2FbFP

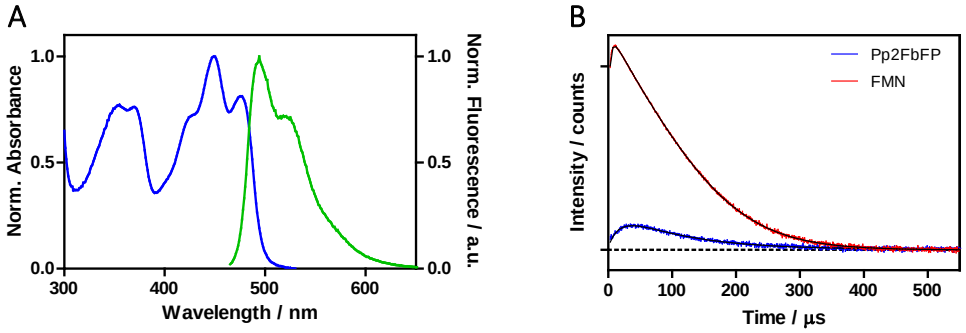

c) Pp2FbFP L30M

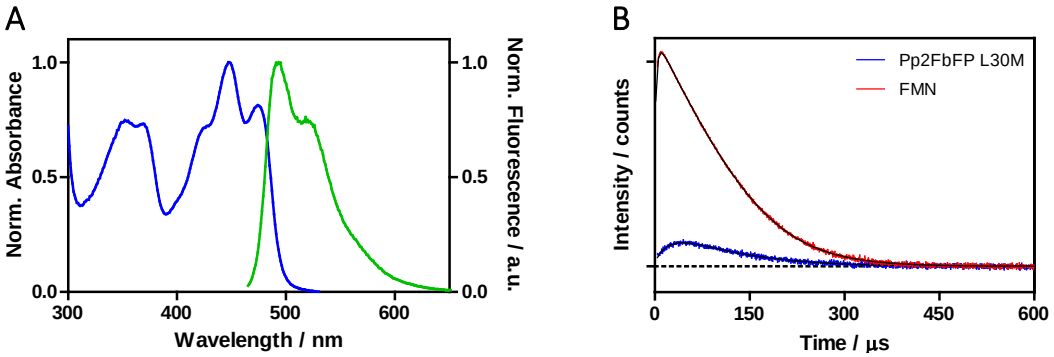

d) DsFbFP

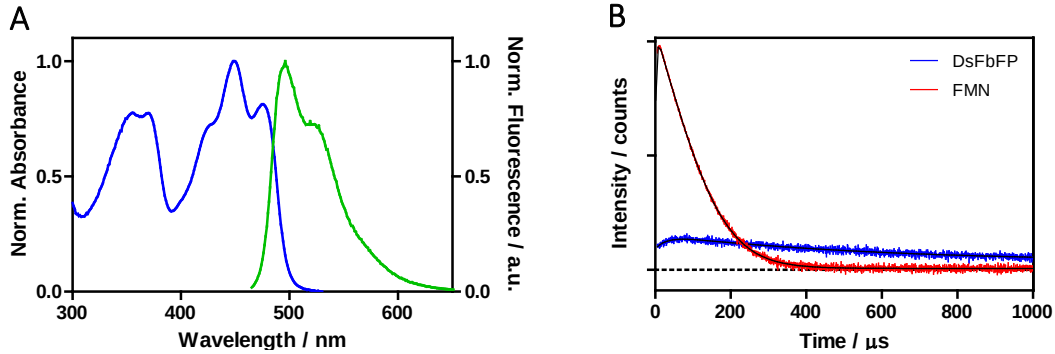

e) DsFbFP M49I

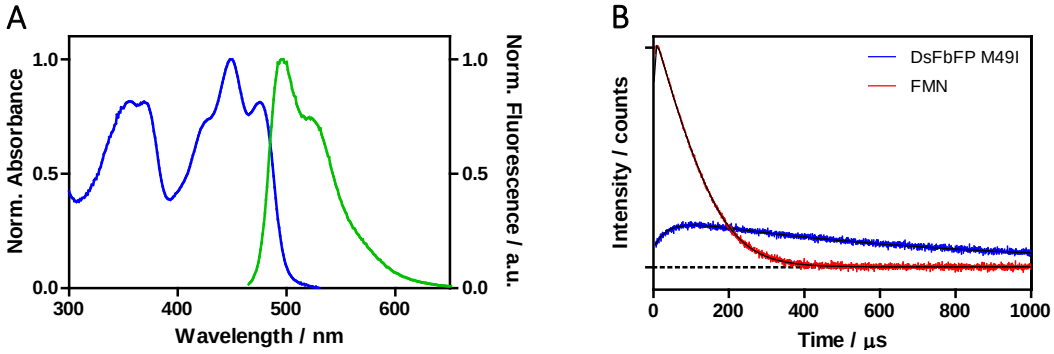

f) EcFbFP

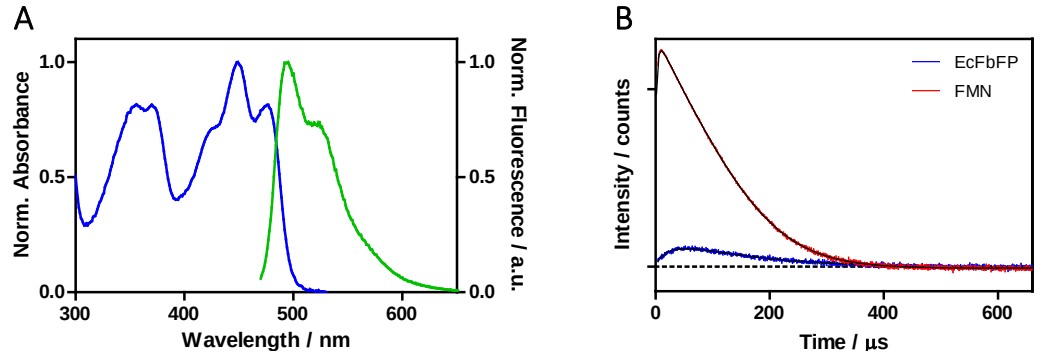

g) PhiLOV2.1

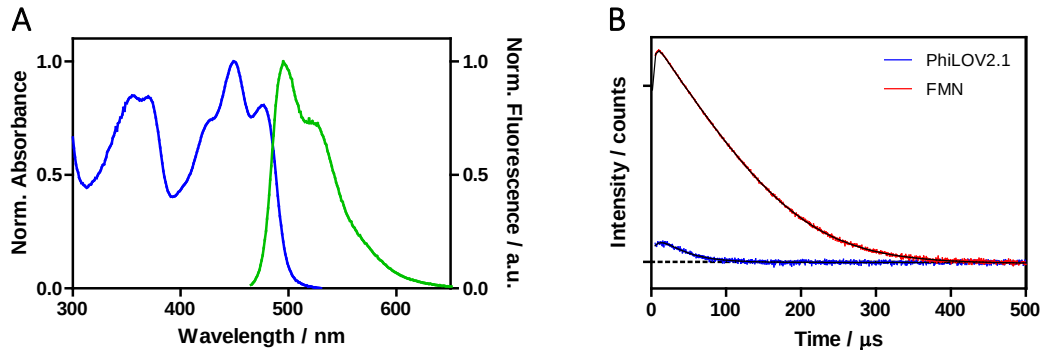

h) iLOV

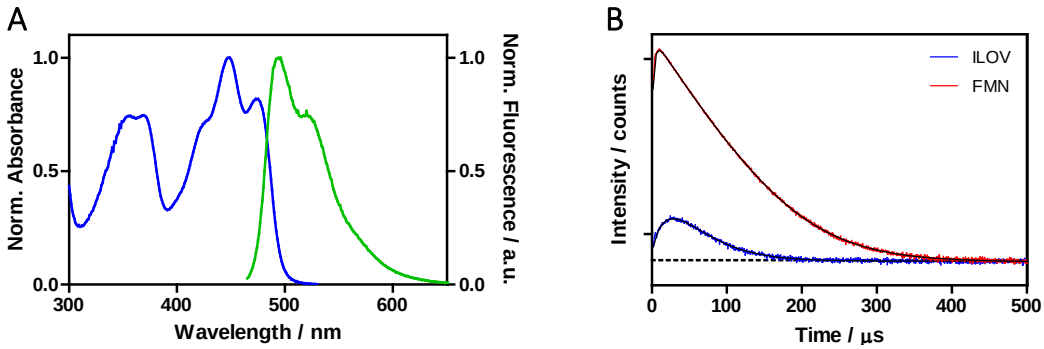

i) SOPP

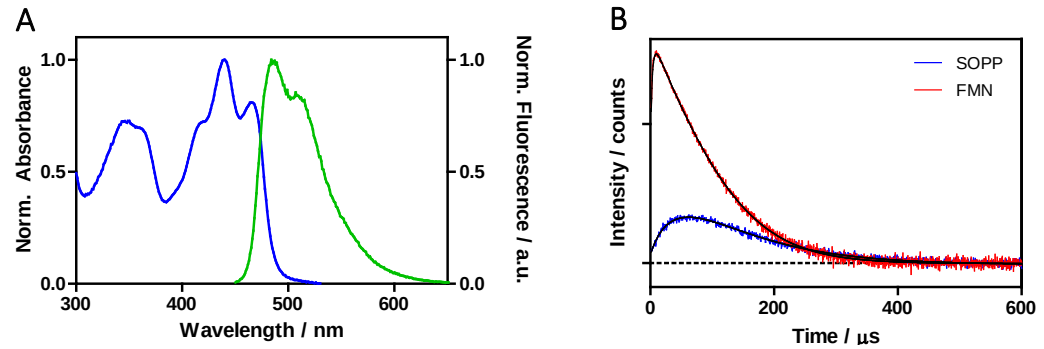

j) CreiLOV

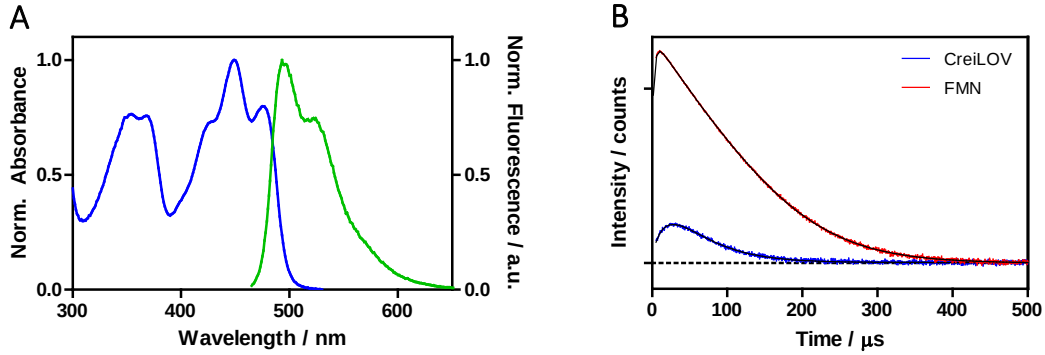

Figure 4.2. Graphics A show the absorption (blue) and fluorescence (green) spectra for the FbFPs. Graphics B show the $^1O_2$ signals of optically matched solutions of proteins (blue) and FMN (red) at 473 nm in air-saturated dPBS. Fitting lines are represented in black. The Y-axes are in log scale. Notice the differences in the time scale in the X-axes, which was conveniently adjusted to show the transients.

Table 4.2. Spectroscopic data for the eleven FbFPs characterized in air-saturated dPBS.

Protein	λ_{abs} / nm	λ_{em} / nm	Φ_F	τ_T / µs	Φ_Δ
Pp1FbFP	449	495	0.27[1]	132	0.23
Pp2FbFP	449	494	0.22[1]	96	0.11
Pp2FbFP L30M	448	493	0.25[4]	100	0.10
DsFbFP	449	496	0.35[1]	>500	0.33
DsFbFP M49I	449	497	0.36	>550	0.42
EcFbFP	449	495	0.44[1]	149	0.08
PhiLOV2.1	449	495	0.33[5]	8.3	0.01
iLOV	448	494	0.20[1]	21	0.05
miniSOG	447	496	0.41[1]	30	0.04
SOPP	440	484	0.33	111	0.23
CreiLOV	449	493	0.32	19	0.04
FMN	450	520	0.25[1]	3.2	0.57[6]

The absorption spectra for all FbFPs showed a structured profile that is attributed to vibronic transitions of the more rigid and confined chromophore molecule in the active pocket.[7] The fluorescence spectra also revealed more resolved bands and a slight blue-shift as compared to the free flavin in solution. The spectroscopic data are consistent with what has been previously observed for other flavoproteins[1,8] and therefore confirms that the FMN chromophore is tightly encased inside the protein.

Interestingly, the properties of the ^{3}FMN* exhibited notorious differences among the FbFPs studied. Since the chromophore is the same for all the proteins, the significant variation in its triplet state lifetimes provides valuable information on both the ^{3}FMN* photoproduction and its quenching processes. Because a single FMN molecule is buried in the protein's binding pocket, O_2 and nearby amino acids arise as potential quenchers. Therefore, the τ_T experimentally determined for each protein provides structural information regarding both the O_2 accessibility to the chromophore and the effect of the specific residues surrounding it.

Triplet lifetimes of tens to hundreds of microseconds in air-saturated buffer solutions reflect very low accessibility of O_2 to the chromophore. This is reasonable since the FMN molecule is buried inside the protein, so O_2 has to diffuse through the amino acid matrix before reaching it. Among the FbFPs studied, PhiLOV2.1, CreiLOV, iLOV and miniSOG revealed shorter τ_t. This observation can be reasoned considering two major factors, (1) the specific amino acid sequence

of these proteins renders FMN more accessible to O_2 or (2) ^{3}FMN* is quenched more efficiently by electron-rich residues surrounding the flavin, such as tryptophan (Trp), tyrosine (Tyr), histidine (His), methionine (Met) and cysteine (Cys).[9,10] Noteworthy, the shortest τ_T value for PhiLOV2.1 is still remarkably longer than typical values observed for organic dyes in air-saturated solution and is therefore consistent with the enclosing effect of the protein on the chromophore.

The second group of proteins showed longer τ_T values, within in the range between 90 to 150 µs (i.e., Pp2FbFP, Pp2FbFP L30M, Pp1FbFP, SOPP and EcFbFP). The increase in τ_T can be explained either by reduced O_2 accessibility (i.e., FMN is buried deeper inside the protein and the amino acid chains make the path more tortuous and difficult for O_2 diffusion) and/or as a consequence of less efficient quenching of ^{3}FMN* by nearby residues.

The third group of proteins comprises DsFbFP and DsFbFP M49I which showed very long τ_T values, beyond 500 µs. Such long lifetimes are unusual for air saturated solutions and therefore reflect an extremely low O_2 accessibility to the chromophore. Noteworthy, the experimental determination of these triplet values raises a tricky mechanistic question for the study of $^1O_2$ production and detection. If ^{3}FMN* lives for more than 500 µs in air-saturated solutions, it can be assumed that it takes more than 500 µs for O_2 to diffuse through the protein to reach the chromophore (in the absence of any other ^{3}FMN* quencher from the protein matrix). Once $^1O_2$ is produced in the immediate vicinity of the chromophore, it is not clear whether it can diffuse out to the external media or it decays inside the protein along its way out. An early assumption considered the latter process, based on the work from Lepeshkevich *et* al.[11] in which the authors observed a strong influence of the protein matrix on the radiative $^1O_2$ deactivation and determined the radiative constant of $^1O_2$ within the protein. The reported value was 1.7 ± 0.3 s^{-1}, which is about eight times larger than the one found in aqueous solutions (0.209 s^{-1}).[11,12] With their results in mind and having observed triplet state lifetimes longer than 500 µs for a chromophore encased system, it was reasonable to apply this approximation for the two DsFbFPs variants. The assumption of this model led to the determination of small Φ_Δ values despite observing an apparently intense and prolonged $^1O_2$ signal. This generated a lot of controversy and discussion and the question remained unsolved for a long time. However, later experimental evidence pointed to the other direction, suggesting that $^1O_2$ indeed escapes from the protein and ultimately decays in the aqueous media. This was unambiguously demonstrated upon exchanging the H_2O-based to D_2O-based phosphate buffer, taking advantage of the deuterium effect on the $^1O_2$ lifetime.[13] While τ_T remained practically unaltered (> 500 µs), τ_Δ increased from 3.4 µs to 42 µs, which is consistent with the $^1O_2$ lifetimes in H_2O and D_2O media,[14] respectively (Figure 4.3).

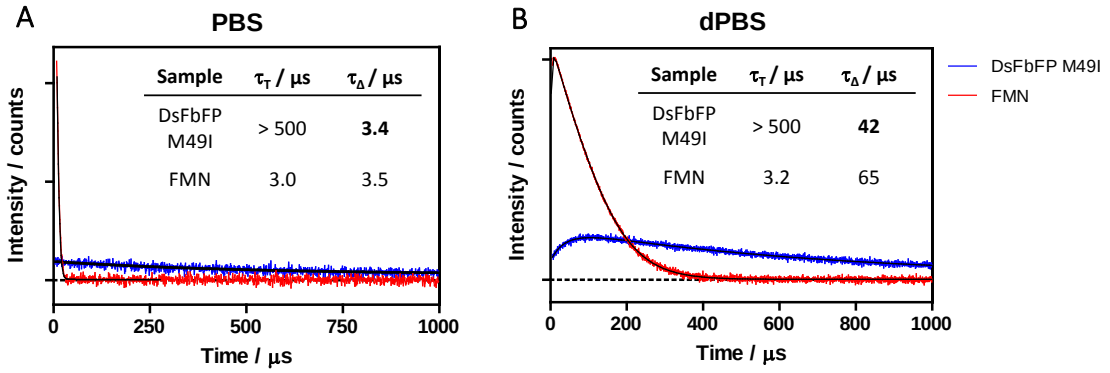

Figure 4.3. $^1O_2$ NIR phosphorescence decays at 1275 nm and kinetic data for DsFbFP M49I upon excitation at 473 nm in air-saturated A) PBS and B) dPBS solution.

As a final piece of evidence, indirect measurements of $^1O_2$ production were performed using UA in dPBS solution (Figure 4.4). The irreversible reaction of UA with $^1O_2$ provides sound evidence of the release of the $^1O_2$ molecules into the solution. The Φ_Δ thus determined was 0.28 and 0.36 for DsFbFP and DsFbFP M49I, respectively, in good agreement with the values obtained by $^1O_2$ luminescence.

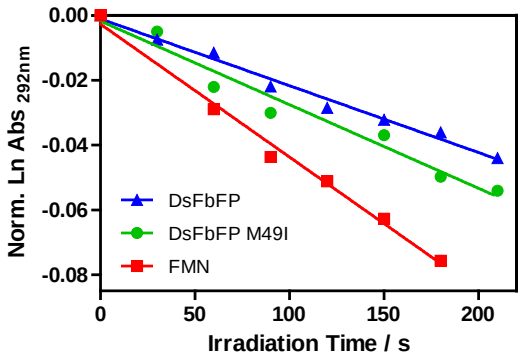

Figure 4.4. Degradation of UA upon illumination at 450 nm of optically matched solutions of DsFbFP, DsFbFP M49I and free FMN. $\Phi_{\Delta FMN}$ = 0.57 in dPBS.[6]

As a consequence, when the radiative constant in aqueous media is applied for calculations, it renders a Φ_Δ value that is about 8-fold higher than the previous estimation (the final Φ_Δ values are included in Table 4.2 above).

Noteworthy, indirect $^1O_2$ measurements for the tow DsFbFP variants were also carried out with the chemical trap 9,10-Anthracenediyl-bis(methylene)dimalonic acid (ABMDMA, also known as ADMA). ADMA is a water soluble and fluorescent anthracene derivative that irreversibly reacts with $^1O_2$ to produce the corresponding non-fluorescent endoperoxide,[15] an therefore, this reaction can be conveniently monitored by means of fluorescence spectroscopy. However, the Φ_Δ values thus obtained were abnormally high (Φ_Δ > 0.73 for DsFbFP M49I, which

taken together with the experimentally determined value $\Phi_F = 0.36$, exceeds the limit $\Phi_\Delta + \Phi_F = 1$). Moreover, large fluctuations of the Φ_Δ value were observed from independent replicates using the ADMA method. Finally, it was observed that the fluorescence of ADMA significantly increases with time after the irradiation of the photoactive protein (Figure 4.5). This is likely consequence of interactions between the protein and the fluorescent probe, which has been previously observed for other anthracene derivatives[2] and therefore hampers the valid characterization of the photosensitizing properties. These possible interactions have not been further investigated since the use of fluorescent probes is beyond the scope of the present work.

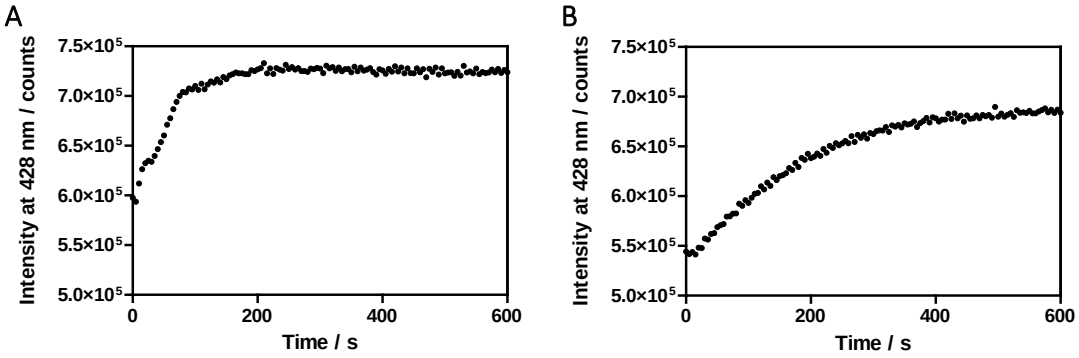

Figure 4.5. Evolution of the fluorescence intensity of ADMA at 428 nm, upon (A) 15 seconds and (B) 90 seconds of blue light irradiation of DsFbFP M49I.

4.2.2. Antimicrobial properties of FbFPs

The antimicrobial capacity of FbFPs was reported for the first time by Ruiz-González *et* al.[2] In that study, the authors demonstrated the superior photokilling ability of miniSOG expressed in *E. coli* cells as compared to the red fluorescent GFP-like protein TagRFP, previously reported as a purely endogenous $^1O_2$ PS by the same authors[16] (Figure 4.5).

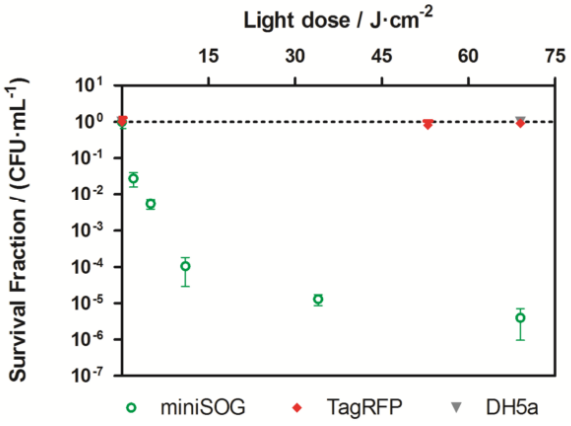

Figure 4.6. Comparison of *E. coli* light-dose dependent photokilling effect of TagRFP and miniSOG upon irradiation with green or blue light, respectively. Noteworthy, more than 1.500 J·cm^{-2} were required to induce a 2-log decrease in the number CFU·mL^{-1} for TagRFP.[16] Image from Ref. 2.

Other authors have tested the phototoxicity of FbFPs, however, all studies have been carried out in nematodes or cancer cells but not in bacteria, the primary target in aPDT. Assessing the capacity of the newly developed palette of FbFPs to kill bacterial cells therefore provides highly valuable information on their underexplored potential for aPDT applications. In addition, from a mechanistic point of view, the ability to kill cells would further demonstrate that $^1O_2$ escapes from the protein matrix and reaches the external media. Moreover, it can also be very interesting to study whether there is a correlation between the capacity of $^1O_2$ production and the killing efficiency observed *in vivo*.

Phototoxicity experiments were performed by the groups of Dr. Drepper and Dr. Gensch at the Forschungszentrum Jülich, in the framework of an ongoing collaboration. *E. coli* cells expressing each FbFP were illuminated with blue light (λ_{ex} = 448 nm, 180 mW·cm^{-2}) for increasing periods of time and cell death was evaluated firstly using the plate spot assay (Figure 4.6). The results demonstrated that almost all of the tested FbFPs exhibit strong light-triggered antimicrobial activities, resulting in pronounced growth impairment already after 10 seconds of blue-light irradiation for some cases (i.e., Pp1FbFP, DsFbFP M49I, miniSOG, SOPP and EcFbFP). Other proteins such as Pp2FbFP, Pp2FbFP L30M or CreiLOV required more extended illumination (>10 seconds) to induce significant photodamage whereas cell viability of phiLOV2.1- and DsFbFP-expressing *E. coli* cells was almost unaffected even after prolonged exposure to intense blue-light (Figure 4.7).

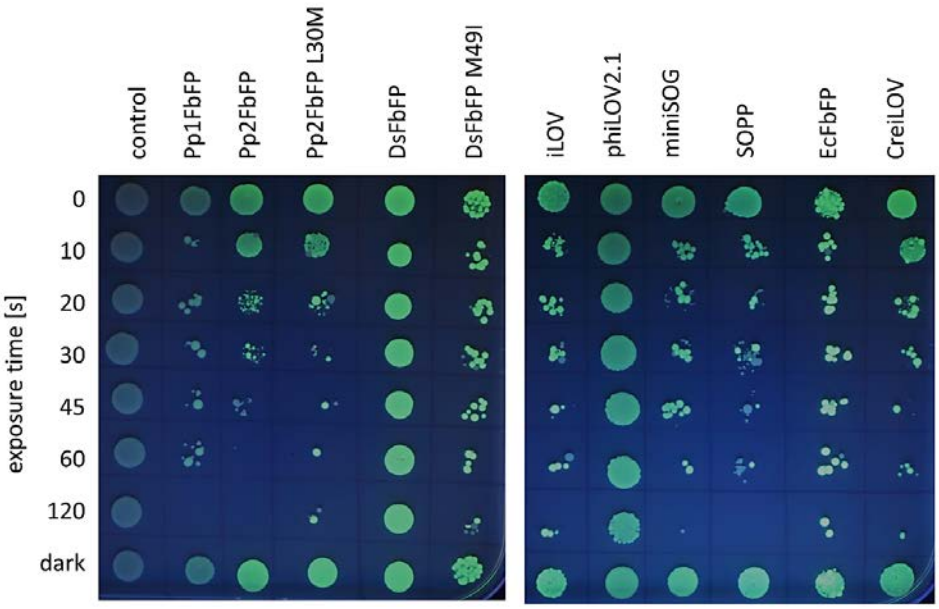

Figure 4.7. Plate spot phototoxicity assay of FbFPs. The empty vector and samples of each culture that were kept in the dark were used as controls. Green colonies represent fluorescing cells while colonies of non-fluorescing cells appear bluish due to UVA-light illumination.

To further characterize the phototoxic activities of FbFPs in *E. coli*, a propidium iodide-based assay was performed. Propidium iodide (PI) is a barely fluorescent and cell impermeable dye;[17] however, when cell membranes are disrupted (e.g., due to ROS-mediated photooxidation), it intercalates into DNA from dead cells and develops a specific, bright, red fluorescence.[17] Therefore, detection of the PI fluorescence allows monitoring FbFP-mediated cell death in a time-resolved manner. The results presented in Figure 4.8 show the increase in PI fluorescence related to the illumination time (0 to 60 minutes). For a more accurate comparison of individual phototoxicities, all cells expressing FbFPs were resuspended to a final cell density of OD_{580} = 0.5 and the PI fluorescence was normalized to the amount of functional protein, which was calculated from the *in vivo* fluorescence and the molecular brightness.

Based on the observed development of PI fluorescence intensities, the phototoxicity of the tested FbFPs can be classified into three different groups: The first encompasses SOPP, DsFbFP M49I, Pp1FbFP and iLOV, where blue-light illumination of *E. coli* cells resulted in a fast and strong increase of PI fluorescence. The second group contains Pp2FbFP, EcFbFP, miniSOG and CreiLOV, whose PI fluorescence signals developed slower after blue-light illumination and exhibited a lower intensity at the longest irradiation times, as compared to those of the first group. The third group contains the apparently less- to non-toxic proteins PhiLOV2.1, DsFbFP and Pp2FbFP L30M since *E. coli* cells expressing these three variants did not show a significant increase in PI fluorescence. In control experiments, aliquots of the same *E. coli* expressing FbFPs were kept in the dark for 60 minutes and no significant changes in the PI fluorescence could be detected, thereby confirming that the observed increase in PI fluorescence is specifically induced by the light-induced phototoxic activity of the tested FbFPs.

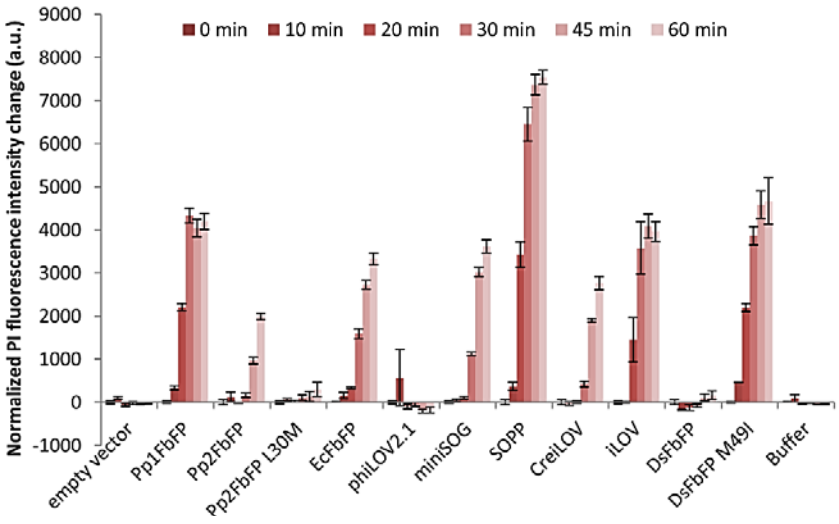

Figure 4.8. Analysis of FbFP phototoxicity using PI marker for dead *E. coli* cells. The bars show the change in PI fluorescence intensity (λ_{ex} = 535 nm, λ_{obs} = 617 nm) over 60 minutes. The data represent the mean values of three independent experiments; the error bars indicate the calculated standard deviations.

These results unambiguously demonstrate that most of the studied FbFPs are capable of cell photokilling and, thus, can potentially be used as PSs for light-controlled antimicrobial applications. In addition, the direct detection of $^1O_2$ upon illumination of the proteins provides solid arguments to link its production with the phototoxicity observed. However, if one attempts to compare the Φ_Δ values obtained for purified proteins in solution with the results from the PI experiments in bacteria, there seems to be no apparent correlation for some of the FbFPs. Many factors may account for this discrepancy since the behavior of the proteins may change as a consequence of the differences in the microenvironment of the protein inside the living cell as compared to free dissolved in solution, including different protein conformations, interactions with other cellular components/biomolecules and/or other external factors. For example, it has been recently observed that the increase of temperature has a remarkable effect on O_2-dependent quenching of ^{3}FMN*.[18]

It is also true that other processes may also compete in the deactivation of ^{3}FMN* and influence in the ultimate efficiency of cell killing. In this regard, it is known that flavins produce ROS other than $^1O_2$ upon illumination and $O_2^{\bullet-}$ has actually been detected and quantified very recently for miniSOG.[19] Therefore, differences in the formation and release of various ROS species could also contribute to different light-induced *in vivo* toxicities of individual FbFPs variants. To assess the participation of other ROS, the production of H_2O_2, (i.e., produced upon $O_2^{\bullet-}$ decomposition), was measured illuminating the purified FbFPs with the Amplex® Red Hydrogen Peroxide/Peroxidase Assay (Figure 4.9).

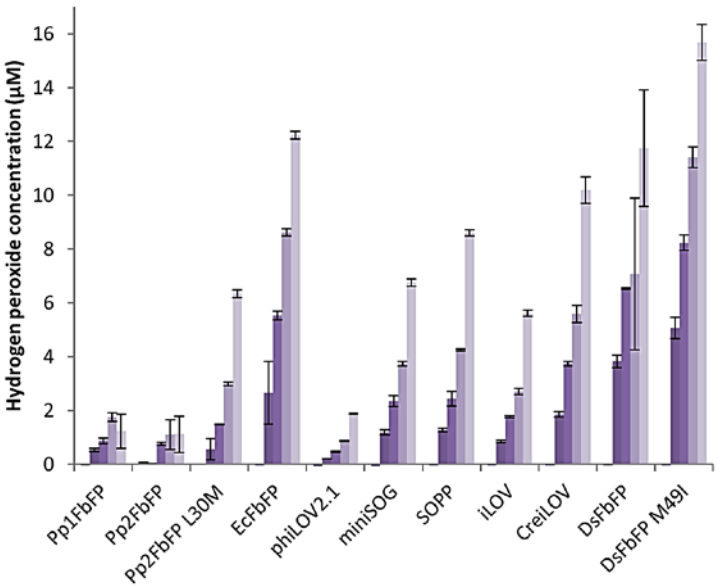

Figure 4.9. Quantification of H_2O_2 formation upon blue-light illumination of FbFPs. The control experiment in the dark did not lead to detectable H_2O_2 production for all tested proteins. The data represent the mean values of three independent experiments; the error bars indicate the calculated standard deviations.

The results of this experiment showed considerable Type-I driven ROS formation of FbFPs, particularly for the two DsFbFPs proteins and EcFbFP. However, as for the $^1O_2$ experiments, no general correlation between phototoxicity and H_2O_2 production ability could be observed.

However, it is worth noting that there are substantial differences in the irradiation time (and thus the light fluence) employed between the PI and the H_2O_2 experiments. While time intervals of 0.5 min were used for H_2O_2 quantification, the first analysis of PI fluorescence was performed at 10 minutes of blue light illumination. Importantly, a closer look at the PI experiments revealed that the time evolution of the PI fluorescence leveled off at different upper-limit values for each protein, resulting in a clear sigmoidal shape (Figure 4.8). This observation is particularly relevant since it implies that photobleaching of the proteins is indeed the critical factor that limits their phototoxic properties. This is consistent with the photobleaching rates reported previously for some of the tested FbFPs in this work.[1] If the protein did not photobleach, the rate of $^1O_2$ production would be stable and the increase in PI fluorescence would not show a sigmoidal shape. Since the Φ_Δ values were determined using much lower light fluences to prevent photobleaching processes, a better comparison between the protein's ability to kill cells and the quantum yields should be made using the initial rate of photokilling. Because photobleaching leads to a loss of protein fluorescence up to 30-40 % within the first 10 minutes of irradiation, it is reasonable to assume that the ability to produce $^1O_2$ decreases accordingly. It is therefore appropriate to use a *corrected* Φ_Δ value. The best way of estimating the *average* Φ_Δ during the 0 - 10 minutes period is by averaging the initial and final Φ_Δ – the final being estimated by normalizing it to the protein fluorescence at 10 minutes. Plotting the corrected values yields a clear correlation between the Φ_Δ values and the cell photokilling efficiency (Figure 4.10).

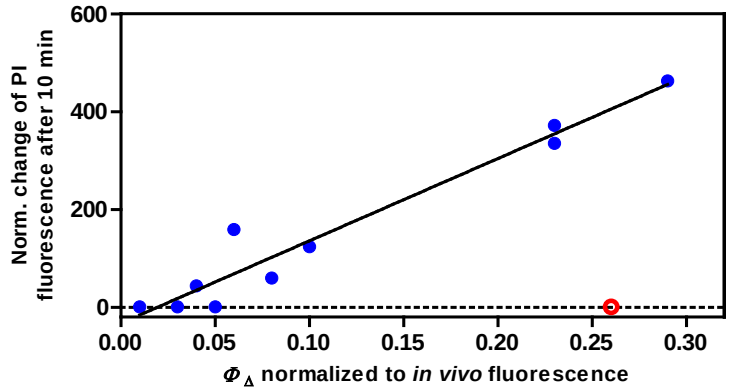

Figure 4.10. Correlation between the $^1O_2$ production and the increase of PI fluorescence after 10 minutes of blue light illumination. Φ_Δ values have been normalized to the decrease in FbFP fluorescence after the 10 minutes. The empty red circle corresponds to DsFbPs and has been excluded from drawing the linear regression, (see text).

Of note, DsFbFP has been excluded from the linear regression analysis since it has been reported that this protein photobleaches much faster as compared to the other FbFPs.[1] Therefore, it can be assumed that the lack of phototoxicity can be explained by the rapid photodegradation of the protein after intense irradiation. Table 4.3 collects the results after 10 minutes irradiation.

Table 4.3. Changes in PI and FbFP fluorescence after 10 minutes irradiation. The normalized Φ_Δ value at 10 minutes has been calculated to the protein fluorescence at the same time elapsed.

Protein	Φ_Δ	Norm. change of PI fluorescence	% *in vivo* fluorescence	Φ_Δ norm. to *in vivo* fluorescence
Pp1FbFP	0.23	335	99	0.23
Pp2FbFP	0.11	124	76	0.10
Pp2FbFP L30M	0.10	60	56	0.08
EcFbFP	0.07	159	71	0.06
PhiLOV2.1	0.01	1	92	0.01
miniSOG	0.04	44	91	0.04
SOPP	0.25	372	84	0.23
CreiLOV	0.04	1	67	0.03
iLOV	0.05	1	89	0.05
DsFbFP	0.33	1	79	0.26
DsFbFP M49I	0.42	463	69	0.29

Regarding the production of other ROS, it is true that some of the proteins form H_2O_2, however, it is not clear to what extent H_2O_2 contributes to cell death. Several studies have actually reported that H_2O_2 is not particularly reactive towards cellular components.[20–22] On the other hand, it cannot be excluded that H_2O_2 may be formed from singlet oxygen[23] (Scheme 4.1). For all these reasons, and supported by the correlation observed in Figure 4.10 and by the well-known reactivity of $^1O_2$ in biological systems, there is now little doubt that $^1O_2$ is the main cell killer.

$$E^{-}_{DONOR} + {}^1O_2 \longrightarrow E^{\bullet+}_{DONOR} + O_2^{\bullet-}$$

$$2\, O_2^{\bullet-} \longrightarrow H_2O_2$$

Scheme 4.1. Reactions involved in the formation of H_2O_2 from $^1O_2$ through the participation of intermediate radical species.

4.3. Conclusions

The photophysical, photosensitizing and antimicrobial properties of eleven FbFPs have been characterized. Fresh protein samples have been prepared following the methodology developed previously and studied on the same day of purification, in order to minimize the possibility of phototransformations. The absorption and fluorescence spectra for all the flavoproteins show structured bands which reflects the more rigid environment of the FMN chromophore inside the protein as compared to the flavin freely dissolved in solution. The position of the fluorescent bands is also slightly blue-shifted for the FMN encased in the active pocket of the proteins. All FbFPs photosensitize $^1O_2$ upon blue light illumination; however, significant differences in both the ability and kinetics have been observed by direct detection of $^1O_2$ NIR phosphorescence at 1275 nm. Because the chromophore is the same for all the flavoproteins, the properties of the triplet excited state reflect the ability of O_2 to diffuse through the protein matrix and the influence that the particular amino acids that make up each protein exert to the FMN chromophore. In addition, the photosensitizing capacity of the FbFPs has been tested for aPDT applications. Phototoxic experiments in *E. coli* cells have demonstrated that most of the proteins are capable of killing bacteria efficiently and selectively upon blue light illumination, being nontoxic in dark conditions. Furthermore, the photokilling properties correlate with the ability to produce $^1O_2$, confirming that, besides other ROS, $^1O_2$ is indeed the prominent cell killer. These results expand the toolbox of flavoproteins for fluorescence imaging and aPDT applications and provide valuable structural information for the rational design of novel and improved flavoproteins with great potential as biological PSs for optogenetic approaches.

4.4. References

(1) Wingen, M.; Potzkei, J.; Endres, S.; Casini, G.; Rupprecht, C.; Fahlke, C.; Krauss, U.; Jaeger, K.-E.; Drepper, T.; Gensch, T. The Photophysics of LOV-Based Fluorescent Proteins – New Tools for Cell Biology. *Photochem. Photobiol. Sci.* **2014**, *13* (6), 875–883.

(2) Ruiz-González, R.; Cortajarena, A. L.; Mejias, S. H.; Agut, M.; Nonell, S.; Flors, C. Singlet Oxygen Generation by the Genetically Encoded Tag MiniSOG. *J. Am. Chem. Soc.* **2013**, *135* (26), 9564–9567.

(3) Pimenta, F. M.; Jensen, R. L.; Breitenbach, T.; Etzerodt, M.; Ogilby, P. R. Oxygen-Dependent Photochemistry and Photophysics of "MiniSOG," a Protein-Encased Flavin. *Photochem. Photobiol.* **2013**, *89* (5), 1116–1126.

(4) Torra, J.; Burgos-Caminal, A.; Endres, S.; Wingen, M.; Drepper, T.; Gensch, T.; Ruiz-González, R.; Nonell, S. Singlet Oxygen Photosensitisation by the Fluorescent Protein Pp2FbFP L30M, a Novel Derivative of Pseudomonas Putida Flavin-Binding Pp2FbFP. *Photochem. Photobiol. Sci.* **2015**, *14* (2), 280–287.

(5) Davari, M. D.; Kopka, B.; Wingen, M.; Bocola, M.; Drepper, T.; Jaeger, K. E.; Schwaneberg, U.; Krauss, U. Photophysics of the LOV-Based Fluorescent Protein Variant ILOV-Q489K Determined by Simulation and Experiment. *J. Phys. Chem. B* **2016**, *120* (13), 3344–3352.

(6) Rodríguez-Pulido, A.; Cortajarena, A. L.; Torra, J.; Ruiz-González, R.; Nonell, S.; Flors, C. Assessing the Potential of Photosensitizing Flavoproteins as Tags for Correlative Microscopy. *Chem. Commun.* **2016**, *52* (54), 8405–8408.

(7) Schüttrigkeit, T. A.; Kompa, C. K.; Salomon, M.; Rüdiger, W.; Michel-Beyerle, M. E. Primary Photophysics of the FMN Binding LOV2 Domain of the Plant Blue Light Receptor Phototropin of Avena Sativa. *Chem. Phys.* **2003**, *294* (3), 501–508.

(8) Salomon, M.; Christie, J. M.; Knieb, E.; Lempert, U.; Briggs, W. R. Photochemical and Mutational Analysis of the FMN-Binding Domains of the Plant Blue Light Receptor, Phototropin. *Biochemistry* **2000**, *39* (31), 9401–9410.

(9) Heelis, P. F.; Parson, B. J.; Phillips, G. O. The PH Dependence of the Reactions of Flavin Triplet States with Amino Acids: A Laser Flash Photolysis Study. *Biochim. Biophys. Acta - Gen. Subj.* **1979**, *587* (3), 455–462.

(10) Tsentalovich, Y. P.; Lopez, J. J.; Hore, P. J.; Sagdeev, R. Z. Mechanisms of Reactions of Flavin Mononucleotide Triplet with Aromatic Amino Acids. *Spectrochim. Acta - Part A Mol. Biomol. Spectrosc.* **2002**, *58* (9), 2043–2050.

(11) Lepeshkevich, S. V.; Parkhats, M. V.; Stasheuski, A. S.; Britikov, V. V.; Jarnikova, E. S.; Usanov, S. A.; Dzhagarov, B. M. Photosensitized Singlet Oxygen Luminescence from the Protein Matrix of Zn-Substituted Myoglobin. *J. Phys. Chem. A* **2014**, *118* (10), 1864–1878.

(12) Schmidt, R.; Shafii, F.; Hild, M. The Mechanism of the Solvent Perturbation of the a 1 Δ g → X 3 Σ g - Radiative Transition of O 2. *J. Phys. Chem. A* **1999**, *103* (15), 2599–2605.

(13) Schweitzer, C.; Schmidt, R. Physical Mechanisms of Generation and Deactivation of Singlet Oxygen. *Chem. Rev.* **2003**, *103* (5), 1685–1758.

(14) Wilkinson, F.; Helman, W. P.; Ross, A. B. Quantum Yields for the Photosensitized Formation of the Lowest Electronically Excited State of Molecular Oxygen in Solution. *J. Phys. Chem. Ref. Data* **1993**, *22* (1), 113–262.

(15) Zhao, B.; Yin, J. J.; Bilski, P. J.; Chignell, C. F.; Roberts, J. E.; He, Y. Y. Enhanced Photodynamic Efficacy towards Melanoma Cells by Encapsulation of Pc4 in Silica Nanoparticles. *Toxicol. Appl. Pharmacol.* **2009**, *241* (2), 163–172.

(16) Ruiz-González, R.; White, J. H.; Agut, M.; Nonell, S.; Flors, C. A Genetically-Encoded Photosensitiser Demonstrates Killing of Bacteria by Purely Endogenous Singlet Oxygen. *Photochem. Photobiol. Sci.* **2012**, *11* (9), 1411–1413.

(17) Crowley, L. C.; Scott, A. P.; Marfell, B. J.; Boughaba, J. A.; Chojnowski, G.; Waterhouse, N. J. Measuring Cell Death by Propidium Iodide Uptake and Flow Cytometry. *Cold Spring Harb. Protoc.* **2016**, *2016* (7), 647–651.

(18) Westberg, M.; Bregnhøj, M.; Etzerodt, M.; Ogilby, P. R. Temperature Sensitive Singlet Oxygen Photosensitization by LOV- Derived Fluorescent Flavoproteins. *J. Phys. Chem. B* **2017**, *121*, 2561–2574.

(19) Barnett, M. E.; Baran, T. M.; Foster, T. H.; Wojtovich, A. P. Quantification of Light-Induced MiniSOG Superoxide Production Using the Selective Marker, 2-Hydroxyethidium. *Free Radic. Biol. Med.* **2018**, *116*, 134–140.

(20) Fee, J. A. Is Superoxide Important in Oxygen Poisoning? *Trends Biochem. Sci.* **1982**, *7* (3), 84–86.

(21) Nordberg, J.; Arnér, E. S. J. Reactive Oxygen Species, Antioxidants, and the Mammalian Thioredoxin System. *Free Radic. Biol. Med.* **2001**, *31* (11), 1287–1312.

(22) Winterbourn, C. C. Reconciling the Chemistry and Biology of Reactive Oxygen Species. *Nat. Chem. Biol.* **2008**, *4* (5), 278–286.

(23) Winkler, B. S.; Boulton, M. E.; Gottsch, J. D.; Sternberg, P. Oxidative Damage and Age-Related Macular Degeneration. *Mol. Vis.* **1999**, *5* (May), 32.

CHAPTER 5

The photochemistry of miniSOG

The photosensitizing flavoprotein miniSOG has been studied in detail. The crystal structure has been solved at 1.17 Å high resolution. The factors that limit the low $^1O_2$ production of miniSOG have been rationalized and the transformations that it undergoes upon photolysis have been explained. In addition, novel miniSOG mutants have been developed and characterized, aiming at enhancing its photosensitizing ability.

An expert is a person who has made all the mistakes
that can be made in a very narrow field.
Niels Bohr

5.1. Introduction

MiniSOG (for mini Singlet Oxygen Generator)[1] is a 106 amino acid protein engineered from the LOV2 (Light, Oxygen and Voltage) domain of *Arabidopsis thaliana* phototropin 2. MiniSOG was originally developed for CLEM applications as it efficiently catalyzes the photo-oxidation of DAB, providing high-resolution images.[1] In addition, miniSOG fluoresces with a moderate quantum yield ($\Phi_F \sim 0.37$)[1] which allows to expanding its potential also for fluorescence microscopy imaging. Combining these techniques, cells and tissues can be studied from the micrometer to nanometer scales.[2] Since its development in 2011 by Shu and coworkers, miniSOG has been used or studied in more than 60 publications so far, aiming at characterizing its properties and exploring its potential for a wide range of applications.[3–5]

Despite great progress made since the first report, a number of fundamental questions remain unanswered concerning the structure and function of miniSOG and, by extension, of other flavoproteins considered for $^1O_2$ photogeneration. First, the actual structure of miniSOG remains still unsolved, and therefore the development of miniSOG mutants has been guided so far by random mutagenesis[6,7] or by a semiempirical approach based on modeled structures obtained from artificially mutated LOV analogs.[8,9] Solving the crystal structure will provide precise knowledge of miniSOG that is essential to understand the trafficking of O_2 and of $^1O_2$ between the external medium and the protein chromophore as well as to get insights on the photochemical behavior of the protein. Other intriguing aspects that require attention are the τ_T and Φ_Δ values. MiniSOG's triplet lifetime is much shorter than that of FMN in nitrogen (N_2)-saturated solutions (33.6 µs[10] vs. 200 µs[11]), whereas its Φ_Δ is much lower than that for the free flavin in PBS (0.03[12,13] vs. 0.51[14]). This has been recently rationalized as the result of O_2-independent competing reactions between the triplet FMN chromophore, ^{3}FMN*, and nearby protein residues, particularly electron transfer processes from tryptophan, and inefficient O_2 diffusion through the protein scaffold.[9]

On the other hand, early results from our laboratory reported the dramatic increase of miniSOG Φ_Δ upon extended exposure of the protein to light,[12] which was later confirmed by independent studies.[13] However, the processes and the compounds involved in the phototransformation, as well as the structural changes and their consequences, have not been assessed so far. A closer look into miniSOG using a combination of structural and photophysical data may provide definitive answers to all these open and puzzling questions, thereby establishing a sound scientific basis for the rational development of the next generation of genetically encoded $^1O_2$ PSs.

5.2. miniSOG explained

The photophysical and photosensitizing properties of miniSOG have been a matter of intense research over the last years.[8,10,12,13] Comprehensive analysis of all the results reported in previous studies, supported and completed with new data from this work (see Chapter 4 for photophysical and photosensitizing data of miniSOG) allow to drawing the whole picture of the current understanding of the photochemistry of miniSOG (Scheme 5.1). Values of relevant photophysical properties are given in Table 5.1.

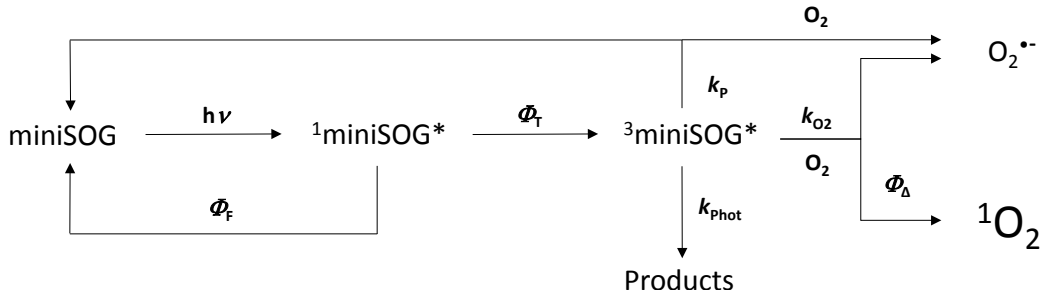

Scheme 5.1. Schematic representation of the photophysical and photosensitization processes of miniSOG.

Upon light absorption, miniSOG is promoted to its singlet excited state, ^{1}miniSOG*, from which it either returns to the ground state emitting fluorescence or it undergoes ISC to populate the triplet state, ^{3}miniSOG*. Other decay pathways such as reaction with nearby amino acid residues can be safely ruled out since no shortening of the fluorescence lifetime or decrease in the Φ_F are observed relative to FMN. The protein matrix confers an enclosing and protective effect on the chromophore, which is reflected by the remarkable increase in the lifetime of ^{3}miniSOG* in air-saturated solutions (~ 31 µs vs. ~ 3 µs). However, τ_T increases only slightly, up to ~ 33.6 µs in O_2-depleted conditions,[10] substantially shorter than that of free ^{3}FMN* in solution (~ 200 µs).[11] This indicates that protein quenching is a major mechanism of triplet decay.[9] Comparison of τ_T values in N_2-saturated solutions of miniSOG and a novel mutant called SOPP3[9] (for Singlet Oxygen Photosensitizing Protein 3), a protein devoid of any electron-rich amino acid in the vicinity of the flavin, allows to estimate the rate constant for protein quenching in miniSOG ($k_P = k_T^{N2} - k_T^{N2}{}_{SOPP3}$, Table 5.1). In the presence of O_2, a second decay pathway is possible, namely quenching to produce $^1O_2$ (energy transfer, type II) or $O_2^{\bullet-}$ (electron transfer, type I), as observed for FMN in solution.[15] It is also possible to produce $O_2^{\bullet-}$ by reaction of O_2 with a radical anion formed during protein quenching. Comparison of the τ_T data in air- and N_2-saturated solutions allows estimating the pseudo-first order rate constant for oxygen quenching ($k_{O_2} = k_T^{Air} - k_T^{N2}$; Table 5.1). Finally, miniSOG undergoes photoproduct formation, albeit with a comparably lower rate constant (k_{Phot}; see Table 5.1).

Table 5.1. Photophysical properties of miniSOG in D_2O and H_2O-based PBS.

Parameter	D_2O	H_2O
τ_S	4.96 ns [a]	4.86 ns [a]
Φ_F	0.43 [a]	0.42 [a]
Φ_T	0.6 [b]	0.6 [b]
$k_T^{N_2}$	2.41 x 10^4 s^{-1} [a]	2.98 x 10^4 s^{-1} [a]
k_P	2.38 x 10^4 s^{-1}	2.95 x 10^4 s^{-1} [c]
k_T^{Air}	2.59 x 10^4 s^{-1} [a]	3.19 x 10^4 s^{-1} [a]
k_{O_2}	1.8 x 10^3 s^{-1}	2.3 x 10^3 s^{-1}
Φ_Δ	0.04 [b,d]	0.03 [e,f]
k_{Phot}	1.3 s^{-1}	-

[a]Ref.[10]. [b]Ref. [8]. [c]Assuming the same value of $k_T^{N_2,SOPP3}$ in H_2O and D_2O. [d]This work. [e]Ref. [12]. [f]Ref. [13]

Analysis of the rate constants in Table 5.1 allows drawing the following conclusions: (1) Protein quenching is the main triplet deactivation pathway in miniSOG, removing 93% of the triplets in air-saturated solutions (k_p / k_p + k_{O_2}). (2) Oxygen quenching only traps 7% of the triplets, which limits the maximum Φ_Δ value to 0.6 x 0.07 = 0.042 (Equation 5.1), in excellent agreement with the experimental value (Φ_Δ = 0.04). It can therefore be concluded that the ability of miniSOG to produce $^1O_2$ is defined by the *competition* between protein- and oxygen quenching.

$$\Phi_\Delta = \Phi_T \times \frac{k_{O_2}}{k_p + k_{phot} + k_{O_2}} \approx \Phi_T \times \frac{k_{O_2}}{k_p + k_{O_2}} \qquad \textbf{Equation 5.1.}$$

5.2.1. Crystal structure

This work has been performed in collaboration with the group of Dr. Antoine Royant at the Institut de Biologie Structurale (IBS) and at the European Synchrotron Radiation Facility (ESRF), Grenoble, France. The crystal structure of miniSOG (Figure 5.1A) has been solved at 1.17 Å high resolution with the molecular replacement method using a previously determined structure of the LOV2 domain of *A. thaliana* phototropin 2[16] (PDB 4EEP). The structures are very close from each other (root-mean-square deviation on Cα atoms of 0.39 Å) and two mutations C40/426G (miniSOG/phototropin 2 numbering) and F84/470L have been identified to affect significantly the FMN-binding cavity. C40G is the photoreaction-hindering mutation, and the removal of a side chain at position 40, added to the smaller size of the side chain at position 84, induce the displacement of three strands towards the isoalloxazine ring, providing the chromophore with a more rigid environment.

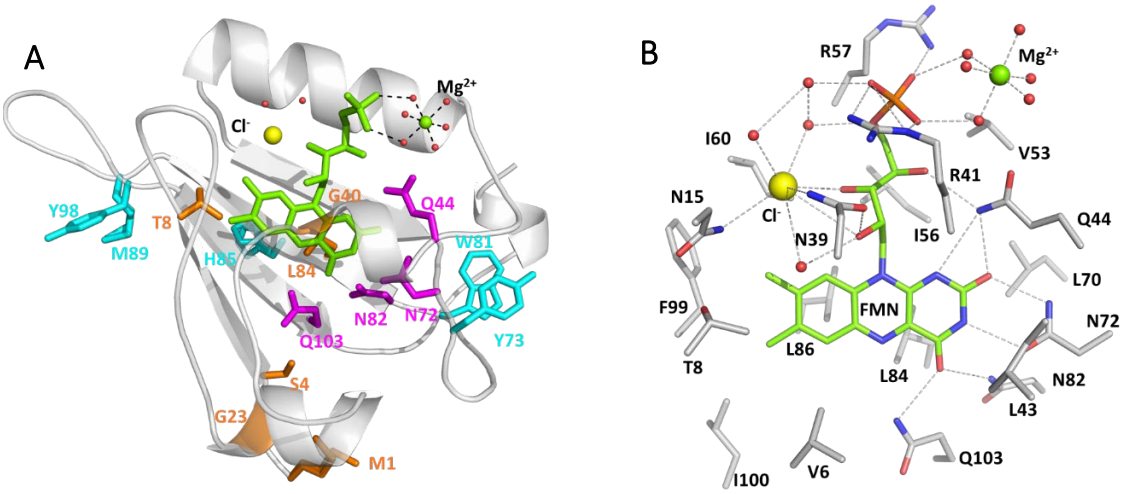

Figure 5.1. A) Secondary structure of the protein (light gray) represented with its chromophore FMN (green), chloride (yellow) and magnesium (green) ions, and H_2O molecules (red). Selected amino acids are represented: mutated residues from LOV2 (orange), residues stabilizing the isoalloxazine ring via hydrogen bonds (magenta), and surface residues susceptible to oxidation (cyan). B) Close-up on the interactions stabilizing the FMN. Hydrogen and coordination bonds are represented as dashed grey lines.

The FMN chromophore is stabilized by the protein through hydrogen bonds on one half of the isoalloxazine ring, and van der Waals interactions on the other half (Figure 5.1B).The ribityl tail lies in a tunnel bridging the bulk solvent and the core of the protein (Figure 5.2), with its terminal phosphate group (PO_4^{2-}) stabilized by two surface arginine residues (R41 and R57) and an hexa-hydrated magnesium ion (Figure 5.1B). A chloride ion is located next to the phosphoribityl tail positioned halfway through the tunnel. The presence of magnesium and chloride is favored by the composition of the crystallization mother liquor. It has been reported that chloride can be a good mimic of O_2,[17,18] which suggests that this location may serve as a transient affinity site for O_2 when diffusing from the solvent to the chromophore via the tunnel.

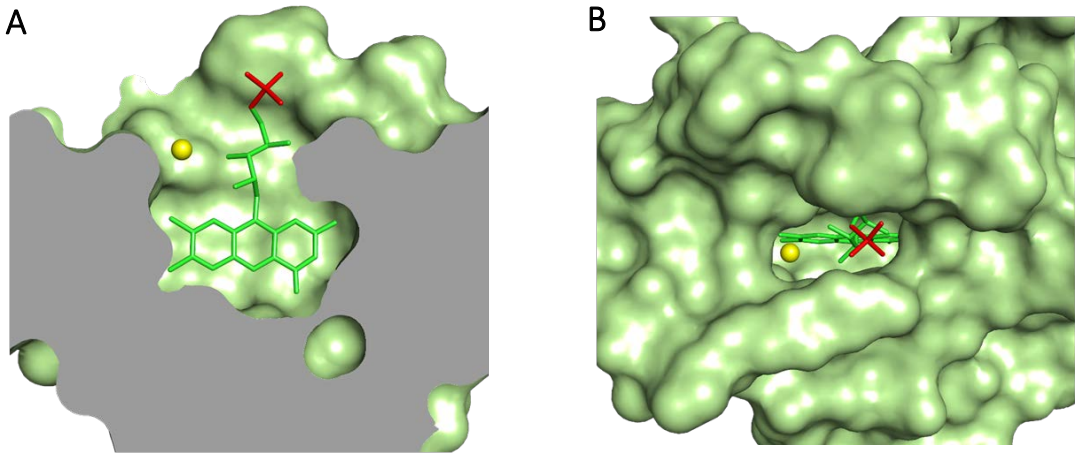

Figure 5.2. Front (A) and top (B) visualization of the surface representation of miniSOG showing the topology of the FMN binding site.

The crystallographic results demonstrated that O_2 access to the chromophore is severely limited by the phosphoribityl tail blocking the tunnel, which explains the low value of k_{O_2}. Therefore, one possible strategy to increase the Φ_Δ value is to remove this tail, thereby enhancing O_2 quenching (see below).

Alternatively, Φ_Δ can also be enhanced by decreasing k_p. Our results show that the electron-rich residues Met1, Tyr73, Trp81, His85, Met89 and Tyr98 are positioned close to the chromophore and can thus act as electron-transfer quenchers of ^{3}miniSOG *. Similarly, residues Glu44, Asp72, Asp82 and Glu103, form hydrogen bonds with FMN (Figure 5.1B), which may enhance protein quenching. Replacing selectively these residues should lead to a lengthening of τ_T of miniSOG, and to a higher fraction of triplets being trapped by O_2, thus to a higher Φ_Δ value. In fact, miniSOG mutants lacking some of these amino acids show considerably longer τ_T values (e.g., 196 μs for miniSOG Q103L (SOPP),[9] 1.0 ms for miniSOG W81F, and 3.3 ms for SOPP3[9] in oxygen-free solutions) and larger Φ_Δ values (0.25, 0.33 and 0.6, respectively), in agreement with Equation 5.1. It is worth noting also that miniSOG produces more $O_2^{\bullet-}$ than FMN,[15] which indicates that the radical anion pathway contributes to the production of $O_2^{\bullet-}$. Consistent with this, the mutant SOPP shows an 8-fold higher Φ_Δ value than miniSOG but only a 1.3 higher yield of $O_2^{\bullet-}$.[8] Thus, removal of electron-rich residues in the vicinity of the chromophore should strongly reduce the formation of $O_2^{\bullet-}$.

5.2.2. Transformations upon photolysis

In an early work, Ruiz-González *et* al. observed a 10-fold increase in miniSOG's Φ_Δ upon prolonged irradiation at 355 nm,[12] which has been reproduced by independent laboratories.[8,13] To get further insights in this phototransformation and understand the processes involved, we performed an extensive spectroscopic study. The pBAD plasmid encoding miniSOG was transformed into competent TOP10 *E. coli* cells and protein expression and purification were performed as described in Chapter 3.

Prolonged exposure of fresh miniSOG to 355 nm light induces a number of remarkable changes in the protein. On the one hand, the FMN chromophore shows photobleaching and new bands appear concomitantly in the 300 - 400 nm region (Figure 5.3A). This is accompanied by the onset of new fluorescence bands at shorter wavelengths (Figure 5.3B). Because severe bleaching is observed for the absorbance bands above 420 nm, and blue light is broadly used for photo-oxidation experiments using miniSOG, the effects of light illumination at 473 nm were

studied as well, where the photoproducts barely absorb. Interestingly, visible light induces similar spectroscopic changes in the absorption and fluorescence spectra (Figure 5.3C and 3D). On the other hand, regarding the photosensitizing properties, a new, shorted-lived component ($\tau_T \sim 3$ µs) can be observed in the triplet decay kinetics upon light excitation at 355 nm and at 473 nm, which leads to a faster rise of the $^1O_2$ NIR phosphorescence signal (Figures 5.3E and 5.3F). In light of Equation 5.1, the 10-fold shortening in τ_T suggests severe changes in k_{O_2}.It is worth noting that the Φ_Δ value remarkably increases when excited at 355 nm, suggesting also remarkable changes in k_p. However, it remains essentially constant if probed at 473 nm, where the photoconverted protein hardly absorbs, and despite the photobleaching observed in the absorption bands. The evolution of the kinetic parameters of the $^1O_2$ photosensitization along the photolysis of miniSOG is collected in Table 5.2 and Table 5.3 for 355 nm and 473 nm light excitation, respectively.

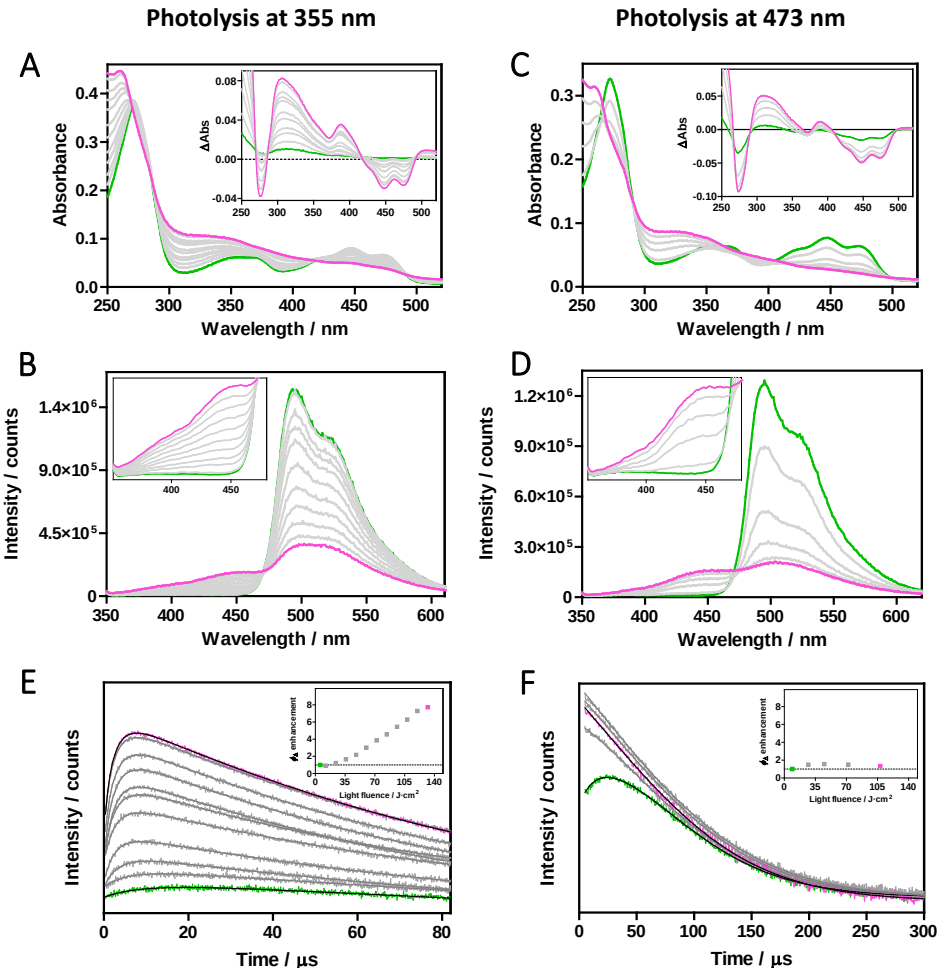

Figure 5.3. Spectroscopic changes of miniSOG upon photolysis (from blue to red lines) at 355 nm (left column panels) and 473 nm (right column panels). Insets in the absorption spectra (A and C) show the difference spectra before and after the successive irradiations. Insets in the emission spectra (B and D) show a zoomed-in image of the new bands formed. (Fluorescence spectra were recorded at λ_{ex} = 320 nm, exciting both the FMN chromophore and the photoproducts). Insets in the $^1O_2$ signals (E and F) show the Φ_Δ enhancement.

Table 5.2. Evolution of miniSOG $^1O_2$ photosensitization kinetics upon photolysis at 355 nm.

Light fluence / J·cm^{-2}	τ_{T1} / µs[a]	τ_{T2} / µs	Relative Φ_Δ
6	27 (2890)	--	1.00
12	27 (1628)	4.6 (996)	0.92
24	27 (1228)	4.3 (2310)	1.22
36	27 (1055)	3.2 (3723)	1.65
48	27 (957)	2.7 (5309)	2.17
60	--	2.9 (8729)	3.02
72	--	2.9 (11121)	3.85
84	--	2.8 (13175)	4.56
96	--	2.8 (15738)	5.45
108	--	2.8 (18173)	6.29
120	--	2.7 (21057)	7.29
132	--	2.6 (22310)	7.72

S_0 values are given in parentheses for comparison.

Table 5.3. Evolution of miniSOG $^1O_2$ photosensitization kinetics upon photolysis at 473 nm.

Light fluence / J·cm^{-2}	τ_T / µs[a]	Relative Φ_Δ
9	29 (7772)	1.00
27	17 (11541)	1.48
45	7.2 (12033)	1.55
72	4.1 (11581)	1.49
108	5.0 (10325)	1.33

S_0 values are given in parentheses for comparison.$^1O_2$ signals could not be conveniently fitted using a tri-exponential model.

In addition to the spectroscopic data, the availability of well-diffracting crystals of miniSOG allowed the study of structural transformations induced by 460 nm blue light irradiation. The light intensity was conveniently adjusted since stronger irradiation led to non-diffracting crystals whereas lower irradiation did not induce substantial structural changes in the crystal. As observed in solution, photolysis of miniSOG crystals induced significant fluorescence bleaching (Figure 5.4). It is interesting to note that the relative intensity of the two bands is the opposite and slightly red-shifted as observed for miniSOG in solution. Although this effect likely reflects differences in the protein's conformation within the ordered crystal as compared to the bulk solution, the determination of these factors is beyond the scope of this work.

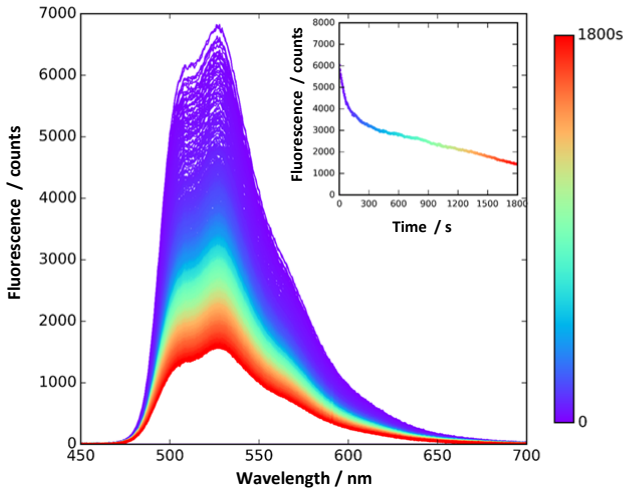

Figure 5.4. Blue light-induced fluorescence bleaching of miniSOG crystals.

Blue light irradiation allowed keeping diffraction around 2.0 Å resolution while generating sufficient damage to be visualized in electron density maps. Inspection of a difference Fourier map calculated from diffraction data sets recorded on a non-irradiated and a blue-light irradiated part of a miniSOG crystal revealed the loss of electron density all along the phosphoribityl tail of the FMN chromophore (Figure 5.5A), strongly suggesting its cleavage.

In order to identify the precise location of the cleavage, LC-MS mass spectrometry was performed on protein samples in solution that had been exposed to increasing blue-light fluences, focusing on the low molecular weight region. Progressive disappearance of the FMN peak at m/z = 457.1 was observed, in favor of a peak at m/z = 243.1 that emerged in a light dose-dependent manner (Figure 5.5B).

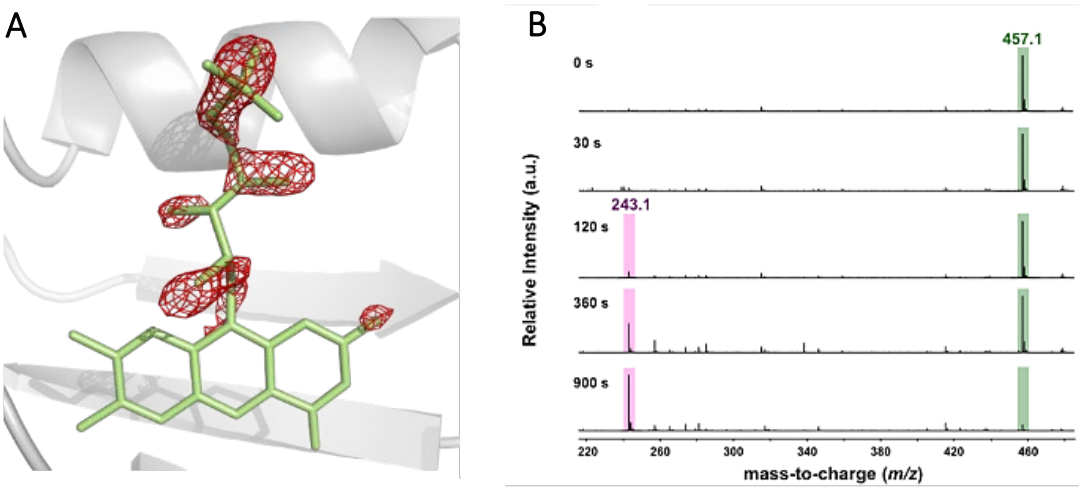

Figure 5.5. A) 2.0 Å resolution difference Fourier map calculated between non-irradiated and blue light-irradiated parts of a miniSOG crystal contoured at a -3.0 σ level (red) superimposed on the FMN molecule (pale green). B) ESI mass spectra of miniSOG irradiated with 460 nm light for 0, 30, 120, 360 and 900 seconds.

On the basis of the structural and spectroscopic data, our results demonstrate that the FMN chromophore in miniSOG is converted into a new product upon blue light illumination. With all this in mind, we sought to identify the photoconverted chromophore. Lumichrome (LC) emerged as the main candidate consistent with the above observations: (1) LC is a photodegradation product of flavins in aqueous solutions,[19] with a molar mass of 242.24 g·mol^{-1} (Figure 5.6A); (2) LC absorbs and fluoresces at shorter wavelengths than FMN (Figures 5.6B and 5.6C), consistent with the observed spectral changes; (3) LC lacks the phosphoribityl tail of FMN, hence access of O_2 to the isoalloxazine ring is favored (Figure 5.6D). This is consistent with the shorter τ_T observed in photolyzed protein samples and implies that k_{O_2} increases. (4) The $\Delta_r G°$ value for quenching of ^{3}riboflavin* by tryptophan is -86.5 kJ·mol^{-1} (riboflavin is analogous to FMN except for the PO_4^{2-}) while is more positive for ^{3}LC*, -67.2 kJ·mol^{-1};[20] hence protein quenching should be less favored and k_p decreases, and (5) LC is also an excellent $^1O_2$ PS,[20–22] Φ_Δ = 0.34 has been determined in dPBS (Figure 5.6D), which is in excellent agreement with literature values.[23]

In summary, in the photoconverted samples of miniSOG encasing LC, the lack of the phosphoribityl tail would imply higher accessibility to O_2 (↑ k_{O_2}), and in combination with lower protein quenching ability (↓ k_p), the Φ_Δ should be reasonably much larger than that of non-irradiated samples since a larger fraction of triplets would be trapped by O_2. It is highly reassuring that a remarkable increase in Φ_Δ is observed when photolyzed miniSOG is excited at 355 nm, where LC absorbs strongly, but not at 473 nm, where it barely absorbs.

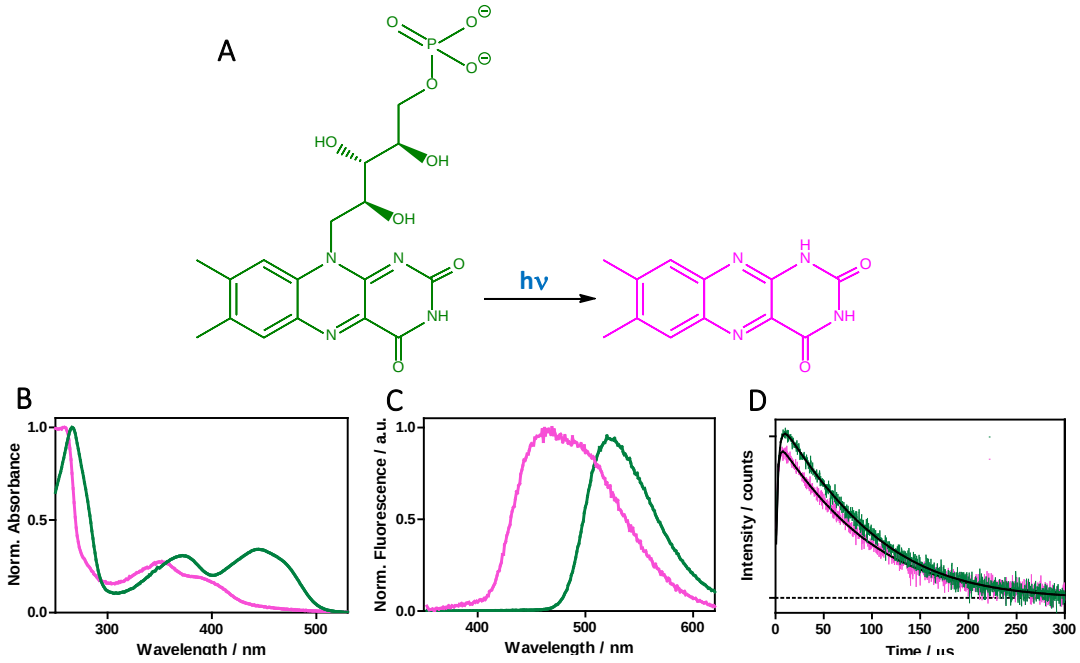

Figure 5.6. (A) Photoconversion of FMN (green) to LC (magenta). Normalized absorption (B) and fluorescence (λ_{ex} = 320 nm, C) spectrum. (D) Time-resolved $^1O_2$ NIR phosphorescence signals of optically matched LC and FMN solutions in air-saturated dPBS (λ_{ex} = 355 nm).

FMN to LC photoconversion is observed also in other miniSOG mutants. For instance, miniSOG W81F lacking the single tryptophan residue shows a Φ_Δ value of 0.33 and a τ_T of 265 µs in air-saturated dPBS solution. Importantly, τ_T also decreases to ~ 3 µs upon extended light irradiation both at 355 nm and at 473 nm. In this case, however, the Φ_Δ value does not increase, indicating that $k_{O_2} >> k_p$ already before photolysis despite the presence of the phosphoribityl tail (Equation 5.1). The spectral and photosensitizing changes induced by prolonged light illumination of this mutant are shown in Figures 5.7 A-F.

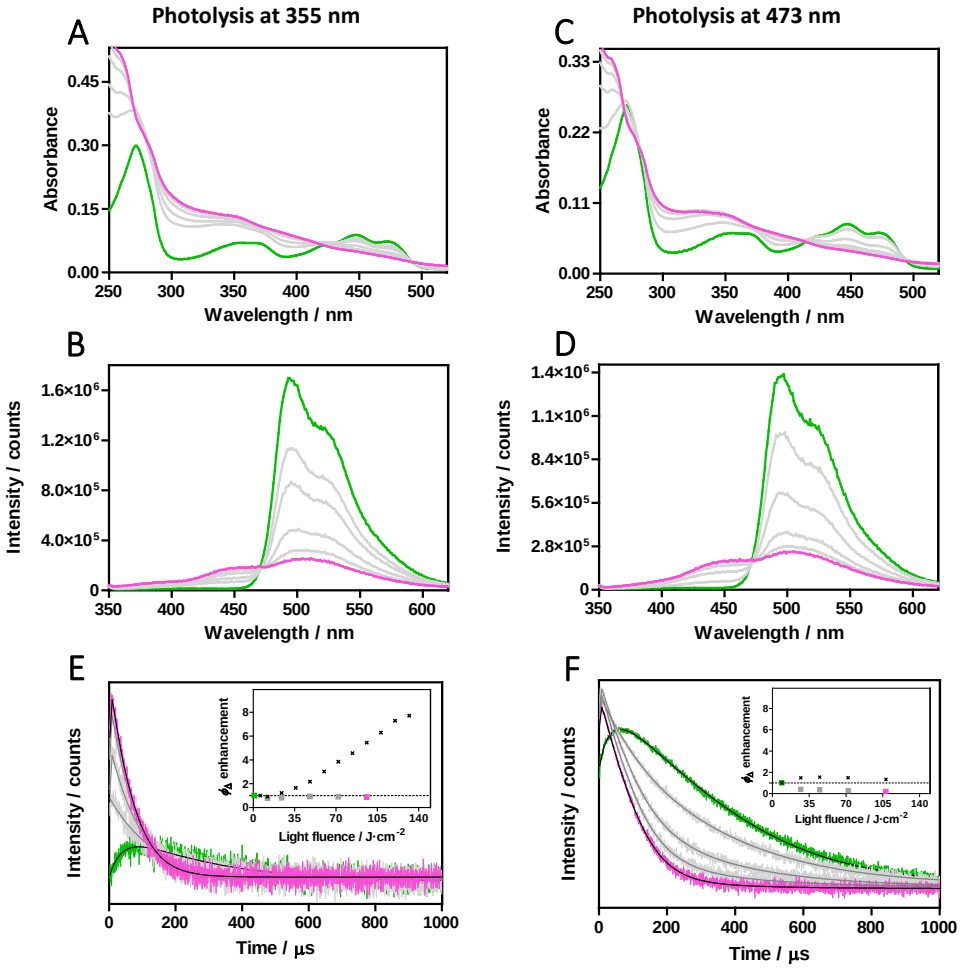

Figure 5.7. Spectroscopic changes of miniSOG W81F upon photolysis (from green to magenta lines) at 355 nm (left column) and 473 nm (right column). Evolution of the absorption (A and C) and fluorescence spectra (B and D) at the two excitation wavelengths. Panels E and F show the time-resolved $^1O_2$ NIR phosphorescence decays upon excitation at 355 and at 473 nm, respectively. Insets show the Φ_Δ enhancement (green to magenta) at the two wavelengths. (Φ_Δ results for miniSOG have been included for comparison (black crosses)).

In addition to the phototransformation of FMN, the oxidation of several amino acid residues is also expected to happen upon illumination and consequent formation of ROS. A closer examination of the $2F_{obs}$-F_{calc} electron density of blue-light irradiated miniSOG revealed that several surface residues had been affected during the irradiation process (Figure 5.8A). The most

obvious structural change occurs on the side chain of Tyr73, consistent with oxidation to yield γ-peroxotyrosine,[24] leading to the tetrahedralization of the Cγ atom. His85 also appears modified, and its two alternate conformations could be modeled by either a singly, or a doubly oxidized histidine, namely 2-oxo-histidine and 2,4 dioxo-histidine[24,25] (Figure 5.8B). Finally, Trp81, which is perfectly ordered in the native structure, has its side chain seemingly partially disordered, which could be modeled by N-formylkynurenine (NFK, Figure 5.8C), a well-known tryptophan oxidation product.[26,27]

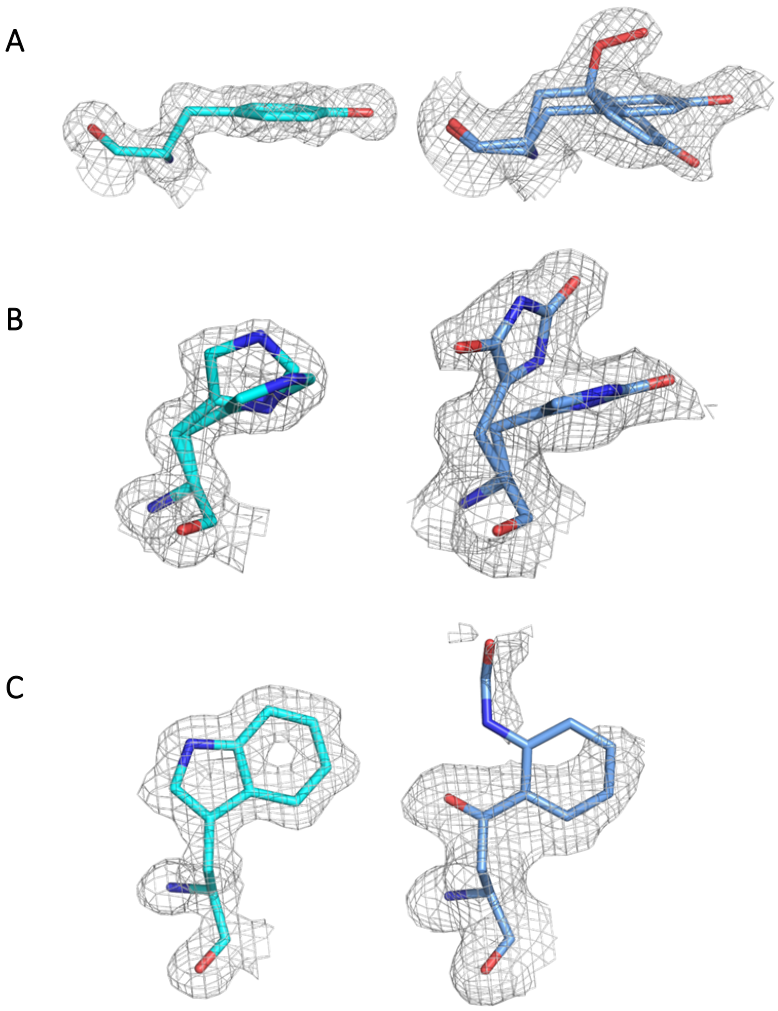

Figure 5.8. Modeled side chains of surface residues Tyr73 (A), His85 (B) and Trp81 (C) before (cyan) and after blue light irradiation (light blue).

Mass spectrometry analysis of blue-light irradiated miniSOG samples revealed increasing additions of 16 Da to the native protein mass of 13882.0 Da, consistent with increasing oxidation of the protein (Figure 5.9). The three structural modifications observed in the crystal structure account for six of the eight additional O_2 atoms evidenced in the mass spectrometry analysis. The two non-assigned additions could well correspond to oxidation of Met89 (+16 Da) and/or Tyr98 (+32 Da), although we did not observe unambiguous oxidation of these two amino acids.

Oxidation of Tyr73, His85 and Trp81 eliminates potential quenchers of ^{3}miniSOG*, thereby decreasing the value of k_p. According to Equation 5.1, this should contribute to an increase in Φ_Δ. However, since protein oxidation occurs simultaneously to FMN to LC photoconversion, which also increases Φ_Δ, it is not possible to ascertain the individual contribution of both effects.

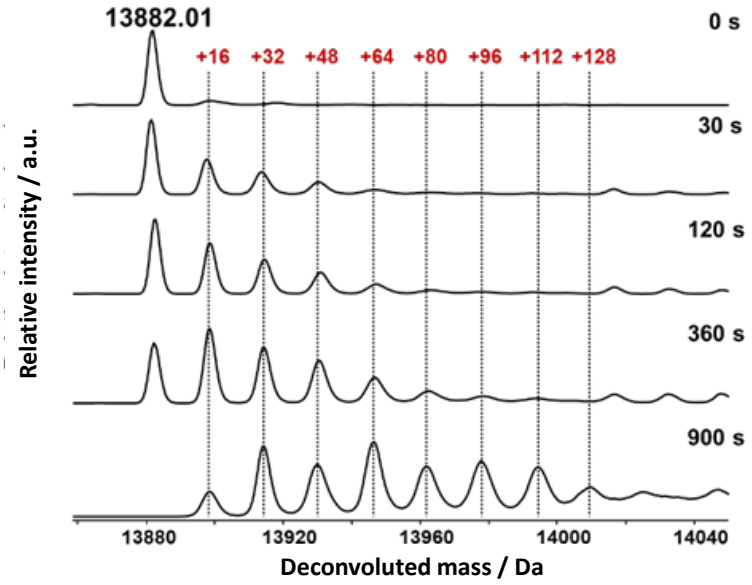

Figure 5.9. Deconvoluted electrospray ionization (ESI) mass spectra of miniSOG in solution irradiated with 460 nm light for 0, 30, 120, 360 and 900 s. The peak at 13882.0 Da corresponds to the native protein.

Finally, it is worth mentioning that oxidation of tryptophan to NFK could contribute to the increased Φ_Δ value observed upon light excitation at 355 nm for the photoconverted miniSOG since NFK absorbs near UV light and it is a potent $^1O_2$ PS (Φ_Δ = 0.17).[28] However, W81F shows a much higher Φ_Δ value (Φ_Δ = 0.33) than miniSOG already before photolysis, on account of its lower k_p value (Equation 5.1), indicating that the potential benefits of producing NFK as secondary PS are of minor value as compared to the effect of eliminating a protein quencher.

All in all, the extensive structural and photophysical characterization of miniSOG have allowed the understanding of its complex photochemistry. It has been demonstrated that the ability of miniSOG to produce $^1O_2$ is defined by the rate constants k_P and k_{O_2}, this is in other words, by the competition between protein- and O_2 quenching. The intriguing observation of the dramatic increase in Φ_Δ upon photolysis has been finally rationalized. Prolonged irradiation leads to the photoinactivation of electron rich residues that are close to the chromophore and are therefore potential quenchers of ^{3}miniSOG*. In addition, photolysis also induces the photoconversion of the FMN chromophore to LC, which is less susceptible to protein quenching and lacks the phosphoribityl tail thereby facilitating the O_2 diffusion.

5.3. Improving miniSOG: towards a more efficient photosensitizer

5.3.1. Characterization of novel miniSOG variants

a) miniSOG Q103V:

The first variant of miniSOG that succeeded in improving the photosensitizing properties was called SOPP.[8] It was developed by introducing a single mutation of the parental sequence at the position 103, replacing the glutamic acid residue into a leucine (Q103L). This mutation induced a remarkable enhancement of the Φ_Δ value, from 0.03 to 0.25.[8] The improvement was rationalized by the positive effect of suppressing competing ^{3}FMN* deactivation channels, particularly, electron transfer processes.[8] However, this Φ_Δ was still far from the value for free FMN and the production of other ROS such as $O_2^{\bullet-}$ and H_2O_2 was also increased,[8] indicating that the competing pathways had not been completely suppressed and leaving room for further improvements.

The development of SOPP was certainly a step in the correct direction. In collaboration with the group of Dr. Cristina Flors at the IMDEA Nanociencia in Madrid, Spain, mutagenesis at the 103 position yielded the miniSOG Q103V mutant,[6] in which a valine replaces the glutamic acid instead of the leucine residue as in SOPP. Early studies on DAB polymerization photosensitized by miniSOG mutants showed improved results for both SOPP and the Q103V variant as compared to the original miniSOG. Therefore, it was interesting to further characterize the photophysical properties of miniSOG Q103V and particularly assess its ability to produce $^1O_2$.

The pBAD plasmid encoding miniSOG Q103V was transformed into competent TOP10 *E. coli* cells and protein expression and purification procedures were performed as described in Chapter 3. The absorption and fluorescence spectra are shown in Figure 5.10.

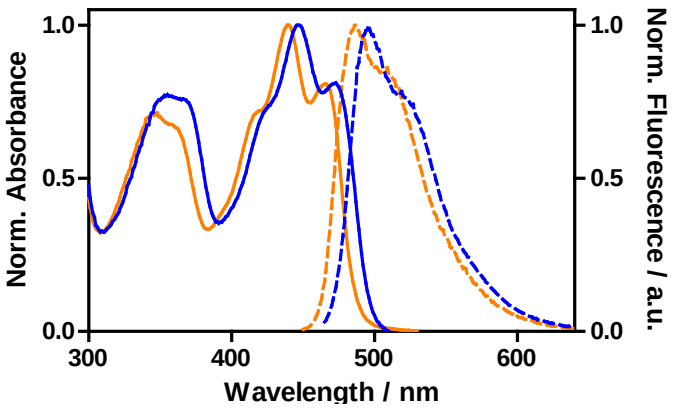

Figure 5.10. Normalized absorption (solid lines) and fluorescence (dashed lines) spectra of miniSOG Q103V (blue) and of the original miniSOG (orange) for comparison.

As previously observed for SOPP, both the absorption and fluorescence spectra showed the typical vibronic profile of the flavin chromophore embedded inside the protein but with a significant ~ 10 nm blue-shift. It has been suggested that the mutation at the 103 position either stabilizes miniSOG ground state or destabilizes ^{1}miniSOG* or both.[8] The Φ_F value for miniSOG Q103V was determined as 0.43, which is similar to the values reported for miniSOG and SOPP (Φ_F = 0.41 ± 0.04)[1,8,10,13,29]

Interestingly, miniSOG Q103V outperformed SOPP in photosensitizing $^1O_2$ by a factor of about 1.5, (0.39[6] vs 0.25 in dPBS, Figure 5.11).

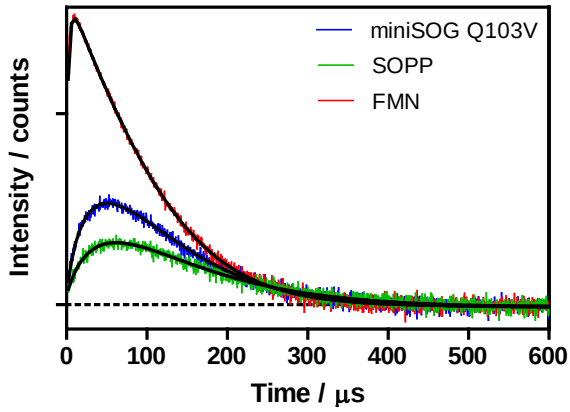

Figure 5.11. Time-resolved $^1O_2$ NIR phosphorescence decays for optically matched dPBS solutions of miniSOG Q103V, SOPP and FMN upon laser excitation at 473 nm.

Therefore, the introduction of a more hydrophobic residue such as valine at the 103 position yielded a more efficient PS, which actually represented a record for a pure genetically encoded $^1O_2$ PS at that time.[6] Interestingly, this mutant showed a shorter τ_T than SOPP (i.e., τ_T ~ 85 µs vs. ~ 111 µs in air saturated dPBS solutions) and later studies correlated the positive effect on $^1O_2$ production with more efficient O_2 diffusion through the protein matrix,[9] which is consistent with the structural results described in Section 5.2.2 for miniSOG.

To determine whether the enhanced $^1O_2$ generation ability correlated with increased cell death, photoinactivation experiments were performed using *E. coli* individually expressing miniSOG, SOPP or miniSOG Q103V. *E. coli* wild-type (wt) (untransformed) were prepared under the same conditions as a control. Bacterial cells were grown until OD_{600} = 0.3 and protein expression was induced by addition of 0.2% Arabinose. Two hours later, cells were harvested by centrifugation and the growth media was washed three times with sterile PBS. Cells were diluted to a final OD_{600} ~ 0.35 in sterile PBS and protein expression was assayed by fluorescence emission, which was comparable for the three FPs, indicating similar protein expression levels. Cells were transferred to an optical non-treated sterile glass chamber and irradiated at

increasing light fluences with blue light (λ = 457 ± 11 nm, 16 mW·cm^{-2}, Figure 5.12). MiniSOG Q103V exhibited the highest photokilling ability, inducing a population reduction of approximately 5-log$_{10}$ in colony-forming units (CFU) per mL after a light fluence as little as 2.7 J·cm^{-2}. SOPP also showed high phototoxicity although slightly less efficient, reducing 3 to 4-log$_{10}$ the number of CFU/mL upon the same light fluence. On the other hand, miniSOG exhibited moderate phototoxicity, requiring 40 J·cm^{-2} to reduce almost 5-log$_{10}$ in CFU/mL, which is in agreement with previously reported data.[12] Noteworthy, no phototoxicity was observed for *E. coli* wt at the highest light fluence tested.

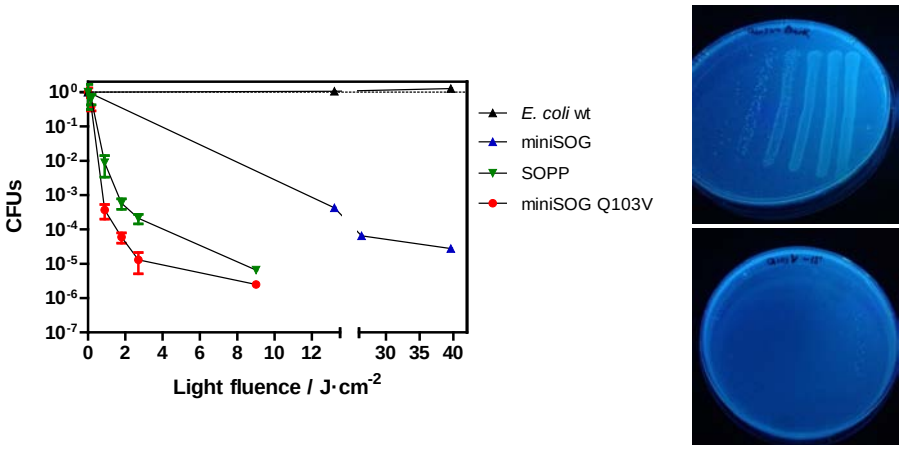

Figure 5.12. Light-fluence dependence on bacterial cell death in *E. coli* expressing miniSOG and the two Q103-mutated variants. Illumination of untransformed *E. coli* cells (*E. coli* wt) under the same light conditions did not induce phototoxicity. Example of viability results in dark conditions and upon blue light irradiation is shown for comparison.

b) miniSOG W81F:

The presence of the tryptophan residue in miniSOG had been previously rationalized in our laboratory as an electron-rich residue capable of quenching either ^{3}miniSOG* or $^1O_2$.[12] For this reason, the mutant W81F in which the tryptophan is replaced by a phenylalanine was developed and characterized in an early work.[12] However, the instruments and techniques available at that time led to an underestimation of its photosensitizing capacity, yielding a Φ_Δ = 0.01 and therefore suggesting that this mutation actually worsen the $^1O_2$ production properties.[12]

MiniSOG W81F was conveniently selected for the study of the phototransformations of miniSOG discussed previously, and therefore its ability to photosensitize $^1O_2$ was re-evaluated. Noteworthy, the characterization was performed using freshly purified protein and the optimized $^1O_2$ detection system. *E. coli* TOP10 cells were transformed with the pBAD plasmid encoding miniSOG W81F and the protein expression and purification were carried out as described in Chapter 3. Absorption and fluorescence spectra were practically identical to

miniSOG (Figure 5.13A). Direct detection of $^1O_2$ NIR luminescence in air-saturated dPBS revealed a long τ_T (~ 265 µs) and high Φ_Δ value (Φ_Δ = 0.33, Figure 5.13B), which is about 8-fold higher than the parental miniSOG. Laser flash photolysis experiments showed τ_T = 334 µs and 1050 µs in air- and argon-saturated dPBS solutions, respectively (Figure 5.13C). These values allowed the determination of the rate constants k_T^{Ar}, k_T^{Air}, k_p and k_{O_2}(Table 5.4).

Table 5.4. Photophysical properties of miniSOG W81F.

k_T^{Ar} / 10^3 s^{-1}	k_T^{Air} / 10^3 s^{-1}	k_p / 10^3 s^{-1}	k_{O_2} / 10^4 s^{-1}
0.91	2.99	0.61	2.08

Such a long τ_T could not be properly measured and analyzed in the early $^1O_2$ experiments and therefore the reported Φ_Δ value for this mutant was underquoted.

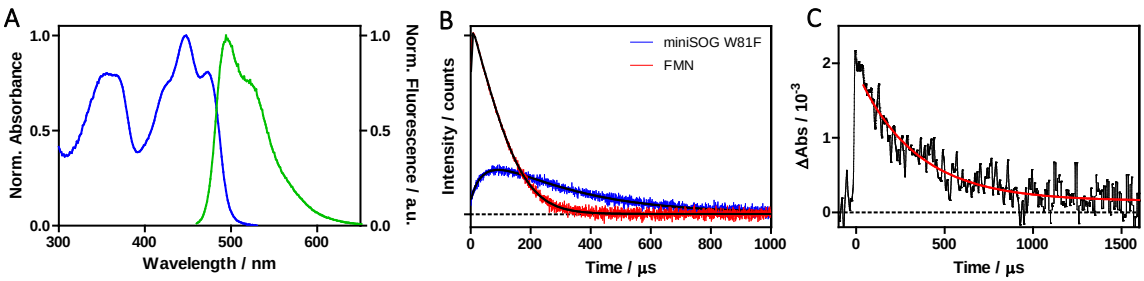

Figure 5.13. A) Absorption (blue) and fluorescence (green) spectra of miniSOG W81F. B) $^1O_2$ signal from optically-matched miniSOG W81F and FMN at the excitation wavelength λ = 473 nm in air-saturated dPBS solutions. Fitting lines in black and Y-axis is in log scale. C) Transient absorption spectrum in air-saturated dPBS solution. Fitting line in red. λ_{ex} = 355 nm; λ_{obs} = 715 nm.

The higher Φ_Δ value determined for miniSOG W81F confirmed the key role of the tryptophan residue on the quenching of ^{3}miniSOG*. The longer τ_T reflects the suppression of a major O_2-independent deactivation pathway, as reflected with a much lower value of k_p. As a consequence, a higher fraction of the triplets are quenched by O_2 and hence, greater amounts of $^1O_2$ are produced. Still, the Φ_Δ value is far from the Φ_Δ ~ 0.6 determined for the free flavin which implies that additional deactivation pathways still occur. Moreover, the long τ_T reflects that O_2 accessibility to the chromophore is limited, which also leaves room for improving the Φ_Δ value. In this regard, experiments on O_2 accessibility have been performed with novel miniSOG mutants encasing more accessible chromophores, and the results are shown and discussed below in Section 5.3.1.

c) miniSOG2:

Random mutagenesis has also been exploited as a tool to develop improved variants of miniSOG. Makhijani and coworkers[7] created a mutant library and used a ROS sensitive FP named IFP1.4[30] as a sensor to select the prominent candidates. The best mutant obtained by this method was called miniSOG2 and its phototoxicity was impressively demonstrated for single and multiple-cell ablation *in vivo*.[7] However, miniSOG2 was not photophysically characterized in detail and the amount and type of ROS produced were not determined.

The pBAD plasmid encoding miniSOG2 was transformed into TOP10 *E. coli* cells and initial attempts of protein expression were carried out following the standard procedure used for miniSOG and all other FbFPs. However, the yield of protein purification for this variant was extremely low. Alternative methods for protein production and purification were tested, however, it was not possible to significantly improve the outcome of the process. The soluble fraction obtained from the bacterial cell lysate presented an intense yellowish color, however, this colored solution was not retained in the Ni-NTA resin and it quickly eluted off the column. Spectroscopic evaluation of the eluted fraction revealed the characteristic features of free FMN. This would suggest that the mutations introduced in miniSOG2 might weaken the binding of the chromophore in the active pocket, and FMN would eventually be expelled when the protein is extracted from the cellular environment. For this reason, only little amounts of miniSOG2 could be purified and characterized by means of fluorescence excitation and emission techniques (Figures 5.14A and 5.14B). Interestingly, excitation spectra showed a ~20 nm hypsochromic shift as compared to miniSOG and narrower UV absorbance bands. Fluorescence emission was very weak and blue-shifted. Unfortunately, the two valleys in the miniSOG2 absorbance matched the wavelength of the two lasers available for $^1O_2$ measurements, which in addition to the tiny amounts of protein obtained, did not allow the determination of the $^1O_2$ production.

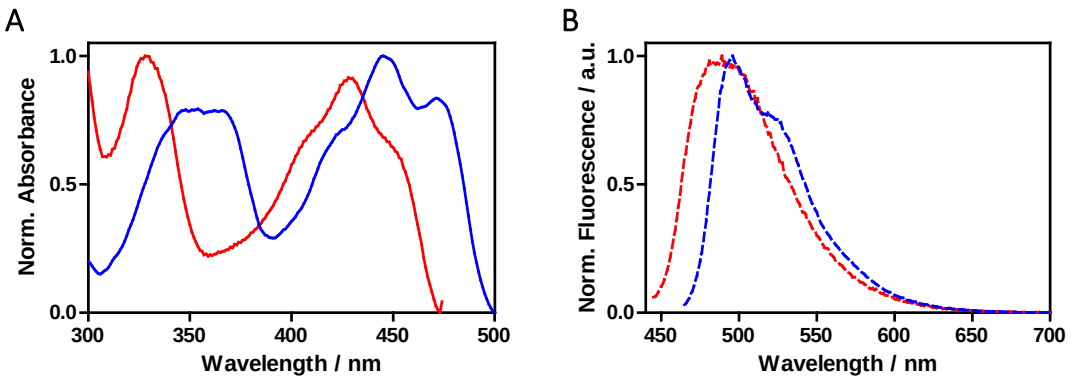

Figure 5.14. Normalized excitation (A) and emission (B) fluorescence spectra of miniSOG2 (red) and of the original miniSOG (blue) for comparison. (Conditions: miniSOG2: λ_{ex}= 430 nm and λ_{obs} = 480 nm; miniSOG: λ_{ex} = 450 nm, λ_{obs} = 530 nm).

d) miniSOG3:

Since the Q103V mutation greatly increased the photosensitizing capacity of miniSOG and the glutamic acid residue is still present in miniSOG2, it was worth developing a new miniSOG2 introducing a valine to test whether it could further improve the phototoxic properties.

To generate the miniSOG2 Q103V variant, hereafter miniSOG3, oligonucleotide primers containing the Q103V mutation were synthesized and used for Quick-Change PCR, using pBAD vector encoding miniSOG2 as a template. Parental DNA was digested with *DpnI* prior to transformation into Stellar competent *E. coli* cells. The mutation was confirmed by re-isolation of the plasmid from a single colony and subsequent sequencing. Primers: miniSOG2(Q103V)_F: 5'-CATCGGGGTTGTGCTGGATGGTGAATTCCATCATCAC-3' and miniSOG2(Q103V)_R: 5'-CACCAT-CCAGCACAACCCCGATGAAGTACTGC.

For protein production, the pBAD plasmid encoding miniSOG3 was transformed into TOP10 competent cells. However, as observed during the purification of miniSOG2, the yellow color from the supernatant eluted off the purification column and it was not possible to characterize the protein.

During the course of this work, independent laboratories have recently developed two improved miniSOG variants, named SOPP2 and SOPP3 with reported Φ_Δ as high as 0.51 and 0.61, respectively.[9] These mutants circumvent the two main causes for the low Φ_Δ observed and discussed for miniSOG; (i) the competing oxygen-independent ^{3}FMN* deactivation mechanisms, k_p, and (ii) the limited O_2 diffusion through the protein matrix and accessibility to the chromophore, k_{O_2}. This was mainly achieved by replacing the electron-rich tryptophan residue and including the Q103V mutation, combining the two big improvements that we had been already observed individually for miniSOG W81F and miniSOG Q103V.

5.3.2. Encasing riboflavin instead of flavin mononucleotide as the chromophore

This work has been performed in collaboration with the group of Dr. Antoine Royant.

Having ascertained the positive effect of removing the tryptophan residue from miniSOG for $^1O_2$ production (i.e., decreasing k_p), it was worth exploring how O_2 accessibility affects the photosensitizing properties (i.e., varying k_{O_2}). The crystal structure of miniSOG shows that the ribityl tail lies in the tunnel that connects the chromophore with the external medium and, in addition to this, the bulky PO_4^{2-} is located at the surface of the protein and it therefore likely

blocks a possible caveat (see section 5.2.1) Noteworthy, PO_4^{2-} presents two negative charges at physiological pH, which may also difficult the approaching of external molecules. As discussed above, the improvement in the Φ_Δ observed upon photolysis of miniSOG occurs concomitantly with a substantial shortening of τ_T. However, the photoproduct LC lacks both the entire phosphoribityl tail, so the data obtained from photoconverted miniSOG does not provide sufficient information to ascertain the individual contribution of each part of the tail.

To determine the role of PO_4^{2-}on O_2 diffusion, the best option is riboflavin (RF), which is the non-phosphorylated flavin that is transformed to FMN by the action of the enzyme riboflavin kinase.[31] The structure of RF is essentially the same as FMN without PO_4^{2-} and so are the optical and photosensitizing properties (Figures 5.14A and 5.14B). Importantly, RF is ubiquitously found in living cells, and hence it can also be used as an endogenous chromophore for genetically encoded PSs. Therefore, if FMN is replaced by RF in miniSOG it is possible to study the individual contribution of PO_4^{2-}.

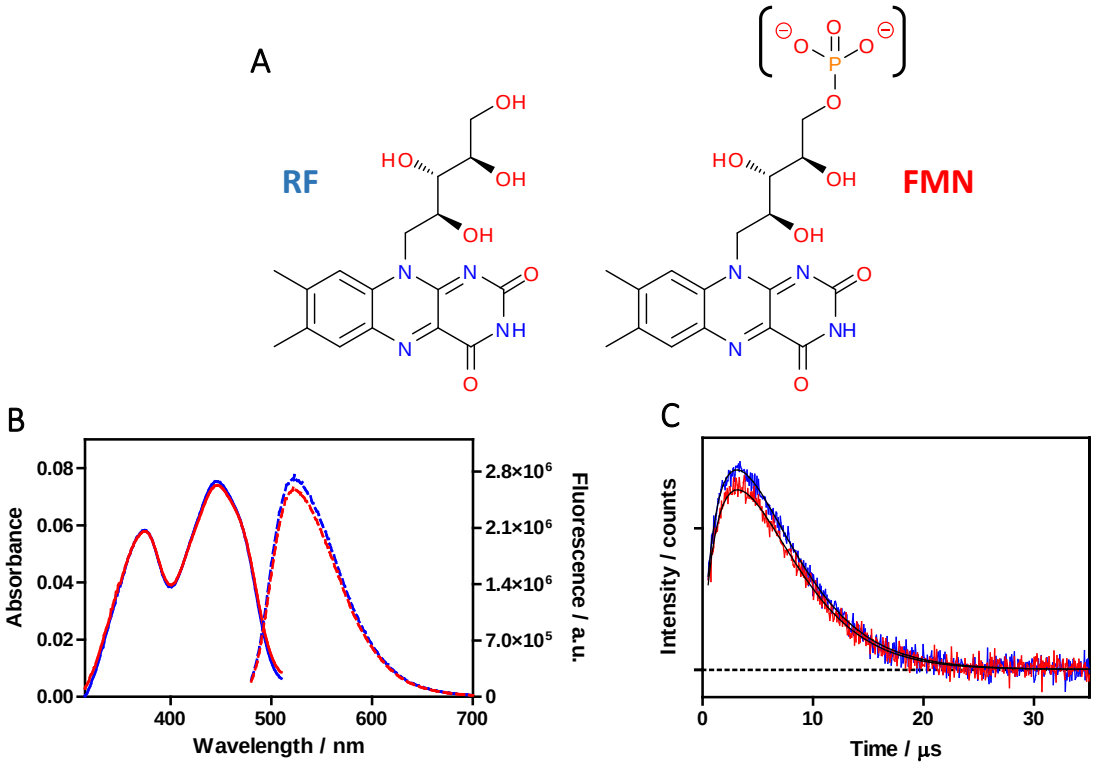

Figure 5.14. A) Chemical structures of RF and FMN. The phosphate group of FMN is highlighted in brackets. B) Absorption (solid lines) and fluorescence (dashed lines) of optically matched PBS solutions at 473 nm of RF (blue) and FMN (red). C) Production of $^1O_2$ of RF is slightly higher than FMN, consistent with reported values.[14]

MiniSOG was purified from *E. coli* cells, denatured with 6 M guanidine hydrochloride solution and reconstituted either with FMN or RF, yielding miniSOG-FMN and miniSOG-RF, respectively. The original miniSOG and the two reconstituted variants were characterized in deuterated

tris(hydroxymethyl)aminomethane (dTRIS) buffer for better comparison with early photo-oxidation results obtained previously by collaborators. Interestingly, miniSOG-RF yielded Φ_Δ = 0.11, about 3-fold higher than the value determined for the original miniSOG (Φ_Δ = 0.04). Moreover, τ_T decreased to 5.1 µs, which correlates with a more exposed flavin to O_2 (Figure 5.15). On the other hand, miniSOG-FMN exhibited essentially the same properties as the original miniSOG, which is not surprising since FMN is the predominant chromophore. Kinetic and Φ_Δ data are collected in Figure 5.15 and Table 5.5.

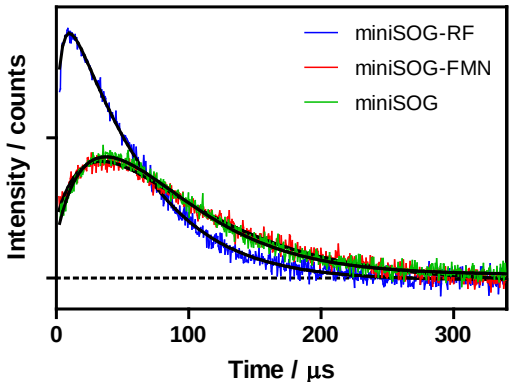

Table 5.5. $^1O_2$ production and kinetics for miniSOG and the RF- and FMN-reconstituted variants.

Protein	τ_T / µs	Φ_Δ
miniSOG	32	0.039
miniSOG-RF	5.1	0.110
miniSOG-FMN	35	0.035

Figure 5.15. $^1O_2$ NIR phosphorescence decays of independent samples of comparable absorbance at 473 nm of the original and RF- and FMN-reconstituted miniSOG. Y-axis is in log scale. Fitting lines are in black.

The substantial shortening in τ_T for miniSOG-RF reveals that PO_4^{2-} has indeed a major contribution on blocking the path to the chromophore. The fact that the τ_T is still a bit larger than the photoconverted miniSOG may account for the ribityl tail of RF, which is not present in LC, and could therefore difficult the diffusion of external molecules.

Comparison between the original miniSOG and the FMN-reconstituted shows subtle differences in τ_T and Φ_Δ that might be in line with the expected effects of RF on miniSOG. The original miniSOG shows slightly shorter τ_T and greater Φ_Δ as compared to the FMN-reconstituted variant. Interestingly, mass spectrometry assays revealed that about 98.5 % of the original miniSOG encases FMN, being RF the remaining 1.5 % chromophore. The presence of small amounts of proteins encasing RF may reasonably explain these minor differences on the photosensitizing properties.

With all these results in mind, the group of Dr. Royant sought to assess and replace the key amino acids in the miniSOG sequence that stabilize the negative charges of PO_4^{2-} and develop mutants that bind predominantly RF over FMN. The positive guanidine group from two arginine residues located at positions 41 and 57 in the sequence of miniSOG were found to interact with PO_4^{2-} (see Section 5.2.1). Several mutants were engineered replacing R57 to neutral and anionic

amino acids to prevent the interaction. Glutamine and asparagine (mutations R57Q and R57N, respectively) were introduced as neutral residues, whereas glutamic acid and aspartic acid (mutations R57E and R57D, respectively) yielded the negative counterparts. Early experiments with $^1O_2$ chemical traps were performed by our collaborators in TRIS buffer and better results were obtained with neutral substitutions over the negatively charged. Particularly, illumination of miniSOG R57Q induced the major fluorescence bleaching of the $^1O_2$ probe ADMA. For this reason, this variant was selected and further studied with the direct $^1O_2$ NIR phosphorescence detection method. It is worth noting that analysis of the chromophore composition revealed 80.2 % RF and 20.8 % FMN content, confirming the positive effect of the R57Q mutation to bind RF predominantly. However, the $^1O_2$ luminescence results revealed a modest increase in the $^1O_2$ production, with Φ_Δ = 0.05. Interestingly, a short component (τ_T = 5.7 µs) was observed in the triplet decay kinetics (Figures 5.16A and 5.16B), which is comparable to the 5.1 µs determined for RF-miniSOG. To further increase the percentage of RF, miniSOG R57Q was denatured and reconstituted with RF, yielding miniSOG R57Q-RF, which exhibited 3.6 % FMN and 96.4 % RF content. In this case, Φ_Δ increased up to 0.07 and the τ_T decreased to 5.0 µs (Figures 5.16C and 5.16D). Table 5.6 collects the τ_Δ and Φ_Δ values for the two miniSOG R57Q.

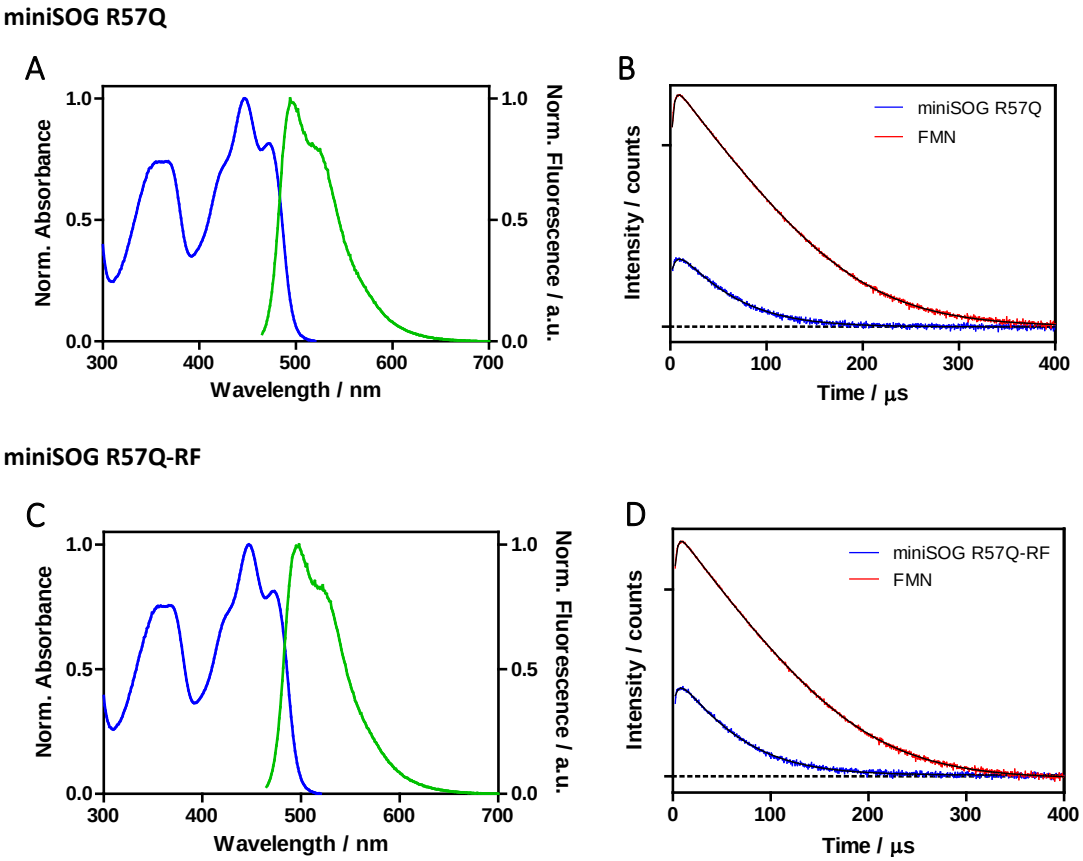

Figure 5.16. Panels A and C show the absorption (blue) and fluorescence (green) spectra of miniSOG R57Q and miniSOG R57Q-RF, respectively. Graphics B and D show the $^1O_2$ signal of optically matched FMN solutions with each miniSOG variant, at 473 nm and in air-saturated dTRIS. Fitting lines are in black. Y-axes are in log scale.

Table 5.6. Photosensitizing data for the RF-binding miniSOG mutants.

Protein	τ_T / μs	Φ_Δ
miniSOG R57Q	5.7	0.05
miniSOG R57Q-RF	5.0	0.07

These results provide further evidence that O_2 diffusion to the chromophore in miniSOG is severely restricted due to the blocking effect of PO_4^{2-} from the FMN tail. However, elimination of this group does not substantially improve Φ_Δ. This implies that k_p is certainly the major limiting factor in the production of $^1O_2$ (Equation 5.1) and therefore, any attempt to design and engineer improved variants of miniSOG must focus in suppressing the O_2-independent ^{3}miniSOG* deactivation pathways.

5.4. miniSOG heterodimers: combining photostability and singlet oxygen production

FbFPs are gaining much attention for advanced imaging techniques, ranging from fluorescence microscopy to photo-oxidation based CLEM. These applications, however, seem to require opposing photophysical properties. On the one hand, photostability of the photoactive protein is a key factor in fluorescence imaging whereas efficient ROS production to oxidize DAB usually leads to rapid photobleaching. Therefore, a protein suitable for fluorescence microscopy has typically a limited application in photo-oxidation based imaging techniques and vice versa. The active development and characterization of novel FbFPs (see Chapter 4) provides numerous alternatives to choose the right protein for each application.

A different approach has been recently designed by the group of Dr. Flors.[32] It relies on the engineering of flavoprotein heterodimers, combining the most photostable FbFP known to date (PhiLOV2.1, for photostable improved LOV)[16] with miniSOG and the improved mutant Q103V as the photosensitizing moieties. Therefore, two tandem dimers have been developed: (1) phiSOG (for "photostable improved Singlet Oxygen Generator"), which has been constructed by fusion of miniSOG and phiLOV2.1 monomers and (2) phiSOG-Q103V, which has been constructed by fusion of the improved mutant miniSOG-Q103V with phiLOV2.1. To obtain the flavoprotein heterodimers, the sequences of the two monomers have been fused by means of a flexible linker (Gly-Ser) in order to avoid possible interactions between fused domains and preserve their structural integrity (Figure 5.17).[32]

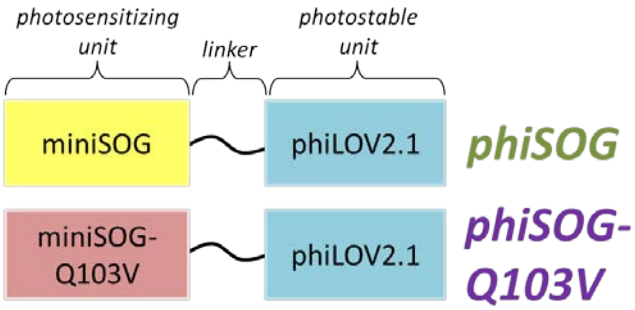

Figure 5.17. Schematic illustration of the monomeric flavoprotein components that yield the heterodimeric tandem: phiSOG and phiSOG-Q103V.

The size of the flavoprotein heterodimers was determined by polyacrylamide gel electrophoresis and mass spectrometry. PhiSOG and phiSOG-Q103V heterodimers showed a size corresponding to that expected by the addition of their respective monomers (~ 26 kDa).[32] It is worth noting that the resulting size of these novel constructs is still sufficiently small, similar to that of a single GFP, which is particularly useful to avoid possible cell function disruptions.

Absorption and fluorescence spectra of the heterodimers and their monomeric components were recorded in PBS (Figures 5.18A and 5.18B). The spectral properties of miniSOG and phiLOV2.1 are almost identical, which therefore results in phiSOG also showing similar spectrum. On the other hand, and as described above, miniSOG-Q103V is slightly blue-shifted, hence the absorption spectrum of phiSOG- Q103V corresponds to the spectral addition of its monomeric components, with a maximum at 444 nm and a less pronounced vibronic structure. The fluorescence spectrum of PhiSOG is also almost identical to the individual emission of its monomers. Interestingly, the emission of phiSOG-Q103V is closer to that of phiLOV2.1, with maxima at 497 and 498 nm, respectively, which may reflect resonant energy transfer from blue-shifted miniSOG-Q103V to phiLOV2.1.

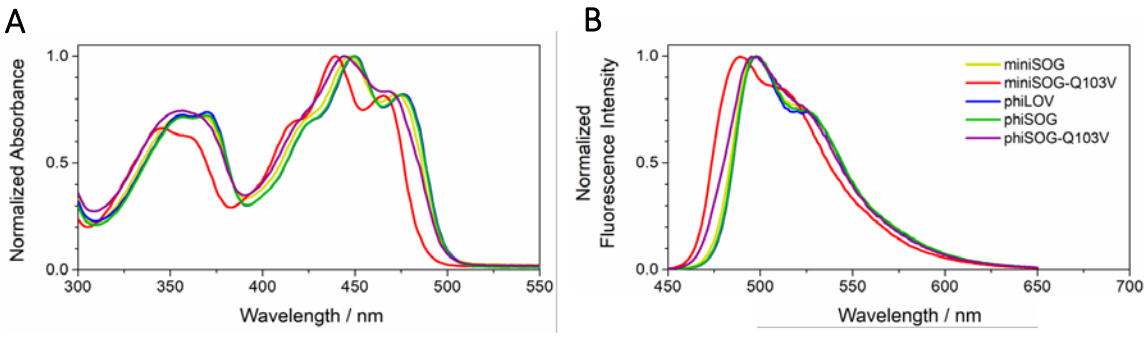

Figure 5.18. Normalized absorption (A) and fluorescence (B) spectra for the flavoprotein heterodimers and the individual components.

We also determined the $^1O_2$ production of all the flavoproteins by detecting directly its NIR phosphorescence upon illumination at 473 nm (Figure 5.19 and Table 5.7). PhiLOV2.1 produced a lower amount of $^1O_2$ (Φ_Δ =0.01), compared to the other two miniSOG monomeric variants. We recall here that phiLOV2.1 was developed as a photostable protein, and it is therefore interesting to note that its Φ_Δ value is still significant, and higher than those measured for GFP-like proteins.[33] The heterodimer phiSOG shows a Φ_Δ = 0.02, approximately averaged between its monomers, miniSOG and phiLOV2.1. On the other hand, the Φ_Δ of the heterodimer phiSOG-Q103V is smaller than the average of its monomers (Φ_Δ = 0.15) and closer to the value of phiLOV2.1. This result reinforces the hypothesis of energy transfer from miniSOG-Q103V to phiLOV2.1, which may (partially) compete with ISC to miniSOG-Q103V triplet state and in turn, energy transfer to O_2 to generate $^1O_2$.

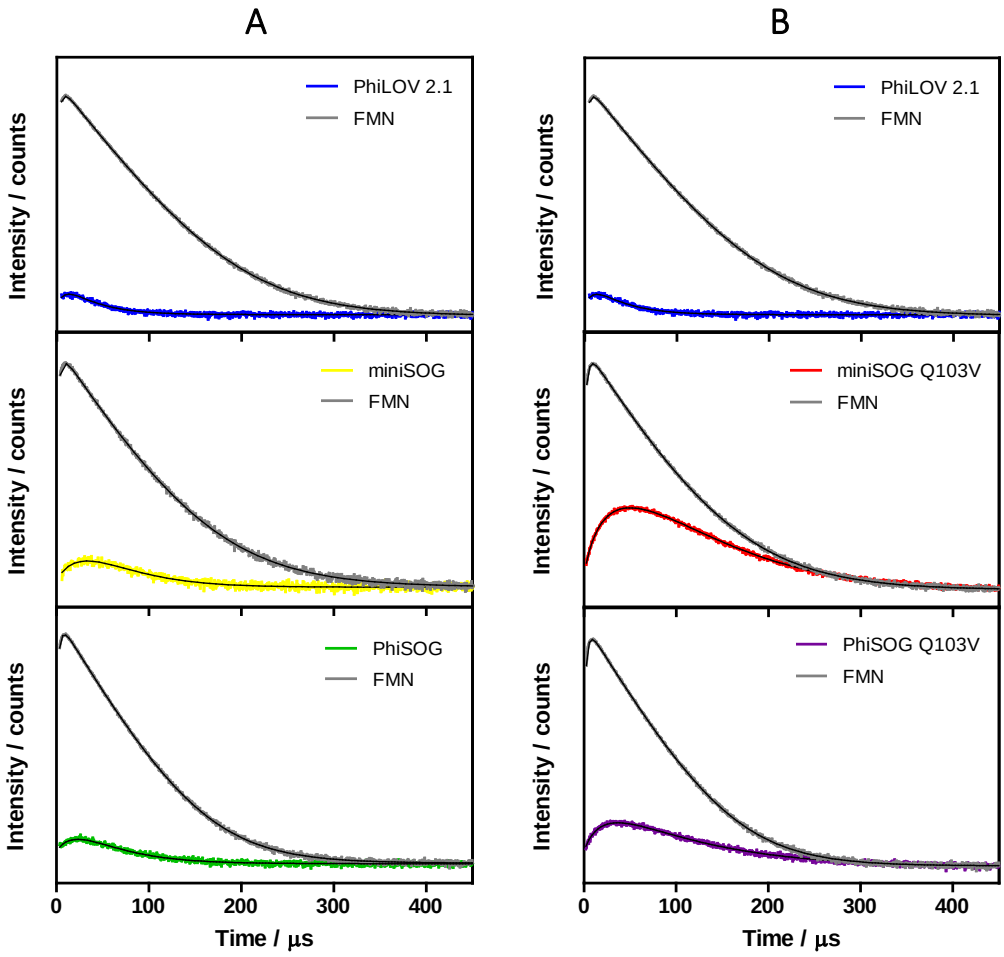

Figure 5.19. Time-resolved $^1O_2$ NIR phosphorescence at 1275 nm for the flavoprotein monomers and the corresponding dimer; PhiSOG (panels column A) and PhiSOG Q103V (panels column B) in air-saturated dPBS solution. The reference signals for optically matched solutions of FMN in air-saturated dPBS are shown in gray. Fitting lines are in black. Y-axes are in log scale.

Table 5.7. Photosensitizing data for the FbFP monomers and heterodimers.

Protein	Protein construct	τ_{T1} / µs	τ_{Δ} / µs	Φ_{Δ}
miniSOG	monomer	32	41	0.04
miniSOG Q103V	monomer	87	35	0.39
phiLOV2.1	monomer	8.3	34	0.01
phiSOG	heterodimer	21	45	0.02
phiSOG Q103V	heterodimer	92	22	0.15

Regarding fluorescence photobleaching, both heterodimers showed enhanced photostability as compared to the miniSOG monomers alone. The most evident improvement was observed in phiSOG-Q103V, considering that miniSOG Q103V is the less photostable protein and further supporting energy transfer processes to phiLOV2.1. Table 5.8 shows the relative rates of fluorescence photobleaching upon blue light irradiation (450 nm, 45 mW·cm^{-2}).

Table 5.8. Relative fluorescence photobleaching and DAB polymerization efficiency for all studied flavoproteins.

Protein	Relative rate of fluorescence photobleaching	Relative ability for DAB polymerization
miniSOG	1.00	1.00
miniSOG Q103V	2.60	1.20
phiLOV2.1	0.12	0.27
phiSOG	0.36	0.51
phiSOG Q103V	0.52	0.51

To assess the suitability of heterodimeric tandem flavoproteins for their application in CLEM, their ability to photo-oxidize DAB was studied by monitoring the increase in optical density at 440 nm, corresponding to the product of DAB photopolymerization.[6,34] polymerization. In agreement with previous results,[6] miniSOG-Q103V only photo-oxidizes DAB about 20% more efficiently than miniSOG upon blue light irradiation (Table 5.8) although their Φ_{Δ} values are much different. As a consequence, both heterodimers behave similarly in terms of DAB photo-oxidation (i. e., are half as efficient compared to miniSOG and twice more efficient compared to phiLOV2.1, see Table 5.8). These results confirm that the ability to polymerize DAB does not clearly correlate with the efficiency of the photosensitizers to generate $^1O_2$, and that other processes such as the participation of radicals or the direct reaction between the PS and DAB may occur, as previously discussed in an early work.[6]

In the light of all these results, these heterodimers are a useful addition to the fluorescent flavoprotein toolbox for an expanding number of advanced imaging technologies, in which the combination of complementary properties including photostable fluorescence, ROS photosensitization and/ or DAB photo-oxidation is required.

5.5. Conclusions

Despite its popularity, the photosensitizing properties of miniSOG are modest and far from the authentic capacity of its FMN chromophore. Two main factors account for the limited production of $^1O_2$: (1) quenching of ^{3}miniSOG* by the protein (high k_p) and (2) poor O_2 accessibility to the chromophore (low k_{O_2}). This has been demonstrated by the combination of structural and spectroscopic studies. The crystal structure of miniSOG has been solved at a 1.17 Å resolution and reveals that the chromophore is surrounded by electron-rich amino acids and that the phosphoribityl tail limits the O_2 diffusion by blocking the tunnel that connects the flavin with the external medium.

The photophysical characterization has allowed key understanding of the photochemistry of miniSOG and drawing of the full picture of the processes that occur upon light absorption. Moreover, the unknown transformations behind photolysis of miniSOG have been finally revealed. On the one hand, FMN is photoconverted to LC, which lacks the phosphoribityl tail and it thus facilitates the O_2 diffusion and is less susceptible to be quenched by the protein. On the other hand, amino acids capable of deactivating ^{3}miniSOG*are inactivated by the $^1O_2$ generated. The result of both processes is the decrease in k_p and the increase in k_{O_2}, which explains the dramatic increase in the Φ_Δ value. The benefits of abolishing these two processes have been tested in novel miniSOG mutants. On the one hand, miniSOG W81F, which lacks the tryptophan residue, exhibits a remarkably long τ_T, which reveals the suppression of O_2-independent deactivation pathways of ^{3}miniSOG* and produces $^1O_2$ with Φ_Δ = 0.33. MiniSOG Q103V outperforms the Φ_Δ of the Q103L mutation in SOPP by a factor of 1.5, which has been rationalized by a more efficient O_2 diffusion through the protein. The highly phototoxic miniSOG2 has been used as a template to introduce the Q103V mutation and generate miniSOG3. Apparently, these two variants do not bind FMN tightly, and the chromophore is released during the protein purification process.

On the other hand, the effect of O_2 diffusion through the protein matrix has been assessed by replacing the FMN for RF, which lacks the bulky PO_4^{2-}. RF-encasing miniSOG shows a

significantly shorter τ_T (~ 5 μs), which is consistent with a more exposed chromophore. MiniSOG variants have been engineered aiming at fostering the preferential binding of RF over FMN. MiniSOG R57Q was found to encase RF efficiently and showed promising results in indirect $^1O_2$ measurements. However, direct detection methods revealed a modest increase in $^1O_2$ production (Φ_Δ = 0.05 vs 0.04 for the original miniSOG). Reconstitution of miniSOG R57Q with RF further improved the Φ_Δ to 0.07. Nevertheless, this value is still far from the Φ_Δ obtained upon suppressing the quenching pathways of ^{3}MiniSOG* by the protein, indicating the major contribution of k_p in the modest overall Φ_Δ of miniSOG.

Finally, flavoprotein heterodimers that combine complementary properties such as photostability and ROS photosensitization have been developed. PhiLOV2.1-miniSOG and phiLOV2.1-miniSOG-Q103V have shown improved photostability and preserved high levels of $^1O_2$ production. Moreover, the resulting size is still small which renders them convenient and powerful alternatives for a growing number of imaging techniques.

5.6. References

(1) Shu, X.; Lev-Ram, V.; Deerinck, T. J.; Qi, Y.; Ramko, E. B.; Davidson, M. W.; Jin, Y.; Ellisman, M. H.; Tsien, R. Y. A Genetically Encoded Tag for Correlated Light and Electron Microscopy of Intact Cells, Tissues, and Organisms. *PLoS Biol.* **2011**, *9* (4), e1001041.

(2) Meisslitzer-Ruppitsch, C.; Röhrl, C.; Neumüller, J.; Pavelka, M.; Ellinger, A. Photooxidation Technology for Correlated Light and Electron Microscopy. *J. Microsc.* **2009**, *235* (3), 322–335.

(3) Ryumina, A. P.; Serebrovskaya, E. O.; Shirmanova, M. V; Snopova, L. B.; Kuznetsova, M. M.; Turchin, I. V; Ignatova, N. I.; Klementieva, N. V; Fradkov, A. F.; Shakhov, B. E.; et al. Flavoprotein MiniSOG as a Genetically Encoded Photosensitizer for Cancer Cells. *Biochim. Biophys. Acta* **2013**, *1830* (11), 5059–5067.

(4) Buckley, A. M.; Petersen, J.; Roe, A. J.; Douce, G. R.; Christie, J. M. LOV-Based Reporters for Fluorescence Imaging. *Curr. Opin. Chem. Biol.* **2015**, *27*, 39–45.

(5) Souslova, E. A.; Mironova, K. E.; Deyev, S. M. Applications of Genetically Encoded Photosensitizer MiniSOG: From Correlative Light Electron Microscopy to Immunophotosensitizing. *J. Biophotonics* **2016**, *15*, 1–15.

(6) Rodríguez-Pulido, A.; Cortajarena, A. L.; Torra, J.; Ruiz-González, R.; Nonell, S.; Flors, C. Assessing the Potential of Photosensitizing Flavoproteins as Tags for Correlative Microscopy. *Chem. Commun.* **2016**, *52* (54), 8405–8408.

(7) Makhijani, K.; To, T.-L.; Ruiz-González, R.; Lafaye, C.; Royant, A.; Shu, X. Precision Optogenetic Tool for Selective Single- and Multiple-Cell Ablation in a Live Animal Model System. *Cell Chem. Biol.* **2017**, *24* (1), 110–119.

(8) Westberg, M.; Holmegaard, L.; Pimenta, F. M.; Etzerodt, M.; Ogilby, P. R. Rational Design of an Efficient, Genetically-Encodable, Protein-Encased Singlet Oxygen Photosensitizer. *J. Am. Chem. Soc.* **2015**, *137* (4), 1632–1642.

(9) Westberg, M.; Bregnhøj, M.; Etzerodt, M.; Ogilby, P. R. No Photon Wasted: An Efficient and Selective Singlet Oxygen Photosensitizing Protein. *J. Phys. Chem. B* **2017**, *121* (40), 9366–9371.

(10) Westberg, M.; Bregnhøj, M.; Etzerodt, M.; Ogilby, P. R. Temperature Sensitive Singlet Oxygen Photosensitization by LOV- Derived Fluorescent Flavoproteins. *J. Phys. Chem. B* **2017**, *121*, 2561–2574.

(11) Fritz, B. J.; Matsui, K.; Kasai, S.; Yoshimura, A. Triplet Lifetimes of Some Flavins. *Photochem. Photobiol.* **1987**, *45* (4), 539–541.

(12) Ruiz-González, R.; Cortajarena, A. L.; Mejias, S. H.; Agut, M.; Nonell, S.; Flors, C. Singlet Oxygen Generation by the Genetically Encoded Tag MiniSOG. *J. Am. Chem. Soc.* **2013**, *135* (26), 9564–9567.

(13) Pimenta, F. M.; Jensen, R. L.; Breitenbach, T.; Etzerodt, M.; Ogilby, P. R. Oxygen-Dependent Photochemistry and Photophysics of "MiniSOG," a Protein-Encased Flavin. *Photochem. Photobiol.* **2013**, *89* (5), 1116–1126.

(14) Baier, J.; Maisch, T.; Maier, M.; Engel, E.; Landthaler, M.; Bäumler, W. Singlet Oxygen Generation by UVA Light Exposure of Endogenous Photosensitizers. *Biophys. J.* **2006**, *91* (4), 1452–1459.

(15) Barnett, M. E.; Baran, T. M.; Foster, T. H.; Wojtovich, A. P. Quantification of Light-Induced MiniSOG Superoxide Production Using the Selective Marker, 2-Hydroxyethidium. *Free Radic. Biol. Med.* **2018**, *116*, 134–140.

(16) Christie, J. M.; Hitomi, K.; Arvai, A. S.; Hartfield, K. A.; Mettlen, M.; Pratt, A. J.; Tainer, J. A.; Getzoff, E. D. Structural Tuning of the Fluorescent Protein ILOV for Improved Photostability ESI. *J. Biol. Chem.* **2012**, *287* (26), 22295–22304.

(17) Roeser, D.; Schmidt, B.; Preusser-Kunze, A.; Rudolph, M. G. Probing the Oxygen-Binding Site of the Human Formylglycine-Generating Enzyme Using Halide Ions. *Acta Crystallogr. Sect. D Biol. Crystallogr.* **2007**, *63* (5), 621–627.

(18) Colloc'h, N.; Gabison, L.; Monard, G.; Altarsha, M.; Chiadmi, M.; Marassio, G.; Sopkova-De Oliveira Santos, J.; El Hajji, M.; Castro, B.; Abraini, J. H.; et al. Oxygen Pressurized X-Ray Crystallography: Probing the Dioxygen Binding Site in Cofactorless Urate Oxidase and Implications for Its Catalytic Mechanism. *Biophys. J.* **2008**, *95* (5), 2415–2422.

(19) Ahmad, I.; Vaid, F. H. M. Photochemistry of Flavins in Aqueous and Organic Solvents. In *Flavins photochemistry and photobiology:*; Silva, E., Edwards, A. M., Eds.; Cambridge: Royal Society of Chemistry, 2006; pp 13–40.

(20) Remucal, C. K.; McNeill, K. Photosensitized Amino Acid Degradation in the Presence of Riboflavin and Its Derivatives. *Environ. Sci. Technol.* **2011**, *45* (12), 5230–5237.

(21) Sikorska, E.; Khmelinskii, I. V.; Prukała, W.; Williams, S. L.; Patel, M.; Worrall, D. R.; Bourdelande, J. L.; Koput, J.; Sikorski, M. Spectroscopy and Photophysics of Lumiflavins and Lumichromes. *J. Phys. Chem. A* **2004**, *108* (9), 1501–1508.

(22) Valerón Bergh, V. J.; Bruzell, E.; Hegge, A. B.; Tønnesen, H. H. Influence of Formulation on Photoinactivation of Bacteria by Lumichrome. *Pharmazie* **2015**, *70* (9), 574–580.

(23) Sikorski, M.; Sikorska, E.; Koziolowa, A.; Gonzalez Moreno, R.; Bourdelande, J. L.; Steer, R. P.; Wilkinson, F. Photophysical Properties of Lumichromes in Water. *J. Photochem. Photobiol. B Biol.* **2001**, *60* (2–3), 114–119.

(24) Pattison, D. I.; Suryo Rahmanto, A.; Davies, M. J. Photo-Oxidation of Proteins. *Photochem Photobiol Sci.* **2012**, *11*, 38–53.

(25) Davies, M. J. Protein Oxidation and Peroxidation. *Biochem. J.* **2016**, *473* (7), 805–825.

(26) Walrant, P.; Santus, R. N-Formyl-Kynurenine, a Tryptophan Photooxidation Product, As a Photodynamic Sensitizer. *Photochem. Photobiol.* **1974**, *19* (6), 411–417.

(27) Fukunaga, Y.; Katsuragi, Y.; Izumi, T.; Sakiyama, F. Fluorescence Characteristics of Kynurenine and N'-Formylkynurenine. Their Use as Reporters of the Environment of Tryptophan 62 in Hen Egg-White Lysozyme. *J. Biochem.* **1982**, *92* (1), 129–141.

(28) Krishna, C. M.; Uppuluri, S.; Riesz, P.; Zigler Jr, J. S.; Balasubramanian, D. A Study of the Photodynamic Efficiencies of Some Eye Lens Constituents. *Photochem. Photobiol.* **1991**, *54* (1), 51–58.

(29) Wingen, M.; Potzkei, J.; Endres, S.; Casini, G.; Rupprecht, C.; Fahlke, C.; Krauss, U.; Jaeger, K.-E.; Drepper, T.; Gensch, T. The Photophysics of LOV-Based Fluorescent Proteins – New Tools for Cell Biology. *Photochem. Photobiol. Sci.* **2014**, *13* (6), 875–883.

(30) To, T.-L.; Fadul, M. J.; Shu, X. Singlet Oxygen Triplet Energy Transfer-Based Imaging Technology for Mapping Protein-Protein Proximity in Intact Cells. *Nat. Commun.* **2014**, *5* (May), 1–9.

(31) Fischer, M.; Bacher, A. Biosynthesis of Flavocoenzymes. *Nat Prod Rep* **2005**, *22*, 324–350.

(32) Rodríguez-Pulido, A.; Torra, J.; Mejías, S. H.; Cortajarena, A. L.; Ruiz-González, R.; Nonell, S.; Flors, C. Fluorescent Flavoprotein Heterodimers: Combining Photostability with Singlet Oxygen Generation. *ChemPhotoChem* **2018**, 1–5.

(33) Jiménez-Banzo, A.; Nonell, S.; Hofkens, J.; Flors, C. Singlet Oxygen Photosensitization by EGFP and Its Chromophore HBDI. *Biophys. J.* **2008**, *94* (1), 168–172.

(34) Deerinck, T. J.; Martone, M. E.; Lev-Ram, V.; Green, D. P.; Tsien, R. Y.; Spector, D. L.; Huang, S.; Ellisman, M. H. Fluorescence Photooxidation with Eosin: A Method for High Resolution Immunolocalization and in Situ Hybridization Detection for Light and Electron Microscopy. *J. Cell Biol.* **1994**, *126* (4), 901–910.

CHAPTER 6

Imaging cell photodamage induced by miniSOG derivatives

Visualizing cell damage processes and the activation of cell death mechanisms in real-time is fundamental to identify the cell structures that are affected and the biomolecules involved. Most of the reporting systems developed so far are based on FRET processes and using externally administered cytotoxic drugs. However, this approach shows several limitations. The combination of genetically encoded PS with cell death fluorescent reporters offers tremendous potential for the study of the phototoxic effects of ROS with high spatiotemporal resolution. Novel fluorescent reporters suitable for imaging diverse cell events, including ROS-mediated photodamage induced by genetically encoded PSs, are characterized.

Things happen for a reason.

Raj, Miao, Zairan and Rahaf

6.1. Introduction

Since the ultimate goal for a molecular or biological PS in the context of PDT is to induce fatal damage to the cell, it is fundamental to have tools that allow (1) to distinguish between live and dead cells, (2) to provide information on the mechanisms or processes involving cell death and (3) to identify the damaged biomolecules that play key roles in the fate of the cell. As described in previous chapters, biological PSs are the best option to spatiotemporally control the production of cytotoxic species and the induction of cellular damage and are therefore ideal tools to study the oxidative effect from the very generation site and its propagation to the molecules nearby. Typical assays for cell death studies are performed with organic dyes that need to be added exogenously and, noteworthy, most of them involve the killing of the cells for data readout. This, of course, limits the real-time visualization of the activation of cell death mechanisms and determination of the biomolecules involved. For this reason, there is a growing interest in developing protein-based fluorescent reporters for the study of cell death processes. Therefore, the combination of the phototoxic action of biological PSs with genetically encoded reporters for cell death processes arise as a powerful tool that might provide valuable data for the study of such mechanisms and identification of the biomolecules involved in a real-time manner. To our knowledge, however, this system comprising fully genetically encoding actuator and reporter has not been explored so far.

Most fluorescent reporters have been traditionally engineered based on FRET process. FRET is a distance-dependent radiationless transfer of energy from an excited donor fluorophore to a suitable acceptor fluorophore.[1] The use of FPs as a FRET tandem under the appropriate conditions allows the genetic introduction of the fluorophores at the target tissue or cellular compartment and the precise study of protein-protein interactions and protease activity.[2] These reporters are useful for imaging events such as activation of caspase proteases during apoptosis in cultured cells, however, their *in vivo* application has been limited because of poor signal to noise ratio and their small dynamic range due to small fluorescence change of the donor and acceptor fluorophores.[3,4] Additionally, fluorescence imaging of living animals is challenging because of tissue autofluorescence, cell heterogeneity and rapid shape and/or position changes.

To overcome limitations of FRET-based reporters, different alternatives have been developed. For example, the group of Dr. Xiaokun Shu at the University of California, San Francisco (UCSF), USA, has been actively working on engineering novel reporters that are initially non-fluorescent or barely fluorescent but become highly fluorescent upon activation by reaction with a cellular or exogenous component,[5,6] including proteases involved in apoptosis processes

such as caspase-3 or apoptosis-modulating factors such as rapamycin.[7] In this work, two novel approaches developed by the group of Dr. Shu have been studied. One relies on the splitting of a FP into fragments that are individually non-fluorescent but become highly fluorescent upon recombination. The second consists of the formation of bright fluorescent droplets based on the FKBP and Frb system which does not interact by itself but it forms a ternary complex upon addition of rapamycin.[8]

To assess the suitability of the new approaches and explore their potential to report photodamage induced by biological PSs, the kinetics of the recombination of the two parts for three novel GFP-like reporters and the droplet formation of an FKBP-Frb conjugate have been studied. For photokilling studies, miniSOG2,[9] an improved variant of miniSOG has been selected as the biological PS. The phototoxicity of miniSOG2 expressed in mammalian cells has been firstly evaluated using an exogenously added organic dye for apoptosis imaging and with the fully genetically encoded reporter.

6.2. Experimental section

6.2.1. Instrumentation

Absorption and fluorescence spectra for protein reconstitution experiments were recorded on an Infinite M1000 microplate reader (Tecan) in PBS buffer pH 7.4 and at 37°C as maintained by the microplate reader. Fluorescence quantum yields were measured using an LS-55 fluorometer (PerkinElmer). Imaging was conducted using a spinning-disk confocal microscopy (Nikon). The confocal scanning unit was equipped with the following emission filters: 525/50 nm for GFP imaging and 610/60 nm for mCherry and caspase-3 dye imaging. Images were processed using NIS-Elements and ImageJ (NIH).

6.2.2. Protein production and purification

Expression vectors encoding all the proteins studied were individually expressed with a polyhistidine tag on pBAD expression vector (Invitrogen) and transformed into competent TOP10 *E. coli* cells (Invitrogen). Bacterial cells were grown from a single colony in 250 mL LB medium supplemented with 100 µg/ml ampicillin (Sigma). Protein expression was induced by addition of 0.02 % (wt/vol) L-arabinose (Sigma). Cells were harvested by centrifugation and the His_6-tagged proteins were purified using the Ni-NTA purification system (Qiagen). The elution fraction containing the fluorescent proteins was loaded on a PD-10 column (GE Healthcare) for

buffer exchange and elimination of imidazole. Protein solutions were assayed by LDS-PAGE using NuPAGE Novex4%–12%Bis-Tris protein gels (Life Technologies) and the protein concentration was determined by the BCA Assay (Pierce).

6.2.3. Phototoxicity experiments in mammalian cells

The HEK293T/17 stocks were obtained from ATCC. Cells were passaged in DMEM supplemented with 10% fetal bovine serum, non-essential amino acids, penicillin (100 units/mL), and streptomycin (100 mg/mL). Cell transfection was performed in 35 mm glass-bottom dish suitable for imaging, mixing 4 µg of plasmid DNA with 71 mL of 1x Hank's balanced salt buffer and 4.3 µL of 2.5 M $CaCl_2$. Cells were then incubated at 37°C and 5 % CO_2 for 24 hours before photoablation experiments. Cells expressing the photoactive protein were illuminated with blue light (λ = 450 nm, ~ 0.8 W/cm^2) for 1 min. The activation of caspase-3 was imaged two hours after the light treatment using the Image-iT™ LIVE Red Caspase-3 and -7 Detection Kit (ThermoFisher). After illumination, cells were returned to the incubator. One hour before the intended time point for imaging, the reagent for apoptosis imaging was added at 1x to the cell culture medium. Cells were then incubated for 60 min under existing culture conditions. Afterward, cells were washed twice with the apoptosis wash buffer provided by the detection kit and imaged in PBS (without fixation) using the confocal microscope. For photokilling experiments using a genetically encoded reporter, a plasmid encoding miniSOG2 fused to mCherry was co-transfected with the GFP cell death reporter. Illumination was performed as described above and cells were imaged for six hours.

6.3. GFP-based novel reporters for the study of cell death processes

6.3.1. FlipGFPs: kinetics and early phototoxic experiments

Because cell autofluorescence is a major problem in fluorescence imaging, the absence of background fluorescence is essential for fluorogenic cell reporters. A good reporter should ideally be non-fluorescent and become bright fluorescent upon activation of a specific cellular event. The group of Dr. Shu has smartly prevented the formation of the fluorescent chromophore by rational splitting a GFP into two parts, named ZipGFP, rendering two non-fluorescent fragments – that only become luminescent upon recombination (Figure 6.1).[6] ZipGFP achieved 10-fold fluorescence increase upon protease activation and thus allowed visualization of apoptosis in the developing zebrafish embryo.[6]

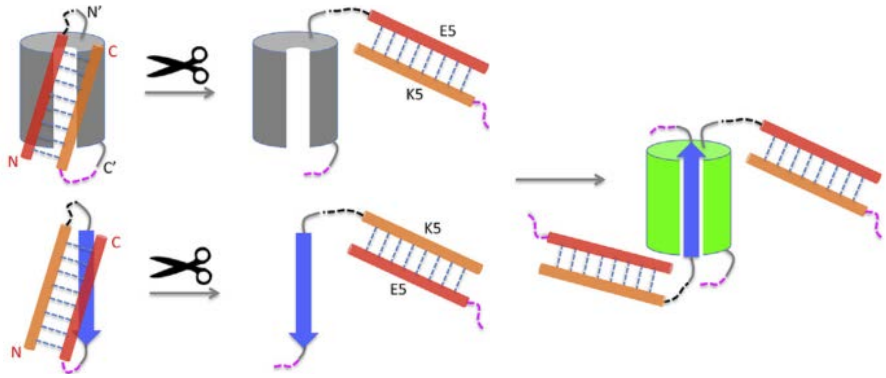

Figure 6.1. Illustration of the formation of a ZipGFP upon recombination of two dark fragments, from Ref. 6.

In the present work, this strategy has been further exploited and improved with a novel GFP-based fluorogenic protease reporter, called FlipGFP. It has been rationally designed by splitting the eleven β strands that constitute the GFP protein[10,11] into three parts. One part contains nine β strands (β1-9), a second part contains the 10th β strand (β10) and the third part contains the 11th β strand (β11). β1-9 contains the three amino acids that form the chromophore,[12] whereas β11 contains the highly conserved Glu222 residue that catalyzes the chromophore maturation.[13] However, it has been shown that when β10 and β11 are linked together or are in close proximity, they rapidly bind to β1-9, and the green fluorescence develops within several tens of minutes.[14] The key point introduced in this approach was to prevent β10-11 binding to β1-9 until protease activation by flipping β11, rendering it parallel to β10 and thus hampering the proper fitting to β1-9 (Figure 6.2A). To flip β11, heterodimerizing coiled coils E5 and K5 were used.[15] In detail, β10 and β11 were linked with the E5 coiled coil, and β11 was followed by the K5 coiled coil. The protease cleavage sequence was inserted between β11 and K5 (Figure 6.2B). Upon protease activation cleavage, β11 is able to flip back forming an anti-parallel structure with β10, which enables self-assembly with β1-9 and leads to the development of fluorescence. This approach has been successfully tested and FlipGFP-based protease reporter increased fluorescence 100-fold after activation and visualized apoptosis in the midgut of *Drosophila* and in live zebrafish embryos with spatiotemporal resolution.

In addition, this strategy has been further employed to design fluorogenic protease reporters with blue and red light fluorescence emission, allowing to cover a broad part of the visible spectrum and providing new tools for multicolor imaging of biological processes in living cells.

The kinetics of the recombination of individual fragments of FlipGFP (green), FlipCherry (red) and FlipBFP (blue) have been characterized in solution. Each protein fragment was expressed in *E. coli* cells, purified and mixed with the corresponding counterpart. A brief description of the experimental procedure, as well as the protein recombination results, are shown below.

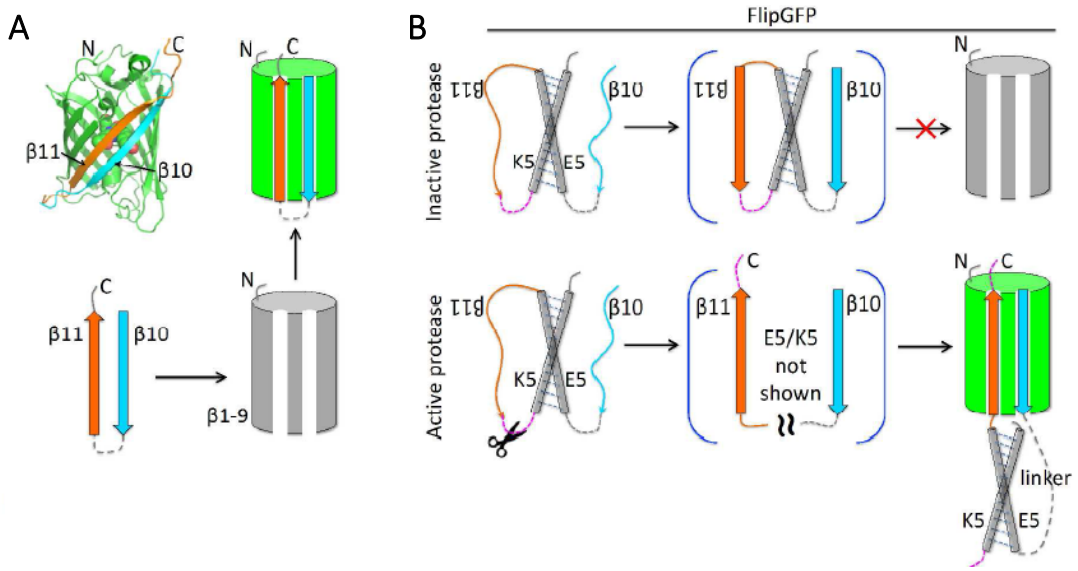

Figure 6.2. A) Structural model of reconstituted tripartite GFP and schematic diagram showing self-assembly of β10-11 and β1-9. (B) Illustration of rationally designed FlipGFP and its working mechanism. β10-11 is "flipped" by the heterodimerizing coiled coils E5 (gray) and K5 (yellow). The protease cleavage sequence is shown in pink.

a) FlipGFP

The two non-fluorescent parts were individually expressed in *E. coli*, purified and mixed in a total volume of 100 µL in a 96-well black plate. The green fluorescence of the reconstituted protein was recorded over time using the microplate reader, upon excitation at 460 nm (Figure 6.3A). FlipGFP emission increased with time to half-maximal fluorescence ($t_{1/2}$) of ~40 min, which is similar to the previously reported kinetics of ZipGFP[6] and the split GFP self-assembly.[16] In control experiments, the two dark parts were analyzed individually under the same experimental conditions, and no increase in fluorescence emission was observed (Figure 6.3B). The Φ_F for the reconstituted FlipGFP was determined (Φ_F = 0.66 ± 0.03) by comparing the AUC of the emission spectra of optically matched solutions of the purified mature protein and fluorescein (Φ_F = 0.925).[17] Thus, FlipGFP is significantly brighter (2.6-fold) than ZipGFP.

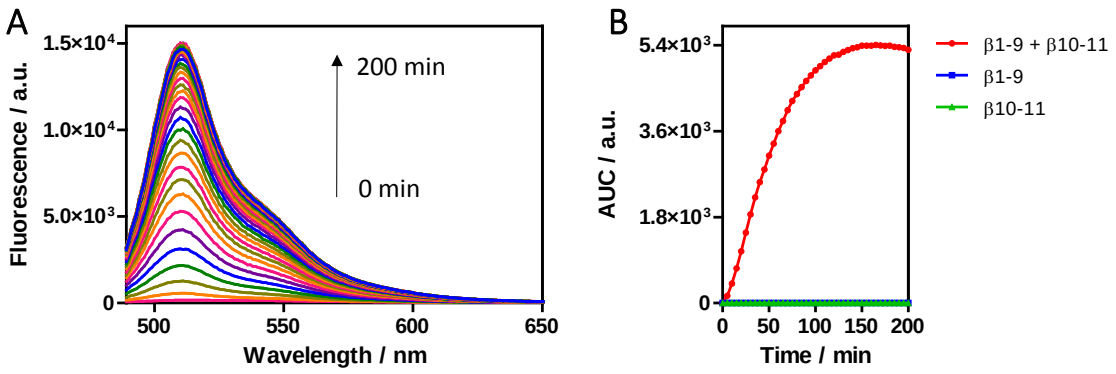

Figure 6.3. A) Fluorescence emission evolution of re-assembled GFP over time. B) Evolution of the AUC for the mixed and individual protein parts over time.

b) FlipCherry

The two non-fluorescent parts were also individually expressed and purified from *E. coli* cells. Protein re-assembling experiments were carried out on the microplate reader, in a total volume of 100 µL and upon light excitation at 545 nm. The red fluorescence increased with $t_{1/2}$ of ~55 min, which is a bit longer as compared to GFP. The results of protein reconstitution kinetics are shown in Figures 6.4A and 6.4B.

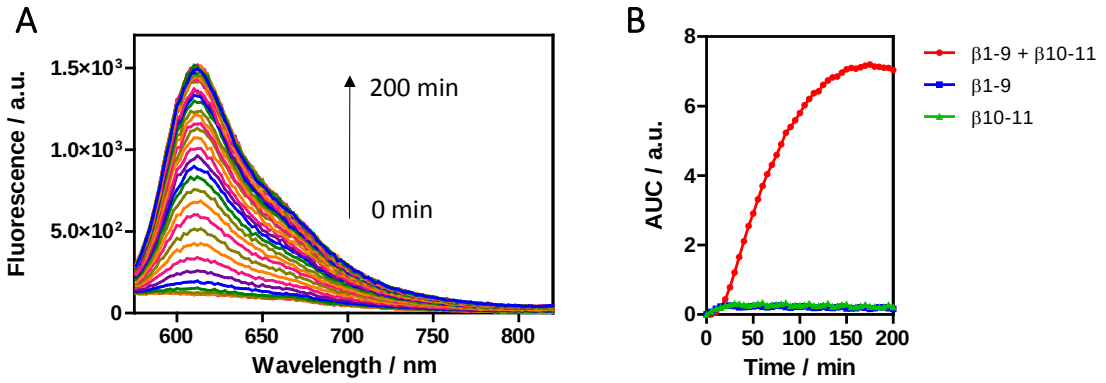

Figure 6.4. A) Fluorescence emission evolution of re-assembled FlipCherry over time. B) Evolution of the AUC for the mixed and individual protein parts over time.

c) FlipBFP

Similarly, the two non-fluorescent parts were purified from *E. coli* cells and mixed in a total volume of 200 µL. The fluorescence spectra were recorded on the fluorometer instead of the microplate reader because this protein is much less fluorescent[18] and it required higher light intensity at the excitation wavelength (λ = 375 nm). The results are shown in Figures 6.5A and 6.4B and reveal that the formation of the chromophore in BFP is less efficient and takes longer maturation times ($t_{1/2}$ ~ 85 min) as compared to the previous FlipGFPs.

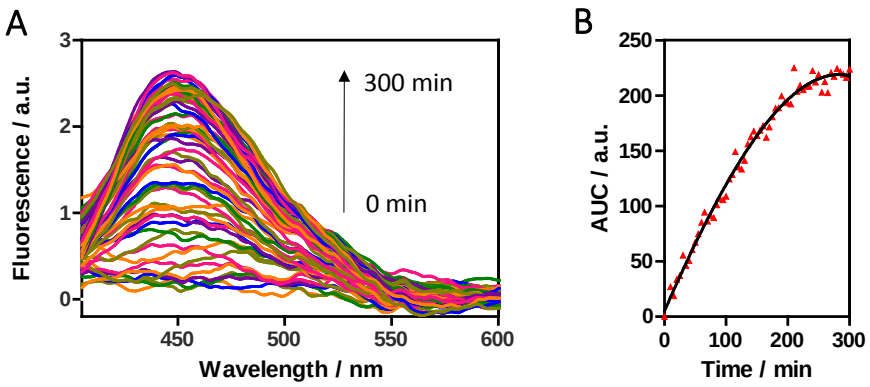

Figure 6.5. A) Fluorescence emission evolution of re-assembled FlipBFP over time. B) Evolution of the AUC for the mixed protein parts over time.

The suitability of these three FlipGFP proteins as fluorescent reporters has therefore been demonstrated in solution. Before testing their performance in living cells, it was pertinent to find an appropriate biological PS. Early studies on miniSOG2 had demonstrated its superior photokilling capacity as compared to other miniSOG variants.[9] Inspired in these previous experiments, the phototoxic properties of miniSOG2 were evaluated in mammalian cells and compared with the photosensitizing protein SOPP,[19] another variant of miniSOG, which produces more $^1O_2$ than miniSOG and had been reported to outperform the parental flavoprotein in cell ablation experiments.[20] Because miniSOG2 is barely fluorescent, nuclear-targeted H2B-miniSOG2 (fused to histone 2B) was co-expressed in HEK293 cells with a green fluorescent marker (H2B-EGFP) to allow identification of transfected cells. Illumination was performed with blue light and two hours after the treatment many cells showed caspase-3 activity (Figure 6.6). As a comparison, only a few cells that expressed SOPP were caspase-3 positive, confirming the grater phototoxicity of miniSOG2. Control cells expressing only H2-GFP did not show caspase-3 activation.

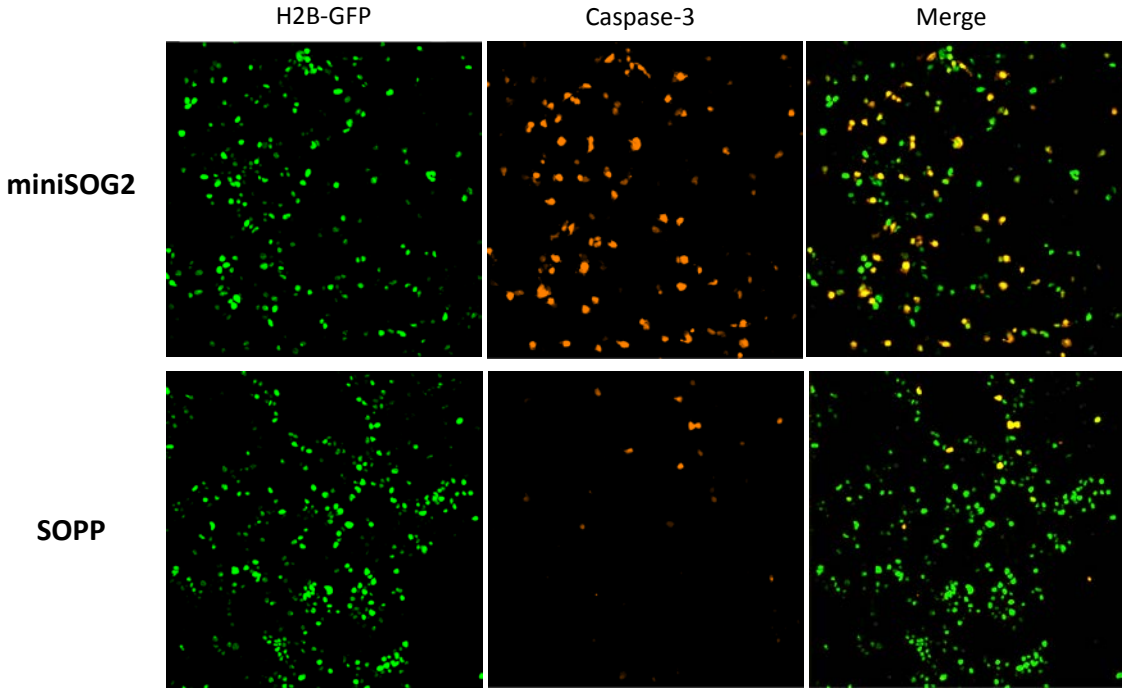

Figure 6.6. Comparison of miniSOG2 with SOPP in cell photokilling upon blue light illumination.

Once the prominent photodamaging capacity of miniSOG2 had been demonstrated with an organic dye, this protein was selected to test the applicability of the novel GFP reporters for apoptosis activation. Among the three GFP-like reporters characterized, the green fluorescent variant was chosen since it had been already expressed in mammalian cells with success and it had shown the brightest luminescence and stability. HEK293 cells were co-transfected with an

H2B-GFP rationally designed to report apoptosis processes – which becomes fluorescent upon activation of caspase-3 – and miniSOG2, which in turn had been fused to mCherry to help to visualize the protein location. Cells were illuminated under the previously described light conditions and imaged over time. Several cells that were initially dark developed bright green fluorescence (Figure 6.7), indicating the activation of apoptotic mechanisms. Unfortunately, cells were imaged only for 6 hours after the light treatment, and only a few cells turned positive. Because the activation of apoptosis may require longer times to occur as well as for the recombination process of the GFP reporter to yield the mature FP, it is therefore reasonable to expect that the number of green cells would eventually increase over time. These results are thus preliminary and further experiments are needed to consolidate the suitability of these novel genetically encoded reporters. However, these results provide encouraging data of their potential for the study of the light-induced cell death mechanisms, particularly in combination with photoactive proteins as PSs.

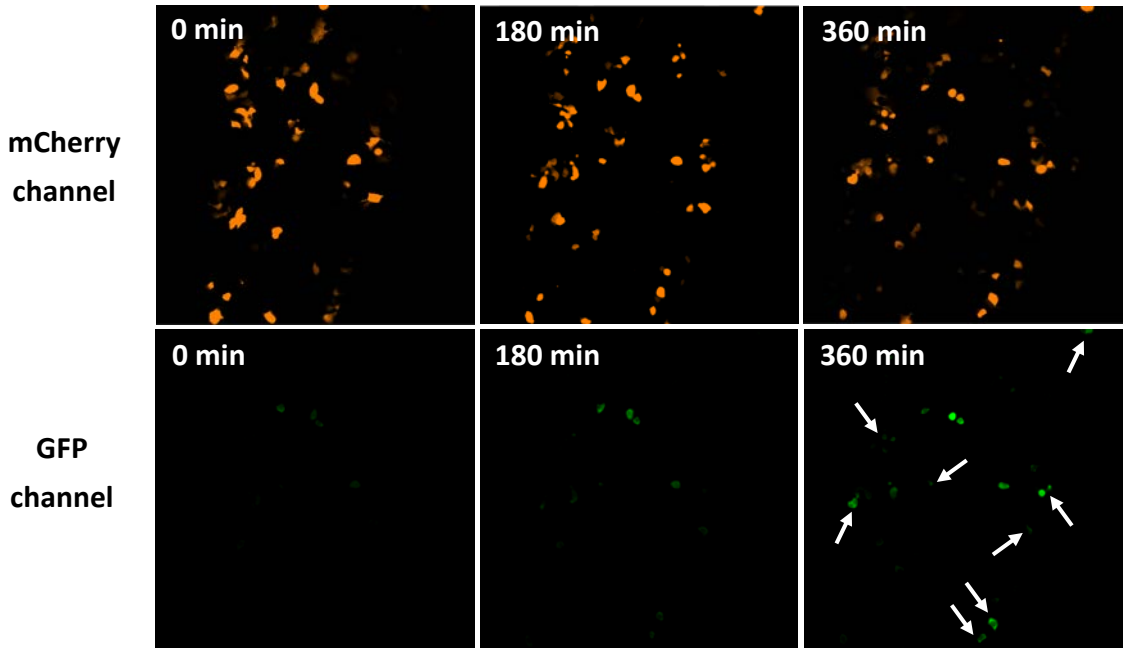

Figure 6.7. Time-lapse microscopy of HEK293 cells co-expressing miniSOG2-mCherry and the GFP reporter for caspase-3 activation. White arrows show some of the individual cells or groups of cells that have developed green fluorescence upon blue light illumination. (mCherry channel, λ_{ex} = 561 nm; GFP channel, λ_{ex} = 488 nm).

6.3.2. EGFP-based fluorescent droplets

The group of Dr. Shu has recently developed a different strategy called SPARK.[21] It is based on the formation of fluorescent droplets of EGFP upon activation of a particular cellular process (Figure 6.8). This is achieved by introducing homo-oligomeric coiled coils (HOTag3 and HOTag6) that are rationally designed to interact with each other only under appropriate conditions.[21]

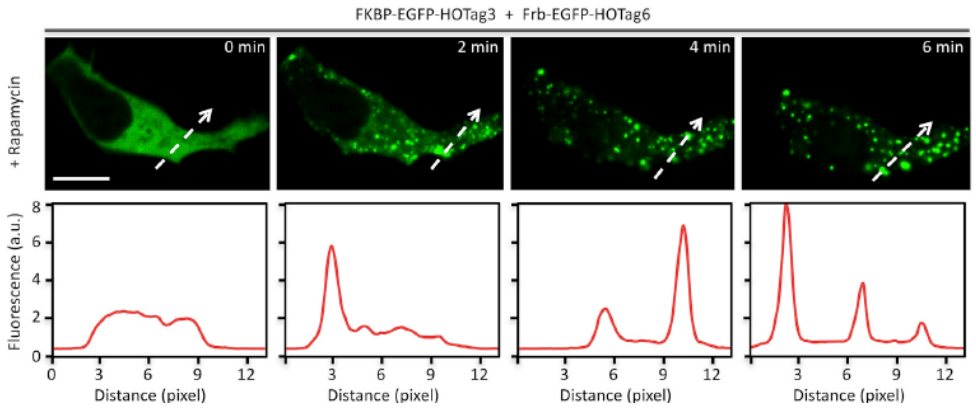

Figure 6.8. Time-lapse images of cells expressing EGFP upon the addition of rapamycin. Histograms are shown corresponding to the dashed arrow in the fluorescence images Figure from Ref. 9.

EGFP-HOTag3 and EGFP-HOTag6 were individually expressed and purified from *E. coli* cells. Aqueous solutions of each protein system were observed both separately and mixed under the confocal microscope (Figure 6.8). In any case, fluorescent droplets were observed. However, bright droplets were readily formed (~20 -30 s) in the mixture solution upon addition of 500 nM rapamycin (Figure 6.9).

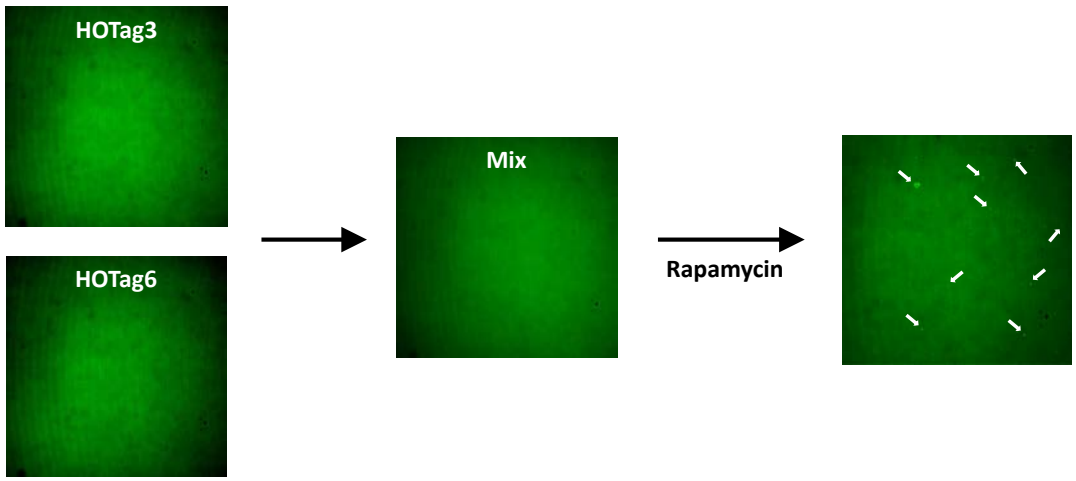

Figure 6.9. Fluorescent droplets are readily formed upon addition of rapamycin to the mixture solution containing EGFP-HOTag3 and EGFP-HOTag6. White arrows show some of the fluorescent droplets.

To estimate the protein concentration in the fluorescent droplets, EGFP was expressed in *E. coli* cells, purified and aliquoted at various concentrations. The protein concentration was determined by both the BCA Assay and by absorption measurements (ε = 56.000 $M^{-1}{\cdot}cm^{-1}$, at 488 nm).[22] The protein samples were then imaged under the confocal microscope. The fluorescence brightness was recorded, corresponding to EGFP concentration (Figure 6.10). The plotted line was then used to estimate EGFP concentration in living cells based on the fluorescence brightness.[21]

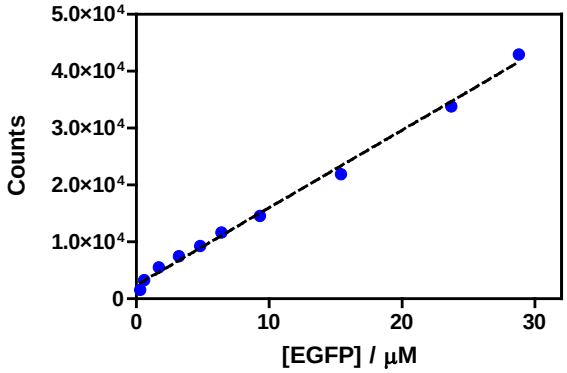

Figure 6.10. Relationship of EGFP fluorescence brightness and concentration.

These results demonstrate that the HOTag system is also a working alternative for the real-time reporting of cellular events. it has been successfully employed for the study of kinase dynamics and signaling in living animals.[21] However, it could not be tested in combination with biological PSs to report cell death processes, which leaves a promising road open to be explored.

6.4. Conclusions

The combination of genetically encoded reporters with biological PSs emerges as a powerful tandem for the study of photodamage with high spatiotemporal resolution. Besides the widely used FRET-based systems, novel fluorescence reporters are being actively developed for the study of cellular processes in real-time. Two novel approaches have been rationally designed by the group of Dr. Shu and part of its characterization and proof of concept covered within this thesis. The first strategy is called FlipGFP and it relies on the recombination of two non-fluorescent fragments that yields a fluorescent entity upon activation of proteases. Three novel variants of FlipGFP reporters, including blue, green and red light emitting proteins, have been produced in *E. coli* cells and characterized. The kinetics of protein self-assembling have been determined in solution. The ability of FlipGFP to report ROS-induced activation of apoptosis has been preliminarily tested in living mammalian cells with the photosensitizing protein miniSOG2. Early results showed the development of FlipGFP green fluorescence in blue light irradiated cells, as a result of the activation of apoptosis processes. The second strategy is named SPARK and it is based on the formation of bright fluorescent droplets of EGFP upon activation of a cellular process or signaling pathway. This approach has been assessed with purified proteins in solution using rapamycin to induce the droplet formation. Moreover, solutions of EGFP at different protein concentrations have been imaged under the confocal microscope. The relationship between fluorescence brightness and EGFP concentration has been determined, which has been used for the estimation of protein concentration in the fluorescent droplets in living cells.

6.5. References

(1) Lakowicz, J. R. *Principles of Fluorescence Spectroscopy*, Third Edit.; Springer: Maryland, USA, 2006.

(2) Lindenburg, L.; Merkx, M. Engineering Genetically Encoded FRET Sensors. *Sensors* **2014**, *14* (7), 11691–11713.

(3) Kardash, E.; Bandemer, J.; Raz, E. Imaging Protein Activity in Live Embryos Using Fluorescence Resonance Energy Transfer Biosensors. *Nat. Protoc.* **2011**, *6* (12), 1835–1846.

(4) To, T. L.; Medzihradszky, K. F.; Burlingame, A. L.; DeGrado, W. F.; Jo, H.; Shu, X. Photoactivatable Protein Labeling by Singlet Oxygen Mediated Reactions. *Bioorganic Med. Chem. Lett.* **2016**, *26* (14), 3359–3363.

(5) To, T.-L.; Piggott, B. J.; Makhijani, K.; Yu, D.; Jan, Y. N.; Shu, X. Rationally Designed Fluorogenic Protease Reporter Visualizes Spatiotemporal Dynamics of Apoptosis in Vivo. *Proc. Natl. Acad. Sci. U. S. A.* **2015**, *112* (11), 3338–3343.

(6) To, T.-L.; Schepis, A.; Ruiz-González, R.; Zhang, Q.; Yu, D.; Dong, Z.; Coughlin, S. R.; Shu, X. Rational Design of a GFP-Based Fluorogenic Caspase Reporter for Imaging Apoptosis In Vivo. *Cell Chem. Biol.* **2016**, *23* (7), 875–882.

(7) Ballou, L. M.; Lin, R. Z. Rapamycin and MTOR Kinase Inhibitors. *J. Chem. Biol.* **2008**, *1* (1–4), 27–36.

(8) Banaszynski, L. A.; Liu, C. W.; Wandless, T. J. Characterization of the FKBP-Rapamycin-FRB Ternary Complex. *J. Am. Chem. Soc.* **2005**, *127* (13), 4715–4721.

(9) Makhijani, K.; To, T.-L.; Ruiz-González, R.; Lafaye, C.; Royant, A.; Shu, X. Precision Optogenetic Tool for Selective Single- and Multiple-Cell Ablation in a Live Animal Model System. *Cell Chem. Biol.* **2017**, *24* (1), 110–119.

(10) Yang, F.; Moss, L. G.; Phillips, G. N.; Phillips Jr., G. N.; Phillips, G. N. The Molecular Structure of Green Fluorescent Protein. *Nat. Biotechnol.* **1996**, *14* (10), 1246–1251.

(11) Ormö, M.; Cubitt, A. B.; Kallio, K.; Gross, L. A.; Tsien, R. Y.; Remington, S. J. Crystal Structure of the Aequorea Victoria Green Fluorescent Protein. *Science* **1996**, *273* (5280), 1392–1395.

(12) Tsien, R. Y. Constructing and Exploiting the Fluorescent Protein Paintbox (Nobel Lecture). *Angew. Chemie Int. Ed.* **2009**, *48* (31), 5612–5626.

(13) Sniegowski, J. A.; Lappe, J. W.; Patel, H. N.; Huffman, H. A.; Wachter, R. M. Base Catalysis of Chromophore Formation in Arg96 and Glu 222 Variants of Green Fluorescent Protein. *J. Biol. Chem.* **2005**, *280* (28), 26248–26255.

(14) Cabantous, S.; Nguyen, H. B.; Pedelacq, J. D.; Koraïchi, F.; Chaudhary, A.; Ganguly, K.; Lockard, M. A.; Favre, G.; Terwilliger, T. C.; Waldo, G. S. A New Protein-Protein Interaction Sensor Based on Tripartite Split-GFP Association. *Sci. Rep.* **2013**, *3*, 1–9.

(15) De Crescenzo, G.; Litowski, J. R.; Hodges, R. S.; O'Connor-McCourt, M. D. Real-Time Monitoring of the Interactions of Two-Stranded de Novo Designed Coiled-Coils: Effect of Chain Length on the Kinetic and Thermodynamic Constants of Binding. *Biochemistry* **2003**, *42* (6), 1754–1763.

(16) Cabantous, S.; Terwilliger, T. C.; Waldo, G. S. Protein Tagging and Detection with Engineered Self-Assembling Fragments of Green Fluorescent Protein. *Nat. Biotechnol.* **2005**, *23* (1), 102–107.

(17) Magde, D.; Wong, R.; Seybold, P. G. Fluorescence Quantum Yields and Their Relation to Lifetimes of Rhodamine 6G and Fluorescein in Nine Solvents: Improved Absolute Standards for Quantum Yields. *Photochem. Photobiol.* **2002**, *75* (4), 327–334.

(18) Patterson, G. H.; Knobel, S. M.; Sharif, W. D.; Kain, S. R.; Piston, D. W. Use of the Green Fluorescent Protein and Its Mutants in Quantitative Fluorescence Microscopy. *Biophys. J.* **1997**, *73* (5), 2782–2790.

(19) Westberg, M.; Holmegaard, L.; Pimenta, F. M.; Etzerodt, M.; Ogilby, P. R. Rational Design of an Efficient, Genetically-Encodable, Protein-Encased Singlet Oxygen Photosensitizer. *J. Am. Chem. Soc.* **2015**, *137* (4), 1632–1642.

(20) Xu, S.; Chisholm, A. D. Highly Efficient Optogenetic Cell Ablation in C. Elegans Using Membrane-Targeted MiniSOG. *Sci. Rep.* **2016**, *6*, 21271.

(21) Zhang, Q.; Huang, H.; Zhang, L.; Wu, R.; Chung, C. I.; Zhang, S. Q.; Torra, J.; Schepis, A.; Coughlin, S. R.; Kornberg, T. B.; et al. Visualizing Dynamics of Cell Signaling In Vivo with a Phase Separation-Based Kinase Reporter. *Mol. Cell* **2018**, *69* (2), 347.

(22) Shaner, N. C.; Steinbach, P. A.; Tsien, R. Y. A Guide to Choosing Fluorescent Proteins. *Nat. Methods* **2005**, *2* (12), 905–909.

CHAPTER 7

Exploring the potential of miniSOG for photodynamic therapy of melanoma

The application of PDT for the treatment of melanoma remains one of the main challenges in the biomedical sciences. Melanoma skin cancer is generally considered to be resistant to PDT due to pigmentation and its intrinsic antioxidant defense mechanisms. Genetically encoded PSs may offer a working alternative to conventional molecular PSs owing to the superior targeting potential conferred by the genetic control of cell expression and subcellular localization. The potential of miniSOG for the treatment of melanoma is evaluated.

Sí arrisca't.
Aquesta és sempre la resposta.
Albert Espinosa

7.1. Introduction

Melanoma is the most dangerous skin cancer, the incidence of which continues to rise in western populations at an alarming rate; only in the last 20 years, the number of cases worldwide has doubled.[1] This type of cancer arises from melanocytes, which are the cells that produce melanin, the pigment responsible for skin and hair color. If diagnosed early, melanoma can be cured by surgical resection, however, prognosis decreases severely once metastasis occurs since melanoma is inherently resistant to traditional forms of chemotherapy and radiotherapy.[2] During the last years, various strategies have been developed and explored to treat melanoma, including immunotherapy, radiotherapy and gene therapy.[3] In addition, recent discoveries in cell signaling have provided significant understanding of the biology of melanoma, and these advances are being exploited to provide targeted drugs and new therapeutic approaches.[3] Although some of these therapies have progressed to human clinical trials, their outcomes remain poor.

PDT has also been explored for the treatment of melanoma as an adjuvant therapy alone or in combination with current therapeutics. However, the application of PDT for the treatment of melanoma remains one of the main challenges in the area. The resistance of melanoma to light therapy mainly arises from pigmentation and its intrinsic antioxidant defense mechanisms[4,5] Attempts to apply PDT to melanoma with conventional molecular PSs have been met only with limited success so far. In this regard, the use of organic dyes as PSs has been typically limited from poor water solubility, low cellular uptake and off-target PS localization.

Genetically encoded PSs may offer a working alternative to overcome the oxidative stress defense of melanoma cells by producing acute and very precise damage to vital organelles. In addition, the superior targeting potential conferred by the genetic control of cell expression provides higher selectivity towards the tumor cells, which is crucial for avoiding injury to the surrounding healthy tissue. On the other hand, the filter effect of melanin in the blue and green regions of the visible spectrum can be circumvented by 2PA PDT, which uses longer wavelength lights that are barely absorbed by the pigment.

In this work, the genetically encoded approach has been explored with miniSOG, since it has been reported that is capable of killing mammalian cells upon blue light illumination[6] (Figure 7.1). In that geminal study, the authors engineered three target vectors to express miniSOG at different subcellular localizations (i.e., plasma membrane, mitochondria and chromatin) and used lentiviruses to generate stable cells lines expressing the photosensitizing flavoprotein at each site.[6] Upon blue light irradiation, they observed pronounced cell death in cancer cells

expressing each of the miniSOG constructs developed, reaching nearly 100% for miniSOG targeted to the membrane, and could therefore demonstrate the phototoxicity of miniSOG in cancer cells for the first time.[6] Of note, the percentage of dead cells in non-illuminated control cells was low in miniSOG-expressing cell lines, although somewhat higher compared to control non-transduced cells.

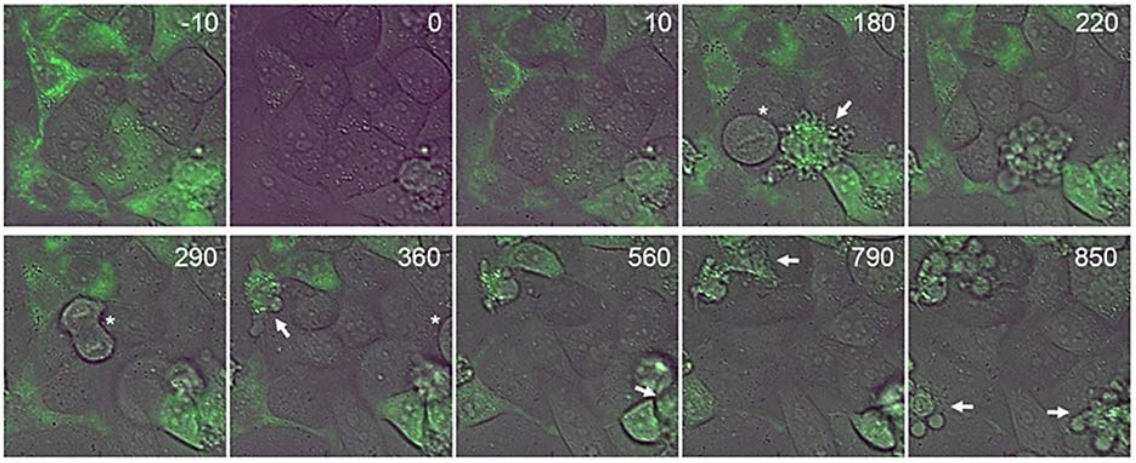

Figure 7.1. Time-lapse microscopy of miniSOG targeted to mitochondria. The numbers indicate the time after illumination in minutes. White arrows point dying cells. Image from Ref. 6.

The study of miniSOG in melanoma cells has been conducted in collaboration with Dr. Àngels Fabra from the Institut d'Investigació Biomèdica de Bellvitge (IDIBELL) in the framework of a research project awarded by Fundació la Marató de TV3. The primary goal of the project was to provide scientific basis for the suitability of the genetically encoded PSs approach for the treatment of cutaneous melanoma. As a proof of concept, the phototoxic properties of miniSOG were initially tested in non-pigmented (amelanotic) melanoma cell lines.

7.2. Strategies to express miniSOG in melanoma cells

7.2.1. Production of lentiviral particles

The three lentiviral vectors expressing miniSOG at the cell membrane (miniSOG-mem), mitochondria (miniSOG-mito) and chromatin (miniSOG-H2B) were kindly provided by the group of Dr. Lukyanov from the Shemyakin-Ovchinnikov Institute of Bioorganic Chemistry in Moscow, Russia. Competent DH5α *E. coli* cells were transformed with each construct to amplify the plasmid. Mammalian cell transfection and lentiviral transduction were performed as described in the literature,[6] with minor changes. Briefly, lentiviral particles were generated by polyethylenimine (PEI):DNA complex[7] transient transfection of host HEK293FT cells. The total of

5.3 µg and 9.7 µg of the two packaging plasmids pMD2 and psPAX2, respectively, and 15 µg of transfer vector plasmid (miniSOG-mem, miniSOG-mito or H2B- miniSOG or) were used for transfection. Additionally, 3.25 µg of pCSEA2 was added for expressing a green fluorescent protein as a control for transfection efficiency in the host cell. All plasmids were mixed with PEI polymer at 3 µL/µg DNA, the solution was incubated for 20 minutes and used for transfection. Twenty-four hours afterward, the medium containing the lentiviral vector particles was filtered (0.45-µm filter). A fraction of the supernatant was mixed with lentivirus transduction enhancer and used for the initial transduction of four amelanotic melanoma cell lines: SK-Mel 131, WM 793, M# 238 and M# 249. To enhance the transduction efficiency, the rest of the vector containing supernatant was mixed with 8.5 % polyethylene glycol (PEG) solution, incubated for 24 hours at 4 °C.[8] Subsequently, the mixture was pelleted by centrifugation, the pellet containing the lentiviral particles was resuspended in 300 µl PBS and used for transduction of melanoma cells.

7.2.2. Evaluation of miniSOG expression on transduced melanoma cells

Epifluorescence microscopy of the virus producers cells HEK293FT showed strong green fluorescence, revealing the successful transfection of the initial DNA complex. In addition, the pellet obtained upon centrifugation of the supernatant also confirmed the formation of the viral particles. However, none of the miniSOG constructs in none of the melanoma cell lines transduced showed fluorescence under the microscope. Moreover, only SK-Mel 131, WM 793 survived the lentiviral process. Many attempts were performed in order to enhance the transduction efficiency, such as increasing the concentration of the viral particles or carrying out successive rounds of infection using the highly concentrated lentivirus-PEG pellets, up to six rounds. In addition to the melanoma cell lines, miniSOG transduction was also tested in other mammalian cells, including HEK293 and HeLa cells; this latter being the cell line used in the reference work of miniSOG in cancer cells that had shown successful results.[6] However, it was not possible to reproduce the reported results and the fluorescence of miniSOG could not be detected for any of the lentiviral vectors expressing miniSOG nor in any of the cell lines assayed.

Noteworthy, quantitative PCR (qPCR, also known as Real-Time PCR) revealed the presence of large amounts of mRNA from the three miniSOG constructs in all infected melanoma cells, confirming that the lentiviral particles had been produced and the plasmid vectors delivered. Of note, miniSOG RNA was not detected in non-transduced cells. With these results in mind, several hypotheses were made to try to rationalize the absence of miniSOG's emission. First, it was

suggested that miniSOG could be misfolded or in a dark state for any reason, which would hamper its detection by means of spectroscopic or microscopy techniques. However, it was not possible to assess the expression of miniSOG in melanoma cells by western blot analysis because the appropriate antibodies were not available. For this reason, initial efforts were made aiming to detect any emission miniSOG by increasing the sensitivity of the fluorescence detection techniques. In particular, control (non-transduced) and transduced melanoma cells of the cell lines SK-Mel 131 and WM 793 were carefully examined by emission and excitation fluorescence spectroscopy. Cells were trypsinized, washed thoroughly with PBS and finally resuspended in PBS buffer. Normalization of the fluorescence emission spectra revealed essentially the same emission profile for both control and transduced cells, which in turn resembled very much the emission spectra of flavin molecules that are present in cellular systems (Figure 7.2). Normalization of the fluorescence excitation spectra showed little differences between the melanoma cells, however, the broad shape of the bands was not likely attributable to miniSOG, which shows a structured profile. Furthermore, cells were lysed, pelleted by centrifugation and the soluble fraction was also analyzed spectroscopically. Again, no significant differences between the control and the transfected cells were observed.

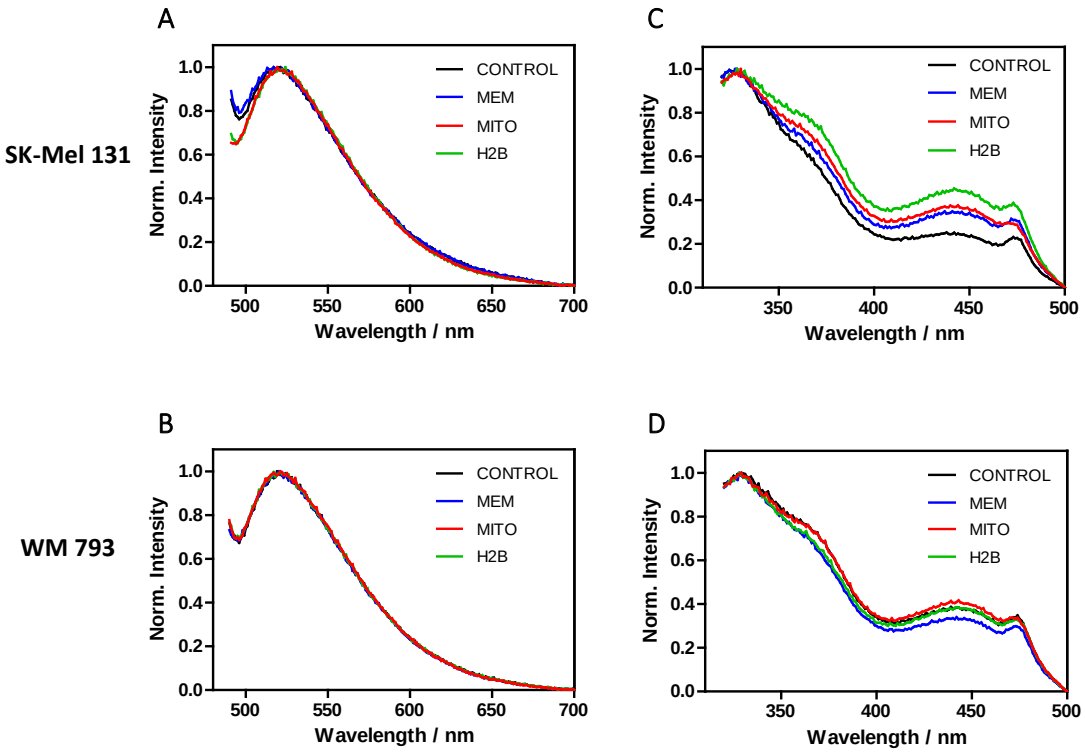

Figure 7.2. Normalized fluorescence emission (A, B) and excitation (C, D) spectra of SK-MEL 131 and WM 793 melanoma cells, respectively, resuspended in PBS. λ_{ex} = 430 nm. λ_{obs} = 540 nm. Control denotes non-transduced melanoma cells of the corresponding cell line. Mem, mito and H2B denote the miniSOG construct used for transduction.

As for the dark state hypothesis, it is worth noting that miniSOG itself is not green fluorescent in the *apo* state (i.e., without the chromophore), and it is the molecule of FMN encased in the protein that bestows the photophysical properties discussed in previous chapters. Thus, in case of lacking FMN in the cellular system, the protein could be expressed, but it would be silenced for optical detection techniques. This hypothesis was tested by supplementing the cellular growth medium of the transduced cells with 0.8 μM and 10 μM FMN. Before analysis, cells were washed thoroughly with PBS to remove any excess of the free flavin. However, the fluorescence of miniSOG could not be observed either by epifluorescence microscopy nor by fluorescence spectroscopy.

With the qPCR results still in mind, further hypotheses to explain the lack of fluorescence in melanoma cells were formulated. One suggested the eventual excretion of miniSOG to the external medium. However, this hypothesis was experimentally ruled out upon centrifugation and analysis of the growth medium. Another explanation pointed to the plausible interaction of miniSOG with any intrinsic cellular component(s) which could eventually quench miniSOG's excited states. If this would be the case, miniSOG would absorb the light delivered to the cells, but the energy would be then transferred to a nearby compound without the emission of a green photon. This process however was unlikely since many studies have observed the fluorescence of miniSOG in mammalian cells. Because the primary goal of this project was to explore the phototoxic properties of miniSOG in melanoma cells, it was worth starting photoirradiation experiments and test whether high doses of blue light were sufficient to induce some degree of cell damage, despite the lack of fluorescence emission.

First attempts of photokilling experiments were carried out using six rounds of virus-infected melanoma cells and having supplemented the growth medium with FMN, which was washed out before the irradiation. Cells were illuminated with blue light (460 nm, 16 mW/cm^2) for 30 and 60 minutes in transparent PBS to avoid filter effects from the colored components that are present the cellular growth medium. Afterward, PBS was removed and cells were and incubated in cell culture medium for 72 hours. Cell death was assayed by the WST-1 colorimetric method, which revealed cell viability higher than 99 % in all cases, by comparing irradiated samples with non-transduced cells and dark controls, concluding the unsuitability of the first approach.

7.2.3. New miniSOG constructs

For a new set of experiments, two commercial miniSOG plasmids for transient transfection were purchased. One, named mCherry-miniSOG-CDC42-C-10 (Addgene number 55087)

engineered for cell membrane targeting, hereafter miniSOG-MEM, and the second named PA-mCherry-miniSOG-Mito-7 (Addgene number 57795) for mitochondria targeting, hereafter miniSOG-MITO. Importantly, both plasmids also encoded (1) a red fluorescent protein (mCherry) fused to miniSOG and (2) resistance to the antibiotic geneticin (G418). Therefore, the new constructs were expected to overcome two of the major problems encountered in the first approach. First, mCherry is excited with green light which is not absorbed by miniSOG and its red fluorescence should be brighter and easier to detect without disturbing miniSOG. Furthermore, the antibiotic resistance provides a powerful tool to select the transfected cells and therefore ensures that all of them carry the plasmid encoding the proteins of interest by the time of the irradiation experiment.

Competent *E. coli* DH5α cells were used to amplify the two miniSOG constructs. Transient transfection was optimized using the lipofectamine method[9] for two melanoma cell lines, SK-Mel 131 (amelanotic, not pigmented) and SK-Mel 128 (melanotic, pigmented). (Transfection of the pigmented cell line was performed to test whether it was possible to excite and detect mCherry in spite of the presence of melanin. No fluorescence could not be detected). As a control to the effectiveness of the cell transfection protocol, an extra batch of SK-Mel 131 cells was co-transfected with a plasmid encoding GFP. The green fluorescence of GFP could be clearly visualized under the epifluorescence microscope. This observation confirmed that transient plasmids were positively and highly efficiently delivered to melanoma cells.

Of note, the red emission was observed under the epifluorescence microscope for the SK-Mel 131 cell line, which therefore confirmed the correct transfection and expression of the proteins. However, the red fluorescence was very weak, almost undetectable in cells expressing the miniSOG-MITO construct. In addition, it was realized that the intensity of the emission dramatically decreased over time, and ultimately disappeared within two to three weeks after transfection. The eventual expelling of the transient plasmid could explain this observation; however, it would also imply the loss of the antibiotic resistance and the concomitant death of the cells soon after. This was not the case since cells survived even after many cell passages in medium supplemented with 500 μg/mL G418. Therefore, it can be safely assumed that the transient plasmid remained inside the cells and hence other unknown events should account for the bleaching of red fluorescence.

On the other hand, extremely dim green fluorescence could be detected under the epifluorescence microscope. However, it was only observed in round-shaped unhealthy melanoma cells and not in healthy ones. To determine whether the green emission could be

attributable to miniSOG, SK-Mel 131 cells expressing miniSOG-MITO and miniSOG-MEM were imaged by confocal microscopy. However, despite the higher laser power and resolution from the confocal microscope as compared to the epifluorescence one, miniSOG's emission was not observed when illuminating with blue light, in any of the melanoma cell lines nor with any of the miniSOG constructs used for transfection.

On the other hand, the confocal microscope allowed visualizing the red fluorescence of mCherry targeted either to the mitochondria or to the cell membrane. Hence, revealing the correct expression and subcellular localization. However, the intensity of the emission was extremely low and most of the cells were not fluorescent (Figure 7.3). Again, this latter is particularly surprising since cells were always grown and kept in medium supplemented with high concentrations of G418 to ensure the selective survival of transfected cells. Of note, imaging experiments were carried out on cells that had been transfected three weeks before, to ensure the complete action of the antibiotic (i.e., at least seven to ten days are typically required for G148 to efficiently kill non-transfected cells).[10] However, the fluorescence of mCherry had already decreased significantly by this time when visualized under the epifluorescence microscope, which raises an apparent incompatibility between high fluorescence intensity and antibiotic selection, which severely limits the optimal study of this system.

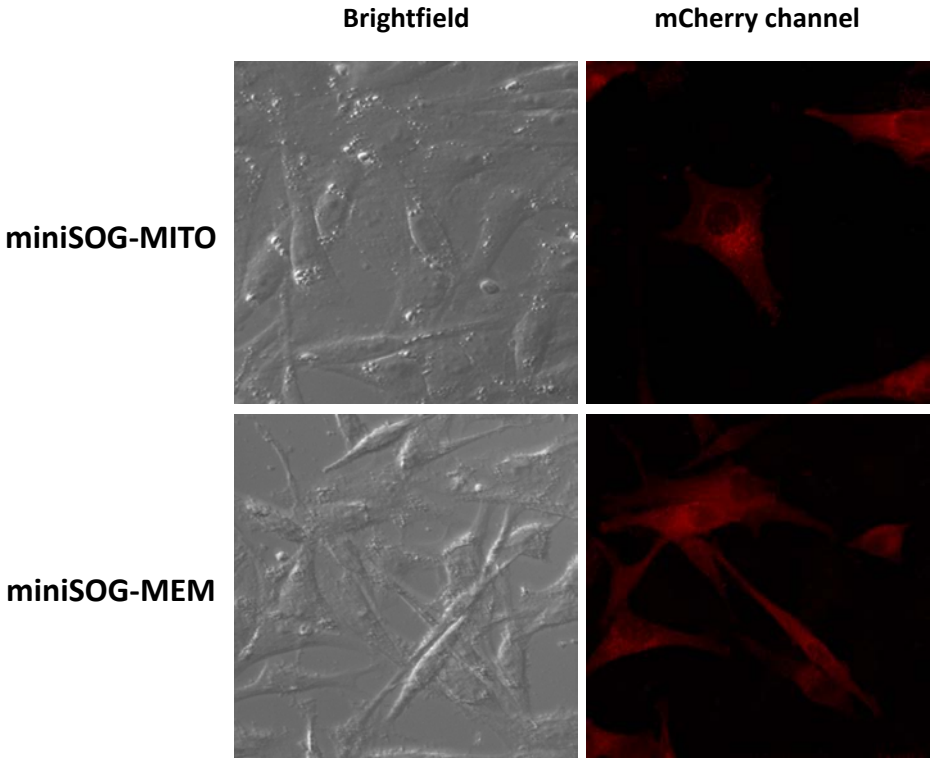

Figure 7.3. SK-Mel 131 melanoma cells expressing miniSOG-mCherry localized at mitochondria and at the cell membrane.

Despite miniSOG's fluorescence could not be observed, photokilling experiments were carried out since the red fluorescence of mCherry guaranteed the correct expression and localization of the protein construct. As proceeded previously, cells were incubated 24 hours in medium supplemented with G418 and FMN and washed with PBS right before irradiation to remove the excess of free flavin. Cells were illuminated in buffer solution for 45 minutes and 90 minutes with blue light. After irradiation, cells were observed under the bright field microscope. Cells expressing either miniSOG-MITO or miniSOG-MEM showed pronounced round shape, (typical morphological indicator of cell damage), while non-transfected cells used as controls showed healthier morphology. Then, the PBS from the wells was exchanged by fresh medium and cells were incubated for 72 hours. At this point, cells were observed under the bright field microscope and surprisingly, all of them had recovered from the irradiation effects and exhibited a normal and healthy morphology. Cell viability was determined by the WST-1 assay and revealed no significant differences between the irradiated cells expressing the photosensitizing protein, the non-transfected cells and the dark controls.

7.3. Novel strategies to improve the photodynamic outcome

Although blue light irradiation did not induce sufficient cell damage to lead to cell death, the morphological changes detected after the treatment apparently reflected some degree of photodamage. This observation would be in agreement with reported studies on photodynamic therapy of melanoma using molecular PSs, where strong resistance of this type of cells towards light therapy has been observed and large light fluences have been required to induce cell death.[4] In attempts to improve the outcome of the photodynamic treatment, three strategies were proposed. (1) To perform successive irradiation cycles to increase the light fluence delivered without exposing the cells out of the incubator for too long times. (2) To design and build a powerful blue light source to increase the fluence and reduce the irradiation time. (3) To mutate the original miniSOG from the commercial constructs to produce the novel mutant named miniSOG Q103V,[11] which has been developed and characterized recently and which photosensitizes $^1O_2$ 10-fold more efficiently, with a reported $\Phi_\Delta = 0.39$[11] (See Chapter 5).

Regarding the first strategy, six cycles of 90 minutes of blue light illumination (460 nm and 16 mW/cm^2) were carried out in combination with 30 minutes of dark recovery inside the incubator. Cell viability was assayed by the 3-(4,5-dimethylthiazol-2-yl)-2,5-diphenyltetrazolium bromide) tetrazolium (MTT) method and revealed that all the cells were dead, including the non-transfected ones. Additional attempts were performed using the same batch of transfected cells

(upon the corresponding cell passages) and reducing the irradiation time out of the incubator. However, none of the experiments showed conclusive results when comparing miniSOG-MEM, MITO and non-transfected controls. The main limitation for all these experiments was that the expression of the proteins could not be ascertained at any time by means of fluorescence or microscopic techniques. Having in mind the fact that fluorescence intensity of mCherry greatly diminishes over time, it was also reasonable to expect the concomitant reduction of the photoactive protein miniSOG. Unfortunately, it was not possible to assess the presence of the fluorescent proteins in the cells before performing the photokilling experiments. In addition, the time required for the antibiotic to select the transfected cells also hampered the study of the cells shortly after cell transfection.

As for the second strategy, a new powerful LED was designed and built up (Figure 7.4). The irradiance of the new LED was ~340 mW/cm^2, about 21 times higher than the previous light source used for cell irradiation. This time, irradiation was performed on different batches of cells that had been transfected 7, 6 and 5 days before the experiment. Admittedly, this time is too short for G418 to fully select the transfected cells. However, this approach was performed in attempts to study cells expressing the maximum amount of photoactive proteins. The new blue LED was used for irradiation and it provided sufficient intensity to supply more than 300 J/cm^2 in less than 15 minutes (reported photokilling experiments with miniSOG in cancer cells[6] were achieved at 280 J/cm^2). Unfortunately, the observation of black spots in the cell cultures prepared for the photokilling experiment as well as in the original flasks of transfected cells revealed apparent contamination which masked the MTT results and all cells had to be discarded.

It has not been possible to further test the new LED for additional experiments by the time of writing this thesis. However, its development now provides a powerful tool with great potential future attempts using blue light-absorbing PSs.

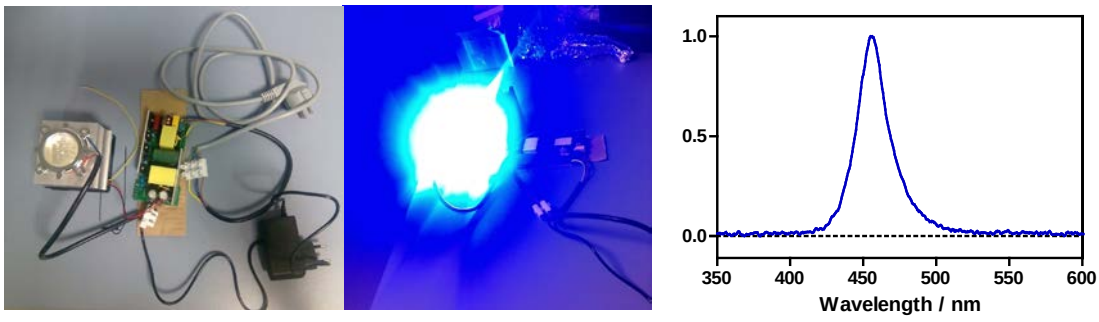

Figure 7.4. Image of the self-customized super bright blue LED emitting with maxima at 455 nm.

Finally, the third approach consisted of performing site-directed mutagenesis of the sequence encoding miniSOG in the commercial plasmids in order to replace the glutamine residue in the position 103 for a valine. The Q103V mutant photosensitizes $^1O_2$ more efficiently and it is also slightly more fluorescent than its precursor, which might be advantageous for its detection. To perform the mutagenesis, it was first necessary to determine the nucleotide sequence of the miniSOG encoded in the commercial constructs, because it was not provided by the depositor laboratory. Since the genetic code is described as degenerate, or redundant, meaning that a single amino acid may be coded by more than one codon, many possible sequences encode miniSOG. For this reason, DNA primers complementary to the most used miniSOG sequence were synthesized and tested for sequencing. However, it turned out that the nucleotide sequence was not the one expected. Luckily enough, one of our primers allowed the reading of the miniSOG-MITO construct. Thus, new primers suitable for the miniSOG MITO construct and containing the Q103V mutation were synthesized. Plasmids were amplified by the polymerase chain reaction (PCR) and the initial methylated template plasmid was afterward digested with the restriction enzyme *DpnI*. Competent *E. coli* DH5β cells were transformed and used for plasmid amplification and isolation. Sequencing confirmed the correct mutation and the construct was named miniSOG Q103V-MITO. Primers: mSOG_F: AAGCTTCGTGATTACT-GACCCGC; mSOG_R: CCGATGAAGTACTGCAGCTCACC.

On the other hand, the nucleotide sequence in the commercial miniSOG-MEM was so different to our primers that the membrane-targeted construct could not be initially read nor determined. Hence, it was not possible to perform PCR for miniSOG-MEM and the mutant miniSOG Q103V-MEM could not be obtained. Several sequencing attempts were performed afterward to identify the nucleotide sequence and it has been finally uncovered, which now enables mutagenesis experiments with this plasmid.

The new construct encoding the improved version of miniSOG targeted to mitochondria could not be tested in melanoma cells by the time of writing this thesis. The potential of this novel mutant for the PDT of melanoma remains to be evaluated, however, its superior photosensitizing ability offers a promising alternative to explore the suitability of the miniSOG approach.

7.4. Conclusions

The use of biological PSs for the PDT melanoma may offer advantages over molecular PSs owing to their greater biocompatibility and their superior targeting capacity to specific organelles. MiniSOG has been selected to assess the viability of the genetically encoded approach because it was the reference photosensitizing flavoprotein at the beginning of the project and its ability to kill cancer cells had been already demonstrated. Lentiviral transduction of melanoma cells was performed similarly as reported in the abovementioned study. However, the green fluorescence of miniSOG was not observed in any of the conditions, miniSOG constructs or cell lines tested. In addition, preliminary phototoxicity experiments revealed cell viability about 99 %.

In a second approach, commercial plasmids encoding miniSOG fused to mCherry were used for transient transfection of melanoma cells. The red fluorescence of mCherry could be detected, albeit very dim in all cases and it gradually bleached over time elapsed after cell transfection. Because the complete action of the antibiotic G418 typically requires at least seven days to be effective, cell selection turned out to be inconvenient for preserving the fluorescent properties of the photoactive proteins. Confocal microscopy revealed that only a few cells in medium supplemented with G418 were expressing mCherry. Unfortunately, it was not possible to monitor the expression levels of the cells before the phototoxicity experiments, and illumination of the cells did not provide evidence of photodamage. Attempts to enhance the outcome of the light treatment included the combination of successive irradiations with dark recovery periods inside the incubator, the build-up of a powerful blue LED to increase the light fluence delivered in a shorter irradiation time, and the site-directed mutagenesis of the commercial miniSOG constructs to produce an improved version of the flavoprotein. None of the strategies carried out has yielded positive results so far, and it has not been possible to draw conclusions on the suitability of biological PSs for the treatment of melanoma. Nevertheless, the successful development of both the LED and the MITO construct encoding the miniSOG Q103V provides valuable alternatives with potential to improve the results in future experiments.

7.5. References

(1) Gray-Schopfer, V.; Wellbrock, C.; Marais, R. Melanoma Biology and New Targeted Therapy. *Nature* **2007**, *445* (7130), 851–857.

(2) Zbytek, B.; Carlson, J. A.; Granase, J.; Ross, J.; Mihm, M.; Slominski, A. Current Concepts of Metastasis in Melanoma. *Expert Rev Dermatol* **2008**, *3* (5), 569–585.

(3) Jilaveanu, L. B.; Aziz, S. A.; Kluger, H. M. Chemotherapy and Biologic Therapies for Melanoma: Do They Work? *Clin. Dermatol.* **2009**, *27* (6), 614–625.

(4) Baldea, I.; Filip, A. G. Photodynamic Therapy in Melanoma - an Update. *J. Physiol. Pharmacol.* **2012**, *63* (7), 109–118.

(5) Huang, Y.; Vecchio, D.; Avci, P.; Yin, R.; Garcia-Diaz, M.; Hamblin, M. R. Melanoma Resistance to Photodynamic Therapy : New Insights. *Biol. Chem.* **2014**, *394* (2), 239–250.

(6) Ryumina, A. P.; Serebrovskaya, E. O.; Shirmanova, M. V; Snopova, L. B.; Kuznetsova, M. M.; Turchin, I. V; Ignatova, N. I.; Klementieva, N. V; Fradkov, A. F.; Shakhov, B. E.; et al. Flavoprotein MiniSOG as a Genetically Encoded Photosensitizer for Cancer Cells. *Biochim. Biophys. Acta* **2013**, *1830* (11), 5059–5067.

(7) Boussif, O.; Lezoualc'h, F.; Zanta, M. A.; Mergny, M. D.; Scherman, D.; Demeneix, B.; Behr, J. P. A Versatile Vector for Gene and Oligonucleotide Transfer into Cells in Culture and in Vivo: Polyethylenimine. *Proc. Natl. Acad. Sci.* **1995**, *92* (16), 7297–7301.

(8) Nasri, M.; Karimi, A.; Allahbakhshian Farsani, M. Production, Purification and Titration of a Lentivirus-Based Vector for Gene Delivery Purposes. *Cytotechnology* **2014**, *66* (6), 1031–1038.

(9) Dalby, B.; Cates, S.; Harris, A.; Ohki, E. C.; Tilkins, M. L.; Price, P. J.; Ciccarone, V. C. Advanced Transfection with Lipofectamine 2000 Reagent: Primary Neurons, SiRNA, and High-Throughput Applications. *Methods* **2004**, *33* (2), 95–103.

(10) Provost, J. J.; Wallert, M. A. Investigating the Biochemistry and Cellular Physiology of NHE1. *Protoc. Stable Cell line Prod.* **1998**, 1.

(11) Rodríguez-Pulido, A.; Cortajarena, A. L.; Torra, J.; Ruiz-González, R.; Nonell, S.; Flors, C. Assessing the Potential of Photosensitizing Flavoproteins as Tags for Correlative Microscopy. *Chem. Commun.* **2016**, *52* (54), 8405–8408.

CHAPTER 8

General discussion

An overview of the entire work presented in the previous chapters is given herein. A general discussion of the main results is provided, whilst offering insights regarding the further development of the use of flavoproteins for PDT, aPDT and in advanced imaging techniques.

Happiness (is) only real when shared.
Alexander Supertramp

8.1. General discussion and future perspectives

The promising predictions formulated over the last decades about the potential of PDT are now a real and consolidated alternative in modern medicine and surgery. PDT is currently applied for the treatment of solid tumors and microbial infections with remarkable success.[1] However, drug delivery and better selectivity towards malignant cells are unsolved drawbacks that still preclude its wider application and are a matter of intense research.

The work performed along the previous chapters is devoted to exploring the suitability of a new family of PSs to circumvent the limitations associated with conventional molecular light-sensitive drugs. The new method relies on biological PSs that are genetically produced by the host cell without the addition of any exogenous compound. The genetic approach provides unprecedented control of the ROS production and the corresponding oxidative cellular damage in time and space. These advantages are gaining much attention and are being actively exploited for cutting-edge optogenetic applications. Because a few natural-occurring chromophores are present in both bacterial and mammalian cells, strategies to develop a fully genetically encoded PS are limited. In the present work, the potential of proteins from the LOV natural blue light receptors has been characterized and evaluated for PDT and aPDT applications. In nature, this family of proteins encases a molecule of FMN which is not photoactive due to the formation of a covalent adduct between a conserved cysteine residue and the excited flavin.[2] The photophysical properties of the chromophore were rationally restored by replacing the active cysteine by an unreactive alanine or glycine,[3,4] and opened up a new road of possibilities of flavin-binding FPs for a wide range of applications.[5,6]

The number of new fluorescent flavoproteins is actively increasing.[7] A palette of FbFPs derived from different organisms were generated from collaborators, and the photophysical, photosensitizing and antimicrobial properties were characterized. Early results showed promising capacity of $^1O_2$ production, outperforming the reported Φ_Δ of miniSOG in most cases. However, the underlying mechanisms for the photosensitization of $^1O_2$ were more complex than previously described examples and involved two independent populations of excited chromophores.[8] The properties of the singlet and triplet excited states for the total of eight FbFPs were initially characterized in detail. However, unexpected phototransformations led to marked changes in their photosensitizing properties, and therefore, the spectroscopic results obtained thus far for those samples did not describe with certainty their putative characteristics and were disregarded.

This situation motivated the development of a new protocol for the in-house expression and purification of the photoactive proteins, enabling the study of fresh flavoprotein samples. A total of 21 proteins from the FbFP-family have been characterized throughout the present work. The photophysical and photosensitizing properties have been determined, which expands the number of available options in the flavoprotein arena and provide a valuable guide for choosing the best option for a given experiment. It is worth noting that besides the spectroscopic data collected, this work also describes the difficulties associated with the study of biological PSs, and aims to help the scientific community that is working with similar systems. It is essential to avoid any light exposure to the photoactive proteins – even white room light – to prevent undesired phototransformations, which are particularly critical for long-term stored samples.

Direct detection of $^1O_2$ NIR phosphorescence revealed that all the FbFPs tested are capable of generating $^1O_2$ upon blue light illumination, although to a different extent. The smallest Φ_Δ was determined for PhiLOV2.1, which is reasonable since this protein was engineered aiming to enhance the photostability of FbFPs.[9] On the other hand, the highest Φ_Δ values were observed in SOPP, an improved version of miniSOG developed specifically for photosensitization purposes[10] and for the two DsFbFP proteins isolated and derived from the marine α proteobacterium *Dinoroseobacter shibae*.[7,11] Interestingly, although all the proteins encase the same chromophore, the properties of the excited triplet state and therefore, the ability and kinetics of $^1O_2$ production, dramatically change from one protein to another. For example, the lifetime of the excited triplet states ranges from dozens to hundreds of microseconds. This provides valuable structural information on both the accessibility to the chromophore from external molecules and the interactions with the amino acids that surround it.

The antimicrobial properties of FbFPs have also been studied. *E. coli* cells individually expressing each flavoprotein were illuminated with blue light and cell death was induced in a light dose-dependent manner. Other ROS have also been detected upon light exposure to the flavoproteins. This was also to be expected since the FMN chromophore is capable of generating ROS other than $^1O_2$ when illuminated with blue light.[12] However, the production of $^1O_2$ correlates with the photokilling rate observed in bacteria, indicating the key role of $^1O_2$ in the fatal damage of the cells.

The photosensitizing and photophysical properties of miniSOG have been characterized in detail to provide a more in-depth understanding of the processes that modulate the fate of its triplet excited state and that affect the ultimate production of $^1O_2$. The crystalline structure has been finally solved in high resolution, and the factors that limit its modest ability to generate $^1O_2$

have been rationalized, in agreement with recently published results.[13] On the one hand, oxygen-independent protein quenching efficiently deactivates ^{3}miniSOG*, decreasing the number of triplets that can react with O_2. This observation is reflected by the high k_p value determined for miniSOG. On the other hand, the phosphoribityl tail of FMN makes tortuous the path for O_2 to diffuse through the protein matrix and reach the chromophore, which is consistent with the lower k_{O_2} value obtained.

The effects of extended photolysis of miniSOG have been elucidated: (1) production of LC, a known photodegradation product of riboflavin which lacks the phosphoribityl tail, absorbs at shorter wavelengths and is capable of photosensitizing $^1O_2$ in high yield, and (2) photo-oxidation of tryptophan and other electron-rich residues. The higher O_2 accessibility to the chromophore increases the k_{O_2} value, whereas the inactivation of protein quenching pathways decreases k_p. The sum of the two processes explains the dramatic enhancement in the Φ_Δ value for the photoconverted miniSOG observed when it is excited at 355 nm, but not at 473 nm LC barely absorbs.

Other miniSOG variants have been developed and characterized aiming to improve the modest Φ_Δ. Inspired by the good results observed for the Q103L mutation in SOPP (Φ_Δ = 0.25),[10] the Q103V mutant was engineered and yielded Φ_Δ = 0.39.[14] The increase in $^{1j}O_2$ production was also reflected in higher phototoxicity of the protein expressed in *E. coli* cells. For the miniSOG W81F mutant, which lacks the single tryptophan residue that is present in miniSOG, Φ_Δ = 0.33 was determined, hence confirming the positive effect of removing this electron rich amino acid on the $^1O_2$ generation (hence decreasing k_p). On the other hand, attempts to characterize the photophysical properties of the highly phototoxic miniSOG2,[15] could not be achieved due to the apparent loss of the flavin chromophore throughout the purification process. Attempts to combine the excellent results of $^1O_2$ production from miniSOG Q103V and the impressive photokilling ability of miniSOG2 yielded the mutant miniSOG2 Q103V, called miniSOG3. However, as observed in miniSOG2, the flavin-protein interaction is apparently weak and this protein could not be purified and characterized in solution.

The effect of O_2 accessibility to the chromophore in the production of $^1O_2$ (i.e., k_{O_2}) has been studied in miniSOG derivatives encasing the non-phosphorylated RF instead of FMN. MiniSOG denatured and reconstituted with RF showed almost identical optical properties, however, its ability to photosensitize $^1O_2$ increased by 3-fold (Φ_Δ = 0.11). Importantly, the triplet lifetime decreased from ~30 μs to ~5 μs, which is consistent with a more exposed flavin to the molecules from the solvent. This effect has been further demonstrated by the rational design of mutants

that bind RF predominantly. One of the mutants, called miniSOG R57Q, was shown to encase RF in 74.4 %, confirming the positive effect of the mutation on the RF binding. Analysis of the $^1O_2$ signal revealed a short component ($\tau_T \sim 5.7$ µs), in agreement with encasing a major proportion of the accessible RF. However, the higher accessibility to the chromophore was not reflected in the Φ_Δ value, which barely improved ($\Phi_\Delta = 0.05$). Denaturation and RF reconstitution of miniSOG R57Q increased the amount of encased RF up to 96.4 %, which resulted in a further shortening of the triplet lifetime ($\tau_T \sim 5.0$ µs) and a slight enhancement in the Φ_Δ value ($\Phi_\Delta = 0.07$). However, Φ_Δ was still far from the improvements observed upon removing protein quenchers, suggesting the major contribution of k_p on the limited production of $^1O_2$ by miniSOG.

The photostability of PhiLOV2.1 and the photosensitizing properties of miniSOG and miniSOG Q103V have been smartly combined for the engineering of flavoprotein heterodimers suitable for fluorescence microscopy and photooxidation-based CLEM.[16] The two heterodimers, named PhiSOG and PhiSOG Q103V, respectively, endured photodegradation significantly, approaching the photostability of phiLOV2.1 while preserving high levels of $^1O_2$ photosensitization.[16] Indeed, the positive effect of merging the complementary properties of the heterodimers has been demonstrated by their ability to polymerize DAB while preserving the emission suitable for fluorescence imaging. In addition, the size of the tandem heterodimers is still small, similar to that of a single GFP, which facilitates its genetic introduction into living cells without significant perturbation of the surrounding cell components. For all these reasons, the development of fluorescent heterodimers opens an alternative and unexplored road which further expands the possibilities of the FbFP family for photosensitization and imaging applications.

Aside from studying the photosensitization properties of FbFPs and understanding their underlying mechanisms to develop better photoactive proteins, the genetically encoded approach is also a powerful tool for reporting the effects of oxidative damage in living cells. Two novel strategies for living cells imaging have been recently engineered and characterized. Regarding the first approach, a novel split GFP called FlipGFP has been developed. The kinetics of the formation of the fluorescent reporter have been studied for three FlipGFP proteins, which emit at different parts of the visible spectrum and therefore provide multiple opportunities to keep track of several cell events simultaneously. FlipGFP has been co-expressed with the phototoxic protein miniSOG2 in mammalian cells, and the green fluorescence of the reporter has been observed after blue light illumination, revealing the activation of apoptosis mechanisms. Still in its infancy, the fully genetically encoded approach for both cell actuators and reporters offers tremendous potential for reporting cellular photodamage processes in high spatiotemporal resolution. The second approach is called SPARK and it relies on the formation

of fluorescent protein droplets upon activation of a cellular process.[17] SPARK has allowed robust and direct visualization of kinase signaling in living animals.[17] In addition, the correlation between fluorescence intensity under the confocal microscope and the concentration of the fluorescent protein has been used to estimate the protein concentration in the fluorescent droplets in living cells.[17]

PDT of melanoma remains an elusive goal due to the resistance mechanisms conferred by the presence of melanin and high levels of antioxidant compounds.[18] The biological PSs approach has shown promising results in other types of cancer cells[19] of less complexity than melanoma cells. In this work, the potential of genetically encoded $^1O_2$ PSs in amelanotic cells been tested with miniSOG. Attempts to express the photoactive flavoprotein in melanoma have been performed by both lentiviral transduction and transient transfection processes. Unfortunately, it has not been possible to ascertain its correct expression by microscopy or spectroscopic techniques in any of the explored cell lines, miniSOG constructs and protocols tested, which has prevented further study and the possibility drawing any conclusions It is necessary to develop novel plasmid constructs and have tools available to visualize the production of the PSs and to assess the optimal time for illumination experiments. The road for the PDT of melanoma with biological PSs is still open, and the potential of this approach is starting to be explored as reflected by early reports that are currently emerging.[20]

Altogether, the results presented in this work unambiguously demonstrate the capacity of FbFPs to photosensitize $^1O_2$ upon blue light illumination. The combination of these abilities with the genetic control offers tremendous potential which can be exploited for a wide array of applications, including CALI, PDT, advanced imaging techniques, theranostics and optogenetics. The characterization of the photophysical and photosensitizing properties of the novel flavoproteins provides a palette of alternatives that may be useful to select the appropriate protein for each study. These results will contribute to consolidate and expand the growing and glowing toolbox of photoactive flavoproteins in the biomedical sciences.

Of particular relevance are the phototoxic properties of the FbFP against bacterial cells. In the actual context of an inevitable move toward the end of the antibiotic era, the development of alternative therapies is urgently needed. Amongst other strategies, aPDT is gaining much attention and firmly progressing to become a reality shortly. In this regard, biological PSs are expected to further improve the outcome of the treatment by increasing the selectivity and reducing the light dose required. The photokilling ability of flavoproteins has been demonstrated, even against Gram-negative bacteria, which are typically more resistant to aPDT.

For all these reasons and in light of the results presented in this work, the use of FbFPs as biological PSs may find a niche in the photodynamic approach to treat microbial infections. On the other hand, the applicability of flavoproteins as genetically encoded PS in mammalian cells has yet to be consolidated. To date, only a few studies have been reported for flavoproteins expressed in mammalian cells, and early experiments in melanoma cell lines performed in this work have not shown positive results. Novel methods to deliver the plasmid selectively and efficiently into cells of high complexity are therefore desired. Particularly interesting is an eventual step towards the development of red-light absorbing optogenetic proteins, which would mitigate the inherent competition from endogenous chromophores for the incident light.

From a structural and mechanistic point of view, it is fascinating how a single mutation changes dramatically the behavior of proteins encasing the same chromophore. It has been shown that the specific amino acid sequence exerts a remarkable effect on the properties of the triplet excited state chromophore, and as a consequence, their ability to generate $^1O_2$. The elucidation of the crystal structure of miniSOG and the transformations that occur upon photolysis provide sound answers to long-awaited open questions. The new mechanistic insights on the formation of $^1O_2$ also allow to rationalize the factors affecting the modest Φ_Δ of miniSOG as compared to the free flavin and offer useful information for the rational development of novel flavin-based proteins as biological PSs. Particularly relevant is the participation of the tryptophan residue in the quenching of ^{3}miniSOG*. FbFPs lacking this amino acid exhibited long triplet lifetimes and remarkable yield of $^1O_2$ production. Therefore, we anticipate that removing the tryptophan residues from the proteins intended for $^1O_2$ applications may enhance the photosensitizing properties. Interestingly, with the exception of the two DsFbFP variants and miniSOG W81F, all other 18 FbFPs studied contain a single tryptophan residue, and thus it would be very interesting to study the consequences of replacing this amino acid. Increasing the O_2 accessibility to the chromophore also has a positive effect on the $^1O_2$ generation. In this regard, the photoconversion of FMN to LC inside the protein unlocks the path for O_2 to easily reach the chromophore. All this information may be useful to expand the toolbox of flavoproteins as reporters for imaging techniques or as biological PSs for the photoablation of malignant cells. The combination of both may therefore result in the development of fully genetically encoded systems that allow both the induction and reporting of cellular photodamage, which has great potential for modern cell biology studies. However, to our knowledge, the potential of this tandem remains unexplored.

8.2. References

(1) Agostinis, P.; Berg, K.; Cengel, K. A.; Foster, T. H.; Girotti, A. W.; Gollnick, S. O.; Hahn, S. M.; Hamblin, M. R.; Juzeniene, A.; Kessel, D.; et al. Photodynamic Therapy of Cancer: An Update. *CA. Cancer J. Clin.* **2011**, *61* (4), 250–281.

(2) Swartz, T. E.; Corchnoy, S. B.; Christie, J. M.; Lewis, J. W.; Szundi, I.; Briggs, W. R.; Bogomolni, R. A. The Photocycle of a Flavin-Binding Domain of the Blue Light Photoreceptor Phototropin. *J. Biol. Chem.* **2001**, *276* (39), 36493–36500.

(3) Drepper, T.; Eggert, T.; Circolone, F.; Heck, A.; Krauss, U.; Guterl, J. K.; Wendorff, M.; Losi, A.; Gärtner, W.; Jaeger, K. E. Reporter Proteins for in Vivo Fluorescence without Oxygen. *Nat. Biotechnol.* **2007**, *25* (4), 443–445.

(4) Shu, X.; Lev-Ram, V.; Deerinck, T. J.; Qi, Y.; Ramko, E. B.; Davidson, M. W.; Jin, Y.; Ellisman, M. H.; Tsien, R. Y. A Genetically Encoded Tag for Correlated Light and Electron Microscopy of Intact Cells, Tissues, and Organisms. *PLoS Biol.* **2011**, *9* (4), e1001041.

(5) Mishin, A. S.; Belousov, V. V; Solntsev, K. M.; Lukyanov, K. A. Novel Uses of Fluorescent Proteins. *Curr. Opin. Chem. Biol.* **2015**, *27*, 1–9.

(6) Buckley, A. M.; Petersen, J.; Roe, A. J.; Douce, G. R.; Christie, J. M. LOV-Based Reporters for Fluorescence Imaging. *Curr. Opin. Chem. Biol.* **2015**, *27*, 39–45.

(7) Wingen, M.; Potzkei, J.; Endres, S.; Casini, G.; Rupprecht, C.; Fahlke, C.; Krauss, U.; Jaeger, K.-E.; Drepper, T.; Gensch, T. The Photophysics of LOV-Based Fluorescent Proteins – New Tools for Cell Biology. *Photochem. Photobiol. Sci.* **2014**, *13* (6), 875–883.

(8) Torra, J.; Burgos-Caminal, A.; Endres, S.; Wingen, M.; Drepper, T.; Gensch, T.; Ruiz-González, R.; Nonell, S. Singlet Oxygen Photosensitisation by the Fluorescent Protein Pp2FbFP L30M, a Novel Derivative of Pseudomonas Putida Flavin-Binding Pp2FbFP. *Photochem. Photobiol. Sci.* **2015**, *14* (2), 280–287.

(9) Christie, J. M.; Hitomi, K.; Arvai, A. S.; Hartfield, K. A.; Mettlen, M.; Pratt, A. J.; Tainer, J. A.; Getzoff, E. D. Structural Tuning of the Fluorescent Protein ILOV for Improved Photostability ESI. *J. Biol. Chem.* **2012**, *287* (26), 22295–22304.

(10) Westberg, M.; Holmegaard, L.; Pimenta, F. M.; Etzerodt, M.; Ogilby, P. R. Rational Design of an Efficient, Genetically-Encodable, Protein-Encased Singlet Oxygen Photosensitizer. *J. Am. Chem. Soc.* **2015**, *137* (4), 1632–1642.

(11) Endres, S.; Granzin, J.; Circolone, F.; Stadler, A.; Krauss, U.; Drepper, T.; Svensson, V.; Knieps-Grünhagen, E.; Wirtz, A.; Cousin, A.; et al. Structure and Function of a Short LOV Protein from the Marine Phototrophic Bacterium Dinoroseobacter Shibae. *BMC Microbiol.* **2015**, *15* (1).

(12) Barnett, M. E.; Baran, T. M.; Foster, T. H.; Wojtovich, A. P. Quantification of Light-Induced MiniSOG Superoxide Production Using the Selective Marker, 2-Hydroxyethidium. *Free Radic. Biol. Med.* **2018**, *116*, 134–140.

(13) Westberg, M.; Bregnhøj, M.; Etzerodt, M.; Ogilby, P. R. No Photon Wasted: An Efficient and Selective Singlet Oxygen Photosensitizing Protein. *J. Phys. Chem. B* **2017**, *121* (40), 9366–9371.

(14) Rodríguez-Pulido, A.; Cortajarena, A. L.; Torra, J.; Ruiz-González, R.; Nonell, S.; Flors, C. Assessing the Potential of Photosensitizing Flavoproteins as Tags for Correlative Microscopy. *Chem. Commun.* **2016**, *52* (54), 8405–8408.

(15) Makhijani, K.; To, T.-L.; Ruiz-González, R.; Lafaye, C.; Royant, A.; Shu, X. Precision Optogenetic Tool for Selective Single- and Multiple-Cell Ablation in a Live Animal Model System. *Cell Chem. Biol.* **2017**, *24* (1), 110–119.

(16) Rodríguez-Pulido, A.; Torra, J.; Mejías, S. H.; Cortajarena, A. L.; Ruiz-González, R.; Nonell, S.; Flors, C. Fluorescent Flavoprotein Heterodimers: Combining Photostability with Singlet Oxygen Generation. *ChemPhotoChem* **2018**, 1–5.

(17) Zhang, Q.; Huang, H.; Zhang, L.; Wu, R.; Chung, C. I.; Zhang, S. Q.; Torra, J.; Schepis, A.; Coughlin, S. R.; Kornberg, T. B.; et al. Visualizing Dynamics of Cell Signaling In Vivo with a Phase Separation-Based Kinase Reporter. *Mol. Cell* **2018**, *69* (2), 347.

(18) Sharma, S. K.; Huang, Y.-Y.; Hamblin, M. R. Resistance to Photodynamic Therapy in Cancer. In *Resistance to Photodynamic Therapy in Cancer*; Rapozzi, V., Jori, G., Eds.; Springer, 2015; Vol. 5, pp 229–246.

(19) Ryumina, A. P.; Serebrovskaya, E. O.; Shirmanova, M. V; Snopova, L. B.; Kuznetsova, M. M.; Turchin, I. V; Ignatova, N. I.; Klementieva, N. V; Fradkov, A. F.; Shakhov, B. E.; et al. Flavoprotein MiniSOG as a Genetically Encoded Photosensitizer for Cancer Cells. *Biochim. Biophys. Acta* **2013**, *1830* (11), 5059–5067.

(20) Takehara, K.; Yano, S.; Tazawa, H.; Kishimoto, H.; Narii, N.; Mizuguchi, H.; Urata, Y.; Kagawa, S.; Fujiwara, T.; Hoffman, R. M. Eradication of Melanoma in Vitro and in Vivo via Targeting with a Killer-Red-Containing Telomerase-Dependent Adenovirus. *Cell cycle* **2017**, *16* (16), 1502–1508.

CHAPTER 9

Conclusions

Conclusions

1. The photophysical, photosensitizing and antimicrobial properties of eleven flavin-binding fluorescent proteins derived from different organisms have been characterized. All proteins are capable of producing $^1O_2$ and most of them are highly phototoxic when expressed in *E. coli* cells. Despite all proteins encase the same FMN chromophore, remarkable variations in quantum yields of fluorescence and singlet oxygen production, as well as in triplet lifetimes and photostability have been found. These observations reveal the strong influence of the specific amino acid sequence of each protein on the optical properties of the chromophore.

2. The photochemistry of miniSOG has been explained. Its modest ability to produce singlet oxygen a consequence of the competition between protein and oxygen quenching of the chromophore. Oxygen quenching is limited by the phosphoribityl tail, which blocks the access tunnel connecting the chromophore with the external aqueous phase. Protein quenching is due to electron transfer from nearby electron-rich amino acids and is favored by hydrogen-bonded residues that affect the electronic structure of the FMN chromophore.

3. The puzzling light-induced increase in miniSOG's ability to produce singlet oxygen has been clarified. Upon light exposure, the FMN cofactor in miniSOG is converted to lumichrome, which absorbs at shorter wavelengths, photosensitizes singlet oxygen in higher yield and lacks the phosphoribityl tail. In addition, electron-rich amino acids are inactivated by singlet oxygen, which also contributes to enhancing the photosensitizing ability.

4. Novel miniSOG mutants have been developed and characterized, including variants lacking electron-rich residues or encasing more accessible chromophores. As expected, higher values of singlet oxygen production have been determined and the improvement has been rationalized in terms of k_p and k_{O_2}, establishing the bases for the rational design of the improved genetically encoded singlet oxygen photosensitizers. Mammalian cells expressing miniSOG and the novel mutants are killed upon blue light illumination, confirming the potential of biological photosensitizers for optogenetic applications.

5. Two novel fluorescent reporters have been developed, characterized and tested in solution and in living cells. FlipGFP has been successfully demonstrated to monitor apoptosis triggered by exposure of miniSOG mutants to blue light, while SPARK is capable of visualizing kinase signaling. The fully genetically encoded approach is a powerful tool both for mechanistic and protein-protein interaction studies with high spatiotemporal resolution.

6. Attempts to use miniSOG as a biological photosensitizer for the treatment of melanoma have not led to positive results. Although several strategies for mammalian cell transduction and transfection have been tested, it has not been possible to detect miniSOG's green fluorescence in any melanoma cell line, which casts doubts about its expression and stability in melanoma cells.

List of abbreviations

$^1O_2$	Singlet oxygen
$^1PS_0$	Ground state photosensitizer
$^1PS^*$	Singlet excited state photosensitizer
$^1PS_1^*$	First singlet excited state photosensitizer
^{1}miniSOG*	miniSOG's singlet excited state
2PA	Two photon absorption
2PE	Two photon excitation
^{3}FMN*	Flavin mononucleotide's triplet excited state
^{3}miniSOG*	miniSOG's triplet excited state
$^3PS^*$	Triplet excited state photosensitizer
$^3PS_1^*$	First triplet excited state photosensitizer
Ala	Alanine
aPDT	Antimicrobial photodynamic therapy
Ara	Arabinose
a.u.	Arbitrary units
AUC	Area under the curve
BFP	Blue fluorescent protein
BLUF	Blue-light receptor using FAD
CALI	Chromophore-assisted light inactivation
CLEM	Correlated light and emission microscopy
cm	Centimeter
CRY	Cryptochrome
Cys	Cysteine
D2O	Deuterium oxide
DIC	Differential interference contrast
DNA	Deoxyribonucleic acid
dPBS	Deuterated phosphate buffered saline
dTRIS	Deuterated tris(hydroxymethyl)aminomethane
DAB	Diaminobenzidine
E. coli	Escherichia coli
EGFP	Enhanced green fluorescent protein
E_T	Energy of the triplet excited state
FAD	Flavin adenine dinucleotide

FbFP	Flavin-binding fluorescent protein
FLIM	Fluorescence lifetime imaging microscopy
FMN	Flavin mononucleotide
FP	Fluorescent protein
FRET	Förster resonance energy transfer
GFP	Green fluorescent protein
Gly	Glycine
GPC	Gated photon counting
h	Hours
H_2O_2	Hydrogen peroxide
HBDI	4-hydroxybenzylidene-1,2-dimethylimidazoline
HEK	Human embryonic kidney
HeLa	Henrietta Lacks
$HO^{\bullet}$	Hydroxyl radical
HOTag	Homo-oligomeric tag
IC	Internal conversion
IPTG	Isopropyl β-D-1-thiogalactopyranoside
IRF	Instrument response factor
ISC	Intersystem crossing
J	Joule
kDa	Kilo Dalton
kJ	Kilo Joule
L	Litre
LB	Luria-Bertani
LC	Lumichrome
LFP	Laser flash photolysis
LOV	Light, oxygen and voltage
M	Molar
MCS	Multichannel scaling
min	Minutes
mL	Milliliter
mM	Millimolar
ms	Milliseconds
mW	Milliwatt
mRNA	Messenger ribonucleic acid

NIR	Near-infrared
nm	Nanometer
Ni-NTA	Nickel- nitrilotriacetic acid
ns	Nanosecond
O_2	Molecular oxygen
$O_2^{\bullet-}$	Superoxide
OD	Optical density
PBS	Phosphate buffered saline
PCR	Polymerase chain reaction
PDB	Protein data bank
PDI	Photodynamic inactivation
PEG	Polyethylene glycol
PEI	Polyethylenimine
PMT	Photomultiplier tube
PNS	1H-phenalen-1-one-2-sulphonate
PI	Propidium iodide
PO_4^{2-}	Phosphate group
PS	Photosensitizer
ps	Picosecond
$P_T^{O_2}$	Fraction of triplets quenched by molecular oxygen
RB	Riboflavin
Ref	Reference
RFP	Red fluorescent protein
RNA	Ribonucleic acid
ROS	Reactive oxygen species
s	Seconds
SDS-PAGE	Sodium dodecyl sulphate-polyacrylamide gel electrophoresis
Ser	Serine
SPARK	Separation of phases-based activity reporter of kinase
TA	Triplet absorption
TCSPC	Time-correlated single photon counting
Tris	Tris(hydroxymethyl)aminomethane
Trp	Tryptophan
Tyr	Tyrosine

UV	Ultraviolet
Vis	Visible
VR	Vibrational relaxation
°C	Degree Celsius
Å	Angstrom
λ	Wavelength
Ɛ	Molar absorptivity
Φ_F	Fluorescence quantum yield
Φ_T	Triplet quantum yield
Φ_Δ	Singlet oxygen quantum yield
$f_{T,\Delta}^{O_2}$	Energy transfer efficiency from the triplet photosensitizer to molecular oxygen
τ_Δ	Singlet oxygen lifetime
τ_T	Photosensitizer's triplet lifetime
τ_s	Photosensitizer's singlet lifetimes
µg	Microgram
µJ	Microjoule
µL	Microliter
µM	Micromolar
µs	Microseconds

List of publications

Papers

- Rodríguez-Pulido, A.; **Torra, J.**; Mejías, S. H.; Cortajarena, A. L.; Ruiz-González, R.; Nonell, S.; Flors, C. Fluorescent Flavoprotein Heterodimers: Combining Photostability with Singlet Oxygen Generation. *ChemPhotoChem* **2018**, 1–5.
- Zhang, Q.; Huang, H.; Zhang, L.; Wu, R.; Chung, C. I.; Zhang, S. Q.; **Torra, J**.; Schepis, A.; Coughlin, S. R.; Kornberg, T. B.; Shu, X.; Visualizing Dynamics of Cell Signaling *In Vivo* with a Phase Separation-Based Kinase Reporter. Mol. Cell **2018**, 69 (2), 347.
- Rodríguez-Pulido, A.; Cortajarena, A. L.; **Torra, J**.; Ruiz-González, R.; Nonell, S.; Flors, C. Assessing the Potential of Photosensitizing Flavoproteins as Tags for Correlative Microscopy. *Chem. Commun.* **2016**, *52* (54), 8405–8408.
- **Torra, J.**; Burgos-Caminal, A.; Endres, S.; Wingen, M.; Drepper, T.; Gensch, T.; Ruiz-González, R.; Nonell, S. Singlet Oxygen Photosensitisation by the Fluorescent Protein Pp2FbFP L30M, a Novel Derivative of *Pseudomonas Putida* Flavin-Binding Pp2FbFP. *Photochem. Photobiol. Sci.* **2015**, 14 (2), 280–287.

Book chapters

- Rodríguez-Amigo, B.; Planas, O.; Bresolí-Obach, R.; **Torra, J**; Ruiz-González, R.; Nonell, S.; Chapter 2: Photosensitisers for Photodynamic Therapy: State of the Art and Perspectives, in *Photodynamic Medicine: From Bench to Clinic*; Kostron, H.; Hasan, T., Eds.; Royal Society of Chemistry, **2016**, 1, 23-62. ISBN: 978-1-78262-451-6.
- Ruiz-González, R.; Rodríguez-Pulido, A.; **Torra, J**.; Nonell, S.; Flors, C.; Chapter 13: Genetically-encoded singlet oxygen photosensitizers, in *Singlet Oxygen: Applications in Biosciences and Nanosciences*, Volume 1; Flors C.; Nonell, S., Eds. Royal Society of Chemistry, **2016**, 1, 23-46. ISBN: 978-1-78262-038-9.
- Planas, O.; Boix-Garriga, E.; Rodríguez-Amigo, B.; **Torra, J.**; Bresolí-Obach, R.; Flors, C.; Viappiani, C.; Agut, M.; Ruiz-González, R.; Nonell S.; Chapter 9: Newest approaches to singlet oxygen photosensitisation in biological media, in *Photochemistry:* Volume 42; Fasani, E.; Albini, A., Eds.; *Royal Society of Chemistry*, **2015**, 42, 233-278. ISBN: 978-1-84973-956-6.

Submitted papers

- Zhang, Q.; Schepis, A.; Huang, H.; Yang, J.; **Torra, J.**; Nonell, S.; Kornberg, T. B.; Coughlin, S. R.; Shu, X.; Designing a green fluorogenic protease reporter by flipping a beta strand of GFP for imaging apoptosis in animals.
- Endres, S.[§]; Wingen, M.[§]; **Torra, J**.[§]; Ruiz-González, R.; Polen, T.; Bosio, G.; Bitzenhofer, N.; Hilgers, F.; Gensch, T.; Nonell, S.; Jaeger, K-E.; Drepper, T.; An optogenetic toolbox of LOV-based photosensitizers for light-driven killing of bacteria. ([§]Co-first author.)

Communications in congresses

- **Torra, J**.; Rodríguez-Pulido, A.; Flors, C.; Agut, M.; Ruiz-González, R. and Nonell, S.; New insights on photoactive proteins suitable for photodynamic therapy, 17th Congress of the European Society for Photobiology (ESP), Pisa (Italy), September 2017.
- **Torra, J**.; Fabra, A.; Puig, S.; Agut, M.; Ruiz-González, R. and Nonell, S.; Genetically-encoded photosensitisers for the treatment of melanoma, XXXVI Reunión BIENAL de la Real Sociedad Española de Química, Sitges (Spain), June 4th – 8th, 2017.
- **Torra, J.**; Beinlich, F.; Ruiz-González, R.; Endres, S.; Wingen, M.; Drepper, T.; Gensch, T. and Nonell, S.; Genetically encoded flavin-binding fluorescent proteins: killing from inside, 16th Congress of the European Society for Photobiology (ESP), Aveiro (Portugal), August 31st – September 4th, 2015.
- **Torra, J.**; Beinlich, F.; Ruiz-González, R.; Endres, S.; Wingen, M.; Drepper, T.; Gensch, T. and Nonell, S.; Singlet oxygen and flavin-binding fluorescent proteins: a deadly tandem in LOV. 40th Congress of The Federation of European Biochemical Societies (FEBS), Berlin (Germany), July 4th – 9th, 2015.
- **Torra, J.**; Burgos-Caminal, A.; Endres, S.; Wingen, M., Drepper, T.; Gensch, T.; Ruiz-González, R.; Nonell, S.; Singlet oxygen photosensitisation by the fluorescent protein Pp2FbFP L30M, a novel derivative of *Pseudomonas putida* flavin-binding Pp2FbFP, XXV IUPAC Symposium on Photochemistry, Bordeaux (France), July 13th – 18th, 2014.

Additional papers are at different stages of publication.

- **Torra, J.**; Lafaye, C.; Signor, L.; Aumonier, S.; Flors, C.; Shu, X., Nonell, S.; Gotthard, G.; Royant, A.; Tailing miniSOG: Structural Bases of the Complex Photophysics of a Flavin-Binding Singlet Oxygen Photosensitizing Protein.
- Bresolí-Obach, R.; **Torra, J.**; Flors, C.; Agut, M.; Shu, X.; Ruiz-González, R.; Nonell, S.; CellROX® Deep Red: Nonspecific Fluorescent Probe for Reactive Oxygen Species.